Innovating surgery for oral squamous cell carcinoma with targeted fluorescent and magnetic tracers

A thesis submitted for the degree of Doctor of Philosophy

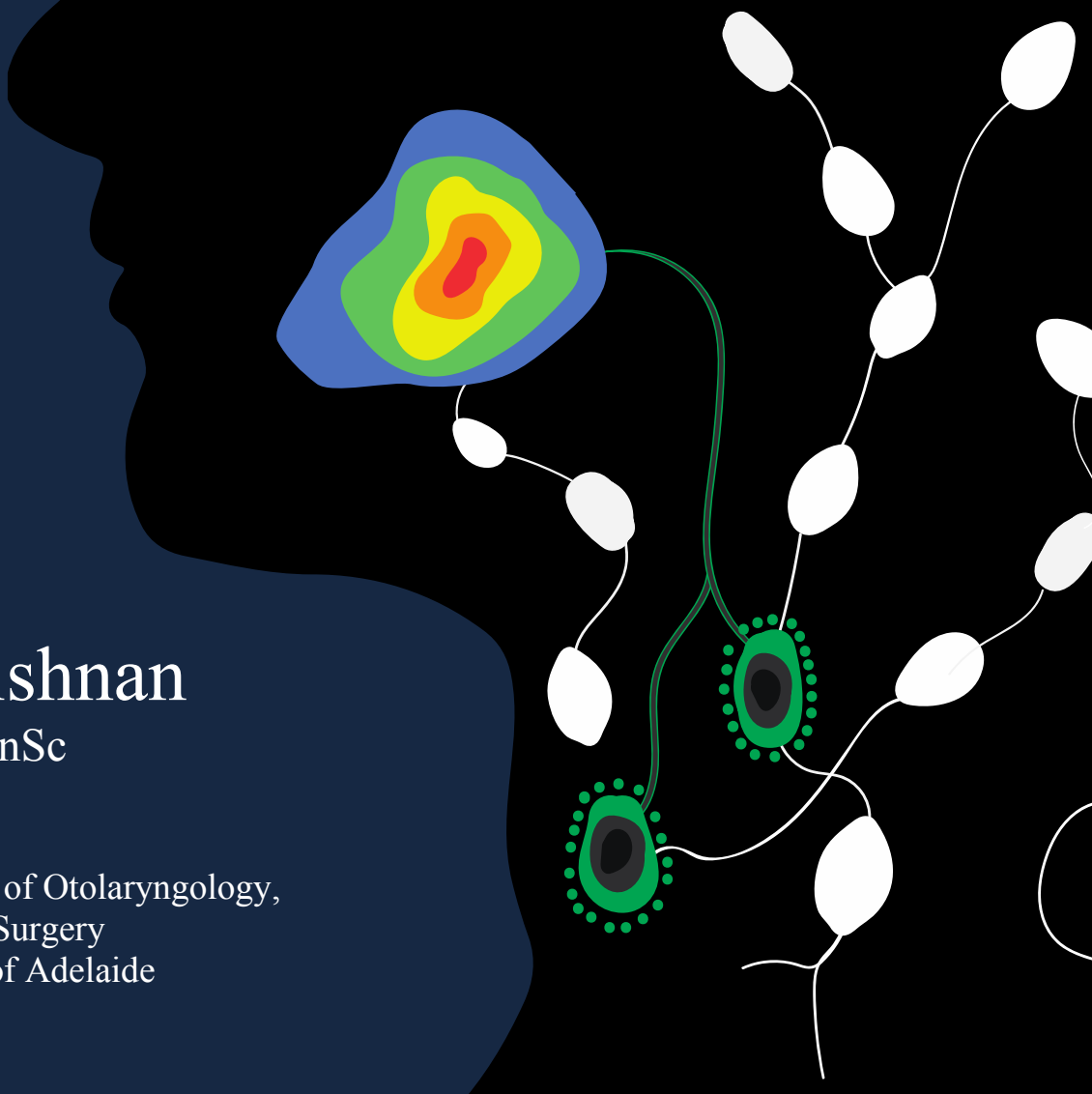

Giri Krishnan
MBBS MClinSc

July 2022

The Department of Otolaryngology,
Head and Neck Surgery
The University of Adelaide

Dedicated to my parents

We chose to go to the moon in this decade and do other things, not because they are easy, but because they are hard

John F. Kennedy 1962

Table of Contents

DECLARATION

I certify that this work contains no material which has been accepted for the award of any other degree or diploma in my name in any university or other tertiary institution and, to the best of my knowledge and belief, contains no material previously published or written by another person, except where due reference has been made in the text. In addition, I certify that no part of this work will, in the future, be used in a submission in my name for any other degree or diploma in any university or other tertiary institution without the prior approval of the University of Adelaide and where applicable, any partner institution responsible for the joint award of this degree. The author acknowledges that copyright of published works contained within this thesis resides with the copyright holder(s) of those works. I give permission for the digital version of my thesis to be made available on the web, via the University's digital research repository, the Library Search and also through web search engines, unless permission has been granted by the University to restrict access for a period of time. I acknowledge the support I have received for my research through the provision of an Australian Government Research Training Program Scholarship.

Dr Giri Krishnan
October 2021

ACKNOWLEDGEMENTS

Matha pitha guru deivam

My first acknowledgement is to my mother. She was my earliest (and continues to be my most important) teacher. If I have achieved success in my life, it is because of the advice I have received from her.

That I have undertaken a career in Otolaryngology, head and neck surgery is because of my father. His care for his patients, passion for surgery and generous service to others has been an inspiration. Every day I am proud to follow in his footsteps.

I am incredibly blessed to have been supervised by Professor PJ Wormald, Dr. Andrew Foreman, Professor Benjamin Thierry and Professor Eben Rosenthal. They have been extraordinary role models and have become dear friends. I have learnt many lessons from them about leadership, science, medicine and surgery, which I will hold with me for the rest of my life. I hope that in the future I can display the same respect, kindness and compassion to my own mentees as they have demonstrated to me.

This work would not have been possible without Dr. Aidan Cousins at the Future Industries Institute at the University of South Australia and Dr. Nynke van den Berg at the Rosenthal Laboratory at Stanford University. I have learnt an enormous amount from these wonderful people and am indebted to them for their significant contribution to the research contained within this thesis. For their generosity of time, wisdom, energy and

spirit, and above all, for their friendship, they will both forever hold a special place in my heart.

There have been many others who have contributed to this work and who have supported me along this journey. Some are listed below:

- Professor Alkis Psaltis, Professor Sarah Vreudge, Dr. Clare Cooksley, Dr. Mahnaz Ramezanpour, Catherine Bennet and the research team at the Basil Hetzel Institute
- The Late Dr. Tim Kuchel, Loren Matthews, Sam Herzog, Robb Muirhead, Paul Herde, Mariah Turelli and the tirelessly hard-working team at the South Australian Health and Medical Research Institute Preclinical Imaging and Research Laboratory at Gilles Plains
- Dr. Naoki Nishio, Dr. Stan van Keulen, Dr. Shayan Fakurnejad and my many friends and colleagues at the Rosenthal laboratory at Stanford University
- Hugh and Aja Minson and Ben Hodgson and Hana Horakova – my family in San Francisco
- Stewart Bartlett and his dedicated team at Ferronova
- My brother, Dr. Shridhar Krishnan, and Dr. James Badlani from the Department of Oral and Maxillofacial Surgery at the Royal Adelaide Hospital
- Dr. Stephen Kao, Dr. Sathish Paramasivan and my Otolaryngology, Head and Neck Surgery Registrar colleagues in South Australia
- My family, including my sister Shuba Krishnan, my grandmother in Perth, and all my uncles, aunties and cousins - In particular, my Uncle Ravi and Uncle Jegan who have been inspirations for my path in science.

Finally, acknowledgement goes to my partner Georgina Juniper and her family. This extraordinary journey has been more rewarding because I have had Georgina by my side. I won't forget the many memories we have shared together over the last several years while completing this thesis, including travelling to the US and working together at Stanford University. In completing this work, I have lent heavily on her for support during challenging times and have asked of her company when a small win called for a celebration. The individual chapters within this thesis amount to an amazing chapter in our lives together.

PUBLICATIONS ARISING FROM THIS THESIS

Included within this thesis:

Intraoperative Molecular Imaging for *ex vivo* Assessment of Peripheral Margins in Oral Squamous Cell Carcinoma.

Fakurnejad S, Krishnan G, van Keulen S, Nishio N, Birkeland AC, Baik FM, Kaplan MJ, Colevas AD, van den Berg NS, Rosenthal EL, Martin BA. Front Oncol. 2020 Jan 10;9:1476.

Metastatic and sentinel lymph node mapping using intravenously delivered Panitumumab-IRDye800CW.

Krishnan G, van den Berg NS, Nishio N, Juniper G, Pei J, Zhou Q, Lu G, Lee YJ, Ramos K, Iagaru AH, Baik FM, Colevas AD, Martin BA, Rosenthal EL. Theranostics. 2021 May 24;11(15):7188-7198.

Fluorescent molecular imaging can improve intraoperative sentinel margin detection in oral squamous cell carcinoma

Krishnan G, van den Berg NS, Nishio N, Kapoor S, Pei J, Freeman L, Lee YJ, Zhou Q, van Keulen S, Fakurnejad S, Condon C, Baik FM, Martin BA, Rosenthal EL. Submitted to Journal of Nuclear Medicine. 2021 August.

Preclinical evaluation of a mannose-labelled magnetic tracer for enhanced sentinel lymph node retention in the head and neck.

Krishnan G, Cousins A, Pham N, Milanova V, Nelson M, Krishnan S, Shetty A, van den Berg N, Rosenthal EL, Krishnan S, Wormald PJ, Foreman A, Thierry B.

Prepared for submission.

Mannose-labelled magnetic tracer for sentinel lymph node biopsy in oral squamous cell carcinoma: Initial results from a phase 1 FerroTrace clinical trial

Krishnan G, Cousins A, Krishnan S, Wormald PJ, Dhatrak D, Otto S, Walls A, Dwyer A, Thierry B, Badlani J, Krishnan S, Forema A.

Prepared for submission.

Feasibility of head and neck robot-assisted sentinel lymph node biopsy using multi-modality magnetic and fluorescence guidance

Krishnan G, Cousins A, Milanova V, Krishnan S, van den Berg N, Rosenthal EL, Krishnan S, Wormald PJ, Thierry B, Foreman A, Krishnan S.

Prepared for submission.

Related publications not included within this thesis:

Fluorescence-Guided Surgery for Sinonasal Cancer Using an Antibody-Dye Conjugate.

Hart ZP, Nishio N, Krishnan G, Lu G, Zhou Q, Fakurnejad S, Wormald PJ, van den Berg NS, Rosenthal EL, Baik FM. Endoscopic Laryngoscope. 2020 Dec;130(12):2811-2817.

Intraoperative Fluorescence-Guided Surgery in Head and Neck Squamous Cell Carcinoma.

Lee YJ, Krishnan G, Nishio N, van den Berg NS, Lu G, Martin BA, van Keulen S, Colevas AD, Kapoor S, Liu JTC, Rosenthal EL. Laryngoscope. 2021 Mar;131(3):529-534.

Safety and Stability of Antibody-Dye Conjugate in Optical Molecular Imaging.

Pei J, Juniper G, van den Berg NS, Nisho N, Broadt T, Welch AR, Yi GS, Raymundo RC, Chirita SU, Lu G, Krishnan G, Lee YJ, Kapoor S, Zhou Q, Colevas AD, Lui NS, Poultsides GA, Li G, Zinn KR, Rosenthal EL. Mol Imaging Biol. 2021 Feb;23(1):109-116.

Effect of Formalin Fixation for Near-Infrared Fluorescence Imaging with an Antibody-Dye Conjugate in Head and Neck Cancer Patients.

Kapoor S, Lu G, van den Berg NS, Krishnan G, Pei J, Zhou Q, Martin BA, Baik FM, Rosenthal EL, Nishio N. Mol Imaging Biol. 2021 Apr;23(2):270-276.

PRESENTATIONS ARISING FROM THIS THESIS

Magnetic nanotechnology for sentinel lymph node biopsy in the head and neck

The 8th international Symposium for sentinel lymph node biopsy

London, United Kingdom, April 2018

Magnetic sentinel lymph node mapping in a rabbit model of head and neck cancer

The Queen Elizabeth Hospital Research Day Expo

Adelaide, South Australia, October 2018

Magnetic sentinel lymph node mapping in a rabbit model of head and neck cancer

The Royal Australian College of Surgeons RP Jepson Medal Presentation

Adelaide, South Australia, November 2018

Magnetic sentinel lymph node mapping in a rabbit model of head and neck cancer

Ron Gristwood Otolaryngology, Head and Heck Surgery Registrar Meeting

Adelaide, South Australia, November 2018

Magnetic sentinel lymph node mapping for oral squamous cell carcinoma

Flinders University Public Health Seminar

Adelaide, South Australia, February 2019

Fluorescent molecular imaging to optimise staging of the neck in clinically node negative oral squamous cell carcinoma (poster presentation)

Stanford University Otolaryngology, Head and Neck Surgery Research Day

Palo Alto, California 2019

Fluorescent molecular imaging to optimise staging of the neck in clinically node negative oral squamous cell carcinoma (poster presentation)

Stanford Molecular Imaging Program Research Retreat

Santa Cruz, California 2019

An innovative approach for sentinel lymph node biopsy in head and neck cancer

The Queen Elizabeth Hospital Research Day Expo

Adelaide, South Australia, October 2020

The future of sentinel lymph node biopsy the head and neck

Ron Gristwood Otolaryngology, Head and Heck Surgery Registrar Meeting

Adelaide, South Australia, October 2020

Magnetic sentinel lymph node biopsy in the head and neck using FerroTrace

The University of Twente Magnetic Detection and Imaging Online Symposium

Enschede, Netherlands, November 2020

Fluorescent molecular imaging in head and neck surgery

The Australian Society of Otolaryngology, Head and Neck Surgery Annual Scientific Meeting

Melbourne, Australia September 2021

A novel magnetic approach to sentinel lymph node biopsy in oral cancer

The Australian Society of Otolaryngology, Head and Neck Surgery Annual Scientific Meeting

Melbourne, Australia September 2021

AWARDS ARISING FROM THIS THESIS

2017

The Fulbright Post-Graduate Scholarship

AVANT Doctors in training Advancement of Medicine Scholarship

The Australia and New Zealand Head and Neck Cancer Society (ANZHNCS) Research Grant

2018

The Garnett Passe and Rodney William's Memorial Foundation Academic Surgeon Scientist Research Scholarship

The Australian Society of Otolaryngology Head and Neck Surgery Ron Gristwood Medal for best South Australian Registrar research presentation

The Queen Elizabeth Hospital Research Day Award for best Junior PhD Laboratory Research Presentation

The South Australian Indian Medical Association President's Award

2020

The Bertha Sudholz Research Scholarship

The Australian Society of Otolaryngology Head and Neck Surgery Ron Gristwood Medal for best South Australian Trainee research presentation

The Queen Elizabeth Hospital Research Day Award for best Senior PhD Clinical Research Presentation

2021

The Jean Littlejohn Prize for best trainee presentation at the Australian Society of Otolaryngology Head and Neck Surgery Annual Scientific Meeting

The Robert Guerin Research Prize for the best trainee research in Australia

The Frank Szallasi Prize for the best Queensland Trainee research presentation

ABBREVIATIONS

2D	Two-dimensional
3D	Three-dimensional
AAS	Atomic absorption spectroscopy
ACOSOG	American College of Surgeons Oncology Group
AHNS	American Head and Neck Society
AJCC	American Joint Committee on Cancer
AUC	Area under the curve
CO2	Carbon dioxide
CI	Confidence interval
CIS	Carcinoma in situ
cN+	Clinically positive neck
cN0	Clinically negative neck
CND	Completion neck dissection
CT	Computed tomography
DFS	Disease free survival
DOI	Depth of invasion
DSS	Disease specific survival
DTPA	Diethylene triaminine pentaacetic acid
DWI	Diffusion weighted images
EGFR	Epidermal growth factor receptor
END	Elective neck dissection
ENE	Extranodal extension
FDA	US Food and Drug Administration
FN	False negative
FNA	Fine-needle aspiration
FOM	Floor of mouth
FP	False positive
FSA	Frozen section analysis
H&E	Haematoxylin and eosin
HNSCC	Head and neck squamous cell carcinoma
HR	Hazards ratio
ICCR	International Collaboration on Cancer Reporting
ICG	Indocyanine green
ICP-MS	Inductively coupled plasma mass spectrometry
IHC	Immunohistochemistry
IJV	Internal jugular vein
IONP	Iron oxide nanoparticle
IRB	Institutional review board
ITC	Isolated tumour cell

IV	Intravenous
LN	Lymph node
LRFS	loco-regional disease free survival
LSG	Lymphoscintigraphy
LVI	Lymphovascular invasion
MFI	Mean fluorescent intensity
MFLA	Modified face-lift approach
MJT	Magnetic tunnel junction
MRI	Magnetic resonance imaging
MRND	Modified radical neck dissection
NBI	Narrow band imaging
NCCN	National Comprehensive Cancer Network
NDII	Neck dissection impairment index
NHMRC	National Health and Medical Research Council
NHS	N-hydroxysuccinimide
NIR	Near infrared
NPV	Negative predictive value
NS	Not significant
OS	Overall survival
OSCC	Oral squamous cell carcinoma
PEG	Polyethylene glycol
PET	Positron emission tomography
PIRL	Preclinical imaging and research laboratory
PNI	Perineural invasion
PORT	Post-operative radiotherapy
PVA	Polyvinyl acetate
QALY	Quality adjusted life years
QOL	Quality of life
R0	Initially negative margins
R1	Initially positive margins
RAFT	Reversible addition-fragmentation chain-transfer
RAND	Robot-assisted neck dissection
RCR	Relative cost ratio
RCT	Randomised controlled trial
RMT	Retromolar trigone
ROC	Receiver operating characteristic
ROI	Regions of interest
SAHMRI	South Australian Health and Medical Research Institute
SBR	Signal-to-background ratio
SCC	Squamous cell carcinoma
SCM	Sternocleidomastoid muscle
SD	Standard deviation
SENT	Sentinel European Node Trial

SLN	Sentinel lymph node
SND	Selective neck dissection
SNR	Signal-to-noise ratio
SPECT-CT	Single photon emission computer tomography fused with CT
SPION	Superparamagnetic iron oxide nanoparticle
SVC	Superficial ventral cervical
T1 WI	T1 weighted image
TIFF	Tag image file format
TN	True negative
TORS	Transoral robotic surgery
TP	True positive
UICC	Union for International Cancer Control
US	Ultrasound
VEGF	Vascular endothelial growth factor
WLE	Wide local excision

LIST OF TABLES

LIST OF FIGURES

ABSTRACT

Oral squamous cell carcinoma (OSCC) is characterised by its locally aggressive nature and its high propensity to metastasise to regional lymph nodes (LN)s. It is well-established that margin status and the presence of LN metastases are two of the most important factors affecting prognosis. While patient and tumour factors cannot be changed after presentation, margin control during primary tumour resection and staging of the clinically occult neck are two components of treatment that are within the control of the head and neck surgeon. Despite this, positive margin rates have not improved over the last three decades and staging of the clinically negative neck continues to rely on elective neck dissection (END), which results in overtreatment of up to 75% of patients.

Molecular imaging, with tracers designed to target specific tissue and tumour ligands, is a growing field that has significant potential to improve outcomes for patients with OSCC. This thesis evaluates how two different tracer technologies could be used to aid either margin assessment during resection of the primary tumour, and/or staging of the clinically negative neck with sentinel lymph node biopsy (SLNB). The tracers studied within this thesis are Panitumumab-IRDye800CW, an EGFR-targeting fluorophore used for fluorescence molecular imaging, and FerroTrace, a superparamagnetic iron oxide nanoparticle (SPION) that has been engineered with mannose end targets for macrophage-specific binding to aid SLNB.

CHAPTER 1: THE CURRENT MANAGEMENT PARADIGM FOR ORAL SQUAMOUS CELL CARCINOMA

INTRODUCTION

The oral cavity is defined by anatomic boundaries, which include the vermillion border of the lip anteriorly, the junction of the hard palate and the soft palate posteriorly and superiorly, the circumvallate papillae inferiorly and the anterior tonsillar pillars laterally. Within this cavity are several subsites where cancers can grow including the lip, dentoalveolar ridge, oral tongue, retromolar trigone (RMT), floor of mouth (FOM), buccal mucosa and hard palate (Figure 1.1).[1]

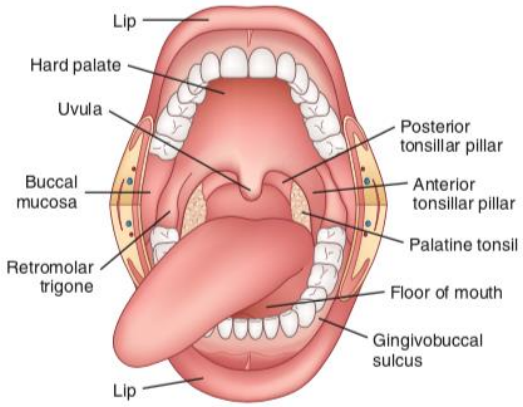

Figure 1.1 Subsites of the oral cavity.

From Atlas of head and neck pathology [2]

Oral squamous cell carcinoma (OSCC) is a malignant neoplasm of the oral cavity and accounts for 95% of cancers in this anatomic site.[2] It is an invasive epithelial neoplasm with varying degrees of squamous differentiation and a has a propensity to metastasise early and extensively to regional lymph nodes (LN)s.[3]

OSCC is most commonly of the keratinising (conventional) type with three histological grades; well, moderately and poorly differentiated. Other types of squamous cell carcinoma (SCC) include verrucous carcinoma, spindle cell SCC, basaloid SCC, adenosquamous carcinoma and lymphoepithelioma-like carcinoma. There are associated premalignant surface epithelial changes called carcinoma in situ (CIS) that is characterized by cellular dysplasia involving the full thickness of the mucosa without compromise of the basement membrane. If the malignant cells penetrate the basement membrane and infiltrate in to the superficial compartment of the lamina propria, the lesion is termed microinvasive carcinoma.[2]

AETIOPATHOGENESIS

The risk factors for OSCC are tobacco, spirits, sharp teeth and, much more rarely now, syphilis. Smoking and alcohol increase the risk four times, and when consumed together have a super multiplicative effect.[4] In India and South East Asia, the practice of chewing betel nut with quid (lime and cured tobacco), is a common cause. Other associations with the aetiology of OSCC are chronic syphilis infection, ill-fitting dentures and long-term immunosuppression.[5]

The pathogenesis of OSCC is multifactorial and is thought to arise from a multi-step process within a clonal population of cells involving sequential activation of genes that have the potential to cause cancer (oncogenes), as well as inactivation of genes that prevent cancer (tumour suppressor genes).[5] A molecular model for the pathogenesis of OSCC describes first a loss of chromosomal regions 3p and 9p21 followed by inactivation

of the p16 gene that leads to histological atypia.[6] Subsequent mutation of the p53 tumour suppressor gene is associated with progression to dysplasia.[7] Finally, gross gene alterations and deletions on 4q, 6p, 8p, 11q, 13q and 14q are thought to lead to malignancy.[8] A late event is amplification and overexpression of the Cyclin D1 gene, which activates cell cycle progression, and confers the ability of the tumour cells to invade.[9]

EPIDEMIOLOGY

OSCC accounts for approximately 14% of head and neck squamous cell carcinomas (HNSCC), which make up the 6th most common neoplasms in the word.[10, 11] Globally, 266,672 cases of OSCC were reported in 2000 representing 5% of all cancers for men and 2% for women. Males are generally affected more than females because of heavier use of alcohol and tobacco in most countries, although in India the highest rates of OSCC are in women who chew tobacco heavily.[3] The majority of cases of OSCC affect people in the developing world, where it ranks the third most common cancer overall after stomach and cervical cancer. It is among the most common cancers in India, Sri Lanka, Pakistan and Bangladesh. In the western world the highest rates are in France, Switzerland, Northern Italy, Central and Eastern Europe.[3]

In Australia there were 3,644 incidences of OSCC and oropharyngeal squamous cell carcinoma in 2013. The highest incidence was for cancer of the lip followed by the tongue. The mortality rate of this disease in Australia has remained relatively unchanged over the last three decades despite a decrease in the incidence of new diagnoses.[12] 55%

of OSCC are detected at an early stage, which is a much higher rate of early disease when compared to other head and neck subsites due to ease of detection and surveillance in the oral cavity where cancer can be much more easily visualized.[4]

CLINICAL WORK-UP

History

Typically, if it is early in the disease process, patients with OSCC will present with any combination of a non-healing ulcer, oral-dental pain or bleeding in the mouth. With progression of tumour growth, patients can have symptoms of otalgia, trismus, halitosis, dysphagia, odynophagia and dysarthria. Weight loss can be a late symptom and signal more advanced disease.

The primary tumour may be ulcerated, 'exophytic' or 'endophytic' (Figure 1.2 A, B and C). Ulcerated lesions have an irregular edge and a firm fibrous indurated feel to the underlying soft tissue. Exophytic lesions grow outward like a cauliflower, while endophytic lesions grow inward with invasion into underlying soft tissue. It is not uncommon for lesions to be heaped with white keratin debris or to bleed from the surface (Figure 1.2 D).

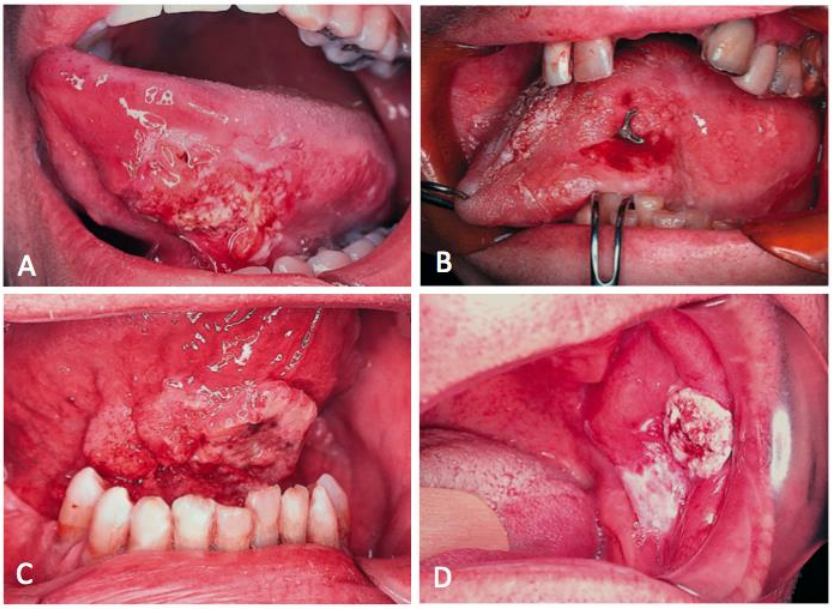

Figure 1.2 Types of oral squamous cell carcinoma.

A. Ulcerative SCC of the ventral tongue, B. Deeply invasive endophytic SCC of the tongue, C. Deeply infiltrating exophytic carcinoma of the FOM, D. An exophytic SCC of the buccal mucosa with white keratin debris. [13]

Physical examination

As part of the physical examination, primary tumour dimensions, subsite involved and potential direct extension within the oral cavity or to adjacent head and neck subsites is evaluated to determine the clinical stage of the cancer and plan the resection. The lesion is palpated to assess for fixation to surrounding bones such as the maxilla or mandible. The neck is palpated to assess the number and location of enlarged nodes, and if present, whether any nodal mass is fixed to underlying structures. Extension of the tumour toward the midline within the oral cavity is checked as this can result in contralateral or bilateral neck metastases.[13]

Imaging

Imaging plays a role in diagnosis, pre-operative planning and staging. The most commonly used imaging modalities are ultrasound (US), computed tomography (CT), magnetic resonance imaging (MRI) and positron emission tomography (PET)-CT.

US is used primarily to characterise an enlarged neck node and when combined with fine-needle aspiration (FNA) biopsy has a diagnostic sensitivity and specificity of 87% and 86%.[14] CT plays a role in assessment of the primary site as well as the cervical LNs. It is more sensitive and specific than physical examination alone for identifying LN metastases, and is the most superior imaging option for assessing cortical bone erosion and mandibular invasion.[14, 15] MRI is the best imaging modality for assessing soft tissue invasion, including into the tongue musculature, as well as perineural invasion (PNI), and extension to medullary bone.[16] PET-CT has excellent diagnostic accuracy for detecting regional nodal and distant metastases and can be used for prognostication and to assess therapeutic response.[17]

DIAGNOSIS AND STAGING

Tissue biopsy is required to confirm the diagnosis of OSCC and the stage is calculated from clinical evaluation combined with imaging. The staging system for oral cavity malignancies is defined by the American Joint Committee on Cancer (AJCC) and follows the 'TNM' scoring system that takes into account primary tumour size, regional nodes

affected, and the presence of distant metastases. At time of writing, the most recent edition of the AJCC Cancer Staging Manual is the 8th edition, which was published in October 2016 and was implemented on January 2018 (Table 1.1). A grouping of the TNM classification provides an overall stage, which is used to guide treatment. In general, early-stage disease is denoted stage I or II, and advanced stage disease is III or IV as summarised in the Table 1.2.[18]

Table 1.1 TNM staging system for oral squamous cell carcinoma.

Primary tumour (pT) staging

pTX	Primary tumour cannot be assessed
pTis	Carcinoma *in situ*
pT1	Tumour ≤2 cm with depth of invasion (DOI) ≤5 mm
pT2	Tumour ≤2 cm with DOI >5 mm *or* tumour >2 cm and ≤4 cm with DOI ≤10 mm
pT3	Tumour >2 cm and ≤4 cm with DOI >10 mm *or* tumour >4 cm with DOI ≤10 mm
pT4	Moderately advanced or very advanced local disease
pT4a	Moderately advanced local disease Tumour >4 cm with DOI >10 mm *or* tumour invades adjacent structures only (eg, through cortical bone of the mandible or maxilla or involves the maxillary sinus or skin of the face)

pT4b	Very advanced local disease Tumour invades masticator space, pterygoid plates, or skull base, and/or encases the internal carotid artery

Regional lymph nodes (pN) staging

pNX	Regional LNs cannot be assessed
pN0	No regional LN metastasis
pN1	Metastasis in a single ipsilateral LN, 3 cm or smaller in greatest dimension and extranodal extension (ENE)(−)
pN2	Metastasis in a single ipsilateral LN, 3 cm or smaller in greatest dimension and ENE(+); *or* larger than 3 cm but not larger than 6 cm in greatest dimension and ENE(−); *or* metastases in multiple ipsilateral LNs, none larger than 6 cm in greatest dimension and ENE(−); *or* in bilateral or contralateral LN(s), none larger than 6 cm in greatest dimension and ENE(−)
pN2a	Metastasis in single ipsilateral node 3 cm or smaller in greatest dimension and ENE(+); *or* a single ipsilateral node larger than 3 cm but not larger than 6 cm in greatest dimension and ENE(−)
pN2b	Metastases in multiple ipsilateral nodes, none larger than 6 cm in greatest dimension and ENE(−)
pN2c	Metastases in bilateral or contralateral LN(s), none larger than 6 cm in greatest dimension and ENE(−)

pN3	Metastasis in a LN larger than 6 cm in greatest dimension and ENE(−); *or* metastasis in a single ipsilateral node larger than 3 cm in greatest dimension and ENE(+); *or* multiple ipsilateral, contralateral or bilateral nodes any with ENE(+); *or* a single contralateral node of any size and ENE(+)
pN3a	Metastasis in a LN larger than 6 cm in greatest dimension and ENE(−)
pN3b	Metastasis in a single ipsilateral node larger than 3 cm in greatest dimension and ENE(+); *or* multiple ipsilateral, contralateral or bilateral nodes any with ENE(+); *or* a single contralateral node of any size and ENE(+)

Distant metastasis (pM) staging

pM0	No distant metastasis
pM1	Distant metastasis present

As per the AJCC Cancer Staging Manual 8th edition.[18]

Table 1.2 TNM stage grouping for oral squamous cell carcinoma.

Stage 0	Tis	N0	M0
Stage I	T1	N0	M0
Stage II	T2	N0	M0
Stage III	T3 T1 – T3	N0 N1	M0 M0

Stage IVa	T4a T4a T1 – T4a	N0 N1 N2	M0 M0 M0
Stage IVb	Any T T4b	N3 Any N	M0 M0
Stage IVc	Any T	Any N	M1

As per the AJCC Cancer Staging Manual 8th edition.[18]

MANAGEMENT OF THE PRIMARY TUMOUR

GENERAL PRINCIPLES

Primary surgery is the mainstay of treatment for patients with OSCC.[19] The general principle of surgery is to resect the tumour with an appropriate margin of normal tissue to provide the best chance of recurrence-free survival.[20] Following tumour ablation, reconstructive surgery to repair the tissue defect is undertaken so that swallowing, breathing and speaking function can be maintained.[21] The size and the location of the tumour determine the need for adjuncts such as temporary tracheostomy and feeding tubes to ensure a secure airway and adequate nutrition in the post-operative period while the upper aerodigestive tract is healing.[22]

SURGICAL APPROACHES TO THE ORAL CAVITY

Surgical access

Effective tumour ablation is achieved by ensuring appropriate visibility and access to the tumour and several surgical approaches are available to aid this depending on the size and site of the lesion.[22] Early-stage lesions of the oral cavity (T1/T2) can be completely resected through a transoral approach (Figure 1.3A). When the transoral approach does not offer enough exposure, the visor flap or upper and lower cheek flap approaches can be used for anteriorly located lesions (Figure 1.3 C, D, E). Large and more posteriorly

located lesions may require a pull-through or mandibulotomy-based technique in order to access the tumour and to effectively reconstruct the defect (Figure 1.3B).[13]

Figure 1.3 Various surgical approaches for resecting oral squamous cell carcinoma.

A. Transoral, B. Mandibulotomy, C. Lower cheek flap, D. Visor flap, E. Upper cheek flap. *Modified from Shah et al.*[13]

Management of the mandible

Mandibular invasion can occur early in tumours of the floor of the mouth, the ventral surface of the tongue and the gingivobuccal sulcus.[23] Tumours invade the mandible through the dental sockets in the dentate mandible, and through the dental pores of the alveolar process in the edentulous mandible.[24] If the tumour invades into the mandible, part of the mandible should be resected to ensure adequate margin control.[25] In the case of mandibular periosteum involvement, this could be achieved by performing a marginal mandibulectomy to shave a margin of bone.[26] If the tumour invades deeper resulting in gross mandibular invasion, a segmental mandibulectomy is indicated where a segment of bone is removed with clear margins on either side.[27]

Reconstructive considerations

Several reconstructive options exist to repair soft tissue and bony defects following tumour ablation in order to preserve breathing, swallowing and speaking function.[28] Smaller surgical defects can be closed primarily with sutures, left to heal by secondary intention, or can be reconstructed with skin grafts. Larger defects are usually reconstructed with regional pedicled flaps or microvascular free tissue transfer.[29] Reconstruction of the mandible typically involves free-tissue transfer with bone from the fibula, iliac crest, radial forearm or scapula.[30] In some instances, if an oral cavity defect involves several areas, multiple free flap reconstruction can be considered.[31]

ADJUVANT TREATMENT

Following surgery, a specialised head and neck multi-disciplinary team convenes to discuss the histopathological results of the resection, which provides accurate staging information to inform subsequent treatment.[32] Adjuvant treatment decisions are typically tailored to the individual patient based on a risk-benefit analysis, and are guided by evidence-based decision making algorithms such as those provided by the National Comprehensive Cancer Network (NCCN) guidelines.[33] Surgery alone can be associated with good oncological control in early-stage tumours, whereas advanced T-stage disease (pT3 or pT4) tends to require multi-modality treatment with additional radiotherapy plus or minus chemotherapy.[34] Other than TNM staging criteria, indications for adjuvant treatment include positive or close surgical margins, PNI and lymphovascular invasion (LVI).[35, 36]

MANAGEMENT OF THE NECK

RATIONALE

OSCC has a propensity to spread through the lymphatics to the regional LNs in the neck.[37, 38] The presence of a tumour deposit in a cervical LN is well-established to be the most significant prognostic factor as it decreases survival by 50%.[37, 39] Therefore, management of the neck is one of the most important aspects of treatment in head and neck cancer.[40-42] For patients with clinically and radiologically positive (cN+) neck disease, neck dissection is the recommended treatment.[43, 44] Treatment of 'cN0' patients with no pre-operative evidence of cervical metastases, however, is an area of ongoing debate and clinical evolution.[45]

NECK DISSECTION

Definition

The neck is divided into 6 levels, which encompass clusters of cervical LNs which receive lymphatic drainage from different primary sites in the upper aerodigestive tract (Figure 1.4).[46] Neck dissection is the surgical operation used to eradicate known or potential metastases in the neck, by systematically removing levels of LNs and fibrofatty tissue in selected compartments of the neck from the mandible and skull base superiorly to the clavicle inferiorly and from the posterior triangle of the neck laterally to the midline viscera.[13] It is classically thought of as being either "therapeutic", when it treats known

LN metastases, or “elective”, when LNs are removed prophylactically in a patient with a clinically and radiologically negative (cN0) neck. The neck dissection is termed ipsilateral when performed on the same side as the location of the primary tumour and contralateral if performed on the opposite side. Bilateral neck dissections are typically performed for midline lesions. When a neck is re-operated on for recurrence the operation is known as a ‘salvage’ neck dissection.

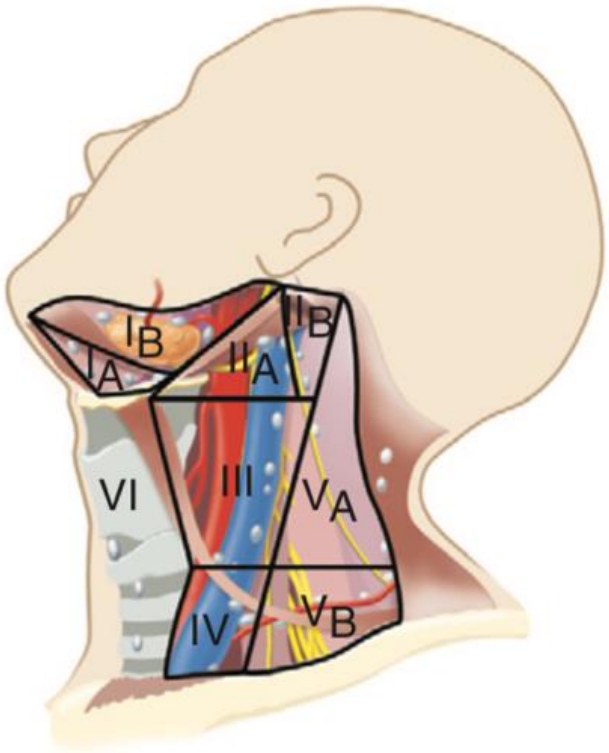

Figure 1.4 Lymph node levels of the neck.

From Jatin Shah's head and neck surgery and oncology [13]

Neck dissection types and indications

The classification of neck dissection as per the American Head and Neck Society (AHNS) is based on a series of modifications to the most radical approach.[47]

The radical neck dissection (RND) involves the removal all of all ipsilateral cervical LNs groups from level I to V as well as resection of the spinal accessory nerve, the internal jugular vein (IJV) and the sternocleidomastoid muscle (SCM).[48] The indication for this is extensive LN metastases with extension beyond the capsule of the node that involve the spinal accessory nerve and the IJV.[48]

A modified radical neck dissection (MRND) is when one or more of the non-lymphatic structures is preserved. The indication for a MRND is to remove grossly visible LN disease that is not invading or fixed to non-lymphatic structures, particularly if several levels are involved.[49]

A selective neck dissection (SND) is when one or more LN groups are preserved in addition to all non-lymphatic structures. This approach is used to electively treat cN0 patients.[44] The lymphatic drainage from each subsite of the head and neck is relatively predictable in untreated patients with early-stage disease, and therefore this approach allows resection of targeted high-risk nodal groups with good oncological outcomes and less morbidity.[50, 51]

Sequelae and complications

Neck dissection, whether radical or selective, is not without morbidity, and in addition to standard surgical risks, has potential for several specific complications. Shoulder dysfunction is one of the most notable sequelae of neck dissection. It occurs most frequently in patients who have undergone RND where the spinal accessory nerve has been removed resulting in a denervated trapezius muscle, with associated pain, weakness and shoulder deformity.[52, 53] Several studies have shown that even when this nerve is preserved in SND, there is still clinically significant shoulder dysfunction, likely caused by stretch and trauma to the nerve during the dissection.[54, 55] Other less common complications of neck dissection include chylous fistula, air leaks into the neck, post-operative haemorrhage, and facial and cerebral oedema (when both IJVs are ligated).[56, 57] A rare, but highly lethal complication is carotid artery rupture, which happens when the artery is exposed in the presence of a salivary fistula.[58]

MANAGEMENT OF THE cN0 NECK

Limitations of clinical and radiological staging of the neck

Currently, the neck is staged by clinical palpation and a variety of different imaging techniques including US, CT, MRI and PET-CT, which are more sensitive than palpation alone.[14] Morphological and size criteria are used to make the diagnosis of cervical metastases on imaging but up to a third of nodal metastases in patients with OSCC are 'microscopic', meaning they are less than 2mm in size.[59] This is smaller than the 3mm

detection threshold of imaging, which limits the sensitivity of radiological staging and results in an occult metastasis rate as high as 20-30%.[60, 61] Pooled data from meta-analyses evaluating the sensitivities and specificities of imaging modalities are summarised in Table 1.3.

Table 1.3 Summary of sensitivity and specificity of techniques for staging the neck.

Staging technique	Study	Sensitivity	Specificity
Physical examination	Merritt et al. [62]	74%	83%
US	van den Brekel et al.[63]	60%	77%
CT	Merritt et al. [62]	83%	83%
MRI	Wu et al. [64]	76%	86%
PET-CT	Sun et al.[65]	84%	96%

The rationale for elective neck dissection

Given the poor prognosis of cervical metastases and the limited sensitivity of currently available imaging techniques to detect them, a policy is in place to treat the neck even if it is cN0 to prevent occult disease becoming more advanced as it progresses to become clinically apparent.[44] This policy was based initially on an often-cited decision analysis model that suggested that elective neck dissection (END) is indicated when the chance of occult nodal disease exceeds 20%.[66] As management of the neck continues to evolve to become increasingly selective, the use of END for all cN0 patients has become an area of debate. Aside from the fact that the historical decision analysis model is now out-dated,

the main issue with this strategy is that it results in 60-70% of patients receiving unnecessary treatment with associated morbidity.[67]

The evidence behind watchful waiting versus elective neck dissection

On the other side of the treatment spectrum, 'watchful waiting' is a management option for cN0 patients that avoids "over-treatment" by carefully monitoring the neck over time with ultrasound-guided fine-needle aspiration cytology.[68, 69] Definitive treatment is given to patients who develop clinically apparent disease, which usually arises within 1-2 years.[70]

There have been numerous retrospective and prospective studies as well as 5 randomised controlled trials (RCT)s that have compared watchful waiting with END.[71-75] In a meta-analysis by Fasunla et al., pooled data from 283 patients from the earliest four RCTs showed that END reduced the risk of disease-specific death compared to observation.[60] In the most recent, and largest of the RCT, D'Cruz et al. showed that in 596 patients at 3-years, END resulted in a significantly improved rate of overall survival of 80% (95% CI: 74.1 - 85.8) compared with therapeutic neck dissection following watchful waiting, which was 67.5% (95%CI: 0.45 - 0.92) (P = .01).[75] Consistent with the results of the meta-analysis, this study showed that END had a higher rate of disease-free survival (69.5% versus 45.9%, P< .001). Rates of adverse events were 6.6% and 3.6% in the END group and therapeutic neck dissection group respectively.

Sentinel lymph node biopsy

Sentinel lymph node biopsy (SLNB) offers a personalised minimally invasive staging strategy for patients with cN0 disease that is more precise than all currently available imaging techniques and less invasive than END.[67] By reliably selecting targeted LNs that potentially contain metastases for biopsy and detailed histopathological assessment, this procedure can accurately detect occult micrometastatic disease, thereby directing which patients will benefit from neck dissection, versus those who can be safely managed with watchful waiting. Many studies have confirmed its diagnostic accuracy and that it is an oncologically sound approach. Furthermore, it is listed in the NCCN guidelines as viable alternative to END for patients with cN0 disease.[43] Despite this, it is not a routinely practiced procedure for a number of reasons which are explored in detail in Chapter 2.

ADJUVANT TREATMENT

Post-operative radiotherapy (PORT) to the neck, with or without chemotherapy, is recommended for patients at risk of recurrence based on the size and number of nodal metastases and the presence of ENE.[76] Specifically, PORT should be administered to patients with pathological N2 or N3 disease.[44] Adjuvant chemotherapy should be offered to any patient where there is ENE in any positive node, regardless of the extent, or number and size of nodes.[44]

CHAPTER 2: A GAP ANALYSIS – COMPONENTS OF THE TREATMENT MODEL CRITICALLY REQUIRING INNOVATION

MARGIN ASSESSMENT DURING PRIMARY TUMOUR RESECTION

THE RATIONALE FOR SURGERY WITH ADEQUATE MARGINS

The goal of surgical treatment of solid tumours is to completely eradicate cancer by removing both gross and microscopic disease during resection.[77] In order to avoid a positive surgical margin where cancer cells are present at the resection edge, surgical resection needs to incorporate a cuff of normal tissue past the invasive tumour front, which theoretically will include any microscopic cancer not able to be detected by the surgeon. For head and neck cancer, this concept was first put forth in 1978 by looser et al., who demonstrated that microscopically positive and "close" margins carry a significantly increased risk of local recurrence.[78] In the decades that have followed, this association has become well-established in the literature providing the basis for current head and neck surgical practice.[79-83] However the amount of normal tissue that needs to be removed to ensure a clear margin is not currently well understood. Importantly in the head and neck, there is a balance between adequate cancer resection and the functional consequences of this, specifically in relation to speech and swallowing.

A recent meta-analysis examining local recurrence rates in 539 patients with OSCC following primary tumour resection without adjuvant therapy demonstrated that margins less than 5mm have significantly higher local recurrence rates than margins 5mm or greater.[84] In this study, recurrence rates were pooled to show a 21% absolute risk reduction in local recurrence with margins more than 5mm (95% CI 12-30%, $P < .00001$) (Figure 2.1).[84]

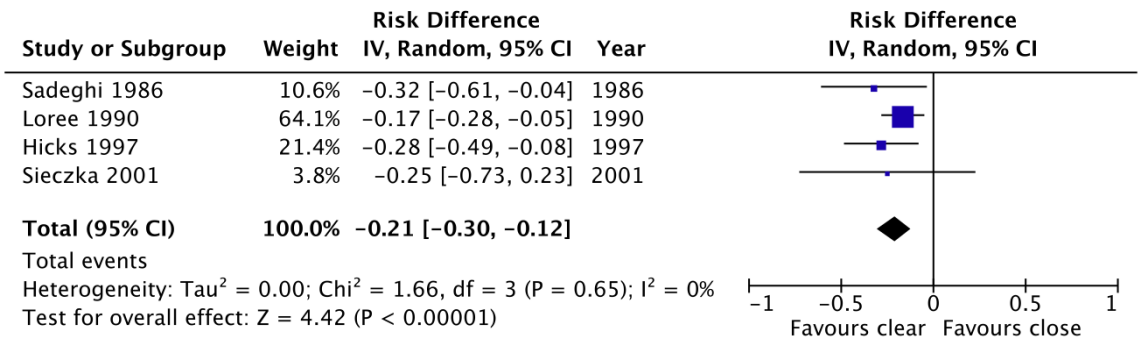

Figure 2.1 Risk difference for random effects models examining the association between pathological margin risk and local recurrence.

(IV: inverse variance) *From Anderson et al.*[84]

DEFINING AN "ADEQUATE" MARGIN – WHAT IS THE EVIDENCE AND WHAT ARE THE GUIDELINES?

Despite an overwhelming consensus in the literature that failure to eradicate tumour at the primary site is associated with increased local recurrence, there is no universal and evidence-based definition of an "adequate" resection margin.[83] Five millimetres is the most commonly used cut-off to define a negative margin in head and neck cancer, however definitions range in the literature from > 0mm (i.e. no ink on tumour) to >7mm.[85, 86] Positive margins are generally defined as tumour at the inked margin, or tumour <1mm from the normal tissue edge, but again, larger margin distances have been reported as positive or inadequate.[87, 88] In addition there is disagreement on what margin status should be designated to cases with dysplasia and CIS at the resection margin.[89, 90]

The lack of standardisation in margin definition stems from an underlying lack of clarity in our understanding of cancer biology and the current research evidence. Studies looking at the relationship between margin size and recurrence have demonstrated broad variability in outcomes, and in some instances conflicting results, where patients with adequate resection margins have had poorer outcomes than patients with inadequate margins.[91-94]

There are several explanations for this. Firstly, several studies have included heterogenous patient populations, by grouping larynx and pharynx cancer patients together with oral cavity cancer patients under the universal umbrella of HNSCC.[95, 96] These will almost certainly introduce confounding results due to clinically significant differences in cancer spread at different head and neck sites, treatment paradigms for tumours at different locations and their differing responses to adjuvant therapy.[97] Even within the oral cavity, studies examining SCC of the buccal mucosa alone have demonstrated higher recurrence rates for both involved and uninvolved margins, which could be related to tumour biology, differences in surgical techniques required to resect these tumours, or difficulties in pathological analysis of tumours at this site compared to other subsites.[98-100] Secondly, studies combining patients who receive PORT with those who don't as part of the analysis will confound the relationship between margin status and outcome because PORT will inherently reduce the risk of recurrence.[101-103] Thirdly, there is often a lack of adjustment for tumour related variables such as size, depth of invasion, differentiation, invasive pattern, and histological features such as PNI and LVI, which are known to affect aggressiveness of disease, so that even with an "adequate" margin, there may still be an inherent increased risk of recurrence.[102-105] Finally, some studies have used survival or loco-regional recurrence as primary outcome measures,

however primary surgery is best assessed by its ability to predict local recurrence.[103, 106, 107] Regional or distant metastases are more likely to be due to metastases in-transit at time of, or prior to surgery, and survival is influenced by many factors and is difficult to interpret as a marker for margin adequacy.[108]

Despite the difficulty in comparing margins outcomes to provide a strong evidence-based definition, the NCCN and the International Collaboration on Cancer Reporting (ICCR) have provided level 2A guidelines as summarised in Table 2.1.[85, 109]

Table 2.1 Summary of margin definitions as recommended in the NCCN and ICCR guidelines.

	NCCN	**ICCR**
Clear	≥ 5mm from invasive tumour	≥ 5mm from invasive tumour
Close	< 5mm from invasive tumour	1 – 5mm from invasive tumour
Positive	invasive carcinoma or carcinoma in situ at a margin	< 1mm from invasive tumour

A BRIEF OVERVIEW OF MARGIN ASSESSMENT AT PATHOLOGY

When a tumour is resected and sent to pathology for analysis, it undergoes a standard sequence of steps as part of its overall evaluation in order for the pathologist to generate a comprehensive synoptic report that is used for prognostication and to guide further management.

Gross specimen review

Initially following resection, the specimen undergoes a gross review at pathology, which involves visual examination, palpation and tissue sectioning to give a global evaluation of the tumour extent in relationship to anatomic structure and three-dimensional (3D) margins. This process is aided by specimen integrity, orientation of the specimen by the surgeon with identification of critical structures or landmarks as appropriate, and also indicating specific areas concern.[89]

Gross assessment of a specimen ranges in difficulty depending on the specimen and resection type and this typically corelates with the difficulty of the surgical resection.[89] Mucosal resections without secondary structures, such as partial glossectomy and wide local excision (WLE) of buccal tumours are generally lower complexity specimens. Orientation is straight-forward, with marking sutures usually employed to designate one or two points on the specimen (i.e. anterior, and lateral). At pathology, these specimen types can easily be serial sectioned into "bread loafs" from anterior to posterior, allowing for several margins to be evaluated in a perpendicular fashion (Figure X). To determine the closest margin on gross assessment, the pathologist inspects for tissue changes caused by tumour infiltration and palpates for corresponding firmness to aid selection of tissue sections for detailed microscopic evaluation. More complex specimens are typically composite resections that involve soft tissue and bone and orientation by the surgeon for these cases is critical (Figure 2.3). Bone can be removed from the en bloc specimen to facilitate assessment of the soft tissue margins.

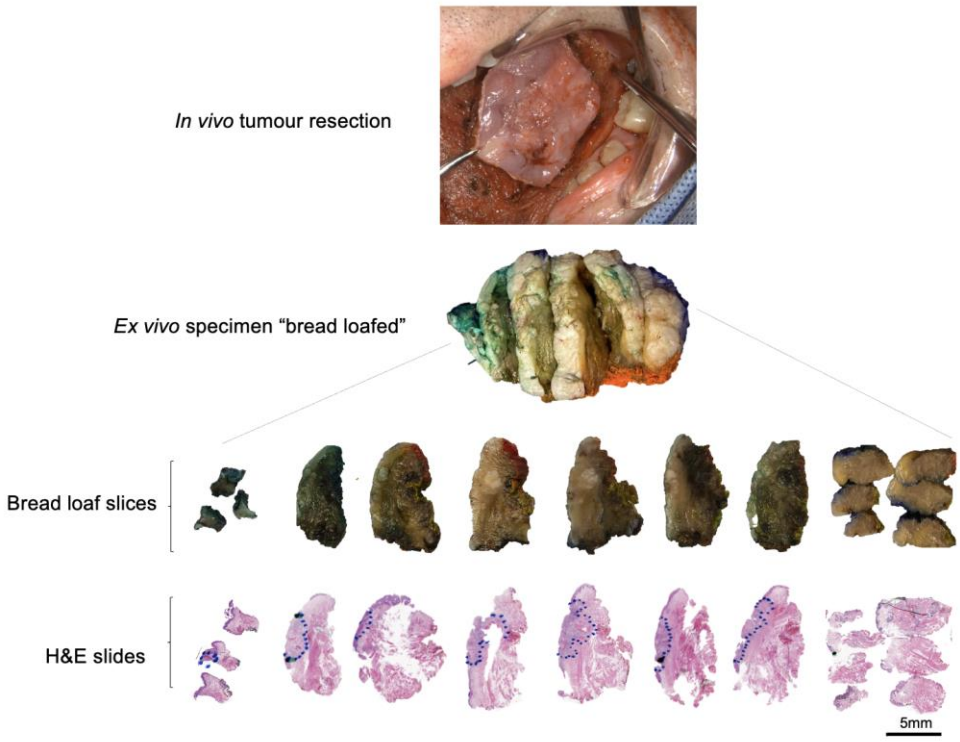

Figure 2.2 "Bread loaf" pathological analysis in a resected tongue specimen.

In the H&E slides, the blue-dotted line outlines tumour.

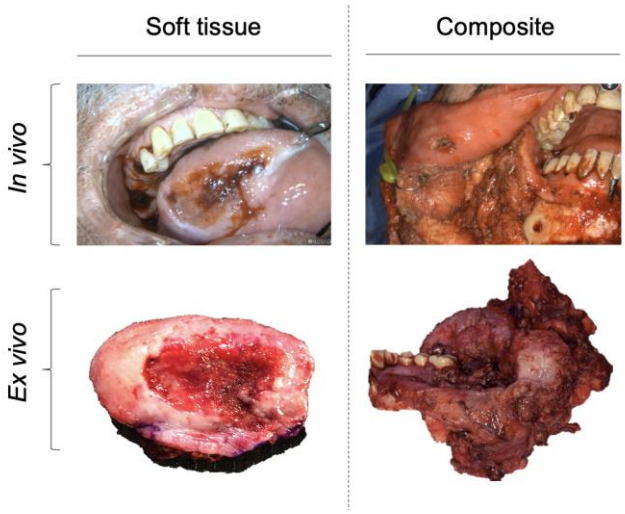

Figure 2.3 Comparison of soft tissue versus composite tissue resections in the oral cavity.

Microscopic margin assessment

Following gross evaluation, the specimen undergoes microscopic margin evaluation, and in order to this, tissue is obtained from the en bloc resection either "en face", or via a "perpendicular" section. The important clinical distinction between these methods is the difference in information that can be obtained by each.

En face tissue is flat peripheral tissue sections, which are taken parallel to the margin of interest. The entire microscopic slide represents the true margin, with the benefit of allowing for a greater surface area to be assessed. This comes with the limitation that margin distance between normal tissue and invasive tumour cannot be determined, so essentially microscopic examination of this tissue provides a binary result as to whether it is positive or negative for tumour cells.

Perpendicular margins represent a cross section through tumour towards the resection edge.

This allows measurements from the tumour cells to the resection margins in millimetres by simply using a standard ruler. A grade for margin interpretation can then be given (i.e. positive / close / negative).

Bone assessment

Histological assessment of bone requires the additional steps of decalcification and processing, and therefore full tissue sections of bone cannot be performed intraoperatively.[89] If there is a requirement for intraoperative assessment of bone

margins, the cut bone edge, or a perpendicular section through the bone at the area of concern can be grossly examined for abnormal finings such as softness or fibroses. Alternatively, scrapings can be taken from the bone resection edge and sent for histology.

Tissue shrinkage

Tissue shrinkage is an issue that must be raised as part of a margin resection discussion. Tissues are not rigid, and there is animal and human evidence to show how surgical resection can result in contraction of tissue and expansion of a wound-bed.[110, 111] In a human study, head and neck cancer patients were shown to have mucosal contraction in specimens following resection in the order of 20-25%.[111] Furthermore, formalin fixation and paraffin embedding of specimens has been well-established to add to the shrinkage in an order of up to 10%.[79, 112, 113] To account for this, some surgeons opt to include up to 25% more tissue in their resection margin and urge pathologists to consider this when providing the final pathology report.[83, 113]

INTRAOPERATIVE MARGIN ANALYSIS

In the oral cavity, an adequate tumour resection is often difficult to achieve because of the complex anatomy, the need to limit tissue resection to preserve function following surgery and considerations of facial cosmesis. During surgery, the surgeon relies only on visualisation with their eyes and palpation with their fingers for real-time margin assessment and studies have demonstrated that this results in adequate tumour clearance

in only 15% of cases. Given that positive margins are well established to confer a poor prognosis, the NCCN guidelines list positive margins as an indication for re-resection.[43]

Intra operative frozen section analysis (FSA) provides a rapid intraoperative pathology consultation that has long been used to guide re-resection of positive margins in a single operative setting, and of all the surgical disciplines, it is most often used in head and neck surgery.[114, 115] Tissue obtained by the surgeon intraoperatively at an area of concern for close or positive tumour involvement is sent fresh to the pathologist for analysis. At pathology, it is immediately frozen in a cryostat machine, then thinly sliced with a razor, fixed to a glass slide and stained for analysis under a microscope. Following examination, typically by an experienced pathologist, results are communicated back to the surgeon in order to guide further resection as deemed clinically appropriate.[116, 117]

Consistent with the general trends in surgical oncology, there are two main approaches to obtain margins for FSA in patients with OSCC; (1) tumour-bed driven, and (2) specimen driven.[114] In a tumour-bed, or 'defect driven' scenario, the surgeon performs a resection and then obtains several tissue samples from the tumour wound bed. This is typically not guided by assessment of the specimen itself and does not involve collaboration with or decision making from the pathologist (Figure 2.4A).[118] In the specimen driven approach the specimen is examined en bloc by the surgeon and/or the pathologist and margins are sampled from the specimen itself (Figure 2.4B).[118]

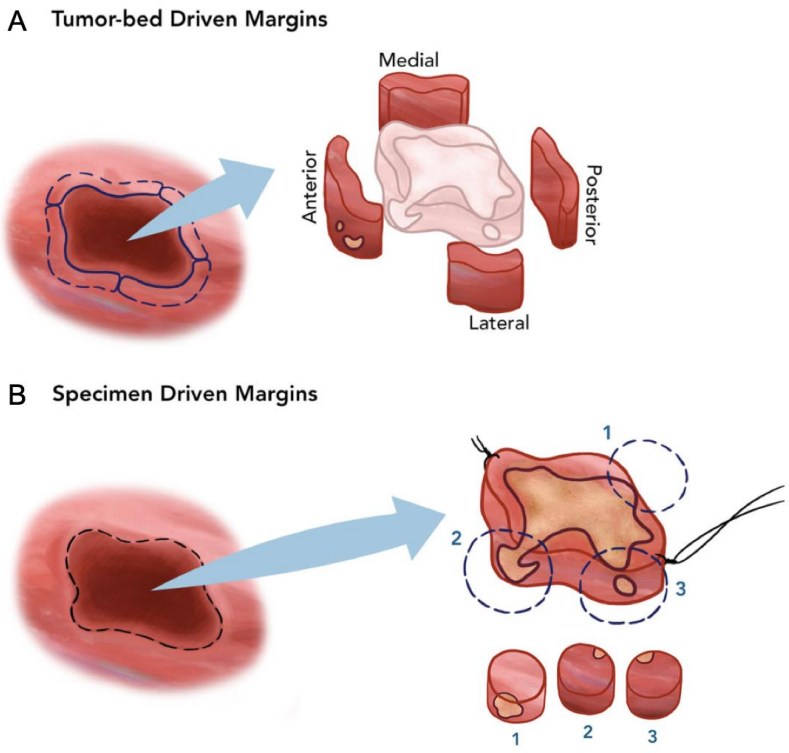

Figure 2.4 Summary of the two surgeon-driven margin sampling approaches.

A. Tumour-bed driven and B. Specimen-driven. *Modified from Kain et al.*[118]

EXAMINING THE EVIDENCE BEHIND INTRAOPERATIVE FROZEN SECTION GUIDED RE-RESECTION

Oncological outcomes following frozen section guided re-resection

Despite the widespread use of FSA for intraoperative margins analysis, there is a growing body of evidence to show that initially positive (R1) margins during surgery (also referred to as "microscopic tumour cut-through"), lead to worse outcomes than initially negative (R0) margins regardless of whether re-resection is performed.[87, 119-121] Additionally,

some studies have demonstrated that patients undergoing simple gross examination of the resection specimen have similar clear margin rates and outcomes compared to those undergoing FSA, calling into question the value of frozen section guided re-resection.[122, 123]

Bulbul et al. conducted a meta-analysis to evaluate the local recurrence-free survival rate in early OSCC patients who a) had initially clear margins during surgery, versus those who underwent intraoperative FSA with a positive/close margin and then were either b) cleared with further resection (i.e. from R1 to R0), or c) not cleared (i.e. remained R1).[124] Eight studies met the inclusion criteria providing data from 1427 patients, of which 952 (67%) were R0, 327 (23%) had R1 to R0 resection, and 149 (10%) had R1 resection. Only primary OSCC patients, previously untreated, were included and margins were defined as negative if they were > 5mm on initial resection. The study was unable to control for a number of important confounding factors including adjuvant radiation, but nonetheless, pooled data showed that patients in the R1 to R0 groups had worse local recurrence free survival than patients who were in the initially R0 group (HR = 2.897, P < .001). Patients in the R1 group were also found to have worse LRFS compared to the R0 group (HR = 3.795, P < .001), and when compared to the final R1 group, the initially R1 to final R0 only showed a trend toward better loco-regional disease free survival (LRFS).

While this meta-analysis clearly demonstrates that FSA guided re-resection does not correlate with improved oncological outcomes, the reasons for this are open to interpretation. It is possible that inaccuracies with frozen section sampling technique in conjunction with the margin revision strategy are responsible for poor local control. On the other hand, it is feasible that positive margins are a marker of aggressive disease and

are likely to be associated with a poor prognosis, regardless of whether FSA is guiding re-resection accurately.

The effect of sampling technique on outcomes – comparing tumour-bed versus specimen driven sampling

Several studies have demonstrated that margin sampling via a tumour-bed driven approach is associated with worse outcomes than via a specimen driven approach.[125-128] This is because in a tumour-bed approach, samples are usually taken en face and therefore lack measurement data. Furthermore, sampling is typically not based on a comprehensive or thorough assessment of the actual tumour specimen itself, and data obtained gives information on only one point on the entire 3D tumour surface. Following from this, when samples are small in size, pathologists become concerned that findings do not reflect the "true" final margin.[129]

In a retrospective multi-centre study, data from 280 patients demonstrated that tumour-bed sampling is associated with worse local control during glossectomy.[127] In this study, patients were grouped into 3 cohorts based on (1) those who did not have margins sampled, and those who had margins sampled via either a (2) specimen driven, or (3) tumour-bed driven approach. The frequency of positive margins was lowest in those patients who did not have margins sampled, compared with those that did ($P < .001$). When margins were sampled from the specimen, the tumour status of the margins (positive or negative), did corelate with local recurrence ($P = .007$), while this was not the case when margins were sampled from the tumour-bed. Furthermore, tumour-bed

driven margin assessment was only 24% sensitive (95% CI: 16-34%) and 92% specific (95% CI: 85-97%).

In a prospective RCT of 71 patients with OSCC, specimen driven margin assessment led to a significant improvement in the rate of negative margins at final pathology.[128] Patients were randomised to have margins assessed intraoperatively, with re-resection as appropriate, by either a tumour-bed driven approach (n = 20), or a specimen driven approach (n = 51). FSA revealed positive/close margins that led to re-resection in 43% of patients in the specimen driven arm, compared to 10% of patients in the tumour-bed driven arm (p = .01). At final pathology the negative margin rate was 84% in the specimen-driven arm compared to 55% in the tumour-bed driven arm (p = .02). While the authors did not evaluate local-recurrence rate, which is probably a more clinically relevant outcome measure, they showed that 38% of patients in the specimen-driven arm, compared with 10% in the tumour-bed driven arm, avoided escalation of adjuvant treatment because of extended surgical re-resection.

The challenge of relocating areas for revision following positive sampled margins

The imprecision of relocating intraoperative sites is likely to be a factor contributing to the increased risk of recurrence in initially R1 to R0 resections.[83, 89] This challenge was first highlighted in a study by Scholl et al. where in 73% of patients who had initially positive margins, when further resection was performed, the repeat margin did not contain tumour.[130] This issue was more recently confirmed in a study where a surgeon was asked to identify the sites of proposed sampling in 14 consecutive cases and then to relocate them after 5 minutes. In 71 examined soft tissue regions of interest, the mean error of

relocating the sample was 9mm at the mucosal margin and 12mm for the deep margin, with the error exceeding 1cm in 32% of cases.[131] To improve relocation of areas in the tumour-bed for re-resection following FSA, another study used numbered tags placed on both sides of the resection in a pair-wise manner, such that after resection, one tag of each pair remained on the specimen and the other remained on the wound bed. Utility of this method in 80 OSCC resections was examined and in all 31 resections where an initially inadequate margin was encountered, accurate re-resection was achieved with the paired tagging method.[132]

Cost considerations

Given the widespread use of FSA, cost and resource requirements related to this procedure deserve attention. From a resource allocation perspective, it is worth remembering that frozen sections require multiple personnel and are considered high priority, which may cause a delay in processing other routine-priority specimens.[129] Cost-benefit was analysed in a retrospective review of 80 consecutive HNSCC patients in whom 420 intraoperative FSA margins were taken and where only 5% of patients benefitted from the FSA guided re-resection. 40% of patients with positive margins on final pathology, and 100% of patients with close margins on final pathology were not detected by intraoperative FSA. The estimated cost of FSA averaged $3,123 per patient, and given the small minority who actually benefitted from it, the resultant cost: benefit ratio was calculated to be 20:1.[133]

Current practice trends

In the last two decades there have been two cross-sectional membership surveys conducted through the AHNS that have evaluated margin practises amongst head and neck surgeons.[86, 90] The first study was conducted in 2005 by Meier et al. and examined margin practises in all head and neck subsites, whereas the second conducted in 2020 by Bulbul et al.[90], focussed on the oral cavity. Examining these studies together provides an insight into head and neck practice trends across this time frame.

Over the 15-year interval between studies it appears that FSA continues to be standard of care for OSCC resections, with 99% of respondents in Meier's study and 97% of respondents in Bulbul's study reporting using it in their daily practise to ensure complete tumour removal. There seems to be a shift from the tumour-bed driven approach to the specimen driven approach (76% used a tumour-bed approach previously compared to 45% now). Despite growing evidence to show otherwise,[124] eighty-one percent of surgeons in Bulbul's study considered a frozen section guided re-resection of a positive margin to negative, an overall negative margin.[90]

SUMMARY OF CHALLENGES

There are many challenges relating to margin management in head and neck surgery, but the key take-home points are summarised below:

1. Adequacy of margins is currently guided by somewhat arbitrary cut-offs and the inaccuracies of a surgeon's macroscopic assessment of tumour. Ideally, given the heterogeneity of evidence directing recommendations, surgeons should realistically tailor resection margins based on an understanding of patient and tumour factors. This is a difficult and inaccurate science.
2. How margins are sampled affects outcomes, with evidence demonstrating that a specimen driven approach is superior to sampling from the wound bed.
3. While FSA is commonly used to guide margin assessment intraoperatively, there is a false belief that re-resection of an R1 tumour will automatically result in a clear margin. Evidence indicates that margin sampling is prone to error and that relocation of positive margins following FSA is highly imprecise. This is consistent with evidence that shows that initial tumour cut through is associated with an increased rate of local recurrence regardless if FSA guided resection is performed with clear margins.

SENTINEL LYMPH NODE BIOPSY FOR MANGEMENT OF THE cN0 NECK

THE SENTINEL LYMPH NODE CONCEPT

The sentinel lymph node (SLN) can be conceptually defined as the first LN to receive lymphatic drainage from a primary tumour.[134] This is of significant clinical relevance because human cancers of epithelial nature metastasize via the lymphatics in an ordered fashion, and therefore the detection, surgical excision and histopathological assessment of the first-draining LN, as part of the SLNB procedure, provides assessment of the overall metastatic status of the regional nodal basin.[135] If the SLN is negative for cancer, an assumption that tumour has yet to metastasise from its primary site to the regional lymphatics can be made, which affects management, because in this scenario, a patient can be spared a lymphadenectomy procedure and its associated surgical morbidity. On the other hand, if the SLN is positive for cancer, a separately staged completion lymphadectomy procedure is required to treat the known metastatic disease. In this way, SLNB is a minimally invasive staging procedure that enables prognostication and guides definitive treatment.

A HISTORICAL PERSPECTIVE

The idea of a 'sentinel lymph node' was first reported in 1960 by Gould during a parotidectomy. A normal-appearing LN was sent for intraoperative frozen section analysis and when it was found to harbour tumour metastases a subsequent full neck-

dissection was performed.[136] Cabanas expanded upon this idea in 1977 and provided the early body of evidence that tumour cells spread in an organised manner and in a predetermined anatomic pathway. During penile cancer surgery he reported that the SLN was the LN that emerged directly from the primary tumour. He recommended that the SLN be excised and assessed at pathology, and if found positive, the primary tumour resection should be extended to include radical removal of the regional LNs.[137]

In 1992 SLNB became incorporated into routine oncological practice. Morton described the process of 'dual mapping' of the SLN, where during melanoma surgery, a dye was injected around the lesion, followed by the injection of a radioisotope and cutaneous lymphoscintigraphy to follow its spread.[138] The SLN was identified pre-operatively on imaging, and then intraoperative visual identification of dye uptake within the node was used to provide additional confirmation. Dual mapping procedures were subsequently validated in breast cancers and showed an increase in sensitivity and detection rate, which lead to the opening of several RCTs that ultimately confirmed the oncological safety of the procedure.[139-141]

Now SLNB is the standard of care for breast cancer and melanoma staging and is used in staging the full spectrum of surgically treated solid malignancies including upper gastrointestinal, thoracic, colorectal, urological and gynaecological cancers.[142-147]

THE EVOLUTION OF HEAD AND NECK SENTINEL LYMPH NODE BIOPSY

SLNB wasn't performed for head and neck cancer until 1996, when it was first described successfully using a gamma probe for guidance in a patient with supraglottic cancer.[148] Following this, several groups attempted variations in the SLNB procedure with limited success, citing challenges unique to the head and neck as possible explanations for failure.[149]

In 1998, Pitman et al. used a peritumoural injection of isosulfan blue dye only to map SLNs in both cN0 and cN+ HNSCC patients. In all 9 patients included, no dye was visualised intraoperatively in the lymphatics. The authors reported that this was likely due to the rapid transit time of the dye resulting in wash-out from the LNs in the time it took to raised flaps and dissect down to the nodes within the deep fascial tissues planes of the neck.[150] They suggested that given the ambiguity of LN drainage patterns in mucosal HNSCC, including the potential for bilateral drainage pathways and drainage to multiple SLNs, future procedures should incorporate lymphoscintigraphy in conjunction with blue dye.

In the same year Koch et al. reported on the results of SLNB following peritumoural injection of 99mTc-labelled sulphur colloid and dynamic lymphoscintigraphy.[151] Here SLNs were identified in only 2 of 5 patients, with the authors reporting multiple issues with the approach, including difficulties associated with intramucosal injection technique, the close spatial relationship between the SLN and the injection site and the potential for bulky metastatic tumour deposits within LNs to obstruct and redirect tracer flow.

In 1999, Shoaib et al evaluated a 'triple method' of SLNB consisting of preoperative lymphoscintigraphy followed by intraoperative localisation with a gamma probe and blue dye. These authors demonstrated improved success with this technique when compared to blue dye alone.[152]

After the success of Shoaib et al, many others began evaluating SLNB in the head and neck and in the light of growing interest in the technique, in 2001, the first international conference on SLNB in mucosal head and neck cancer was held in Glasgow, United Kingdom. Here, 22 centres contributed staging data from their early SLNB experience, demonstrating improved sensitivity with increased case-volume.[153] At the second conference in 2003, in Zurich, Switzerland, 20 centres presented their data and a consensus was reached that SLNB for early OSCC and oropharyngeal SCC was sufficiently valid and that the use of the triple method of radiotracer, lymphoscintigraphy, and a hand-held gamma probe was the minimum requirement for lymphatic mapping.[154]

In the decade that followed, several large prospective observational trials demonstrated validity of this technique,[155-157] and in 2013, SLNB was incorporated into the NCCN guidelines as an alternative to END for the identification of occult metastases in patients with T1-2 N0 oral cancer, with advantages cited as "decreased morbidity and improved cosmetic outcomes".[158]

CURRENT BEST PRACTICE GUIDELINES

Although simple in theory, SLNB in practice is highly complex. It entails a sequence of specialised procedures requiring expert input, each with scope for variation in technique and interpretation. The procedure can be broadly broken down into the following three components: 1. pre-operative imaging to identify SLNs, 2. Surgery to intraoperatively localise and then harvest SLNs, and 3. pathological analysis of harvested SLNs to guide further management. Several guidelines and protocols based on expert consensus and best evidence have been developed providing recommendations for each element of the procedure.[159-162]

INDICATIONS AND PATIENT SELECTION

Patients with biopsy proven OSCC who have clinically and radiologically negative neck disease can be considered for SLNB for the following three indications:

1. For staging of the ipsilateral cN0 neck
2. To assess bilateral metastatic spread in a cN0 neck, where the primary tumour crosses midline
3. To assess metastatic spread to a contralateral cN0 neck, in primary tumours approaching midline where the ipsilateral neck is positive for nodal disease, to guide the decision as to whether the patient should undergo bilateral or ipsilateral neck dissection.[160]

Generally, the final consensus on staging of the patient's neck and indication for SLNB should be agreed upon by the head and neck multi-disciplinary team prior to surgery.

SLNB is contraindicated for staging the ipsilateral neck where there is clinically positive neck disease, because gross lymphatic involvement can lead to distortion of the normal lymphatic architecture, leading to aberrant drainage patterns and false negative results.[163] Paradoxically however, SLNB can be offered to patients who have had a previously treated neck, as it can map true lymphatic drainage in these cases where there may be altered lymphatic pathways leading to the metastatic deposition of tumour in unexpected locations.[164] While there is no definite cut-off criteria for tumour T-stage, generally SLNB is reserved for T1-T2 tumours, but ultimately the important clinical indication is whether the tumour can be reliably resected with adequate margins and the defect repaired locally without requiring access to the neck.

PRE-OPERATIVE IMAGING

Radiotracer injection

In order to map the lymphatic drainage pathway from the primary tumour to the regional nodal basin, a radioisotope conjugated with a colloid is injected around the tumour and its lymphatic flow is imaged with lymphoscintigraphy. There are many radiopharmaceuticals that can be used for this purpose, and in general terms, an ideal tracer should combine rapid and predictable transport toward the SLN with persistent retention within the node.[165] These properties are highly dependent upon colloid particle size and stability, as the radiopharmaceutical has to be uniform in particle size distribution and small enough to translocate from the interstitial injection site into the lymphatic

channels, but large enough to delay transit time within the lymphatics.[166] Addition of molecules to target reticuloendothelial cell receptors can enhance uptake and binding of particles in SLNs, such as the use of mannose moieties to target CD206 mannose-binding receptors in macrophages as deployed by the recently US Food and Drug Administration (FDA)-approved radiopharmaceutical 99mTc-Tilmanoscept.[167] Several different types of radiopharmaceuticals available for commercial use and their size dimensions are listed in Table 2.2.[159]

Table 2.2 Types of 99mTc-lableled radiotracers and their size characteristics.

Agent	Particle size (nm)	
	Maximum	Mean
Sulphur colloid (Sulphur Colloid®)	350–5000 (see text)	100–220 (filtered)
Antimony trisulphide (Lymph Flo®)	80	3–30
Sulphide nanocolloid (Lymphoscint®)	80	10–50
Nanocolloidal albumin (Nanocoll® and NanoTOP®)	100	5–80
Rhenium sulphide nanocolloid (Nanocis®)	500	50–200
ICG-99mTc-Nanocolloid	100	5–80
Tin colloid	800	30–250
Labelled dextran	800	10–400
Hydroxyethyl starch	1000	100–1000
Stannous phytate	1200	200–400
Tilmanocept (Lymphoseek®)	About 7 (equivalence)	About 7 (equivalence)

From Pfister et al.[159]

Injection is typically performed by a nuclear physician or head and neck surgeon on the eve or morning of surgery. The total injected activity depends on individual institution protocols and ranges from 15MBq to 120MBq, where higher doses are typically used when the window between injection and procedure is increased. Lidocaine hydrochloride spray or gel, or a high lingual nerve block, are recommended for local anaesthesia prior

to injection. Radiotracer is administered with 4 submucosal injections at 3, 6, 9 and 12 o'clock and should be delivered 0.1- 0.5cm from the macroscopic tumour margin (Figure 2.5), with a total injection volume of roughly 0.4 -1.0ml in 2-4 aliquots.

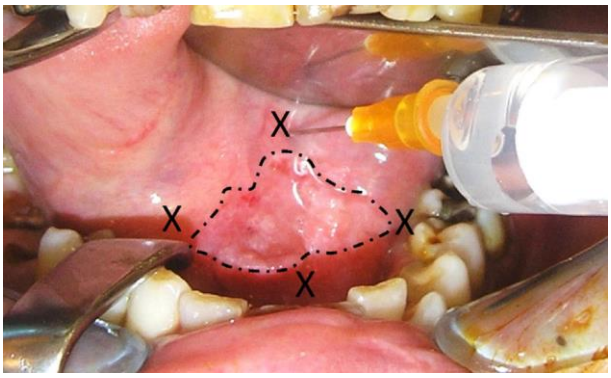

Figure 2.5 Injection of radiotracer in a quadrant around an oral floor of mouth tumour.

From Garrel et al.[162]

Imaging with lymphoscintigraphy and SPECT-CT

Lymphoscintigraphy is the nuclear medicine technique used to visualise the spread of radioactivity from the site of injection of radiopharmaceutical to the fist LN relay known as the "hotspot". Imaging is achieved by acquiring planar and dynamic images with a gamma camera consisting of a large field-of-view detector, parallel-hole collimator and an associated appropriate energy setting.

A typical lymphoscintigraphy protocol involves the following sequence of image acquisition:

1. Dynamic images of the neck in the anterior view are acquired immediately after tracer injection to identify lymphatic vessels that drain to the tumour (performed within 5 minutes and encompassing at least the first 10-15 minutes post injection).
2. Early static views of the anterior and lateral neck are acquired to localise the LNs in three dimensions.
3. Late static views are acquired at 60-120 minutes post injection to identify LNs that receive a slower drainage from the tumour and to distinguish between the surgically relevant SLNs and the irrelevant higher echelon LNs.
4. The skin is marked by the nuclear physician based on the acquired images to guide the surgeon. This can be done with a collimated hand held-gamma probe as an adjunct for transcutaneous confirmation. Ideally, the skin marking should be made with the head extended and rotated laterally to replicate positioning during surgery.

Single photon emission computer tomography fused with CT (SPECT-CT) is thought to improve localisation and is recommended immediately after static images for anatomic localisation and depth evaluation, although there is no consensus agreement that it must be routinely used in addition to lymphoscintigraphy.[162]

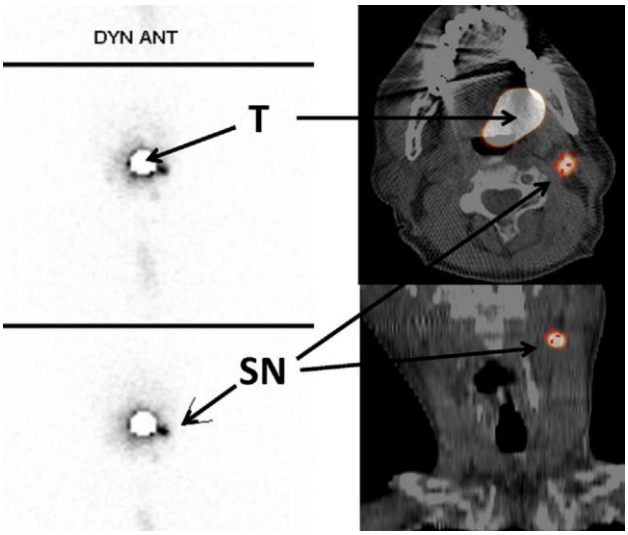

Figure 2.6 Lymphoscintigraphy in sentinel lymph node biopsy.

(Left) Dynamic lymphoscintigraphy images of the anterior neck in a patient with a FOM tumour taken following peri-tumoral radiotracer injection. (Right) Fusion of scintigraphy images with CT. (T: tumour, SN: sentinel lymph node). *From Garrel et al.*[162]

A synoptic imaging report is generated by the nuclear physician which should summarise:

a. Visualisation of lymphatic ducts
b. The order of appearance of LNs
c. Which LN basins are involved
d. The intensity of tracer uptake within LNs

On the basis of these factors, visualised radioactive LNs may be defined into one of three categories of probability for being the SLN[159, 168] as summarised in table 2.3.

Table 2.3 Defining SLN probability based on lymphoscintigraphic features.

SLN Probability	Lymphoscintigraphic features
Definite	a. LNs draining from the site of primary tumour are visualised with their own afferent lymphatic vessel, or b. A single radioactive LN in a LN basin is seen
Highly probable	a. LNs that appear between the injection site and a first draining LN, or b. A LN with increasing uptake that appears in other LN station c. Additional LNs found on the contralateral neck with SPECT-CT
Less probable	A second echelon LN in the neck that appears only in delayed planar images

SURGICAL PROCEDURE

Operative approach

The decision on which nodal hotspots to be explored during surgery should be based on communication between the surgeon and the nuclear medicine physician. Primary tumour excision and SLNB are performed during the same procedure. SLNB is typically more

complex and some surgeons will elect to perform it first, however, when the SLN is in close proximity to the primary tumour, it is recommended that the primary should be excised first to reduce the risk of shine through (although there is no evidence to show that this improves accuracy).[161]

Incisions should be made to provide optimal access to SLNs and only secondarily to facilitate completion neck dissection (CND). For aesthetic and functional benefit, they should be smaller than the required incision for END, and if multiple SLNs at different levels need to be accessed, depending on which levels need to be accessed, one single incision or multiple short ones can be used. New incisions may be required in CND and there is no evidence for recurrence within an incision.[160] Following incision, subplatysmal skin flaps are not routinely raised and upon reaching the SLN, resection should conserve the LN capsule.[162]

Localisation with optical tracers

Optical tracers, such as blue or fluorescent dyes, are delivered in the operating theatre at the beginning of the procedure in the same locations as used for lymphoscintigraphy. Following incision, they can aid detection of SLNs during dissection by providing visualisation of the targeted nodes or the lymphatic ducts leading to them. They are recommended by the consensus group, especially in FOM tumours, with evidence suggesting that the additional modality improves sensitivity.[169] While generally safe, their biggest downside is increased expense and resource requirement, particularly in the case of fluorescent dyes, which require a fluorescent camera in order to be visualised.

The Blue dyes available include patent blue V sodium, isosulfan, or methylene blue. Their small particle size results in rapid flow to SLNs with almost no retention, meaning they are susceptible to 'wash-out' by time of retrieval. They do have a 1% risk of allergy, including smaller risk of anaphylaxis and can stain the injection site, although there no evidence to suggest this adversely affects the surgeon's ability to identify tumour margins.[170]

Indocyanine green (ICG) does not stain the injection site under white light and provides a fluorescent signal that has a penetration depth of 1cm through overlying tissue, allowing localisation of the lymphatics and SLNs through tissue.[171] This is particularly significant in the FOM, where this property can overcome the unfavourable effect of shine through. While free ICG, like blue dye, is a small molecule with rapid flow and early wash-out, when mixed with 99mTc-Nanocoll, it forms a covalent bond, resulting in a multimodal tracer (ICG-99mTc- Nanocoll) that is retained within the SLNs for longer.[172]

Localisation with gamma probe

A gamma probe is a hand-held device that works as a radiation detector by providing a radioactivity count rate from identified gamma rays in counts per second.[173] It can take the form of either a crystal or solid-state device and has a surrounding metal shielding and collimation to give a restricted field of view. It is connected to a power supply and has an analyser unit which receives electrical signals from the radiation detector (Figure 2.7). The analyser provides a response related to the detected count rate by audible pitch or volume variation and visual display.

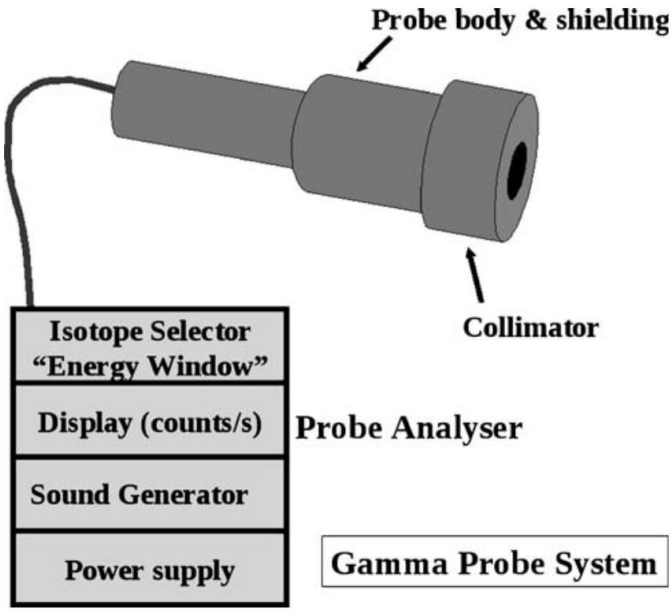

Figure 2.7 Schematic diagram demonstrating components of the gamma probe.

From Alkureishi et al.[160]

For a LN to be considered 'sentinel' when using measured radioactivity with the gamma probe, the count must be at least 10-times that of the background and more than 10% of the hottest node excised.[159] During surgery, all nodes in the area of the scintigraphic first echelon LN that are hot and coloured, only hot, or only coloured, should be harvested.[160, 174] The gamma count of each node must be confirmed *ex vivo* by the average reading taken over 10 seconds.

The resection site and other cervical regions are tested for any other significant residual radioactivity, in which case further LNs are taken. Other LNs from a hotspot, if suspicious in appearance but not meeting the above specified sentinel criteria, should be resected

and labelled as ‘non-sentinel’ and sent separately for routine analysis. If no SLN is detected, then an END should be performed.[160]

In FOM tumours, some authors recommend sampling level 1B, bilaterally in the case of midline tumours, to account for the chance of a missed SLN because of the shine through effect.[154] Stoeckli et al. described a reliable system for routine exploration and superselective resection of the preglandular triangle of level 1, whereby the fat-pad is detached from the mandible and then flipped down to allow use of the gamma probe from a craniocaudal direction while pointing the probe to the SLN (Figure 2.8).[175]

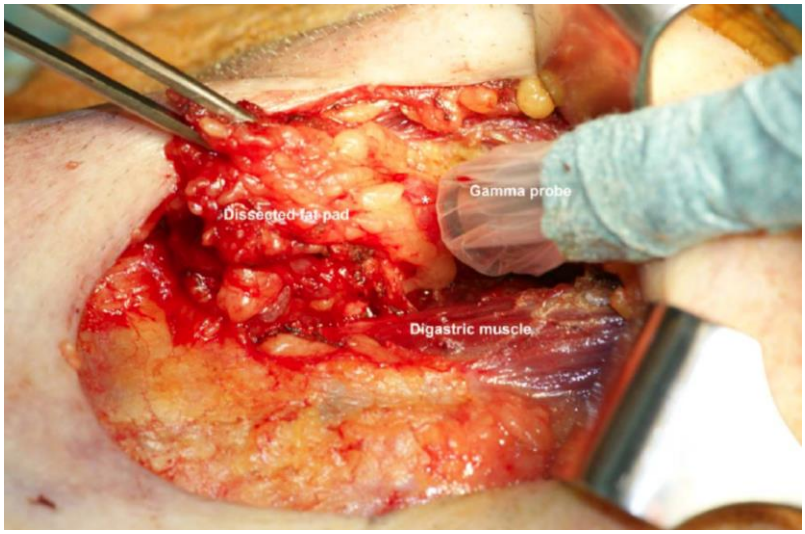

Figure 2.8 Pre-glandular level 1 fat-pad dissected and flipped down for exploration with a gamma probe in a patient with a FOM tumour.

From Stoeckli et al.[175]

When resected, all individual SLNs are ranked according to their tracer uptake, where SN1 represents the node with the highest activity, followed by SN2 and so on.[160] A number of studies have confirmed that 2-3 SLNs are normally removed per patient, and rarely, more than 5 are encountered, which typically occurs when there is bilateral drainage.[161, 176]

PATHOLOGICAL ANALYSIS

In order to detect microscopic metastatic disease (tumour deposits less than 2mm in size), dissected SLNs undergo a specialised pathological protocol, which involves routine sectioning followed by serial step-sectioning as summarised in the Table 2.4.[177, 178] A first reading of all slices is undertaken by the pathologist and, if negative, immunohistochemistry (IHC) is then performed using anti-pan cytokeratin AE1AE3 antibody every 150-250um.[160, 179] The classification of SN invasion is assed using the January 2003 Union for International Cancer Control (UICC) TNM classification as outlined in the Table 2.5.[180]

Table 2.4 Summary of typical pathology protocol for sentinel lymph nodes.

Sectioning:
• Nodes < 2mm process whole • Nodes 5mm bisected through hilum or longest pole, process both halves en face • Nodes > 5mm cut into 2mm slices longest pole to pole, process all slices en face
Step sectioning:
• Routine H&E, report metastatic disease if present. If negative, continue to next step • Mount six exact serial sections numbered separately 1-6 • Discard 150um (may be saved for research) • Mount further six numbered serial sections, continue through entire block • Stain all number 3 sections by H&E • Report metastatic disease. If negative or equivocal continue to next step • Immunohistochemistry on all number 2 sections using anti-pan cytokeratin AE1AE3 antibody • Examine for positivity • Compare positivity with H&E • Use remaining sections if required

Table 2.5 IUCC TNM classification of sentinel lymph node invasion.

Term	Definition
Isolated tumour cell (ITC)	Isolated tumour cells or small clusters within lymphatic sinus
Micrometastasis	LN infiltration by tumoral parenchyma of less than or equal to 2mm
Macrometastasis	LN infiltration by tumoral parenchyma > 2mm diameter

Frozen section is not used mandatorily during SLNB and has a sensitivity of only 10% when a single cross-section of a LN is examined.[181] Some surgeons employ FSA for large suspicious appearing LNs where the chance of a macroscopic metastasis is higher. In 10-15% of cases where a LN is found to be positive on intraoperative FSA, the procedure should then be converted to a selective neck dissection as part of the same procedure.[181]

FOLLOW-UP / FURTHER TREATMENT

Follow-up when SLNB is negative

If a SLNB procedure is negative, patients should be closely followed up with 3-monthly serial examination and US of the neck for the first 12-18 months. This is so that false-negative cases and recurrences can be detected early with improved chance for salvage and survival. The median time to recurrence is 9 months with no isolated neck recurrence seen after 2 years.[182]After this, patients re-join routine follow-up patterns for HNSCC patients.

Further treatment when SLNB is positive

If a SLNB is found to be positive, patients should undergo further treatment with CND in a timely fashion (withing 2-3 weeks).[161] The extent of CND should be planned as if the patient had presented with a clinically positive node.[161] If the positive node is on the contralateral neck only, then a careful review of the ipsilateral neck should be undertaken. CND is more challenging than END in a virgin neck with increased risk of complications.[183] Following CND, patients should be considered for adjuvant post-operative radiotherapy to the neck as per standard indications.[184]

THE EVIDENCE FOR SENTINEL LYMPH NODE BIOPSY IN ORAL SQUAMOUS CELL CARCINOMA

Diagnostic accuracy

Over the last decade there have been many studies evaluating the diagnostic accuracy of SLNB for OSCC. The majority of these have been retrospective observational cohort studies from single institutions. Two meta-analyses have examined pooled data from these studies to show that SLNB has a high diagnostic accuracy in patients with early stage OSCC.[185, 186]

In 2013, Govers et al. conducted a meta-analysis with 21 included studies comprising data from 847 patients.[185] 60% of the patients included had OSCC, although oropharyngeal SCC patients were also included, resulting in some clinical heterogeneity. The pooled data showed an overall sensitivity of 0.93 (95% CI 0.90 – 0.95), with negative predictive values ranging from 0.88 to 1. A subgroup analysis of 508 patients with OSCC demonstrated a pooled sensitivity of 0.92 (95% CI 0.86 – 0.95) (Figure 2.9).

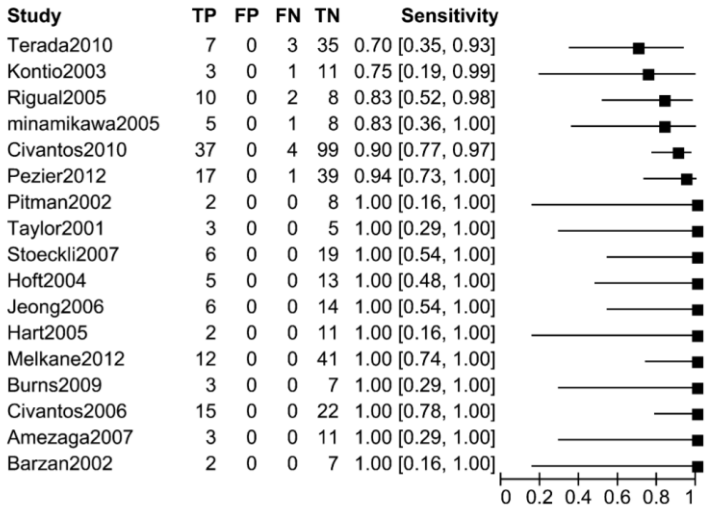

Figure 2.9 Forest plot of sentinel lymph node biopsy sensitivity in oral cavity cancer.

(TP: true positive, FP: false positive, FN: false negative, TN: true negative).

From the meta-analysis by Govers et al.[185]

More recently, in 2017, Liu et al. conducted a meta-analysis with 66 included studies comprising data from 3566 patients with T1-2 N0 OSCC only.[186] The pooled SLN identification rate was 96.3% (95% CI 0.85 – 0.89), the pooled negative predictive value (NPV) was 0.94 (95% CI 0.93-0.95) and the area under the curve (AUC) was 0.98 (95% CI 0.97 – 0.99). An overall summary receiver operating characteristic curve (ROC) showed an AUC of 0.98 (95% CI 0.97 – 0.99) (Figure 2.10).

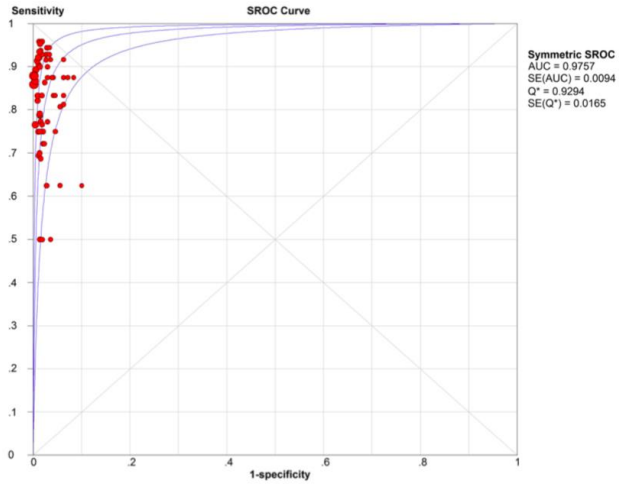

Figure 2.10 A summary receiver operating characteristic curve (ROC) of SLNB sensitivity in OSCC.

From the meta-analysis by Liu et al.[186]

Therapeutic outcomes

As well as being shown to be an accurate technique for staging the neck, SLNB has also been shown to be reliable and safe from an oncological perspective. This is perhaps best demonstrated by the 3-year results from the Sentinel European Node Trial (SENT), which thus far has been the largest prospective observational study examining therapeutic outcomes following SLNB for T1-T2 N0 OSCC.[182]

In this multi-centre trial, fourteen European centres recruited 415 patients, and SLNs were found in 99.5% cases, with an average of 3.2 SLNs harvested per patient. These were found to be positive for tumour metastases in 23% of cases. A false negative result occurred in 15/109 (14%) of patients, of whom 8 underwent salvage surgery and the overall sensitivity of SLNB int this study was 86% with a NPV of 95%. Follow-up at 3-

years demonstrated an overall survival (OS), disease free survival (DFS) and disease specific survival (DSS) of 88%, 92% and 94% respectively. The SLN status (P = .003) and number of positive nodes (P = .0008) were shown to be the two factors that significantly affected OS (Figure 2.11).

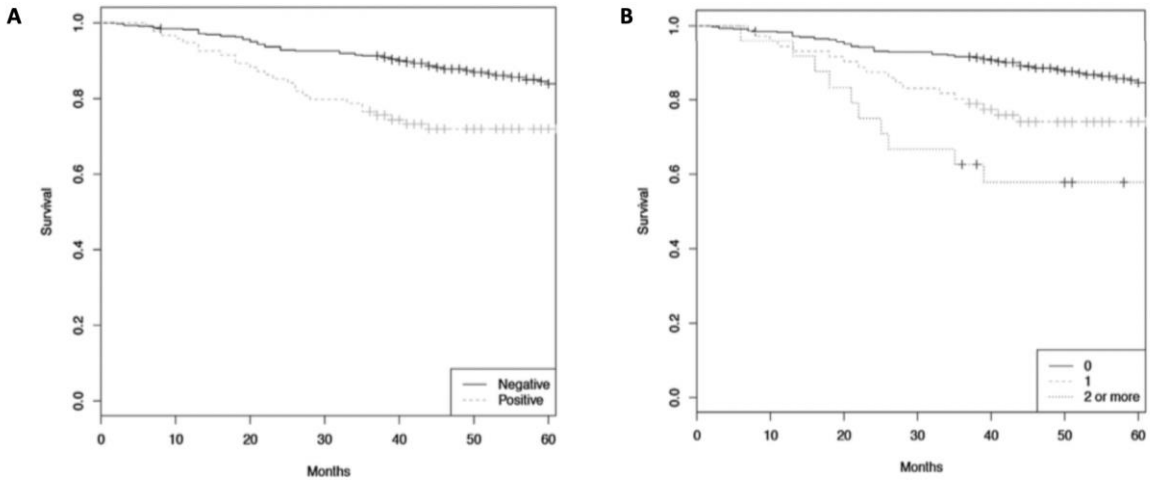

Figure 2.11 Kaplan Meier curves for overall survival generated in the Sentinel European Node Trial.

Overall survival based on A. SLN status, and B. number of positive nodes. *From Schilling et al.*[182]

Functional outcomes

The general philosophy of SLNB is to provide nodal staging with the highest level of accuracy, while performing the least amount of tissue dissection. It therefore promises as its core benefit over extensive lymphadenectomy procedures, lower surgical morbidity,

fewer complications and improved functional outcomes. Two studies have directly compared SLNB verses END with respect to functional outcomes such as scar length, shoulder disability and quality of life, confirming significant benefit with SLNB in all of these domains.

In a study by Murer et al. 62 consecutive patients were enrolled prospectively and underwent either SLNB alone (n=33) or SLNB with completion END (n=29).[187] Subjective shoulder impairment was assessed with the validated neck dissection impairment index (NDII) questionnaire that has ten items measuring the impact of shoulder disability on quality of life with a 5-point Likert scale (where a lower score reflects greater disability).[188] In this study, SLNB alone showed a significantly higher NDII than in the SLNB plus END group with a median score of 99.7 (range 90 – 100) versus 94.3 (range 32.5 – 100) (p = .0044). Objective shoulder function was examined using the validated Constant Shoulder Score, which includes measures of shoulder range of movement with goniometry.[189] Again, shoulder function was significantly better following SLNB compared with END, mean 99.87% versus 96.13% respectively (P = .0018). In addition, there was a significant difference in scar length between the two groups with a median of 5cm (range 2.5-6.5cm) versus 9cm (range 5-19cm) in the SLNB and END groups respectively (P < .001, Wilcoxon test).

In another prospective study, by Schiefke et al., patients either underwent SLNB (n = 24) or selective neck dissection of levels 1-3 (n = 25) and underwent quality of life and psychosocial assessment with the EORTC QLQ-C30 questionnaire, the disease specific EORTC QLQ-H&N35 module, the hospital anxiety and depression scale and the fear of progression questionnaire.[183] In this study, there was no difference in health related

quality of life (QOL) outcomes. Disease specific QOL scores showed fewer swallowing problems in SLNB patients (P = .043). SLNB patients felt less fear of progression, experience significantly less impairment from cervical scars and had less sensory dysfunction and better shoulder function.

Cost effectiveness

As an important secondary benefit associated with the reduced invasiveness of the procedure, SLNB has been shown in several studies across different health care systems to be cost effective when compared to END.

In a European study by O'Connor et al., the treatment model and data derived from the 481 patients included in the European Sentinel Node Trial (SENT) was used to calculate a relative cost ratio (RCR) for 100 hypothetical patients passing down each treatment pathway (i.e. either END alone, or SLNB with or without completion SND).[190] In the trial, 25% of patients had a positive SLNB result, 75% had a negative SLNB result and in 2.5% of patients there was a false negative result.[182] Based on this, the authors extrapolated that treatment of 100 hypothetical patients using a SLNB pathway is 0.35-0.60 the cost of treating the same cohort using END alone. Furthermore, the study showed that even if 100% of SLNBs were positive, the SLNB approach still offered an overall saving, at 0.91 of the cost of the traditional surgical approach.

In a Japanese study, Kosuda et al. used a similar decision tree sensitivity analysis designed on ipsilateral neck dissection versus SLNB to examine the difference in billed costs to the Japanese national insurance reimbursement system.[191] In this study, introduction of

SLNB in place of ipsilateral END was projected to yield a cost saving of $1218 (USD) per cN0 patient in Japan and avoid 7 surgical deaths per 1000 patients who would have undergone END. A break-even point analysis demonstrated that savings would begin to accrue after reaching a threshold of 41 patients.

Using a different approach, Govers et al., employed a Markov decision analytic model to evaluate the cost effectiveness of five different possible strategies for diagnosis and treatment of early stage OSCC.[192] The management strategies evaluated were: 1. END, 2. Watchful waiting, 3. gene expression profiling followed by neck dissection or watchful waiting, 4. SLNB followed by watchful waiting or neck dissection, and 5. gene expression profiling and SLNB for positive gene expression profiling, followed by neck dissection or watchful waiting. In this study SLN followed by neck dissection or watchful waiting was the most effective and cost-effective strategy. Compared with END the incremental cost-effective ratio was 3356 Euros per quality adjusted life years (QALY) gained. At 66%, SLNB was found to have the highest probability of being cost effective of the five strategies at a willingness to pay of 88,000 euros per QALY (Figure 2.12).

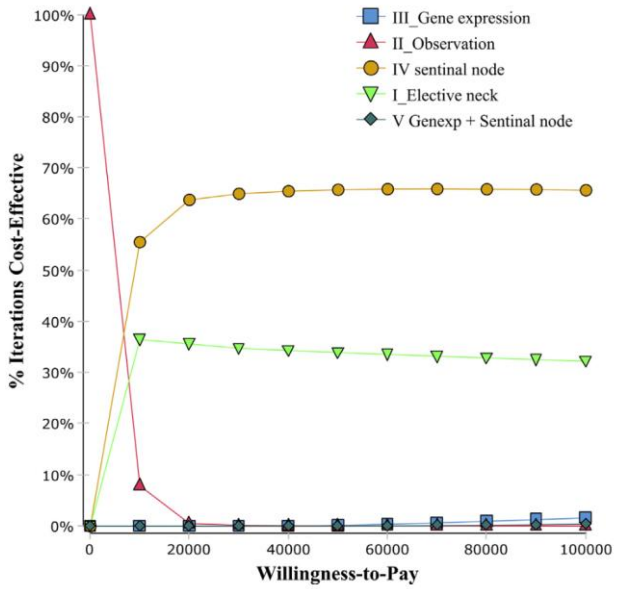

Figure 2.12 Acceptability curve for five treatment strategies for neck disease in OSCC.

At a willingness-to-pay of 88,000 euros per QALY, SLNB had the highest probability of cost-effectiveness at 66%. At this threshold, END was cost effective in 33% of the simulations. *From Govers et al.*[192]

Randomised controlled trials comparing sentinel lymph node biopsy with elective neck dissection

Recently two prospective RCTs have directly compared SLNB with END, generating high-level evidence to show oncological equivalence between the two techniques, with significantly lower morbidity and improved functional outcomes using SLNB.[193]

In a Japanese study published in 2019 by Hasegawa et al., 270 patients with T1-2 OSCC were recruited from 16 centres and randomised to SLNB (n=134) or END (n=137).[194]

3-year OS in the SNB group was 89% (95% CI 82-93%), versus 86% (95% CI 79-91%) in the END group, demonstrating non-inferiority. 3-year relapse free survival was 80% (95% CI 72-86%) in the SNB group and 81% (CI 73-87%) in the ND group. In addition, arm abduction was examined in patients in both groups at 1- and 3- months following surgery, with significantly better results reported in the SLNB group.

Even more recently, a study published in 2020 by Garrel et al. reported results from a phase III multicentre RCT conducted in France.[195] Here, 307 patients with cT1-T2N0 OSCC were recruited and randomised to SLNB or END, with data from 279 patients analysed (140 SN and 139 END). Neck node RFS at 2 years was 90.7 (95% CI 0.84 - 0.95%) versus 89.6% (95% CI 0.83% - 0.94%) in the SLNB and END arms respectively, confirming equivalence with $P < .01$. Furthermore, the 5-year RFS and the 2- and 5- year DSS and OS were not significantly different between arms. The study also measured the median hospital length of stay in both arms, with a median of 8 days in the END arm and 7 days in the SLNB arm ($P < .01$). Notably, consistent with the other RCT, the functional outcomes were significantly worse in the END arm until 6 months after surgery.

CHALLENGES AND BARRIERS TO WIDESPREAD ADOPTION

Despite good evidence to show that SLNB for OSCC is an accurate and oncologically sound technique that can improve functional outcomes and minimise costs when treating patients with early-stage OSCC, it is still yet to be widely adopted in many regions around the world including Australia and North America.[196] In a review of the national cancer database in the United States between 2012 and 2015, of the 8,328 patients who

underwent surgical treatment for stage I and II OSCC, just 240 or 2.9% were treated with SLNB.[197]

While the data presented thus far highlights the beneficial outcomes of SLNB, there are technical and logistical challenges associated with the procedure that have been commonly cited as barriers to widespread adoption in the head and neck. These challenges can be distilled broadly into three core overlapping themes: 1. Limitations of the radionuclear approach, 2. Unique complexities of head and neck lymphatic anatomy and 3. Logistical and system challenges (Figure 2.13).

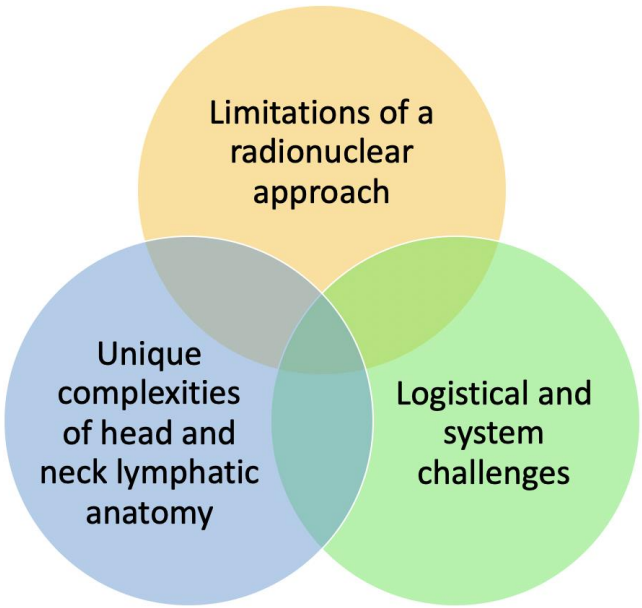

Figure 2.13 Summary of overlapping themes which are barriers to adoption of SLNB in OSCC.

Limitations of a radionuclear approach

Perhaps the most frequently reported issue with SLNB in OSCC is the clinically significant impact of the "shine-through phenomenon". This phenomenon is where radioactive tracer deposited at the injection site produces a large hotspot on lymphoscintigraphy that hides any SLN that lies in close proximity to it and masks SLN gamma probe signal intraoperatively, overall leading to SLN non-visualisation and non-detection (Figure 2.14).[198] While this tends not to be an issue for SLN mapping in breast cancer and melanoma, it does become a significant problem in the head and neck, where the SLNs are located a very short distance from the primary tumour. This is particularly evident in FOM tumours where level 1 nodes are the most common site of metastasis and lie in close proximity to the primary tumour. Multiple studies have demonstrated a significantly lower accuracy of SLNB in FOM tumours than other tumour locations in the oral cavity.[155, 199-201] Given the significant impact on survival of positive neck disease, a false negative result in this highly curable setting is regarded by many as an unacceptable risk.

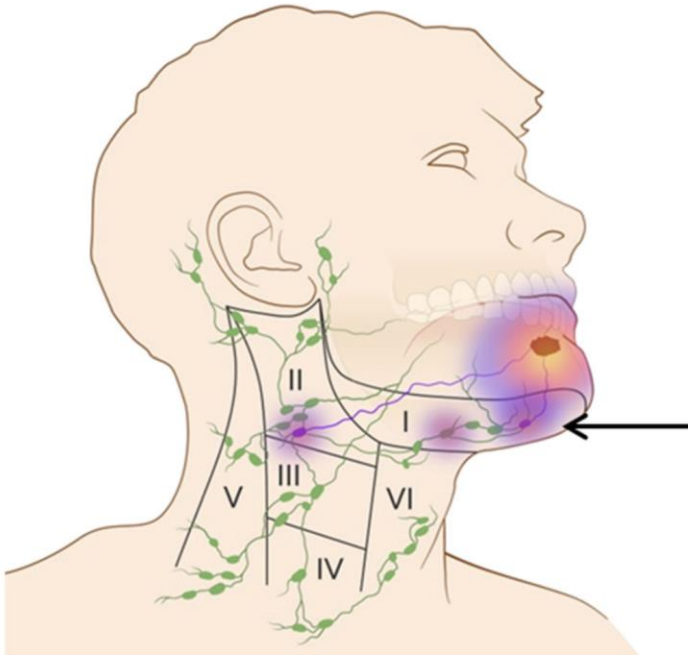

Figure 2.14 The "shine through" phenomenon.

A large hotspot generated by the radiation at the primary tumour masks the signal from the first echelon LN that lies in close proximity (arrow). *From den Toom et al.*[202]

Unique complexities of head and neck lymphatic anatomy

The next barrier to adoption is related to the complex and in many instances unpredictable, lymphatic drainage pathways in the head and neck, resulting in a perception that limited nodal dissection during SLNB has significant potential to miss metastatic disease, again presenting the unacceptable risk of a false negative result in a highly curable setting.[203] There can be multiple first draining LNs from the oral cavity, located in a variety of different levels and sometimes in the contralateral neck, which can make incision placement difficult and require the need for multiple small incisions.[204] Furthermore, there is a small but well-known risk of "skip metastases" in the neck, where

metastatic cells directly bypass common locations of spread to be deposited in unexpected locations such as level IV or V.[37, 205] To address the risk of false negatives in this setting, techniques to improve sensitivity such as the use of the 'triple method" of detection, and additional imaging with SPECT-CT, are recommended.[154, 198]

Logistical and system challenges

There are a myriad of technical, logistical and system challenges which have been reported as barriers to adoption of SLNB in the head and neck.

One technical challenge is the difficulty of local tracer injection in the head and neck. Access to tumours can be limited, particularly those located posteriorly in the oral cavity or originating in other head and neck subsites such as the oropharynx, larynx or hypopharynx. Poor access is a clinically significant issue in the head and neck where meticulous injection technique is critical. This is because the tumour often lies adjacent to many surrounding lymphatic pathways that do not necessarily drain the primary, and therefore, small volumes of radiotracer must be injected subcutaneously close to the margin of the tumour with a high level of accuracy to ensure there is no unphysiological uptake of tracer into adjacent lymphatics that do not represent true primary draining basins.[206, 207] For all of these reasons, many centres require that surgeons perform this process rather than nuclear medicine technicians, increasing demands on surgical departmental resources.[197]

In addition, there is also the logistical challenge of precisely coordinating timing of radiotracer injection with timing of surgery. Increasing the window of time between

lymphoscintigraphy and surgery can impact accuracy of intraoperative detection.[201] Therefore, successful SLNB requires a high level of planning, coordination and communication between nuclear medicine physicians and surgeons, which can be particularly difficult when either or both departments have busy schedules and limited resources.[198]

Another cited barrier to adoption is the logistical requirement for staged CND because intraoperative pathology is not sensitive enough to direct definitive treatment on the day of procedure.[208] Delayed definitive treatment of the neck does come with oncological risk[209, 210] and therefore guidelines for SLNB recommend that it must only be performed where it is known that a CND can be undertaken within 3 weeks of the SLNB procedure.[161] Furthermore, where there is a requirement for free-tissue reconstruction following resection of larger primary tumours, the added tissue dissection performed within the neck as part of this procedure can undermine the minimally invasive approach provided by SLNB.

SLNB does have a significant learning curve and therefore specialised training and surgical experience also become critical components affecting uptake.[207] In centres with an experience of ten or less cases, a sensitivity of only 57% could be obtained compared with 94% in centres with an experience of more than ten cases.[154] The American College of Surgeons Oncology Group (ACOSOG) validation trial found that more experienced surgeons performed better than less experienced surgeons, with 0% false negatives versus 13.3% respectively.[201] In the US, academic centres performed 63% of SLNB procedure, consistent with the observation that smaller centres may need more experience before adopting the technique.[197]

Finally, a less commonly reported, but nonetheless significant barrier to adoption relates to financial reimbursement, whereby repayments for SLNB are less than for END.[197] Given the substantial expertise, time and resources required to complete SLNB, this undoubtedly impacts utilisation of this procedure.

CHAPTER 3: A ROLE FOR FLUORESCENT AND MAGNETIC MOLECULAR IMAGING

MOLECULAR FLUORECENCE IMAGING

GENERAL PRINCIPLES OF NEAR-INFRARED FLUORECENCE GUIDED SURGERY

The visible spectrum versus the near infrared spectrum and the phenomenon of fluorescence

Humans can detect light in the visual spectrum (400 – 750nm) with a high resolution of approximately 50μm, however the human eye cannot differentiate between spectra with a small separation in wavelengths (i.e. differentiating two different objects with an almost same colour).[211] This is the phenomenon used by the defence force to mislead the human eye with camouflage. During surgery there is no clearly defined optaical margin to visually discriminate tumour and nearby benign fibrotic or dysplastic tissue when analysing margins.[211] Furthermore, microscopic extensions of tumour are not visible at all. Using an optical imaging method that can clearly discriminate normal tissue from cancer has potential to aid margin delineation.

Fluorescence is the phenomenon that occurs when a molecule absorbs a photon activated at a certain wavelength (excitation) that then triggers the release of photons at a longer wavelength (emission).[211] Among the wavelengths of light on the electromagnetic spectrum, near infrared (NIR) wavelengths range from 750 – 1000nm (Figure 3.1) and have been of great interest in fluorescence guided surgery for several reasons. Firstly, unlike light in the visible range, light in the NIR range can penetrate tissue to a depth of 2cm, which can be useful for detecting tumour cells through normal tissue.[212] Secondly,

the wavelength range of NIR light has the lowest absorption coefficients of haemoglobin, lipid, and water.[212] This decreases the amount of autofluorescence and minimizes the background noise, which provides a better signal-to-noise ratio (SNR) to enhance optical imaging and allow quantification of fluorescent intensities of targeted tissues during surgery.[213]

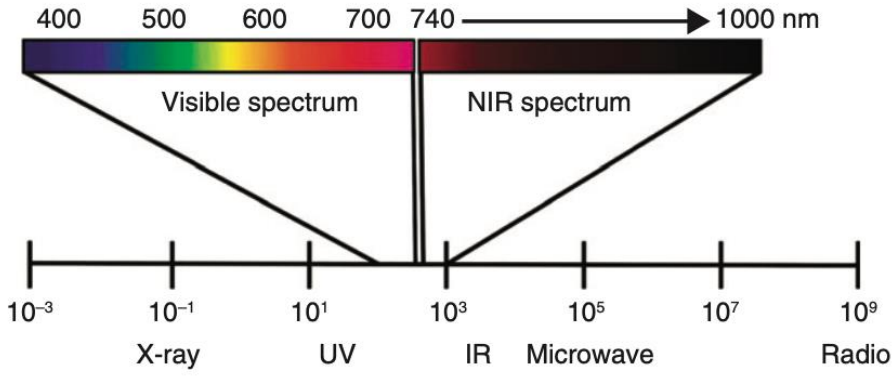

Figure 3.1 Optical imaging related to the electromagnetic spectrum.

The visible spectrum (400-750nm) and the near-infrared spectrum (750 – 1000nm) are highlighted. *From de Boer et al.*[211]

The role of a sensitive charge-coupled camera in fluorescence imaging

Light in the NIR wavelength is not visible to the human eye, and therefore, fluorescent imaging in clinical practice requires that released photons following excitation are detected with a sensitive charge-coupled camera.[212] Such cameras typically incorporate two different light sources. First, a white light source is used for colour registration of the tissue combined with a filtered white light source (light-emitting diode or laser) in the

wavelengths needed for excitation of the fluorescent optical contrast agent to be used to detect tumour.[211] The light emitted from the field of surgical view is then guided through optics and divided into different detectors. Computer software reconstruct the fluorescence signal typically projecting a pseudocolour overlay on the colour image displayed on a monitor, which allows quick interpretation of the distributed fluorescence through the tissue.[214] These cameras can be used to inspect the entire operating field in real-time as part of "open-field imaging" (Figure 3.2). Alternatively, "closed-field imaging" can be performed, where cameras housed in a closed environment image the resected specimen ex vivo, thereby removing disturbance by ambient light.[215, 216] This typically takes place on the operating back-table in near real-time.

Figure 3.2 A hand-held sensitive charge-coupled camera being used during head and neck surgery for in situ open-field imaging.

The role of "Fluorophores" as fluorescent contrast agents

As part of fluorescent imaging, a fluorescent contrast agent or "fluorophore" is required for the excitation and emission of photons that are detected by the sensitive charge-coupled camera (Figure 3.3). There are many different types of fluorophores, including endogenous molecules within tissue such as collagen and elastin, as well as exogenous agents that are delivered to tissue.[217] Of the exogenous molecules, several agents are already FDA approved and in clinical use including, fluorescein, which is used for assessing the retina, and ICG which is used for blood perfusion studies and SLN mapping.[218, 219] Both of these contrast agents are non-targeted, meaning they are not tissue or tumour-specific.

To enhance demarcation between normal and cancerous tissue, tumour-targeted, or molecularly-targeted, fluorophores have been developed that combine fluorescent dyes with antibodies that bind to tumour-specific receptors for fluorescent molecular imaging.[220] Examples of these are cetuximab-IRDye800CW and panitumumab-IRDye800CW, which target the epidermal growth factor receptor (EGFR) and have been used in head and neck, pancreas, brain and lung cancer.[221-224] For breast cancer, trastuzumab-IRDye800CW, which targets Her2/neu, and bevacizumab-IRDy800CW, which targets vascular endothelial growth factor (VEGF)-A, have been used.[225]

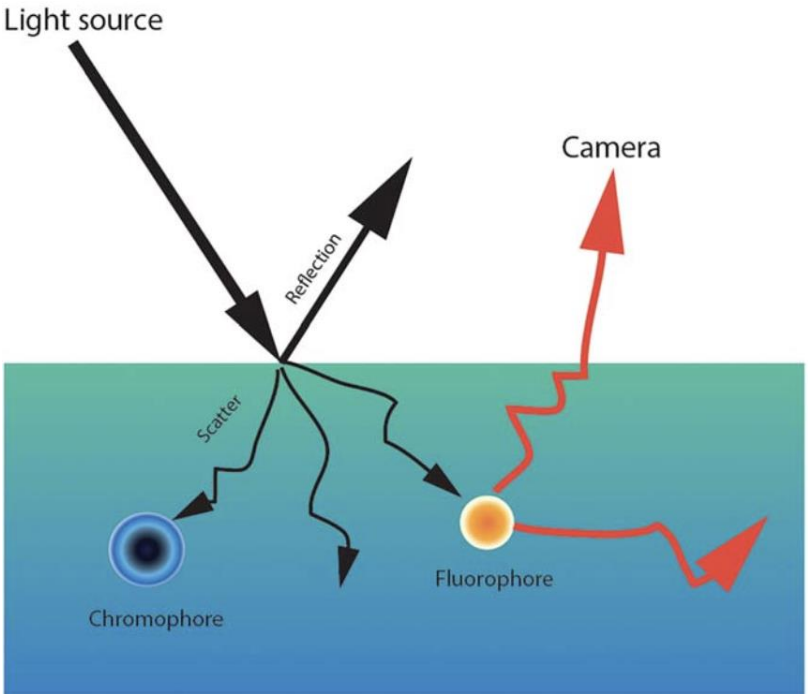

Figure 3.3 Fluorescent imaging using a "fluorophore" for excitation and emission of photons that are detected by a sensitive charge-coupled camera.

When a light source is applied to tissue it can be reflected, scattered and absorbed by molecules within the tissue (chromophores). In fluorescent imaging, a fluorescent contrast agent (fluorophore), either endogenous or exogenously administered, is excited by the applied light and emits light at a different wavelength, which can be detected by a sensitive charge-coupled camera. *From Teraphongphom et al.*[217]

PANITUMUMAB-IRDYE800CW – A MOLECULARLY-TARGETED FLUOROPHORE

Panituumab-IRDye800CW

Pantiumumab-IRDye800CW is a tumour targeted fluorophore composed of the antibody Panitumumab (Vectibix; Amgen, Thousand Oaks, California, United States), which is conjugated with a near-infrared fluorophore called IRDye800CW (Figure 3.4), which has an absorption maximum of 774nm and an emission maximum of 789nm.[226-228] Panitumumab is a fully-humanized monoclonal IgG2 antibody, that binds with high-affinity to the EGFR, a protein of the ErbB family that is overexpressed in, amongst others, head and neck, glioma, pancreatic and lung cancers.[229] It was initially approved by the FDA in September 2006 as a chemotherapeutic agent for EGFR-expressing metastatic colorectal cancer.[226]

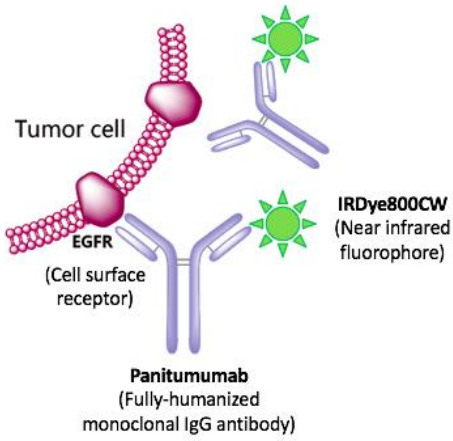

Figure 3.4 Schematic diagram demonstrating the tumour-targeted fluorophore Panitumumab-IRDye800CW binding with EGFR expressed on a tumour cell surface.

Conjugation, safety and stability

IRDye800CW has been demonstrated to have low toxicity and short half-life when unconjugated.[230] As part of the conjugation process, a N-hydroxysuccinimide (NHS) ester reaction binds randomly to lysines throughout the antibody during a relatively simple labelling method that has been performed successfully for chimeric and fully human antibodies with a consistent dye to protein ratio and good imaging results.[231, 232] Studies have demonstrated that re-purposing the therapeutic antibody Pantiumumab, as a diagnostic imaging agent with its fluorescent IRDye800CW label, has been deemed safe and stable in studies. It has a rate of adverse events (7.4%) that is consistent with the rate of panitumumab alone, although in this context is being used. As a diagnostic rather than a therapeutic agent.[232-235] The common side effects of panitumumab are skin changes including acne, dry skin, rash and itching, swelling or irritation of fingernails or toenails, loss of appetite, nausea and diarrhoea and tachycardia.

CLINICAL APPLICATIONS OF MOLECULAR FLUORECENT IMAGING IN HEAD AND NECK SURGERY USING PANITUMUMAB-IRDYE800CW

Fluorescence-guided surgery clinical trial workflow

Currently, fluorescence guided surgery is not a part of routine practice but has been investigated for several different applications in head and neck surgery as part of prospective phase I and II clinical trials.[236] These trials generally follow a similar workflow (Figure 3.5).[237-240] Patients are infused intravenously (IV) with 50mg of

Panitumumab-IRDye800CW (which has been shown to be the optimum dose for imaging) 1-5 days prior to surgery.[236] Imaging is then performed during surgery at three different time points. Firstly, open-field fluorescence imaging is performed to visualise the tumour *in situ* in real-time. The overhead, head lamp, and room lights are turned off to minimize ambient light and reduce noise.[241] This can be utilised during primary tumour resection as well as during neck dissection.[242] Secondly, immediately following tumour resection, a closed-field imaging system is used for ex vivo specimen mapping in near-real time on the operating back-table.[240] Finally after surgery at pathology, sectioned specimens are imaged on a closed-field, flat bed scanning device for target validation. Here, the mean fluorescence intensities of regions of interest (ROI)s on the fluorescent images are cross-referenced with histopathologic findings.[237]

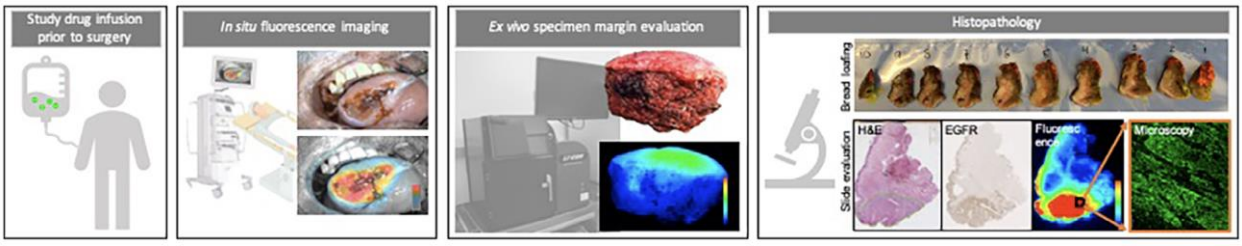

Figure 3.5 Summary of general workflow of fluorescence guided surgery in head and neck clinical trials with in situ and *ex vivo* imaging in the operating room, followed by imaging at pathology for target validation.

From Lee and Krishnan et al.[212]

***In situ* margin analysis in real-time**

During primary tumour resection, open-field fluorescence imaging can enhance intraoperative decision making by guiding extended or additional resection in real-time. In a trial enrolling 14 HNSCC patients, fluorescence imaging made a clinically significant improvement to decision making during surgery in 3 cases (21.4%) by identifying a close margin in two cases (Figure 3.6) and an unanticipated region of primary disease in one case.[239]

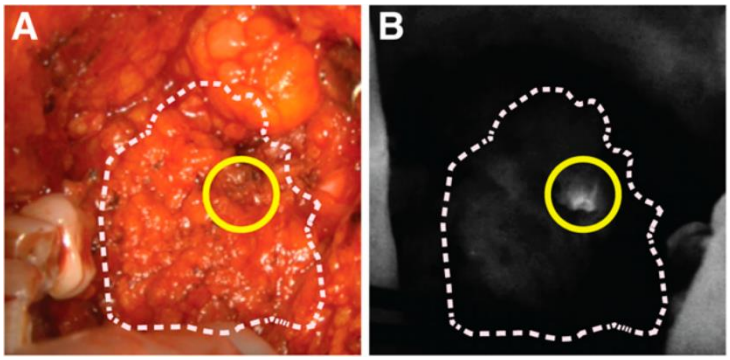

Figure 3.6 intraoperative detection of a close deep margin with open-field fluorescence imaging.

The deep aspect of a specimen being resected in A. bright-field and B. fluorescent views respectively. The yellow circle indicates the area of increased fluorescence on the deep aspect of the resection, representing where tumour comes close to the resection edge.

From van Keulen et al.[239]

Ex vivo margin analysis in near-real time

To aid ex vivo margin assessment, resected specimens can undergo closed-field imaging. The close-field devices that have been used in clinical trials have typically been small animal imaging platforms that have been repurposed for human use. The closed device allows for a controlled imaging environment, with a stationary specimen and camera, and elimination of ambient light.[241]

A study by van Keulen et al. developed a novel concept for ex vivo specimen mapping using relative fluorescence intensity.[240] In this study, imaged specimens were analysed with signal-mapping computer software to identify areas on the deep margin of highest fluorescence, which were called fluorescence intensity peaks. It was demonstrated that the highest fluorescent intensity peak consistently detected the point on the deep surface where tumour came closest to the resection edge. Furthermore, the margin distance increased in an orderly fashion with successively lower intensity peaks on the specimens (Figure 3.7). By using the relative fluorescence values (i.e. by comparing first and second peaks within a specimen, rather than setting a broad and generalised fluorescent intensity threshold across different patients), issues of heterogeneity in imaging between different patients with different tumours were controlled for. The authors proposed that the highest intensity peak could be used to identify the "sentinel margin", a term they coined to represent the true closest margin. They proposed focussed assessment of this point would reduce sampling error by improving accuracy of detection of close margins on the specimen.

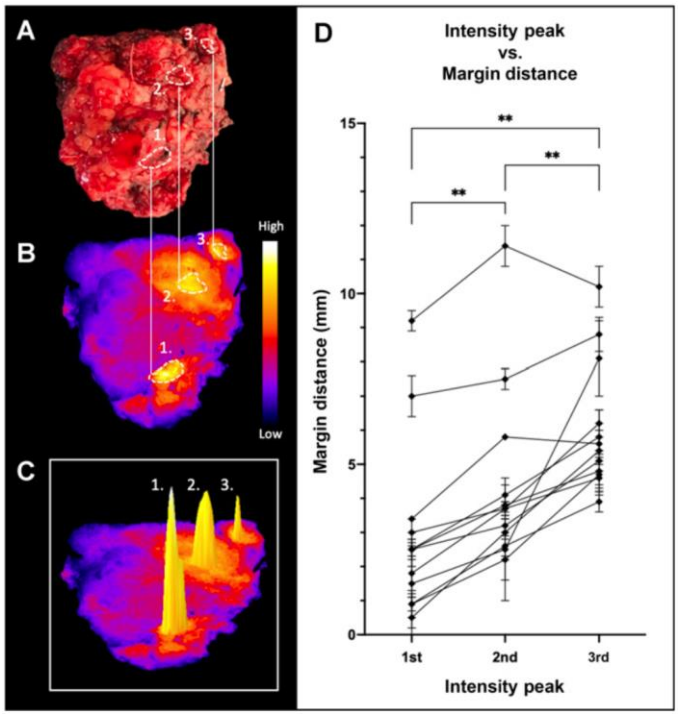

Figure 3.7 fluorescent intensity peaks versus margin distances.

Representative tumour resection in A. Brightfield, and B. Fluorescent views. C. Identification of the highest three fluorescent intensity peaks on the deep surface of the specimen. D. Graph demonstrating the increasing margin distance with decreasing intensity peaks per patient. *From van Keulen at al.*[(240)]

Metastatic lymph node detection

The feasibility of molecular fluorescence imaging for metastatic LN detection has also been shown, although the clinical utility of an open-field approach to guide neck dissection in real-time has yet to be elucidated. In a study by Nishio et al.,[(243)] 1012 LNs (39 metastatic and 973 benign) underwent closed-field imaging following neck dissections in 22 patients who were pre-operatively infused with panitumumab-IRDye800CW. The authors demonstrated that metastatic LNs had a significantly higher

mean fluorescent intensity (MFI) and signal-to-background ratio (SBR) than benign LNs with a sensitivity and specificity of metastatic LN detection of 94.9% and 76.4% for MFI, and 87.2% and 86.1% for SBR when set at optimum thresholds. Based on this, the authors proposed a fluorescent-guided pathology strategy, whereby molecular imaging could be used to preselect at-risk LNs (above a certain MFI or SBR threshold) for rigorous pathological examination, while stratifying lower-risk LNs for sectioning only as required, in this way improving prognostication and efficiency of pathology (Figure 3.8).

Another incidental finding in this study was that higher doses of systemically delivered panitumumab-IRDye800CW correlated with a higher false-positive rate, prompting microscopic examination of benign LNs, which demonstrated a non-specific accumulation of panitumumab-IRDye800CW in a dose-dependent fashion at the lymphatic sinuses even in the absence of EGFR expression. This lead the authors to hypothesise that when given in higher doses, panitumumab-IRDye800CW could potentially be oversaturating EGFR at the primary site, leading to extravasation into the lymphatics, with resultant circulation to first draining LNs (regardless of their metastatic/EGFR status) – a physiochemical property that could be leveraged for SLNB.

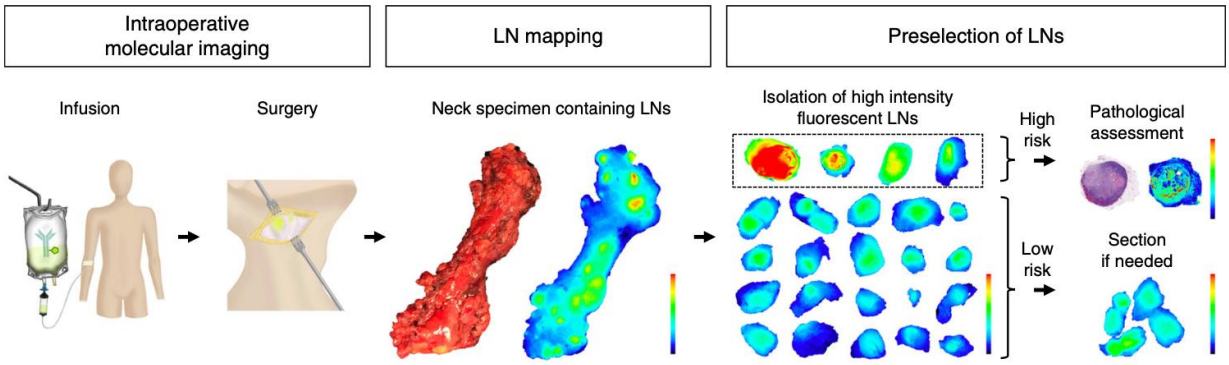

Figure 3.8 Proposed work-flow for fluorescent molecular image-guided pathology to aid preselection of at-risk lymph nodes for detailed histopathological assessment.

From Nishio et al.[243]

TARGETED LYMPHOTROPIC SUPERPARAMAGNETIC IRON OXIDE NANOPARTICLES

GENERAL PRINCIPLES OF SENTINEL LYMPH NODE MAPPING WITH CONTRAST AGENTS

The effect of particle size on lymphatic transport

When performing SLNB, the ideal tracer should have fast uptake into the lymphatics with rapid clearance from the primary injection site, thereby reducing the effect of shine through. The tracer should then swiftly migrate to the SLN, and once there, be retained for long enough to provide the optimum time-window for imaging and intraoperative identification. After reaching the SLN, there should be excellent retention with limited flow-through to lower echelon nodes in order to maximise the sensitivity and specificity of detection.

Unfortunately, no such perfect tracer exists as the dominant factor influencing each of these aspects of lymphatic transport is particle size, and of critical significance, particle size confers antagonistic effects between migration, diffusion, and retention.[244, 245] Smaller particles have a quick uptake into and migration through the lymphatics, but this can be a disadvantage if the imaging window is too short. They are also more likely to diffuse out of the lymphatics resulting in unwanted background signal. Furthermore, they have poor retention in the SLN with higher flow-through to lower echelon nodes.[246] On the other hand, large particles migrate slowly which can be of benefit in widening the imaging window, but if there is poor migration past the injection site, shine through effect

becomes a significant problem.[202] Furthermore, large particles are at risk of being diverted past first echelon LNs if they contain metastatic tumour deposits which obstruct their lymphatic flow.[148, 150] The right contrast agent for SLNB therefore requires a particle size that strikes an optimal balance between each of these components of lymphatic transport.[247] Figure 3.9 demonstrates the variation in sizes of SLNB tracers currently used and the effect of this on their migration, diffusion and retention properties.

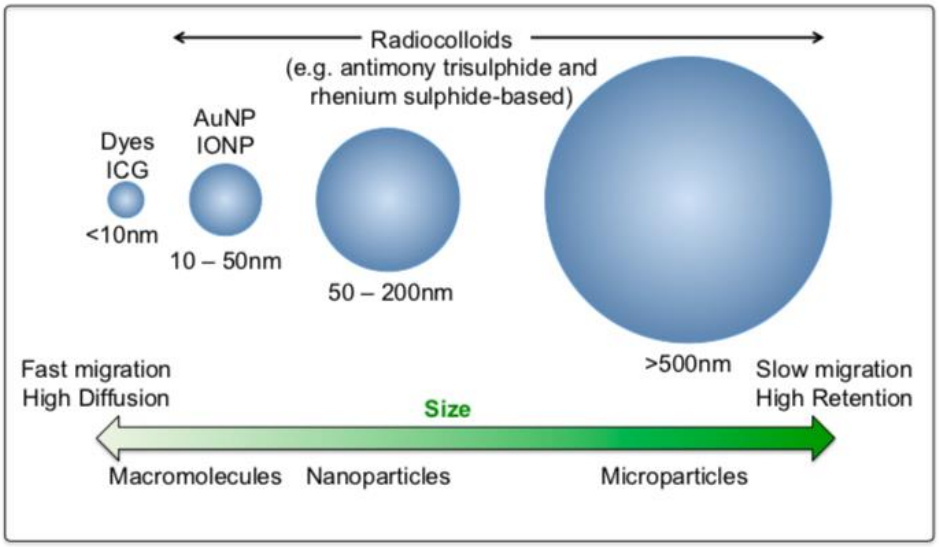

Figure 3.9 Size comparison of different tracers with summary of size effect on lymphatic migration, diffusion and retention.

(ICG: indocyanine green, AuNP: gold nanoparticle, IONP: iron oxide nanoparticle).

From Cousins et al.[247]

Targeted sentinel lymph node tracers

Given the difficulties of optimising tracers for SLNB by manipulating hydrodynamic diameter alone, modern tracers have been engineered to be coupled with molecules that target biological receptors on specific lymphoid cells in order to enhance retention. One such example is 99m-Tc Tilmanocept or "Lymphoseek" (Neoprobe Copr., Dublin, OH), which has been FDA approved and is now widely used.[246] It consists of a dextran backbone to which multiple units of mannose are attached, which serve as substrates for recognition and binding to the mannose-binding protein receptor (CD206) found on reticuloendothelial cells within LNs.[248] For nuclear imaging and gamma probe detection, it is labelled with Tc-99m, using diethylene triaminine pentaacetic acid (DTPA) as a chelating agent (Figure 3.10). The resultant mannose-based low molecular weight soluble imaging agent can be produced with a sub 20nm hydrodynamic diameter, compared with diameters ranging to > 500nm with radiocolloids. Therefore, Lymphoseek is designed to exhibit properties of rapid clearance from the administration site, with sustained sentinel LN uptake without distal LN accumulation, which holds great potential to minimise the effect of shine through and improve results of SLNB in floor of mouth tumours.[249] Prospective clinical trials have demonstrated its safety and efficacy, as well as its combined rapid injection site clearance and promising intraoperative SLN localisation.[167, 202, 250]

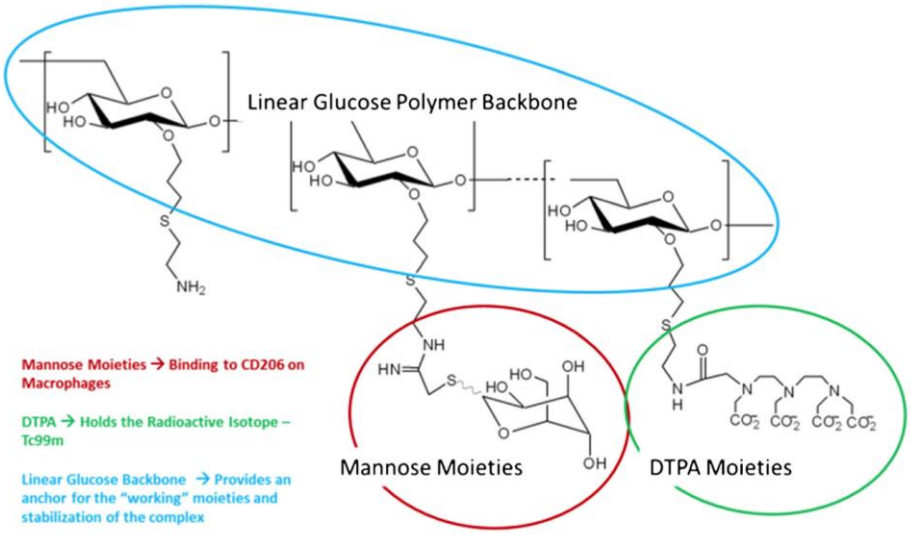

Figure 3.10 99m-Tc Tilmanocept or "Lymphoseek" molecular structure.

The dextran backbone to which mannose units are attached to target the CD206 receptor on macrophages. DTPA moieties are attached for labelling with Tc99m.

From den Toom et al.[202]

THE RATIONALE FOR USING MAGNETIC TRACERS IN SENTINEL LYMPH NODE BIOPSY

Comparing radionuclear versus magnetic technology

The SLN concept hinges completely on the use of an exogenous contrast agent to map the lymphatic drainage from a primary tumour to one or more first draining LNs - but the procedure does not need to be limited to any specific contrast type, or imaging and intraoperative detection technology.[247] While radionuclear technology has historically always been used for SLNB, it has inherent limitations that have affected its application

in complex lymphatic networks such as the head and neck, as has been discussed in detail in chapter 2.

Pivoting to a magnetic approach holds great potential to overcome some of the inherent shortcomings associated with radionuclear technology. For example, unlike lymphoscintigraphy, MRI provides excellent spatial resolution with high sensitivity to soft tissues, which makes it ideal for lymphatic mapping and surgical planning.[251] In addition, using magnetic tracers and MRI avoids exposure to ionising radiation which is highly attractive from a safety viewpoint. From a logistical viewpoint, magnetic tracers are not burdened by considerations associated with short half-life radioactive compounds that impact timing of injection, imaging and surgery.[252] Magnetic tracers, unlike radiocolloids, have a dark brown or black colour which has potential to provide optical feedback without the use of an additional blue-dye injection.[253] Furthermore, with appropriate magnetic tracers, a magnetometer probe can be used to detect magnetic signal within LNs intraoperatively, much like a gamma probe.[254] With these advantages in mind, a magnetic approach presents an attractive next generation technique with significant potential to increase adoption of SLNB in the complex head and neck lymphatic environment.

Magnetic resonance imaging with superparamagnetic iron oxide nanoparticles

Conventional MRI contrast agents such as gadolinium chelates are poor lymphatic contrast agents as they have poor retention in the lymphatics and a high rate of diffusion out of vessels, which results in increased background noise.[255] Furthermore, their fast

clearance can lead to wash-out, affecting the ability of imaging to accurately identify the first draining LNs.[256]

Iron oxide nanoparticles on the other hand, have potential to make great contrast agents for lymphatic mapping with MRI, as they offer a stable platform for coating with dextran or biocompatible polyethylene glycol (PEG) and polyvinyl acetate (PVA) (which gadolinium chelates do not). This can be used to increase their size, thereby reducing migration speed and increasing SLN retention.[257, 258] Furthermore, they have low toxicity, high biocompatibility, tuneable signal strength and ease of manufacture, and they provide the high magnetic signals required for detection with a magnetometer probe.[259]

Successful clinical application of FDA approved iron oxide tracers to SLN mapping include the use of Ferumoxides in japan[260, 261] and the repurposing of ferumoxytol, an iron supplement used for anaemia, as a preoperative contrast agent in USA.[262] In Europe, the use of MagTrace (previously called Sienna+), a superparamagnetic carboxy-dextran-coated iron oxide nanoparticle with a hydrodynamic diameter of 60nm, has been the most successful commercially used tracer for magnetic SLNB.[253, 263]

Intraoperative superparamagnetic signal detection with a magnetometer probe

A magnetometer is a device capable of conveying the presence and strength of direction of magnetic fields through conversion to an electronic source.[247] To do this it emits a signal to induce alignment and net magnetisation of tracer particles and then picks up their magnetic signal with a magnetic sensor (Figure 3.11). Unlike gamma probes,

magnetometer probes do not measure signal intrinsic to the particles, but rather the particles' response to an externally applied magnetic field, which in the case of iron oxide nanoparticles, is their superparamagnetic behaviour.[247] Of significant potential advantage, magnetic signals measured by hand-held probes have been shown to greatly reduce over distance compared to gamma rays (Figure 3.12), presenting a property that could be leveraged to eliminate the shine-through effect.[254]

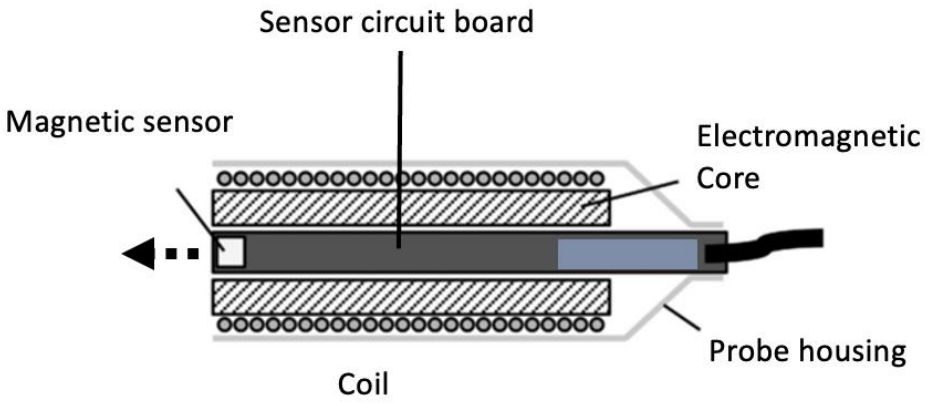

Figure 3.11 Schematic diagram of a magnetometer probe indicating technical components.

Modified with permission from Cousins et al.[247]

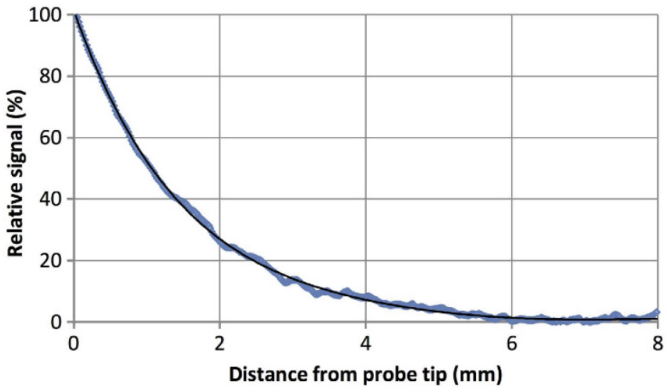

Figure 3.12 Magnetometer range of magnetic signal.

In a proof-of-concept study, the relative magnetic signal from a simulated LN approximately 6mm in diameter was demonstrated to decrease as probe distance increased. *From Cousins et al.*[254]

Many magnetometer probes are available on the market but few are suitable for detecting a small quantity of magnetic particles in an intraoperative environment.[247] Probes for SLNB need to discriminate between signals from particles and unwanted background signals including the earth's magnetic field and mains power.[264] From a commercial-use stand-point, they must be hand-held, sterilizable, portable and easy to operation and maintain.[264] 'Sentimag' (Endomagnetics, London, UK) has been the most successful commercially utilised magnetometer for SLNB, with use for breast and prostate cancer and melanoma.[263, 265, 266]

CLINICAL PRECEDENTS FOR MAGNETIC SENTINEL LYMPH NODE BIOPSY

Clinical trials in breast cancer using Sienna+ and Sentimag

The magnetic technique for SLNB was first demonstrated to be clinically feasible in 2014 in a multicentre trial for breast cancer using Sienna + with the SentiMag magnetometer probe.[253] Since then, there have been several other large prospective non-inferiority trials for breast cancer evaluating this technology. A metanalysis published in 2016 by Zada et al. found seven clinical trials comparing magnetic SLNB to the standard technique. Pooled data from 1118 patients included in these studies showed that the magnetic technique was non-inferior to the standard technique with a high identification rate but a significantly higher LN retrieval rate.[267]

Clinical trials in Melanoma using Sienna+ and Sentimag

Following from the early success of magnetic SLNB trials in breast cancer, results from the MELAMAG trial for melanoma were published in 2016.[266] Here, data from 129 patients across multiple centres showed a SLN detection rate of 97.7% with the standard technique compared to 95.3% with the magnetic technique (2.3% difference, 95% upper confidence limit 6.4, 5.4% discordance). The LN retrieval rate was 1.99 nodes per patient overall, with 1.78 with the standard technique and 1.87 with the magnetic technique. While it was shown to be a feasible technique for melanoma, it was associated with skin staining from the magnetic tracer and did not meet the predefined non-inferiority margin,

so the authors concluded that the magnetic technique was not indicated for SLNB in melanoma.

Challenges

Despite the fast rate of early diffusion of the magnetic approach for SLNB following the success of the first clinical trial, several limitations of Endomagnetic technology have since been unveiled that have stunted its ongoing use. In addition to the MELAMAG trial, several breast cancer studies also reported postoperative skin staining secondary to the Sienna+ injection affecting between 19.4 - 47.3% of patients.[268, 269] In one study, this continued to be a problem after a mean follow-up of 5.9 months and worsened in 1.4% of patients affected.[269] Furthermore, the persistent tracer stains at the subareolar injection sites complicated subsequent surveillance MRI scans with void artefacts greater than 5mm causing risk for potentially obscuring clinical findings. In at least one patient this was present 25 months after injection.[270] In addition technical difficulties relating to the probe were cited, such as the fact that it had a large diameter and therefore necessitated a larger incision for use.[271] It also needed to be pressed in contact with the node to detect signal. Furthermore, it interrupted the operative workflow because of its requirement for regular calibration during surgery and the need to remove metallic retractors and instruments during use to avoid signal disruption.[271]

"FERROTRACE" – A NOVEL TARGETED LYMPHOTROPIC SUPERPARAMAGNETIC IRONOXIDE NANOPARTICLE

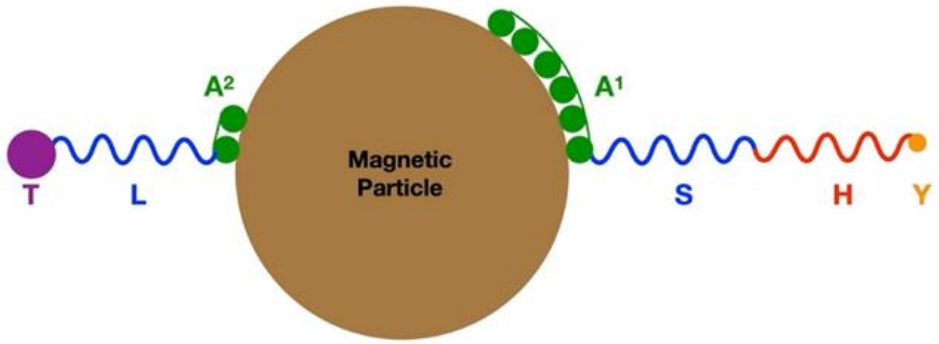

Figure 3.13 Schematic structure of FerroTrace.

(T: Mannose targeting end group, L and S: stabilising polymers, A1 and A2: anchoring polymers, H: hydrophilic polymer, Y: alkyl end group)

Two critical shortcomings of MagTrace have been the significantly higher LN retrieval rate compared with standard nanocolloid, and the clinically adverse outcome of skin staining as a result of aggregation of particles at the injection site.[268, 270] To address these problems, a novel superparamagnetic iron oxide nanoparticle (SPION) has been designed in Australia called "FerroTrace", which is made up of a maghemite iron oxide core coated with a 2-part block copolymer consisting of a 70:30 mixture of stabilising and targeting polymers (Figure 3.13). The nanoparticle has a hydrodynamic diameter of roughly 70nm and a high iron content (60%). The stability block consists of anchoring, stabilising and hydrophilic polymers and an end alkyl group to prevent degradation and aggregation in a biological environment.[272-274] The targeting block copolymer

incorporates mannose to recognise and bind to the CD206 mannose-receptors on macrophages in the same fashion as Lymphoseek.[248] The particle has therefore been designed to optimise magnetic SLNB in complex lymphatic environments such as the head and neck with properties of improved stability to minimise staining at the injection site, and enhanced SLN retention by way of the mannose target, to improve specificity. An early preclinical study has demonstrated promising stability and biocompatibility of the particle, thereby setting the foundation for further preclinical and clinical evaluation.[275]

CHAPTER 4: HIGH-LEVEL SUMMARY OF REVIEW AND RESEARCH OBJECTIVES

THE CASE FOR DISRUPTING THE CURRENT SURGICAL TREATMENT MODEL

OSCC is characterised by its locally aggressive nature and its high propensity to metastasise to regional LNs. Consistent with this, it has been well-established over a long period of time that margin status and the presence of LN metastases are two of the most important factors affecting prognosis.[36, 276] Positive margins double the rate of local recurrence and decrease survival by approximately 13%.[80] The presence of a positive LN, independent of all other factors, halves survival, even if metastatic disease is microscopic and clinically occult (as occurs in roughly 25% of patients).[39] While patient and tumour factors cannot be changed after presentation, margin control during primary tumour resection and staging of the clinically occult neck are two components of management that are within the control of the head and neck surgeon. Despite this, positive margin rates have not improved over the last 30 years[77] and staging of the clinically negative neck continues to rely on a historically invasive approach, unnecessarily overtreating 75% of patients.[67] Therefore, ironically, while both surgical margin assessment and staging of clinically occult disease are two of the most critical components of the management paradigm, they are also the two that most critically require improvement.

TARGETED FLUORECENT AND MAGNETIC TRACERS AS TOOLS FOR INNOVATION

Advancements in conventional surgical approaches do not appear to be improving margin outcomes or minimally invasive nodal staging, providing impetus to seek innovative

solutions with new surgical technologies. Molecular imaging, with tracers designed to target specific tissue and tumour ligands, is a growing field that may hold the answers.

Molecular fluorescent imaging employs the use of tumour-targeted fluorescent tracers to provide optical guidance during cancer resection. For head and neck cancer surgery, an EGFR-targeting fluorophore, Panitumumab-IRDye800CW, has been shown to be able to accurately identify points on the deep surface of resected specimens where tumour comes closest to the margin edge. Given, 97% of head and neck surgeons use intraoperative FSA to guide margin assessment and tumour re-resection, clinical translation of an ex vivo fluorescent guided approach to margin sampling holds great potential for increased precision.

Molecular fluorescent imaging could also be employed for minimally invasive nodal staging. SLNB is a highly accurate and oncologically safe staging procedure that guides personalised treatment of the neck in patients with no clinical evidence of metastatic disease, yet it is not routinely practiced. One reason for this relates to the logistical and technical difficulties of injecting tracer locally around the tumour in the oral cavity. Panitumumab-IRDye800CW has been shown to identify tumour metastases in regional LNs and has also been hypothesised to overflow into the lymphatics from the primary tumour after systemic administration. Further research in this area could lead to the development of a novel SLNB approach built around the IV delivery of panitumumab-IRDye800CW.

Probably the most significant barrier to adoption of SLNB in the head and neck, however, relates to the inherent limitations of conventional radionuclear techniques in this

particularly complex lymphatic environment. Unlike nuclear imaging techniques, lymphatic imaging with MRI provides excellent spatial and anatomic resolution and the combination of SPIONs with a magnetometer probe could eliminate the issues of tumour shine-through that have plagued adoption of SLNB for OSCC. Despite this, magnetic SLNB has not been trialled in the head and neck cancer because currently commercially available magnetic particles lack specificity and have been demonstrated to aggregate at the injection site leading to skin staining and void artefacts on surveillance MRI in breast cancer and melanoma trials. In addressing these issues, a novel SPION has been engineered with mannose end targets for macrophage-specific biding and has shown promising pre-clinical biocompatible and stability findings, holding great value for use in head and neck cancer surgery.

STUDIES TO BE PERFORMED AS PART OF THIS THESIS

1. As an extension to the *ex vivo* sentinel margin concept developed for use on the deep surface of resected head and neck specimens, undertake a proof-of-concept study to evaluate if the same principal using panitumumab-IRDye800CW can be applied to the mucosal surface of specimens to accurately identify the closest peripheral margin to guide pathological sampling.
2. Understand the actual clinical value of using *ex vivo* molecular fluorescent imaging for sentinel margin detection and margin sampling for both deep and mucosal surfaces of resected head and neck specimen in a prospective clinical trial
3. Determine whether IV infusion of panitumumab-IRDye800CW in patients with OSCC undergoing neck dissection can identify sentinel and metastatic LNs.

4. Evaluate the feasibility of using a novel mannose-labelled magnetic tracer for SLNB in the head and neck in a preclinical animal model
5. Translate these preclinical findings into a Phase 1 study evaluating the safety and feasibility of using a novel mannose-labelled magnetic tracer for SLNB in patients with OSCC
6. Determine the value of a robotic approach to SLNB in a preclinical model leveraging both magnetic and fluorescent imaging technology

Part I: Innovating intraoperative margin analysis

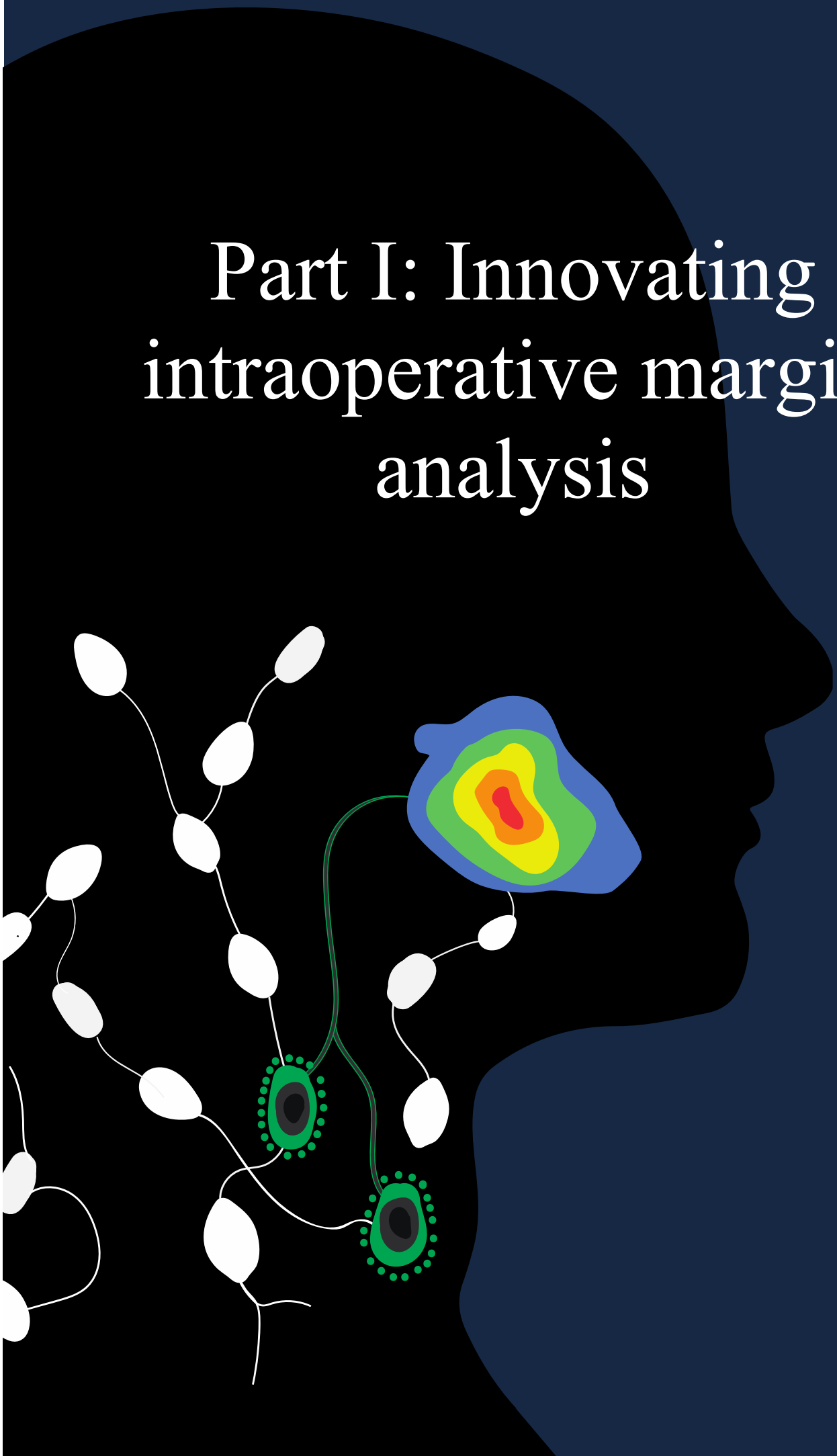

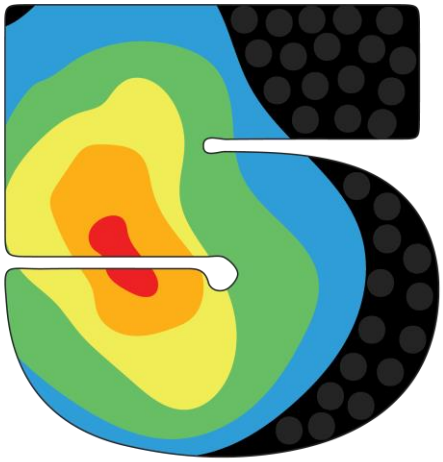

CHAPTER 5: INTRAOPERATIVE MOLECULAR IMAGING FOR EX VIVO ASSESSMENT OF PERIPHERAL MARGINS IN ORAL SQUAMOUS CELL CARCINOMA

STATEMENT OF AUTHORSHIP

Title of paper	Intraoperative molecular imaging for *ex vivo* assessment of peripheral margins in oral squamous cell carcinoma
Publication status	✓ Published ☐ Accepted for Publication ☐ Submitted for Publication ☐ Unpublished and Unsubmitted work written in manuscript style
Publication details	Fakurnejad S, Krishnan G, van Keulen S, Nishio N, Birkeland AC, Baik FM, Kaplan MJ, Colevas AD, van den Berg NS, Rosenthal EL, Martin BA. Intraoperative Molecular Imaging for *ex vivo* Assessment of Peripheral Margins in Oral Squamous Cell Carcinoma. Front Oncol. 2020 Jan 10;9:1476.

Principal Author

Name of Principal Author (candidate)	Giri Krishnan		
Contribution to the Paper	Data collection, analysis and interpretation. Manuscript preparation.		
Overall percentage (%)	50%		
Certification	This paper reports on original research I conducted during the period of my Higher Degree by Research candidature and is not subject to any obligations or contractual agreements with a third party that would constrain its inclusion in this thesis. I am the primary author of this paper		
		Date	20.09.2021

Co-Author Contributions

By signing the State of Authorship, each author certifies that:

i. The candidate's stated contribution to the publication is accurate (as detailed above);
ii. Permission is granted for the candidate in including the publication in thesis; and
iii. The sum of all co-author contributions is equal to 100% less the candidate's stated contribution.

Name of Co-Author	Shayan Fakurnejad		
Contribution to the Paper	Data collection, analysis and interpretation. Manuscript preparation		
Signature		Date	27.09.2021

Name of Co-Author	Stan van Keulen		
Contribution to the Paper	Data collection, analysis and interpretation.		
Signature		Date	03.10.2021

Name of Co-Author	Naoki Nishio		
Contribution to the Paper	Data analysis and interpretation. Manuscript editing.		
Signature		Date	23.09.2021

Name of Co-Author	Andrew C. Birkeland		
Contribution to the Paper	Study conception and design. Manuscript editing.		
Signature		Date	24.09.2021

Name of Co-Author	Fred M. Baik		
Contribution to the Paper	Study conception and design. Manuscript editing.		
Signature		Date	06.10.2021

Name of Co-Author	Michael J. Kaplan		
Contribution to the Paper	Surgical management of patients and acquisition of tissue samples		
Signature		Date	06.10.2021

Name of Co-Author	A. Dimitrios Colevas		
Contribution to the Paper	Study conception and design. Manuscript editing.		
Signature		Date	06.10.2021

Name of Co-Author	Nynke S. van den Berg		
Contribution to the Paper	Study conception and design. Data analysis and interpretation. Manuscript preparation and editing.		
Signature		Date	28.09.2021

Name of Co-Author	Eben L. Rosenthal		
Contribution to the Paper	Supervision of study. Study conception and design. Data analysis and interpretation. Manuscript preparation.		
Signature		Date	24.09.2021

Name of Co-Author	Brock A. Martin		
Contribution to the Paper	Study conception and design. Data analysis and interpretation. Manuscript preparation.		
Signature		Date	24.09.2021

ABSTRACT

Objectives

Complete surgical resection is the standard of care for treatment of oral cancer although the positive margin rate remains 15-30%. Tissue sampling from the resected specimen and from the wound bed for FSA remains the mainstay for intraoperative margin assessment but is subject to sampling error and can require the processing of multiple samples. We sought to understand if an *ex vivo* imaging strategy using a tumor-targeted fluorescently labelled antibody could accurately identify the closest peripheral margin on the mucosal surface of resected tumor specimen, so that this 'sentinel margin' could be used to guide pathological sampling.

Materials and Methods

Twenty-nine patients with OSCC scheduled for surgical resection were consented for the study and received systemic administration of a tumor-targeted fluorescently labelled antibody (Panitumumab IRDye800CW). After surgical resection, the tumor specimen was imaged using a closed-field fluorescent imaging device. Relevant pathological data was available for five patients on retrospective review. For each of these five patients, two regions where the highest fluorescence intensity was closest to the peripheral margin and one region of lowest fluorescence intensity were identified, and results were correlated with histology to determine if the region of highest fluorescence intensity along the mucosal margin (i.e. the sentinel margin) was truly the closest margin.

Results

Imaging acquisition of the mucosal surface of the specimen immediately after surgery took approximately thirty seconds. In all of the specimens, the region of highest

fluorescence at the specimen edge had a significantly smaller margin distance than other sampled regions. The average margin distance at the closest, “sentinel”, margin was 3.2 mm compared to a margin distance of 8.0 mm at other regions ($p<0.0001$).

Conclusions

This proof-of-concept study suggests that, when combined with routine FSA, *ex vivo* fluorescent specimen imaging can be used to identify the closest surgical margin on the specimen. This approach may reduce sampling error of intraoperative evaluation, which should ultimately improve the ability of the surgeon to identify the sentinel margin. This rapid sentinel margin identification improves the surgeon’s orientation to areas most likely to be positive in the surgical wound bed and may expedite pathology workflow.

Keywords

Near-infrared, fluorescence imaging, molecular imaging, margins, head and neck cancer, oral cavity, antibody

INTRODUCTION

Surgical resection with curative intent remains a mainstay in the treatment of solid tumours. Patient outcomes are largely dependent on obtaining clear surgical margins, as locoregional recurrence rates are significantly higher when residual disease exists at or near the margin.[277] Unfortunately, the rates of positive margins in most branches of surgical oncology have remained stagnant over the past 15 years.[278] This has been a particular burden in the management of head and neck cancers, with positive margin rates ranging from 15-30%.[279]

To obtain a tumor-negative margin in head and neck cancer, the surgeon must attain a 5-mm margin of normal tissue around the tumor, based on extensive survival data demonstrating that smaller margins result in worse survival.[280] To accurately measure this margin of normal tissue, the margin should be assessed on the specimen rather than the wound bed, although this remains controversial.[83, 127] Obtaining a consistent 5-mm cuff of normal tissue is challenging since surgeons largely rely on visual and tactile cues when operating. While many novel technologies have emerged to assist in delineation of margins, none have been incorporated into the standard surgical and pathological workflow.[281] Therefore, currently the standard of care for intraoperative margin assessment is the use of FSA. Here, the specimen margins are sampled by the surgeon and/or pathologist for immediate processing and evaluation in parallel to surgery. Results are communicated back to the surgeon so that further resection can be performed if required.

There are two critical limitations with this current practice of identifying positive margins. The first limitation is the fact that sampling of the tumor margin, whether by the surgeon or by the pathologist, is subject to error. Most specimens are 5-10 cm in diameter, and only a fraction of the margin can be sampled; therefore, the likelihood of a false negative assessment is high. The second limitation is that following resection, the tumor specimen must leave the operating room, and the orientation of the specimen is often lost to the wound bed. Consequently, when the pathologist reports the FSA results to the operating room, it is challenging for the surgeon to correlate where in the patient the positive margin was identified.

Several novel imaging technologies have been utilized in surgical oncology and have been met with variable success. Narrow band imaging (NBI) has been available for many years and has been used for both early detection and screening of head and neck cancer, as well as for intraoperative margin assessment.[282, 283] The technology relies on the detection of haemoglobin, which in turn allows for enhanced visualisation of neoangiogenesis, a known phenomenon in solid tumours.[284] However, the technique is challenging to master, and is heavily reliant on the subjective interpretation of the images. Furthermore, the technique is influenced heavily by tissue properties and modified vascularity, which are often seen with tumours of the head and neck.[285] Another emerging technology for intraoperative margin analysis during oncological surgery is the use of fluorescence molecular imaging.[286-288] Fluorescently labelled antibodies allow for highly specific targeting of cancer cells and can be utilized for a myriad of imaging techniques. Leveraging this technology in the current study, we propose a novel methodology for rapid, objective and reproducible identification of the closest margin on the peripheral mucosal surface of the resected tumor specimen, termed the ‘sentinel

margin'. We have previously demonstrated that the sentinel margin strategy can be applied to evaluate the deep surface of the surgical specimen, and here we focus on the mucosal margin.[289]

Successful validation of the proposed fluorescent imaging-based specimen mapping technique would allow for more accurate sampling for FSA from the tumor specimen. This would lead to improved accuracy of intraoperative tumor margin analysis and ultimately improve patient prognosis. Furthermore, by targeting the sentinel margin for FSA, fewer samples would be required to adequately assess the entire peripheral margin, with secondary benefits such as a significantly reduced burden on the pathologist and fewer delays in operating time.

The objective of this retrospective proof-of-concept study was to determine if the 'sentinel margin' as identified by our proposed fluorescent imaging-based specimen mapping technique could accurately identify the closest surgical margin at the peripheral, mucosal border in order to improve accuracy of FSA sampling and to improve surgical orientation to the wound bed when further resection is required.

MATERIALS AND METHODS

Study design

A Phase I study evaluating panitumumab-IRDye800CW was approved by the Stanford Institutional Review Board (IRB-35064; NCT02415881). The study process, safety of panitumumab-IRDye800CW, and pharmacokinetics of the drug have been previously reported.[234] Consented patients were infused 1-5 days prior to surgery with a 50 mg dose of panitumumab-IRDye800CW. Following primary tumor resection, the mucosal surface of the tumor specimen was imaged in a closed-field fluorescence-imaging device (PEARL Trilogy, LI-COR Biosciences Inc., Lincoln, NE). The specimen was then sent to pathology for standard-of-care histological assessment. Specimens were formalin-fixed overnight and serially cross-sectioned at 5 mm intervals. These cross-sections were then further divided as necessary to fit in cassettes for paraffin embedding, after which a representative 5 μm section was cut from each paraffin block for routine H&E staining. Histopathological assessment was performed by a board-certified pathologist who outlined regions of squamous cell carcinoma on the slide. The slides were then digitized (NanoZoomer 2.0-RS; Hamamatsu Photonics K.K., Hamamatsu, Japan) and analysed for study purposes. Included in the current retrospective study were patients with OSCC whose primary tumor had less than a 1 cm depth of invasion and no cortical bone involvement. This was because patient specimens needed to be amenable to the retrospective histological analysis as described below. Therefore, 5 patients were included in this proof-of-concept study.

Fluorescent imaging-based specimen mapping

The brightfield and fluorescence images obtained from the closed-field imaging device were loaded into ImageJ (version 1.50i, National Institute of Health, Washington D.C.,

ML). Using the brightfield image of the primary tumor specimens, a mask was manually created along the periphery of the specimen, approximately 1 mm within the edge. This was to avoid any potential for edge artifact during fluorescence imaging. This mask was then applied onto the fluorescence image obtained from the closed-field imager, allowing for measurement of the fluorescence signal along the length of the mask. The raw fluorescence data is analysed in an 8-bit grayscale format, where black is taken as 0 and white is taken as 255. A graphical representation of the workflow can be found in Figure 5.1.

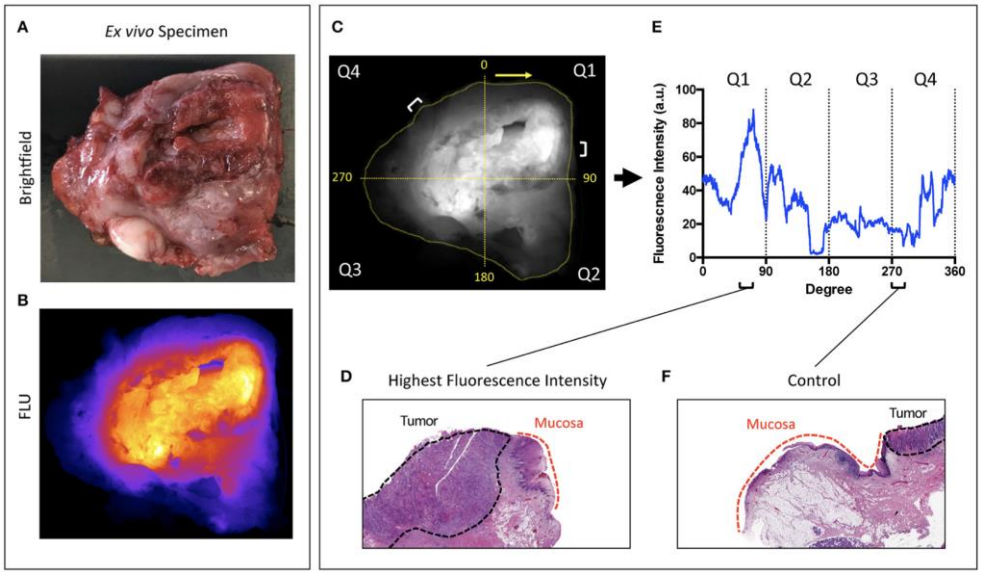

Figure 5.1 Overview of study workflow.

Representative A. brightfield and B. closed-field fluorescence image of a resected specimen. C. Fluorescent image with mask applied circumferentially around tumour margin. Specimen divided into 4 quadrants labeled Q1 – 4 clockwise from 0 degrees. D. and F. H&E slides taken from regions of highest fluorescence intensity and control region of low fluorescence intensity with tumor and normal mucosa delineated. E. Graph illustrating corresponding fluorescence intensities to peak and control at location on circumferential mask.

As the specimens were processed according to current standard-of-care for gross histological assessment, only a portion of the periphery was retrospectively analysable with available perpendicular sections of tumor to peripheral margin. From this analysable portion of the specimen, two regions of highest fluorescence intensity were selected, as well as one region of lowest fluorescence. Careful annotation of brightfield images taken throughout each stage of gross specimen processing allowed for a direct correlation of specimen fluorescence in the regions of interest with corresponding microscopic histology.

To decrease interference of interpatient variables such as dose, infusion-to-surgery window, EGFR-expression and other biological factors, patients were used as their own internal control by comparing high fluorescence regions to low fluorescence regions on the same specimen as was previously described and validated in our deep sentinel margin mapping study.[289]

Correlation of Fluorescence Signal with Margin Distance

Along the periphery of the specimen, for each of the two regions of the highest fluorescence intensity and for one region of low intensity (which served as a control), the margin distance was measured. The margin distance was defined as the distance in millimeters between the tumor edge and the specimen edge (i.e. the surgical cut) on the H&E-stained microscopic sections. First, the margin distance at the region of highest fluorescence within the analysable domain was compared to the margin distance at the lowest fluorescence intensity region. Second, to determine if the margin distance

correlated with the fluorescence signal, the margin distance at the highest fluorescence intensity region was compared to the second highest fluorescence intensity region.

In order to register the microscopic findings to the fluorescence signal on the intact specimen, the specimen was virtually reconstructed from the 5 mm thick macroscopic cross-sections. This process has been described previously. [237, 290] As the cross-sections are approximately 5 mm thick with each submitted for microscopic evaluation, the margin of error is less than 5 mm, and this margin of error does not influence the margin distances measured as the distances are in perpendicular planes. On each histological section, the margin distance was measured using ImageJ (US NIH, Bethesda, MD USA) three independent times and then averaged.

Statistical Analysis

Data was imported into GraphPad, Version 8.0c (La Jolla, California, USA), and the intra-specimen comparison of margin distance was done using the Wilcoxon-signed-ranked test. P-values of less than 0.05 were considered statistically significant.

RESULTS

Subjects

Between December 2015 and June 2018 a total of 29 patients underwent infusion of panitumumab-IRDye800 for intraoperative fluorescent imaging including *ex vivo* fluorescence imaging of their tumor specimen directly after resection. Of these patients, only five had sufficient pathological data to be included in the study. Patient and tumour characteristics are presented in Table 5.1. Imaging acquisition of the peripheral surface of the specimen took approximately 30 seconds, after which the specimen was sent to pathology and processed for standard of care assessment. As part of the retrospective analysis, the sentinel margin was identified by determining the region of highest fluorescence intensity that was closest to the specimen edge. Each serial cross-section of the specimen was also assessed by fluorescence imaging, and the sentinel margin distance was compared to all the other margin distances with low fluorescence signal obtained in the tissue sections (approximately 8-18 analysable margins per specimen). We chose to evaluate two margins as potential sentinel margins (where the fluorescence was highest and second highest at the specimen edge).

Table 5.1 Patient and tumour characteristics.

#	Age	Sex	Tumor site	Tumour stage	Tumour grade	Smoking	Alcohol	LVI
1	62	M	Buccal	T2N0Mx	II	N	N	N
2	46	M	Lateral tongue	T1N0Mx	I-II	Y	Y	N
3	69	F	Buccal	T1N0Mx	I-II	N	N	N
4	65	F	Buccal	T2N2bMx	II	Y	Y	N
5	70	F	Buccal	T3N0Mx	I	N	Y	N

Tumor stage was the pathologic staging, and tumor grade was the histologic grading (I: well-differentiated, II: moderately-differentiated, III: poorly-differentiated). Smoking and alcohol use were considered 'yes' if the patient had a prior history or was an active user. (LVI: lymphovascular invasion. N: No, Y: Yes.)

High fluorescence intensity regions (sentinel margin) vs low fluorescence intensity regions (controls)

From each primary tumor specimen, two sentinel margins were identified by determining the regions of highest fluorescence that most closely approached the cut mucosal surface of the specimen. To validate the hypothesis that this would identify the closest margin, we evaluated the margin distance at the sentinel margin compared to the margin distance at other sites, with low fluorescence available for measurement from the specimen cross-sections. In all specimens (100%), as shown in Figure 5.2, the margin distances at the sentinel margins were significantly lower than the margin distances at other regions; the average margin distance at the sentinel margins was 3.2 mm compared to 8.0 mm in other regions evaluated ($p<0.0001$).

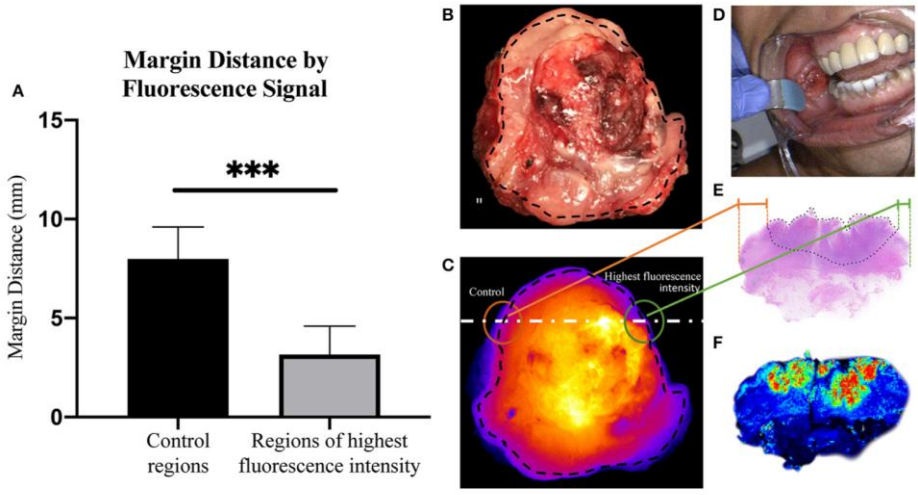

Figure 5.2 Margin distance by fluorescent signal.

A. Graph showing increase in margin distance at control regions when compared to sampled regions of highest fluorescence intensity. Representative brightfield image of resected tumor specimen B. (taken from buccal region in patient, seen in D). C. Corresponding close-field fluorescent image of resected tumor specimen with black dotted line indicating overlaid circumferential mask, white dashed line indicating slice from which H&E slide E. was taken, highlighting the difference in margin distance at the periphery between control region and region of highest fluorescence intensity. F. High resolution image taken from Odyssey demonstrating fluorescence distribution within microscopic section.

Comparison of Margin Distances at the Fluorescence Extremes

Next, we sought to determine if margin distance would increase linearly in the regions of highest to lowest fluorescence intensity along the periphery of the mucosal surface. A significant difference was found for margin distance when comparing each group (first sentinel margin, second sentinel margin, and low-fluorescence control). The sentinel margin (highest fluorescence region closest to the cut edge of the specimen) measured on average 2.4 mm, compared to 4.0 mm for the second sentinel margin and 8.0 mm for control regions ($p<0.0001$). As shown in Figure 5.3, in all the imaged specimens, the margin distance was closest at the point of highest fluorescence signal, the sentinel margin, compared to the second, with the largest margin at the low fluorescence intensity region. The average increase in margin distance when comparing the first and the second sentinel margins was 1.5±0.90 mm. Importantly, the fluorescence intensity also accurately predicted the closest margin distances when correlated with final standard-of-care histopathologic assessments by H&E staining.

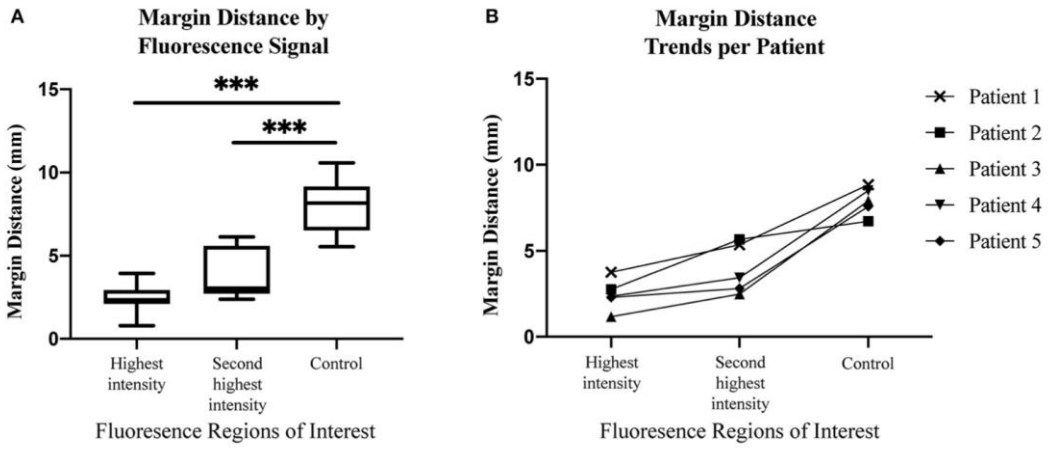

Figure 5.3 Margin distance by fluorescence regions of interest.

A. Box and whisker plots demonstrating margin distance by fluorescent signal. B. Graph demonstrating margin distance trends from region of highest fluorescence intensity to second highest fluorescence intensity, to control region per patient.

DISCUSSION

The present study demonstrates that after systemic administration of a targeted fluorescent agent, resected oral tumor specimens can be quickly imaged to determine the closest or 'sentinel' margin on the peripheral mucosal surface. This proof-of-concept study has two important clinical implications for future specimen analysis in near real-time during surgery. First, it will reduce sampling error when selecting tissue for FSA from the primary specimen. And second, by generating an immediate intraoperative image available to the surgeon and pathologist, it improves the surgeon's ability to remain oriented to which areas are sampled for FSA and aids with the accurate, targeted re-resection from the wound bed if required.

The proposed approach has previously been described by our team for targeting the closest tumor margin on the deep surface.[289] The term 'sentinel margin' was first introduced to designate the closest margin, which may or may not be positive but will be the margin most at risk. If the sentinel margin is identified as negative (>5 mm) on FSA, one could reliably predict that the rest of the margins from other areas of the tumour specimen would also be negative in the current study. Accurately selecting margins that are most at risk for being close and/or positive on FSA has potential to not only decrease the burden on the pathologist, but also to shorten the surgical procedure time. In the case where the sampled margin returns positive for carcinoma within 5 mm of the cut edge, the surgeon can resect additional tissue and repeat the FSA procedure until the margin is clear. In these instances, because tumor specimen imaging takes place on the back table in the operating room, in parallel with the operation, the surgeon can assess the fluorescence image from re-resected tissue in near-real time.

The other potential contribution of this technology to the surgical workflow is the opportunity to perform the initial assessment immediately after removal of the specimen so that the surgeon can remain oriented to the wound bed. Once the sentinel margin is identified, the surgeon can confirm the corresponding area in the wound bed and then send the specimen for pathological determination by FSA. Fluorescence images can then also be made available to the pathologist, allowing for more direct and accurate communication of the margins at risk and those sampled by FSA.

This proposed technique is built upon the knowledge that 90% of SCC in the head and neck have upregulated EGFR.[291] Antibody-based contrast agents, such as panitumumab-IRDye800CW, leverage this fact and strongly and specifically bind tumor cells with higher affinity than adjacent, healthy tissue. This allows for a robust imaging technique that can detect regions of tissue harbouring cancer. Specificity for this antibody-dye bioconjugate for its receptor has been thoroughly studied, and previous studies have demonstrated excellent specificity for EGFR.[292, 293] Although demonstrated for EGFR, this proposed technique can be used for margin assessment to any highly specific targeted-imaging agents, provided the expression of the target in tumor tissue is vastly different from that of normal tissue. Furthermore, since this technique relies on using relative fluorescence intensity differences where each patient serves as their own control, the methodology is not influenced by differences in infusion time or dosing. It is known that fluorescence imaging techniques have suffered from limitations with tissue auto-fluorescence. Fluorescent dyes in the near-infrared range of the light spectrum do not suffer from these limitations to any reasonable extent, allowing for improved contrast and deeper penetration. Depths up to around 6 mm have been reported with IRDye800CW, which is fortuitous as positive surgical margins in the head and neck are 5 mm or less.[83]

Breast and skin cancer are two other cancer types that leverage these facts and may also be amenable to the proposed intraoperative imaging-based specimen mapping technique.

A limitation of this study is its retrospective nature and therefore the low number of patients that could be included. Because accurate assessment of the margin distance requires taking a perpendicular section of tumor to the closest (sentinel) margin, microscopic assessment of the relevant fluorescent area was possible only in select cases retrospectively. Nevertheless, we feel that since each specimen had numerous peripheral margins analysed, the current data is sufficient to ensure the robustness of this methodology. However, in order to further evaluate the clinical efficacy of this technique, a larger prospective trial is warranted where sentinel peripheral margins highlighted fluorescently on the back table are correlated to clinical suspicion prior to undergoing selective FSA as appropriate. Such a trial investigating the accuracy of sentinel deep and peripheral margins using this technology is currently underway at our institution.

CONCLUSION

This retrospective, proof-of-concept study demonstrates that regions of highest fluorescence intensity on the periphery of the resected tumor specimen correlate with the closest mucosal margin, the 'sentinel margin'. The clinical application of this specimen mapping technique to surgical management would allow identification of the sentinel margin for more accurate and efficient intraoperative sampling. Fluorescence-guided FSA could thus reduce diagnostic error secondary to specimen sampling and expedite the pathology workflow. When additional resection is required following FSA, near real-time fluorescent imaging can facilitate improved communication of positive or close margins between the surgeon and pathologist by maintaining orientation of the specimen to the wound bed and aiding with completeness of resection. With these benefits in mind, this *ex vivo* near real-time imaging strategy has great potential to ultimately improve margin control rates in oncological head and neck surgery.

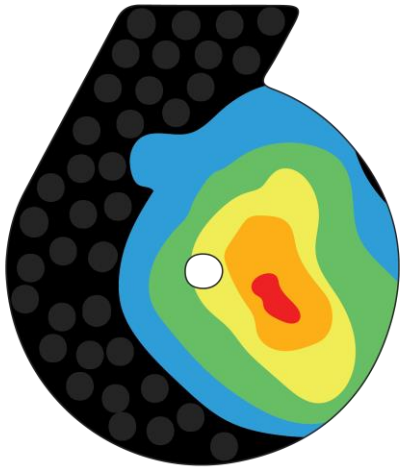

CHAPTER 6: FLUORESCENT MOLECULAR IMAGING CAN IMPROVE SENTINEL MARGIN DETECTION IN ORAL SQUAMOUS CELL CARCINOMA

STATEMENT OF AUTHORSHIP

Title of paper	Fluorescent molecular imaging can improve intraoperative sentinel margin detection in oral squamous cell carcinoma
Publication status	☐ Published ☐ Accepted for Publication ✓ Submitted for Publication ☐ Unpublished and Unsubmitted work written in manuscript style
Publication details	Krishnan G, van den Berg NS, Nishio N, Kapoor S, Pei J, Freeman L, Lee YJ, Zhou Q, van Keulen S, Fakurnejad S, Condon C, Baik FM, Martin BA, Rosenthal EL. Fluorescent molecular imaging can improve intraoperative sentinel margin detection in oral squamous cell carcinoma. *Submitted to Journal of Nuclear Medicine. 2021 August.*

Principal Author

Name of Principal Author (candidate)	Giri Krishnan		
Contribution to the Paper	Study conception and design. Data collection, analysis and interpretation. Manuscript preparation.		
Overall percentage (%)	75%		
Certification	This paper reports on original research I conducted during the period of my Higher Degree by Research candidature and is not subject to any obligations or contractual agreements with a third party that would constrain its inclusion in this thesis. I am the primary author of this paper		
		Date	20.09.2021

Co-Author Contributions

By signing the State of Authorship, each author certifies that:

i. The candidate's stated contribution to the publication is accurate (as detailed above);
ii. Permission is granted for the candidate in including the publication in thesis; and
iii. The sum of all co-author contributions is equal to 100% less the candidate's stated contribution.

Name of Co-Author	Nynke S. van den Berg
Contribution to the Paper	Study conception and design. Data collection, analysis and interpretation. Manuscript preparation.

Signature		Date	28.09.2021

Name of Co-Author	Naoki Nishio		
Contribution to the Paper	Data analysis and interpretation. Manuscript preparation.		
Signature		Date	23.09.2021

Name of Co-Author	Shrey Kapoor		
Contribution to the Paper	Data organisation.		
Signature		Date	06.10.2021

Name of Co-Author	Jaqueline Pei		
Contribution to the Paper	Data collection and analysis.		
Signature		Date	05.10.2021

Name of Co-Author	Laura Freeman		
Contribution to the Paper	Data collection and analysis.		
Signature		Date	28.09.2021

Name of Co-Author	Yu-Jin Lee		
Contribution to the Paper	Data collection and analysis.		
Signature		Date	23.09.2021

Name of Co-Author	Quan Zhou		
Contribution to the Paper	Data collection and analysis.		
Signature		Date	24.09.2021

Name of Co-Author	Stan van Keulen		
Contribution to the Paper	Study conception and design. Data collection, analysis and interpretation.		
Signature		Date	03.10.2021

Name of Co-Author	Shayan Farkurnejad
Contribution to the Paper	Study conception and design. Data collection, analysis and interpretation.

Signature		Date	27.09.2021

Name of Co-Author	James Condon		
Contribution to the Paper	Statistical design. Statistical data analysis and interpretation.		
Signature	JJJ Condon	Date	24.09.2021

Name of Co-Author	Fred M. Baik		
Contribution to the Paper	Surgical management of patients and acquisition of tissue samples. Manuscript preparation.		
Signature		Date	06.10.2021

Name of Co-Author	Brock A. Martin		
Contribution to the Paper	Pathological assessment of all specimens. Data analysis and interpretation. Manuscript preparation.		
Signature		Date	24.09.2021

Name of Co-Author	Eben L. Rosenthal		
Contribution to the Paper	Supervision of study. Study conception and design. Surgical management of patients and acquisition of tissue samples. Data analysis and interpretation. Manuscript preparation and finalisation.		
Signature		Date	24.09.2021

ABSTRACT

Rationale

Current practices during head and neck cancer resections result in a 20-30% rate of positive margins which translates to an increased risk of local tumour recurrence. A major limitation of current intraoperative margin analysis is the ability to detect areas most likely to be positive based on specimen palpation. This is especially true for larger specimens where sampling error limits detection of positive margins. This study aims to address this by prospectively examining the clinical value of fluorescent molecular imaging to accurately identify "the sentinel margin," the point on a specimen where tumour lies closest to the resected edge in real-time during frozen section analysis.

Methods

Eighteen patients with OSCC were enrolled into a prospective clinical trial and infused IVly with 50mg of Panitumumab-IRDye800CW 1-5 days prior to surgery. Resected specimens were imaged in a closed-field near-infrared optical imaging system in near-real time, and custom designed software was used to identify locations of highest fluorescence on deep and peripheral margins. The surgeon identified the sentinel margin blinded to optical specimen mapping, and then the regions of highest fluorescence were identified and marked for frozen analysis. Final pathology based on specimen reconstruction was used as reference standard.

Results

Resected specimens were imaged immediately in the operating room and included partial glossectomy (5/18, 28%), hemiglossectomy (2/18, 11%), total glossectomy (1/18, 6%), partial maxillectomy (2/18, 11%), RMT composite resections (6/18, 22%), buccal

mucosal wide local excisions (2/18, 11%). Fluorescence had a higher interobserver agreement with pathology (Cohen kappa value 0.96) than the surgeon (Cohen kappa values of 0.82) for the location of the closest margin. Plotting margin distance at the predicted sentinel margin location of each observer versus the actual closest margin distance at pathology demonstrated best correlation between fluorescence and pathology ($R^2 = 0.98$), with surgeon ($R^2 = 0.75$).

Principal conclusions

Fluorescent image-guided analysis of specimens can improve identification of the true closest margin in resections when compared to currently accepted clinical standards of care and holds significant promise for rapid identification of positive margin rates and improve oncological outcomes in head and neck cancer.

Key words

Head and neck cancer, Oral squamous cell carcinoma, Tumour margins, Fluorescent image-guided surgery, Surgical oncology

INTRODUCTION

In HNSCC, surgery requires balancing complete tumour clearance with conservation of uninvolved tissue to preserve breathing, speaking and swallowing function. Achieving adequate margins can be particularly challenging [82] and it is well-established that positive margins in HNSCC are associated with local recurrence and decreased OS and despite advances in operative technique and surgical technology, positive margin rates have remained unchanged over the past 30 years [278, 294].

Assessment of the tumour specimen to identify positive margins immediately following removal allows the surgeon the opportunity to resect further tissue from the wound-bed if required to ensure adequate tumor clearance. Currently this involves visual inspection and palpation of the specimen by the surgeon, with sampling of areas of concern from the specimen or wound bed intraoperatively for FSA [118]. This process is inconsistent, surgeon dependent and is complicated by sampling error in larger specimens [295].

In a retrospective analysis of HNSCC specimens from patients that were pre-operatively infused with a fluorescent antibody-dye conjugate (panitumumab-IRDye800CW), our group recently demonstrated that ex vivo fluorescent imaging allowed the identification of the point on a specimen surface where tumour comes closest to the resection edge – the ‘sentinel margin’ in peripheral mucosal margins and for the deep margin [240, 296]. Based on this, we hypothesize that an objective, focused assessment of the specimen using optical imaging may reduce false negatives during intraoperative margin assessment, maintain orientation of sampled areas on the specimen to the wound bed and streamline the margin assessment process. The aim of the present study was to evaluate

the accuracy and clinical value of fluorescent molecular imaging for intraoperative sentinel margin identification in HNSCC by comparing it prospectively to current clinical practice.

MATERIALS AND METHODS

Clinical Trial Design

Between June 2018 and December 2019, patients with biopsy proven primary or recurrent OSCC scheduled for curative surgery were enrolled into a prospective single centre, non-randomised, clinical trial evaluating the fluorescence molecular imaging agent panitumumab-IRDye800CW. The trial was approved by the Stanford University Administrative panel on Human Subjects research and the FDA, and registered with ClinicalTrials.gov (NCT03733210; NCT02415881; NCT03405142). This study was performed in accordance with the Helsinki Declaration of 1975 and its amendments, FDA's ICH-GCP guidelines and the laws and regulations of the United States. Written informed consent was obtained from all patients.

Panitumumab-IRDye800CW

Pantiumumab-IRDye800CW is a tumour targeted fluorophore composed of the antibody panitumumab (Vectibix; Amgen, Thousand Oaks, California, United States), which is conjugated with the near-infrared fluorophore IRDye800CW, which has an absorption maximum of 774nm and an emission maximum of 789nm [226-228]. Panitumumab is a fully-humanized monoclonal IgG2 antibody, that binds with high-affinity to EGFR, a protein of the ErbB family that is overexpressed in head and neck cancers [229]. IRDye800CW has been demonstrated to have low toxicity and short half-life when unconjugated [230]. As part of the conjugation process, a NHS ester reaction binds randomly to lysines throughout the antibody during a relatively simple labelling method that has been performed successfully for chimeric and fully human antibodies with a consistent dye to protein ratio and good imaging results [231, 232]. Studies have

demonstrated that re-purposing the therapeutic antibody pantiumumab, as a diagnostic imaging agent with its fluorescent IRDye800CW label, is safe and stable, with a low rate of adverse events (7.4%) that is consistent with the rate of panitumumab alone [232-235].

Study Workflow

Enrolled patients were infused IVly with 50 mg of panitumumab-IRDye800CW 1-5 days prior to surgery. The study workflow is outlined in Figure 6.1. In the operating room, primary tumour specimens, as well as sampled margins for FSA, were imaged *ex vivo* on the back table immediately following removal from the patient in a closed-field near-infrared optical imaging system IGP-ELVIS, LICOR Biosciences, Inc. Nebraska, US [241]. All primary tumour resections were 3D and were therefore repositioned within the closed-field near-infrared optical imaging system to capture each surface in a two-dimensional (2D) plane. Imaged surfaces were denoted 'mucosal' if they primarily captured the mucosal aspect of the resection (Figure 6.1A). All other surfaces were denoted 'deep' (Figure 6.1B). Only imaged surfaces that required pathological evaluation by the surgical team were included in the study analysis.

Acquired images were exported as tag image file format (TIFF) files from the optical imaging system to a laptop for near-real time fluorescent analysis of the sentinel margin using ImageJ software (version 1.50i, NIH, Washington D.C, MD). This analysis has been previously described by our team [240, 296]. Briefly, for images taken of mucosal surfaces, a mask was manually fitted around the periphery of the specimen within 1mm of the resection edge using a free-hand drawing tool. The standard 'plot profile' analysis function was then used to graph the raw fluorescence data of each point along the mask in an 8-bit grayscale format enabling isolation of the area of highest fluorescence on the

periphery (Figure 6.1C). For images taken of specimen deep surfaces, a 3D signal-mapping tool (ImageJ plugin, interactive 3D surface plot) was used to scale and isolate the area of highest fluorescence intensity (Figure 6.1D). Areas of highest fluorescence on the deep and mucosal surfaces were denoted the presumptive sentinel margins as per fluorescence analysis.

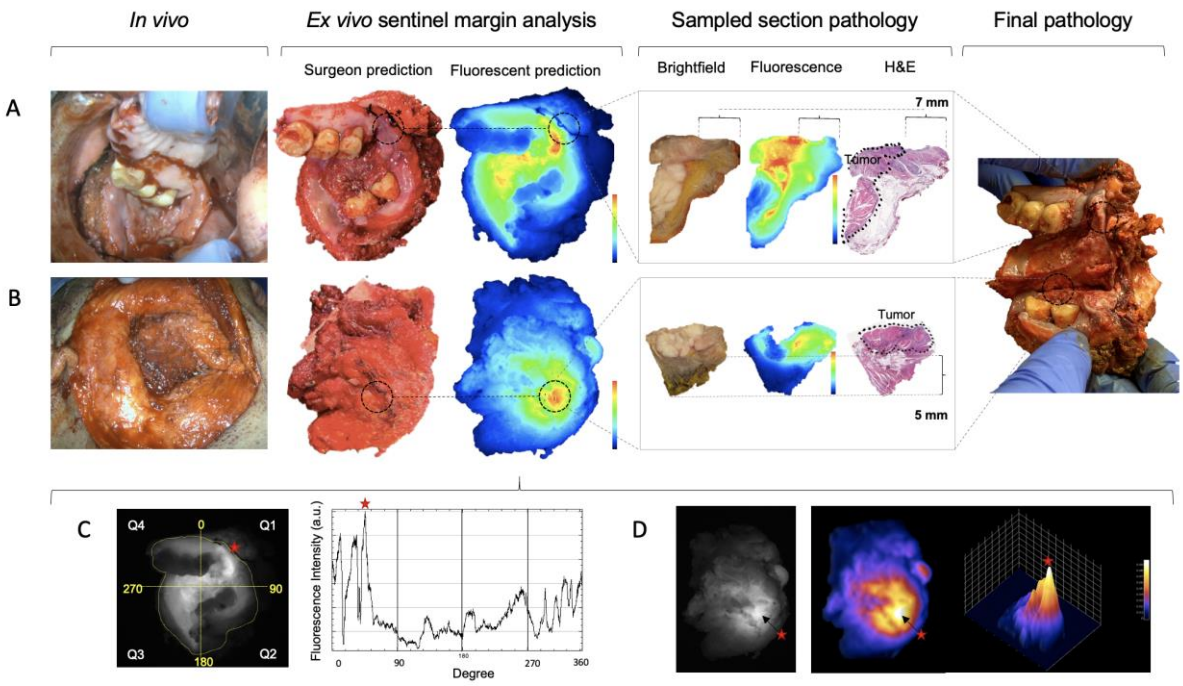

Figure 6.1 Study workflow.

Study workflow demonstrated in representative patient 18 with a right sided RMT squamous cell carcinoma. The patient was infused with 50mg of IV Panitumumab-IRDye800CW three days prior to surgery. From left to right, the workflow shows the lesion in vivo and then ex vivo, examining the (A) mucosal, and (B) deep surfaces of the resection. On both surfaces the surgeon and fluorescence agreed as to the location of the sentinel margin. Sampled tissue from these locations underwent closed-field fluorescent imaging and then H&E staining to evaluate the margin distance. Following

this the specimen was examined at final pathology. C. Mucosal surface fluorescent sentinel margin analysis in this patient as demonstrated by a mask manually fitted around the periphery of the specimen within 1mm of the resection edge followed by a graph showing the raw fluorescence data of each point along the mask in an 8-bit grayscale format enabling isolation of the area of highest fluorescence on the periphery (represented by the red star). D. Deep surface fluorescent sentinel margin analysis as demonstrated by using the 3D signal-mapping tool to scale and isolate the area of highest fluorescence intensity (represented by the red star).

To compare our fluorescent analysis against current clinical practice, the primary board-certified surgeon involved in the case and blinded to fluorescence was asked to identify the point where they thought that tumour came closest to the specimen edge after specimen removal from the patient. This was often done following specimen removal at pathology in collaboration with the pathologist. Their orientation of the specimen and demarcation of the sentinel margin was photo and video documented. This photo was then used to compare the point of highest fluorescent signal on that surface by registering the two images against each other. A margin of error equivalent to one bread-loaf at pathology was used when comparing each prediction against final pathology as gold-standard. Individual bread loafs are approximately 5mm thick[89], therefore if the surgeon or fluorescence is within 5 mm of the true sentinel margin, this would fall within the realms of "close enough" to ink activating the pathologist to do selected radial margins in the area of concern. Where there was clinical concern that the specimen had close or positive margins, frozen sections were taken from the presumptive sentinel margins demarcated by the surgeon. These frozen sections were processed and analysed as

standard of care and the results were reported to the operating team for intraoperative action as appropriate. As per the NCCN guidelines, margins were defined in this study as "clear" if ≥ 5mm from invasive tumour, close if < 5mm from invasive tumour and positive if invasive carcinoma or carcinoma in situ was present at the specimen edge [43, 96].

At the completion of surgery, the primary tumour specimen underwent routine pathological processing and assessment. All tissue cassettes were re-imaged in the closed-field imaging device (LI-COR Biosciences) prior to paraffin embedding. A standard synoptic report was generated by a board-certified pathologist, which included identification of the final closest margin location and distance on mucosal and deep surfaces as seen on H&E slides. This served as the gold-standard to compare the sentinel margin predictions of the surgeon and fluorescence against.

EGFR expression and quantification

To examine the expression of EGFR at regions of interest where tumor came closest to the resected specimen edge, automated IHC staining was performed on contiguous sections with Dako Autostainer (Agilent Technologies, Santa Clara, CA, USA) for EGFR (prediluted, RM-2111-RQ, Thermo Fisher Scientific, Waltham, MA, USA) with secondary antibody: Envision FLEX+ rabbit (linker) (prediluted, SM805, Agilent Technologies). Immunoreactivity was visualized with diaminobenzidine and magenta chromogens (Dako EnVision, Glostrup, Denmark). Digital images of IHC-stained EGFR slides were obtained at 4 – 20 magnification with a whole slide scanner (NanoZoomer 2.0-HT slide scanner; Hamamatsu Photonics, Hamamatsu City, Japan). Tumor regions were annotated on slides using Aperio's annotation software (ImageScope Viewing Software: Positive Pixel Count v9.1, Aperio ImageScope®; Leica Microsystems Inc.) and

the intensity of staining was graded as follows: negative, weak positive (Intensity Threshold weak [upper limit] = 220, [lower limit] = 175), medium ([upper] = 175, [lower] = 100), and strong ([upper] = 100, [lower] = 0) by default. The staining of EGFR was quantified by IHC positivity, which was calculated as the number of positive pixels stained at each positive intensity level divided by the total number of pixels (the number of positive and negative pixels).

Statistical Analysis

All tumour specimen surfaces analysed were entered into a spreadsheet (Microsoft Excel version 2019) and the location of the predicted sentinel margin from each observer was recorded. In order to map all predicted sentinel margin locations against final pathology, locations were recorded categorically according to which pathology cassette they belonged to. Where two sentinel margin predictions were located on separate areas of the same tumour cassette, they were further differentiated with reference to their orientation on the cassette. A ruler was used to measure the distance in millimetres from tumour edge (marked by a board-certified pathologist) to the specimen edge at each predicted sentinel margin on stained H&E slides. MFI, defined as total counts per pixel area, divided by pixel area, was calculated for each acquired image of tissue taken intraoperatively for FSA using ImageStudio software (LI-COR Biosciences Inc.). MFI data was correlated to final tumour status (positive or negative).

Scipy (version 1.4.1), Scikit-learn (version 0.22.2) and GraphPad Prism (version 8.0c) were used for statistical analysis. Cohen kappa (k) statistic was used to assess the strength of agreement of sentinel margin location of the two observers (surgeon and fluorescence) independently against the gold-standard (final-pathology). Accuracy and error rate of

sentinel margin location of each observer was calculated using standard statistics. The 95% confidence interval of each observer's accuracy was calculated based on a t-distribution. Accuracy p-values were calculated based on the number of cassettes for each specimen, with respect to random choices. Pearson and spearman correlation coefficients were calculated for margin distances at predicted sentinel margin locations of each observer against the actual closest margin distance at final pathology. A two-sided p-value of 0.05 or less was considered statistically significant.

RESULTS

Primary tumour specimens from 18 patients were included in this study with 28 specimen surfaces imaged and analysed. Of the surfaces imaged, 16 (57%) were mucosal and 12 (43%) were deep. Tumours were located in the lateral tongue (8/18, 44%), RMT (4/18, 22%), buccal mucosa (4/18, 22%), hard palate (1/18, 6%) and alveolus (1/18, 6%).

The pT-stages of included tumours were pT2 (6/18, 33%), pT3 (4/18, 22%), pT4 (8/18, 44%). Resections performed included partial glossectomy (5/18, 28%), hemiglossectomy (2/18, 11%), total glossectomy (1/18, 6%), partial maxillectomy (2/18, 11%), RMT composite resections (6/18, 22%), buccal mucosal wide local excisions (2/18, 11%)

Observer Agreement and Accuracy in Sentinel Margin Prediction

The predicted sentinel margin location and corresponding measured margin distances at these locations per observer compared to final pathology is summarised in Table 6.1. Overall, areas of highest fluorescence intensity strongly correlated final pathology with a Cohen kappa value of 0.96. The surgeon also had a relatively lower correlation with final pathology (Cohen kappa value of 0.81). The accuracy of fluorescence intensity to identify the true sentinel margin was 96.4% (95% CI 89.1 – 100, P <0.001) compared to the surgeon at 82.1% (95% CI 67.0 – 97.3, P < 0.001) as summarised in Table 6.2. Plotting the margin distance at the predicted sentinel margin of each observer versus the actual closest margin distance at final pathology demonstrates better correlation betw een fluorescence and final pathology (R^2 = 0.98, 95% CI 0.93 – 1.00, P < 0.001) compared to the surgeon and final pathology (R^2 = 0.75, 95% CI 0.73 – 1.00, P < 0.001) (Figure 6.2).

Table 6.1 Summary of interobserver prediction of sentinel margin location and corresponding margin distance versus actual closest margin location and distance at pathology.

Specimen					Predicted sentinel margin location (pathology cassette)			Distance at predicted sentinel margin (mm)		
#	Tumor site	pT	Resection	Surface	Surgeon	Flu	Pathology	Surgeon	Flu	Pathology
1	Lateral tongue	T3	Partial glossectomy	Deep	C11	C11	C11	0	0	0
				Mucosal	C4	C11	C11	10	2	2
2	Lateral tongue	T3	Partial glossectomy	Deep	C8	C14	C14	2	1	1
3	Lateral tongue	T4a	Partial glossectomy	Deep	A1	A1	A1	3	3	3
4	Lateral tongue	T4a	Hemi glossectomy	Deep	FSD 1	FSD 1	FSD 1	2	2	2
				Mucosal	D6	D6	D6	11	11	11
5	Hard palate	T4a	Maxillectomy	Deep	FSB	FSB	FSB	1	1	1
				Mucosal	FSD	FSD	FSD	7	7	7
6	Retromolar trigone	T4	Maxillectomy	Deep	FSA	FSA	FSA	0	0	0
				Mucosal	FSD	FSD	FSD	5	5	5
7	Retromolar trigone	T3	RMT composite resection	Mucosal	FSC	FSC	FSC	0	0	0
				Mucosal	C2	C2	C2	4	4	4
8	Lateral tongue	T2	Partial glossectomy	Mucosal	A5	A5	A8	3	3	1
9	Lateral tongue	T2	Partial glossectomy	Mucosal	A6	A6	A6	5	5	5
				Deep	C4	C4	C4	6	6	6
10	Retromolar trigone	T4a	RMT composite resection	Deep	FSB3	FSB3	FSB3	1	1	1
				Mucosal	FSB2	FSB2	FSB2	1	1	1
11	Lateral tongue	T2	Partial glossectomy	Mucosal	FSB1	FSB1	FSB1	0	0	0
				Deep	B1	B1	B1	1	1	1
12	Lateral tongue	T4a	Hemi glossectomy	Deep	FSC1	FSC1	FSC1	0	0	0
				Mucosal	FSC2	FSC2	FSC2	5	5	5
13	Retromolar trigone	T4a	Mandibulectomy	Mucosal	O9	O20	O20	8	4	4
14	Retromolar trigone	T4a	RMT composite resection	Mucosal	FSI	FSI	FSI	10	10	10
15	Buccal	T2	WLE	Deep	FSB	B10	B10	1	1	1
16	Alveolar ridge	T2	Mandibulectomy	Mucosal	D8	D8	D8	4	4	4
16	Buccal	T2	WLE	Mucosal	FSA	FSA	FSA	2	2	2
18	Retromolar trigone	T3	RMT composite resection	Mucosal	B11	B11	B11	7	7	7
				Deep	B16	B16	B16	5	5	5

(pT: pathological T-stage, RMT: Retromolar trigone, Flu: Fluorescence)

Table 6.2 Accuracy of observer at identifying the final closest margin location.

	Interobserver agreement with final pathology (Cohen kappa)	**Accuracy (%)**	**95% confidence interval**	**Error rate (%)**	**P value**
Surgeon	0.82	0.64	(0.45, 0.83)	17.9	< 0.001
Fluorescence	0.96	0.86	(0.72, 1.00)	3.6	< 0.001

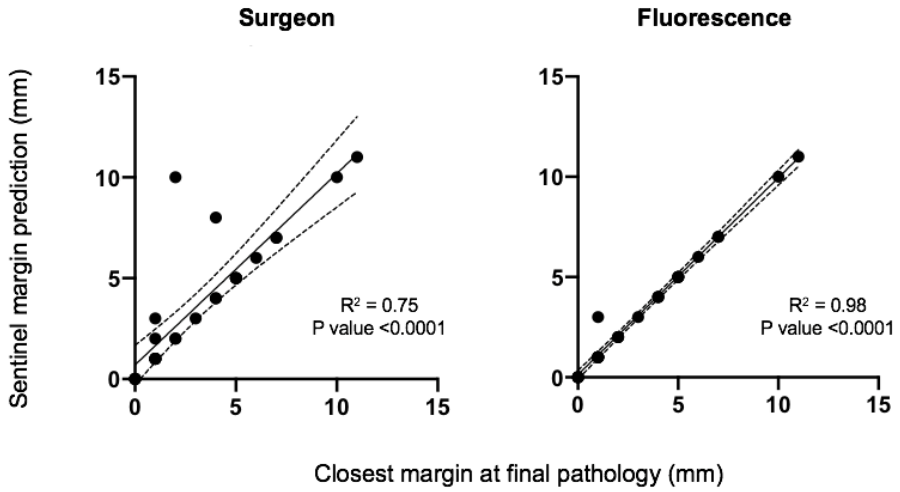

Figure 6.2 Correlation between distance at predicted sentinel margin by observer with distance of closest margin on final pathology.

Clinical Value of Fluorescence in Sentinel Margin Analysis

Closer examination of the cases where the techniques of margin assessment failed to correctly identify the sentinel margin can aid understanding of the clinical value of ex vivo molecular imaging. Overall, the surgeon's prediction of the sentinel margin disagreed with final pathology in 4 out of 28 cases compared to 1 out of 28 cases with fluorescence. In the one instance where fluorescence disagreed with final pathology, the fluorescent predicted sentinel margin location was in concordance with the surgeon's prediction. Therefore, if improved surgical decision making is defined as instances when fluorescence imaging changes the surgical procedure to improve surgical outcomes, there would have been a clinically significant improvement in intraoperative frozen section sampling in 3/28 (10.7%) surfaces analysed.

Figure 6.3 demonstrates a case where there was a separate smaller focus of tumor that was close (1mm) to the mucosal surface of a partial glossectomy specimen that was not identified by fluorescence as being the area of greatest signal. In this case, the main centrally located tumor measured 1.3cm in diameter and invaded to a depth of 6mm. At final pathology, it came closest to the specimen edge superiorly, at a point accurately identified by both fluorescence and the surgeon to be the closest margin for this tumour (3mm). The smaller separate focus of tumor, measured 8mm in diameter and invaded to a depth of 3.5mm, and was not macroscopically visible. It registered as the third highest region of fluorescent signal on the peripheral margin. IHC staining and EGFR quantification of the regions where each focus of tumour came closest to the peripheral margin demonstrated EGFR expression at both points, but with higher EGFR expression (81.2%) where there was macroscopically visible disease on the main tumour focus versus (43.2%) on the smaller secondary focus.

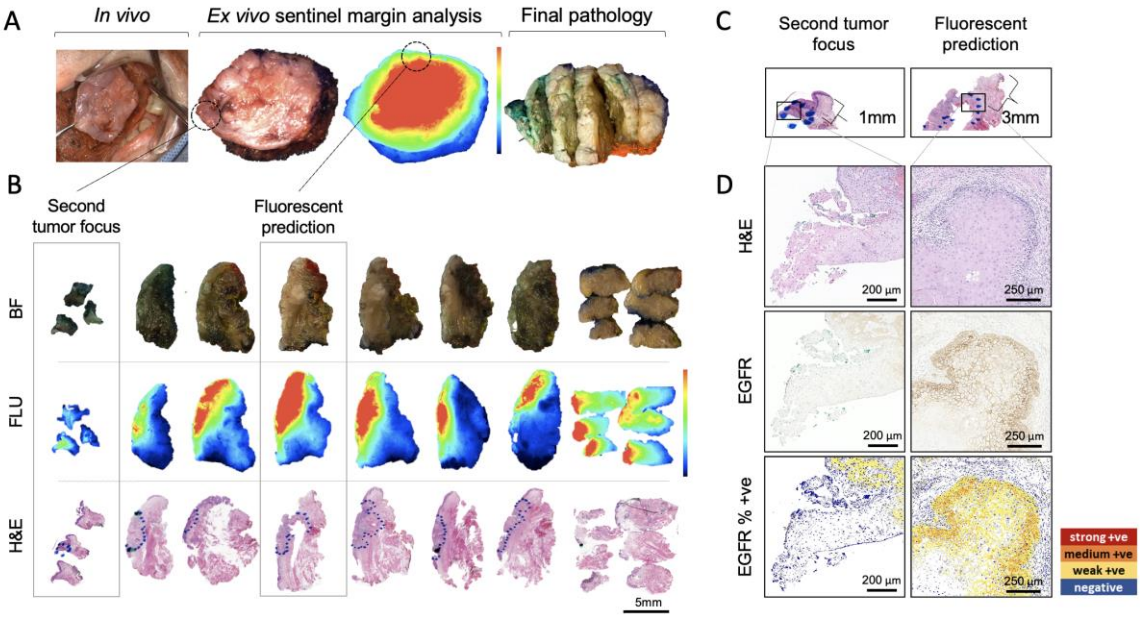

Figure 6.3 Closer analysis of the case where both molecular imaging and conventional margin analysis missed a sperate microscopic focus of tumor that was identified at final pathology to come closer to the resection edge.

A. Specimen evaluation workflow demonstrating firstly the partial glossectomy resection in situ, and then the ex vivo specimen imaged in brightfield and closed-field fluorescence, followed by a depiction of the specimen bread loafed at final pathology. B. Bread loafs of the specimen taken during pathological grossing are lined-up to demonstrated their appearance in brightfield, fluorescence and corresponding H&E slides with blue dots outlining tumour boundaries on the mucosal surface of the specimen as marked by the board-certified pathologist. C. Magnified view of two bread loafs demonstrating margin distance of 3mm, where surgeon and fluorescence predicted the sentinel margin on the main tumor, compared to a margin distance of 1mm where a the sperate secondary focus of tumor came close to the anterior specimen edge. D. Slides confirming the presence of SCC and EGFR expression at the point on each tumor focus closes to the margin edge. In the main tumour, EGFR expression was quantified at 81.2% compared to 43.2% at the secondary focus.

In the three cases where the fluorescent sentinel margin prediction outperformed conventional palpation by the surgeon, the final margin was close (<5mm) in all cases. The three cases are summarized in Figure 6.4. Figure 6.4A shows a pT3 right lateral tongue SCC, where the surgeons prediction appears to show ulcerated tumour close to the anterior/inferior margin, however, measurement of the tumour edge to the mucosal margin at the floor of mouth revealed a distance of 10mm. In comparison, fluorescence identified the location of highest signal posteriorly and at final pathology, tumour was found extending just under the surface to within 2mm of the peripheral resected edge. Figure 6.4b demonstrates pT4a right lateral tongue SCC, where the surgeon palpated a nodule on the deep surface that was slightly more anterior to the true sentinel margin and was only was within 1 mm of the final closest margin distance. Figure 6.4C demonstrates a composite T4a resection where all peripheral margins were reported by the pathologist to be greater than 5mm from tumour. Fluorescence identified an area of increase signal in the inferior medial aspect of the specimen which was found to be soft tissue underlying the mucosal fold where tumor came within 4mm of the resected peripheral margin.

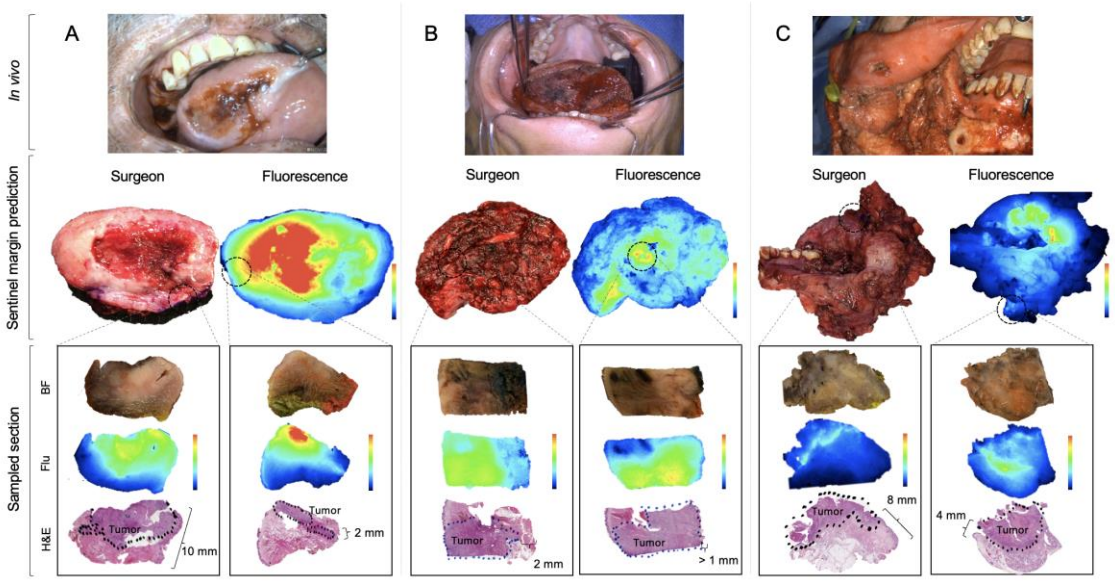

Figure 6.4 Cases where fluorescence sentinel margin identification demonstrated improved identification of the true closest margin when compared to conventional analysis technique by the surgeon.

A. Demonstrates Patient 1 with a pT3 right lateral tongue SCC. This patient was infused with Panitumumab-IRDye800CW 2 days prior to surgery. B. Demonstrates Patient 2 with a pT4a right lateral tongue SCC. This patient was infused with Panitumumab-IRDye800CW 1 day prior to surgery. C. Demonstrates Patient 13 with a pT4a right retromolar SCC infused 2 days prior to surgery.

(Flu: Fluorescence, BF: Brightfield)

DISCUSSION

This prospective study compares fluorescence with current intraoperative margin assessment, evaluated against final pathology as the gold-standard. It builds on previous retrospective studies conducted by our group where we developed the concept of sentinel margin detection using fluorescence in which we described the identification of the sentinel margin on the deep and mucosal surface using relative fluorescence intensities [240, 296]. In these studies we found that margin distance inversely correlated with the areas of highest fluorescent intensity such that margin distances decreased from areas of highest fluorescence to lowest fluorescence in each specimen. These studies laid the foundation for the current prospective trial, but were limited by their retrospective nature, which meant that only specimens where measurable bread loafs coincided with the intensity peaks on the deep surface, or areas of highest fluorescence intensity on the peripheral surface, could be included for analysis. It is important to note that tissue is relatively homogenous so the optical properties are disrupted allowing this technique to work consistently across specimens. Furthermore, although EGFR is heterogenous across the different patient cancer specimens, it is high enough to allow fluorescence to penetrate through the tissue margin. This study, unlike previous research in this technique is a prospective comparison to the surgeon.

This study demonstrates that *ex vivo* fluorescent molecular imaging of head and neck resections can improve objective detection of tumour that comes closest to the specimen edge when compared to standard of care, which was exemplified in 11% of cases where fluorescence-based sentinel margin assessment outperformed standard of care pathological assessment by the surgeon, suggesting that this approach has the potential to

improve positive margin rate outcomes. Accurate isolation of the sentinel margin within minutes of resection, in the operating room has several significant benefits. Of highest clinical priority, it promises to minimize false negative intraoperative margin assessment [127]. From a hospital resource utilisation standpoint, reduced tissue sampling and reduced frozen section analyses during surgery streamlines operative workflow and decreases demand on pathology [133, 297]. By identifying the sentinel margin in the operating room immediately after surgical resection, there is also promise for improved *in vivo* and *ex vivo* orientation of the resected specimen to the wound bed by the surgeon, which is necessary for precise re-resection from the wound bed when required, although this particular benefit was not assessed here and requires focused evaluation in future studies [131, 132]. Anecdotally in this study, fluorescence imaging followed by sentinel margin analysis took approximately 5 to 10 minutes to complete (depending on the complexity of the specimen and how many surfaces were being imaged) whereas frozen sectioning typically takes 20-30 minutes per FSA. Hence, additional benefit can be found in providing directional information to the pathologist for areas to be assessed by FSA.

All 18 HNSCC specimens in this study originated from the oral cavity, but resection units varied, including glossectomies, maxillectomies, mandibulectomies and composite resections. Our findings demonstrate that fluorescence molecular imaging of complex 3D resections involving soft tissue and bone is feasible and this is a significant strength of this study, as current *ex vivo* margin analysis in these complex specimens is particularly difficult [298]. It is in these resections that there is a short window-of-opportunity for surgeon orientation of specimen to wound bed, and where communication of margin locations between surgeon and pathologist are prone to error [299].

Evaluation of the four clinically relevant cases where the sentinel margin prediction was wrong revealed significant insights. In the single case where fluorescence failed to identify a close margin, traditional methods of palpation and visualization in white light were also unsuccessful. In this case, while accurately identifying the closest margin where the main tumour came within 3mm of the resection edge, fluorescence missed a microscopic separate focus tumour that came within 1mm of the resection edge. Prior to undertaking this study, we hypothesized that there could be two potential factors that could impact on the accuracy of fluorescent sentinel margin identification, which were positioning and intratumoural heterogeneity of EGFR [240, 286]. This case however, highlights the possibility that fluorescence is susceptible to missing smaller tumour satellites that come close to the resection surface. In this case, the incidental secondary focus of tumor which came closer to the resection margin was significantly smaller in size and tumour burden than the main focus and had an associated lower EGFR expression (43.2% versus 81.2%) that corresponded to a lower fluorescence intensity. In this particular case, the small tumour satellite registered the third highest peak in fluorescence on the periphery of the specimen providing some insight into the resolution of this technique for picking up microscopic disease. While it is probably not practical to sample multiple areas of high fluorescence for all cases, based on this finding and in line with the results of our previous studies, we would advise for future use of this technology that the clinician examine at least the first two to three regions of high fluorescent signal on a specimen surface and sample from these as appropriate in the context of clinical suspicion [240]. In this case, sampling the three areas of highest fluorescence on the peripheral margin would have picked up this separate focus of microscopic disease that was not visually detectable or palpable consistent with results from previous studies that have employed this approach for fluorescent margin assessment.[296].

In one of the three cases where fluorescence was superior to the surgeon sentinel margin prediction, the standard approach still identified a close margin of 2mm. This highlights an important clinically relevant point, which is that there may be more than one location on a specimen surface, and multiple surfaces on one specimen for that matter, where tumour comes close to the resection edge. It is precisely in these cases where fluorescence can be of significant added value, as re-resection from the wound-bed at multiple locations may be necessary and without fluorescence guidance may be missed.

In this study we used a fixed dose of 50mg of panitumumab-IRDye800CW, which we have previously identified as part of a dose-ranging study to be the optimal dose for use in the clinic [300]. Panitumumab was initially approved by the FDA in September 2006 as a chemotherapeutic agent for EGFR-expressing metastatic colorectal cancer and is currently used for this indication at a dose of 6mg/kg [226]. As such, our fixed dose of the antibody-dye conjugate for diagnostic purposes is actually a subtherapeutic dose of panitumumab. IRDye800CW has been demonstrated to have low toxicity and short half-life when unconjugated [230]. We have previously demonstrated that re-purposing the therapeutic antibody as a diagnostic imaging agent fluorescent labeling is safe and effective [232-235].

Patients were infused 1-5 days prior to surgery with panitumumab-IRDye800CW although the ideal timing of infusion prior to surgery lies at < 3 days based on data showing that MFI significantly increased when the infusion-to-surgery window was within this range [300]. The window was left broader than this range in order to improve

study recruitment and improve logistical challenges of appointment availability and surgery scheduling.

The work is agnostic to the fluorescent agent used for surgical imaging. The specimen imaging techniques described will apply to any of the many agents currently under development, including the use of γ-glutamyl hydroxymethyl rhodamine green [301], indocyanine green [302] and urokinase-like plasminogen activator receptor [303]. In addition, it is also worth mentioning that several non-fluorescent optical dyes have been investigated for margin analysis with promising results including Lugol's iodine [304, 305] and toluidine blue [306].

There are some limitations of this study worth highlighting. Firstly, where there was a specimen surface that the surgeon and/or the pathologist were not concerned for close margins, a fluorescence analysis was not performed and no frozen section was sampled. This was done to reduce intraoperative pathology time and allow focus on clinically relevant margin assessment, which is consistent with the philosophy that this margin assessment strategy should be used for clinical guidance only. Despite this, there is no data from this study examining margin distances at high fluorescent areas on specimen surfaces where there was no clinical suspicion for close margins. As such we cannot comment on the accuracy of fluorescent imaging at identifying the sentinel margin in all surfaces of all specimens resected in this study. Future similar trials could circumnavigate the issue of intraoperative delay, by prospectively collecting tissue samples at pathology of the identified sentinel margin location on all surfaces of all specimens (based on both fluorescent analysis and surgeon prediction) and then retrospectively analysing the margin distances on these tissue samples at later time point. Secondly, fluorescence

margin analysis was performed by one person during the period of this study. While this kept variability in fluorescent margin analysis and interpretation constant, learning curve for performing the analysis and discrepancies in analysis between users was not examined as part of this study. With increasing adoption of artificial intelligence technology in surgery, it is foreseeable that future use of this strategy may move toward a computer automated technique.

CONCLUSION

Image-guided analysis of specimens can improve identification of the true closest margin in 3D resections and has the potential to reduce positive margin rates; results of the current study determined a clinically significant value of fluorescence-based margin assessment in 11% of patients. A study examining the value of this technique in improving communication of margin location between surgeon and pathologist as well as evaluating the efficacy of surgical guidance during re-resection should follow.

KEY POINTS

Question

How does ex vivo fluorescent molecular imaging of head and neck cancer resections compare with current standard of care in identifying the true closest margin?

Pertinent findings

In this prospective observational clinical trial including 18 consecutive patients who underwent head and neck cancer surgical resections, fluorescence-based sentinel margin assessment outperformed the surgeon at identifying the true closest margin at final pathology in 11% of cases. Fluorescence had a higher interobserver agreement with final pathology (Cohen kappa value 0.96) than the surgeon (Cohen kappa values of 0.82) and plotting the margin distance at the predicted sentinel margin location of each observer versus the actual closest margin distance at final pathology demonstrated best correlation between fluorescence and final pathology ($R^2 = 0.98$).

Implications for patient care

Broad translation of an ex vivo fluorescent molecular image-based approach to sentinel margin identification could improve accuracy of intraoperative margin sampling, with overall potential to reduce positive margin rates in surgery.

Part II: Innovating sentinel lymph node biopsy

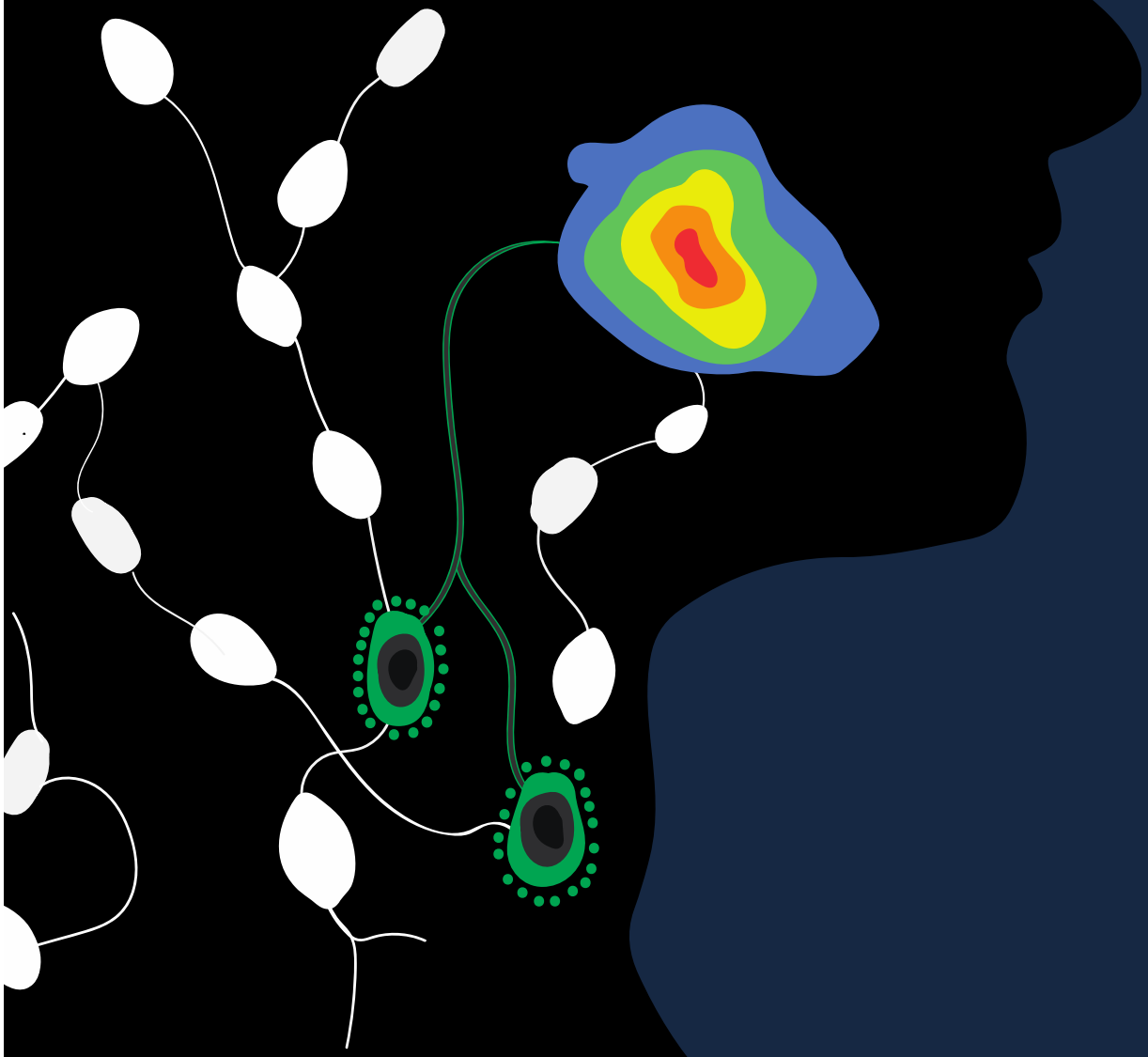

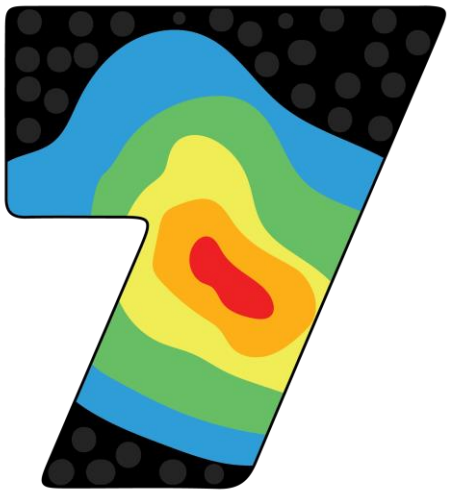

CHAPTER 7: METASTATIC AND SENTINEL LYMPH NODE MAPPING USING INTRAVENOUSLY DELIVERED PANITUMUMAB-IRDYE800CW

STATEMENT OF AUTHORSHIP

Title of paper	Metastatic and sentinel lymph node mapping using intravenously delivered Panitumumab-IRDye800CW
Publication status	✓ Published ☐ Accepted for Publication ☐ Submitted for Publication ☐ Unpublished and Unsubmitted work written in manuscript style
Publication details	Krishnan G, van den Berg NS, Nishio N, Juniper G, Pei J, Zhou Q, Lu G, Lee YJ, Ramos K, Iagaru AH, Baik FM, Colevas AD, Martin BA, Rosenthal EL. Metastatic and sentinel lymph node mapping using intravenously delivered Panitumumab-IRDye800CW. Theranostics. 2021 May 24;11(15):7188-7198.

Principal Author

Name of Principal Author (candidate)	Giri Krishnan		
Contribution to the Paper	Study conception and design. Data collection, analysis and interpretation. Manuscript preparation.		
Overall percentage (%)	75%		
Certification	This paper reports on original research I conducted during the period of my Higher Degree by Research candidature and is not subject to any obligations or contractual agreements with a third party that would constrain its inclusion in this thesis. I am the primary author of this paper		
		Date	20.09.2021

Co-Author Contributions

By signing the State of Authorship, each author certifies that:

i. The candidate's stated contribution to the publication is accurate (as detailed above);
ii. Permission is granted for the candidate in including the publication in thesis; and
iii. The sum of all co-author contributions is equal to 100% less the candidate's stated contribution.

Name of Co-Author	Nynke S. van den Berg
Contribution to the Paper	Study conception and design. Data collection, analysis and interpretation. Manuscript preparation.

Signature		Date	28.09.2021

Name of Co-Author	Naoki Nishio		
Contribution to the Paper	Study conception and design. Data collection, analysis and interpretation. Manuscript preparation.		
Signature		Date	23.09.2021

Name of Co-Author	Georgina Juniper		
Contribution to the Paper	Data analysis and interpretation		
Signature		Date	11.10.2021

Name of Co-Author	Jaqueline Pei		
Contribution to the Paper	Data collection and analysis.		
Signature		Date	05.10.2021

Name of Co-Author	Quan Zhou		
Contribution to the Paper	Data collection and analysis.		
Signature		Date	24.09.2021

Name of Co-Author	Guolan Lu		
Contribution to the Paper	Data collection and analysis.		
Signature		Date	03.10.2021

Name of Co-Author	Yu-Jin Lee		
Contribution to the Paper	Data collection and analysis.		
Signature		Date	23.09.2021

Name of Co-Author	Kimberly Ramos		
Contribution to the Paper	Study execution in Division of Nuclear Medicine. Patient supervision. Data collection and analysis.		
Signature		Date	24.09.2021

Name of Co-Author	Andrei H. Iagaru
Contribution to the Paper	Study supervision of patients in Nuclear Medicine division. Data interpretation. Manuscript editing.

Signature		Date	23.09.2021

Name of Co-Author	Fred M. Baik		
Contribution to the Paper	Surgical management of patients and acquisition of tissue samples. Manuscript editing.		
Signature		Date	06.10.2021

Name of Co-Author	Alexander D. Colevas		
Contribution to the Paper	Patient eligibility confirmation. Study conception and design. Data interpretation. Manuscript editing.		
Signature		Date	06.10.2021

Name of Co-Author	Brock A. Martin		
Contribution to the Paper	Pathological assessment of tissue specimens. Data analysis and interpretation. Manuscript editing.		
Signature		Date	24.09.2021

Name of Co-Author	Eben L. Rosenthal		
Contribution to the Paper	Study conception, design and responsibility for supervision. Surgical management of patients and acquisition of tissue samples. Data analysis and interpretation. Manuscript preparation. Securing funding.		
Signature		Date	24.09.2021

ABSTRACT

Rationale

SLNB is a well-established minimally invasive staging procedure that maps the spread of tumour metastases from their primary site to the regional lymphatics. Currently, the procedure requires the local peri-tumoural injection of radiolabelled and/or optical agents, and is therefore operator dependent, disruptive to surgical workflow and restricted largely to a small subset of malignancies that can be readily accessed externally for local tracer injection. The present study set out to determine whether IV infusion of a tumour-targeted tracer could identify sentinel and metastatic LNs in order to overcome these limitations.

Methods

We examined 27 patients with OSCC, 18 of whom were cN0. Patients were infused with 50mg of IV Panitumumab-IRDye800CW prior to surgical resection of their primary tumour with neck dissection and/or SLNB. Lymphadenectomy specimens underwent fluorescence molecular imaging to evaluate tracer distribution to LNs.

Results

A total of 960 LNs were analysed, of which 34 (3.5%) contained metastatic disease. Panitumumab-IRDye800CW preferentially localized to metastatic and sentinel LNs as evidenced by a higher fluorescent signal relative to other LNs. The median MFI of metastatic LNs was significantly higher than the median MFI of benign LNs (0.06 versus 0.02, $p < 0.05$).

Furthermore, selecting the highest five fluorescence intensity LNs from individual specimens resulted in 100% sensitivity, 85.8% specificity and 100% NPV for the detection of occult metastases and 100% accuracy for clinically staging the neck. In the cN+ cohort, assessment of the highest 5 fluorescence LNs per patient had 87.5% sensitivity, 93.2% specificity and 99.1% NPV for the detection of metastatic nodes.

Conclusion

When intravenously infused, a tumour-targeted tracer localized to sentinel and metastatic LNs. Further validation of an IV tumour-targeted tracer delivery approach for SLNB could dramatically change the practice of SLNB, allowing its application to other malignancies where the primary tumour is not accessible for local tracer injection.

Key words: Head and neck cancer, Oral squamous cell carcinoma, sentinel lymph node biopsy, Fluorescent molecular imaging, Translational science

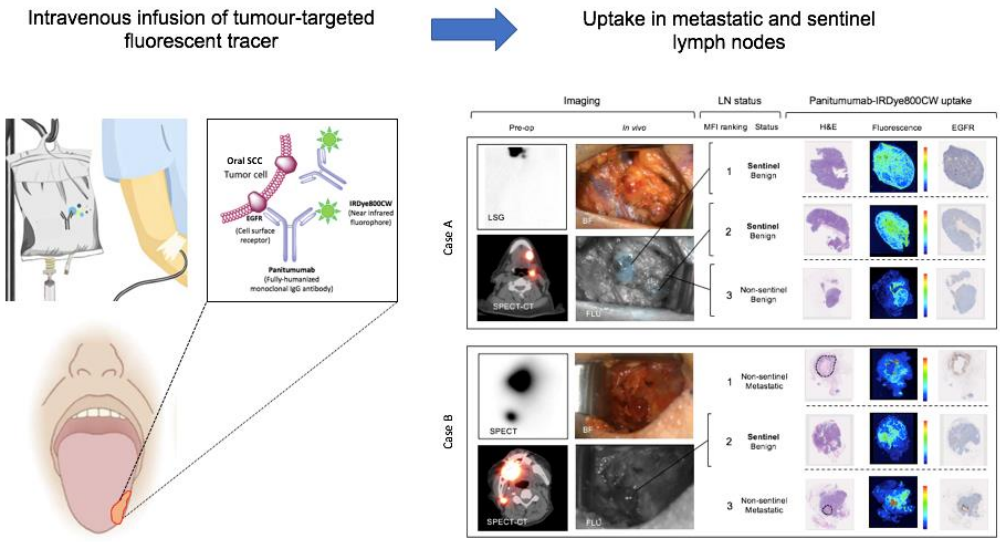

Figure 7.1 Graphical abstract.

INTRODUCTION

Head and neck cancer is a major cause of global morbidity and mortality [307]. OSCC is one of the most common types and has a high propensity to metastasise to cervical LNs [307, 308]. Because the presence of cervical metastases is associated with reduced survival, management of the neck focuses on optimizing staging accuracy while minimising treatment morbidity [309-313]. This is challenging as occult metastases are present in 25% of patients who have negative clinical and radiographical staging (cN0) [61, 67, 310, 314-316]. Currently the standard practice in the United States is to have cN0 patients undergo END if there is a possibility (20%) that the LNs harbor micro-metastatic disease. This procedure consists of removal of the cervical fibrofatty lymphoid tissue in selected neck levels to evaluate for tumour positive LNs [159, 317, 318].

SLNB is an alternative method of identifying micrometastatic disease which is supported by the NCCN guidelines [43, 319]. This technique requires a local peri-tumoural radiotracer injection and assumes that the tracer follows the same route of lymphatic spread as metastatic cells. Subsequent excision and histopathological assessment of the SLN (the first LN receiving afferent flow of tracer) predicts the metastatic status of the neck [320-322]. This technique offers lower morbidity than END with equal diagnostic yield, however it has not been adopted in the United States because it is dependent on appropriate local tracer injection, which can be disruptive to operative work flow, and is additionally restricted in the head and neck to those cancers arising in the oral cavity (since cancers arising from the pharynx and larynx cannot be accessed externally for local tracer injection) [162, 197, 206, 323-326]. IV tracer delivery would overcome these limitations [327, 328].

Recently, our group demonstrated that IV infusion of a fluorescent antibody-dye conjugate (panitumumab-IRDye800CW) can detect metastatic LNs during pathological processing [243]. Based on these findings, we hypothesized that IV panitumumab-IRDye800CW could potentially replace local tracer injection as a method for identification of SLNs during surgery. The present study aims to identify whether systemically delivered panitumumab-IRDye800CW can identify metastatic and sentinel LNs in resected neck dissection specimens by using the fluorescence signal of LNs to evaluate preferential tracer distribution.

MATERIALS AND METHODS

Clinical trial design

Two prospective single centre, non-randomized, phase I-II clinical trials evaluating the fluorescence molecular imaging agent pantimumamab-IRDye800CW were approved by the Stanford University Administrative Panel on Human Subjects Research and the FDA and registered with ClinicalTrials.gov (NCT02415881; NCT03405142). The studies were performed in accordance with the Helsinki Declaration of 1975 and its amendments, FDA's ICH-GCP guidelines, and the laws and regulations of the United States. Written informed consent was obtained from all patients.

Between June 2018 and December 2019, adult patients with biopsy proven primary or recurrent OSCC scheduled for curative surgical treatment with a subsequent neck dissection (n = 25) or SLNB procedure (n = 2) were enrolled. Patients were divided into cN0 (clinically node negative (n = 18)) and cN+ (clinically node positive (n = 9)) cohorts based on consensus staging at the Stanford tumour board meeting after review of clinical findings and pre-operative imaging.

Panitumumab-IRDye800CW

All patients received a flat dose of 50 mg of panitumumab IRDye800CW, infused via a peripheral IV catheter 1-5 days prior to surgery. Panitumumab (Vectibix; Amgen, Thousand Oaks, CA) is a recombinant, fully humanized monoclonal antibody, that binds with high affinity to the extracellular domain of the human EGFR, overexpressed in up to 90% of patients with HNSCC [237]. IRDye800CW is a near infrared fluorophore, which is ideal for surgical visibility since it has higher tissue penetration depth than fluorescence

in the visible range (400-700nm) and is not limited by endogenous autofluorescence.[227] It has been demonstrated to have low toxicity and short half-life when unconjugated.[230]

Panitumumab (Vectibix; Amgen; 147 kDa) was conjugated to IRDye800CW-NHS by a 2-hour incubation at 20C in the dark with a dye-to-protein ratio of 2.3:1. The NHS ester reaction binds randomly to lysines throughout the antibody during a relatively simple labelling method that has been performed successfully for chimeric and fully human antibodies with a consistent dye to protein ratio and good imaging results.[231, 232] Quality control of the conjugate included analysis of drug product in a sterile vial for particulates and integrity of the sterilizing filter. Upon production and vialing, vials were transported to Stanford University (Stanford, CA) where they were stored at the Stanford Health Care Investigational Pharmacy prior to use[237]. The safety profile and pharmacokinetics of the antibody-dye conjugate have been previously reported [234]. Furthermore, the antibody-dye conjugate has been found to have a stability profile non-inferior to panitumumab alone.[329]

Intra-operative fluorescence imaging

The intraoperative fluorescence imaging workflow during END is shown in Figure 7.2A. Briefly, fluorescence imaging was performed before, during and after neck dissection using the Spy-Phi camera and the IR9000 optical imaging platform modified for IRDye800CW fluorescence imaging (Novadaq, Burnaby, Canada) [215, 239]. A closed-field near-infrared optical imaging system ((modified) PEARL Triology, LI-COR Biosciences Inc.) was used on the back table for *ex vivo* imaging of surgical specimens [240, 241].

Ex vivo fluorescence imaging and histopathology

Pathological processing and assessment of neck dissection specimens was conducted as standard of care and previously described [243]. Cassetted tissue was re-imaged in the closed-field imaging device (LI-COR Biosciences) prior to paraffin embedding (Figure 7.2B). Stained slides were evaluated by a board-certified pathologist blinded to fluorescence. Tumour deposits were outlined and ENE was reported (Figure 7.2C). Selected slides underwent fluorescence microscopy as previously described [237].

Sentinel lymph node biopsy

Two cN0 patients underwent conventional SLNB and IV infusion of panitumumab-IRDye800CW prior to END. In these patients, the afternoon prior to surgery, ^{99m}Tc-tilmanocept (Lymphoseek, Cardinal Health, Dublin, OH, USA) was administered via 4 peri-tumoural injections of 0.125 mCi. Dynamic images were obtained during the first 10 minutes using a GE Discovery 870 CZT camera (GE Healthcare, Waukesha, WI, USA) followed by static planar images and SPECT/CT imaging. Images were evaluated by a board-certified nuclear medicine physician who reported the number and location of SLNs. Following primary tumour resection, a handheld gamma ray detection probe (Neoprobe, Johnson&Johnson Medical, via Leica Biosystems, Cincinnati, Ohio, United States) was used to track SLNs as seen on preoperative images. When localised, the count rate in SLNs was measured in triplicate. Next, fluorescence imaging was performed using a handheld near-infrared fluorescence camera (Spy-Phi, Novadaq). Identified SLNs were excised and CND performed.

At pathology, SLNs were step-sectioned at 150 μm intervals to obtain slides from three levels. Routine immunohistochemistry was performed to confirm the presence of EGFR,

cytokeratin 5/6, CD68, and CD31 using an autostainer (DAKO Link48 and PT link, Agilent Technologies Inc., Santa Clara, California, USA) as previously described [243]. Stained slides were scanned digitally using a whole slide scanner (Hamamatsu NanoZoomer 2.0-RS, Hamamatsu, Japan). The presence of panitumumab-IRDye800CW was evaluated by imaging slide-mounted sections on the Odyssey imaging platform (LI-COR Biosciences Inc.)

Statistical analysis

MFI, defined as total counts per pixel area, divided by pixel area, was calculated for each LN on acquired images using ImageStudio software (LI-COR Biosciences Inc.). MFI data was correlated to LN status (benign or metastatic) (Figure 7.2B and C). For LNs sent for intraoperative FSA, MFI was calculated from images acquired on the back table to avoid wash-out artefact as a result of altered tissue handling. MFI values for all LNs were entered into a spreadsheet (Microsoft Excel version 2019).

GraphPad Prism (version 8.0c) was used for statistical analysis. The Fisher exact test or chi-square test was used to compare categorical values between groups. The Mann-Whitney U-test was used to compare continuous values between groups and the MFIs between metastatic and benign LNs. Sensitivity and specificity of panitumumab-IRDye800CW to identify metastatic LNs was calculated using ROC curves. The likelihood ratio was defined as sensitivity / (1 – specificity). All tests were two-sided. Data was presented as mean or mean ± standard deviation (SD), and a two-sided p-value of 0.05 or less was considered statistically significant (*$p < 0.05$; **$p < 0.01$; *** $p < 0.001$; NS not significant).

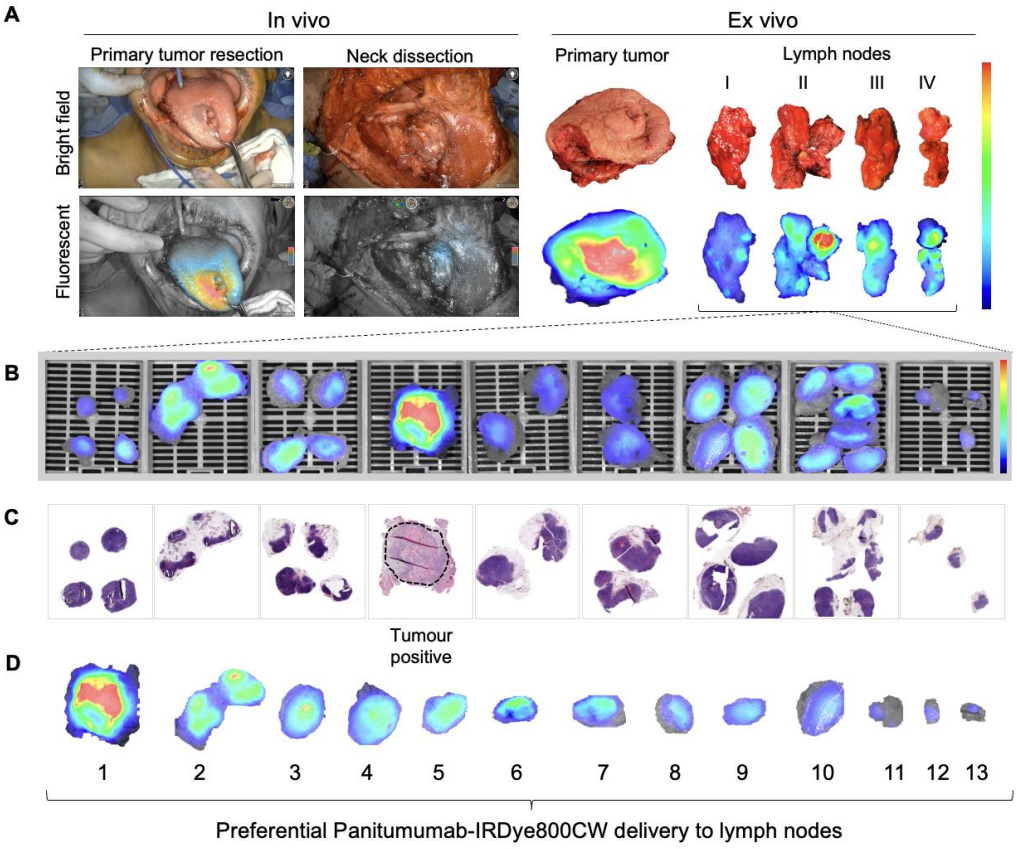

Figure 7.2 Lymph node fluorescence imaging workflow.

A. Representative case demonstrating intraoperative fluorescence imaging during resection of an anterior tongue tumour and elective level I – IV neck dissection B. Fluorescence image of cassetted LNs from the neck dissection specimen C. Corresponding H&E slides generated from the cassetted LNs enabling co-localisation of tumour status to fluorescence. D. Ranking of individual LNs by mean fluorescence intensity to evaluate the preferential delivery and uptake of panitumumab-IRDye800CW to individual lymph nodes from the neck dissection specimen.

RESULTS

Patient characteristics

Twenty-seven patients underwent IV infusion of panitumumab-IRDye800CW 1-5 days prior to END. There were 18 patients preoperatively staged as cN0 and 9 staged as cN+. There were no statistical differences in baseline demographics between groups (Table 7.1). Twenty-three unilateral and 4 bilateral neck dissections were performed, as well as two conventional SLNB procedures.

A total of 960 LNs were collected from neck dissections for analysis, of which 34 (3.5%) contained metastases. In the cN0 group, 10 out of 581 LNs (1.7%) were metastatic, and in the cN+ group 24 out of 379 LNs (6.3%) were metastatic. On average, 37 LNs were dissected per patient. Of the 18 patients with cN0 disease, five had metastatic disease at final pathology and were upstaged to pN1 in two (11.1%), pN2 in one (5.6%) and pN3 in two cases (11.1%). Of the 9 patients with cN+ disease, two (22.2%) had no metastases at final pathology and were down-staged to pN0 disease.

The majority (70.4%) of patients were infused within 2 days of surgery. Eight patients (4, 5, 6, 7, 11, 12, 15, 20) were infused the day before surgery and eleven patients (1, 2, 3, 9, 10, 13, 16, 18, 21, 23, 27) were infused 2 days prior to surgery. Three patients (14, 17, 22) were infused three days prior to surgery, and four patients (8, 24, 25, 26) were infused 4 days prior to surgery. Patient 19 was the only patient infused 5 days prior to surgery.

Table 7.1 Patient, primary tumour and lymph node characteristics.

Variable	Clinical LN status		P - value	Total
	cN0	cN+		
Patient characteristics				
Number of patients, No. (%)	18 (100)	9 (100)	0.10 [c]	27 (100)
Gender			0.67 [b]	
Female	7 (38.9)	3 (33.3)		10 (37.0)
Male	11 (61.1)	6 (66.7)		17 (63.0)
Age, mean (SD), y	63.2 (9.5)	60 (11.3)	0.53 [c]	62.2 (10.1)
Weight, mean (SD), kg	67.6 (15.8)	78.1 (11.9)	0.06 [c]	71.1 (15.3)
Days from infusion to surgery, No. (%)			0.66 [a]	
1	6 (33.3)	2 (22.2)		8 (29.6)
2	7 (38.9)	4 (44.4)		11 (40.7)
3	2 (11.1)	1 (11.1)		3 (11.1)
4	3 (16.7)	1 (11.1)		4 (14.8)
5	-	1 (11.1)		1 (3.7)
Primary tumour characteristics				
Tumour sub-site, No. (%)			0.83 [a]	
Tongue	7 (38.9)	5 (55.6)		16 (59.3)
Buccal mucosa	6 (33.3)	3 (33.3)		9 (33.3)
RMT	3 (15.8)	1 (11.1)		4 (14.8)
Alveolar ridge	1 (5.6)	-		1 (3.7)

Hard palate	1 (5.6)			1 (3.7)
Final T stage, No. (%)			0.10 [a]	
pTx	-	1 (11.1)		1 (3.7)
pT1	5 (27.8)	-		5 (18.5)
pT2	6 (33.3)	1 (11.1)		7 (25.9)
pT3	3 (15.8)	4 (44.4)		7 (25.9)
pT4	4 (22.2)	3 (33.3)		7 (25.9)
Recurrence, No. (%)	5 (27.8)	1 (11.1)		6 (22.2)
Maximal dimeter, mean (SD), cm	2.8 (1.5)	4.6 (2.3)	*0.03 [c]	3.4 (2.0)
Depth of invasion, mean (SD), mm	9.5 (7.5)	26.6 (22.1)	*0.02 [c]	15.8 (16.4)
Lymph node characteristics				
LNs, No. (%)				
Total	581 (100)	379 (100)	**0.001 [a]	960 (100)
Mean LNs per patient	33.9	42.1		37
Metastatic	10 (1.7)	24 (6.3)		34 (3.5)
Benign	571 (98.3)	355 (93.7)		926 (96.5)
Extra nodal extension (ENE), No. (%)				
Number of nodes	2 (0.3)	5 (1.3)		7 (0.7)
Patients with ENE	2 (11.1)	4 (44.4)		6 (22.2)
Clinical N-stage, No. (%)			****<0.0001 [a]	
N0	18 (100)	-		18 (66.7)

N1	-	3 (33.3)		3 (11.1)
N2	-	4 (44.4)		4 (14.8)
N3	-	2 (22.2)		2 (7.4)
Pathological N-stage, No. (%)			*0.02 [a]	
N0	13 (72.2)	2 (22.2)		15 (55.6)
N1	2 (11.1)	-		2 (7.4)
N2	1 (5.6)	3 (33.3)		4 (14.8)
N3	2 (11.1)	4 (44.4)		6 (22.2)
Neck dissection type, No. (%)			0.9 **[b]**	
Unilateral neck dissection	17 (94.4)	6 (66.7)		23 (85.2)
Bilateral neck dissection	1 (5.6)	3 (33.3)		4 (14.8)
Pre-operative imaging modality, No. (%)			0.12 [a]	
CT	4 (22.2)	1 (11.1)		5 (18.5)
PET/CT alone	-	3 (33.3)		3 (11.1)
MRI	7 (38.9)	3 (33.3)		10 (37.0)
PET/CT and MRI	4 (22.2)	2 (22.2)		6 (22.2)
Unknown	2 (11.1)	-		2 (7.4)

Chi-squared test[a], Fisher's exact test[b], Mann-Whitney test[c]

Panitumumab-IRDye800CW distribution to metastatic and benign LNs

The median MFI of metastatic LNs was significantly higher than the median MFI of benign LNs (0.06 versus 0.02, $p < 0.05$). Ranking LNs by MFI in individual patients shows that metastatic LNs tend to exhibit a higher MFI than benign LNs (Figure 7.3A),

with up to an 800% increase in signal between the median MFI of benign and metastatic LNs per patient (Figure 7.3C). This is statistically significant when comparing the fluorescence intensity of metastatic LNs to the fluorescence intensity of benign LNs within the same patients, in both the cN0 and cN+ cohorts (Figure 7.3B).

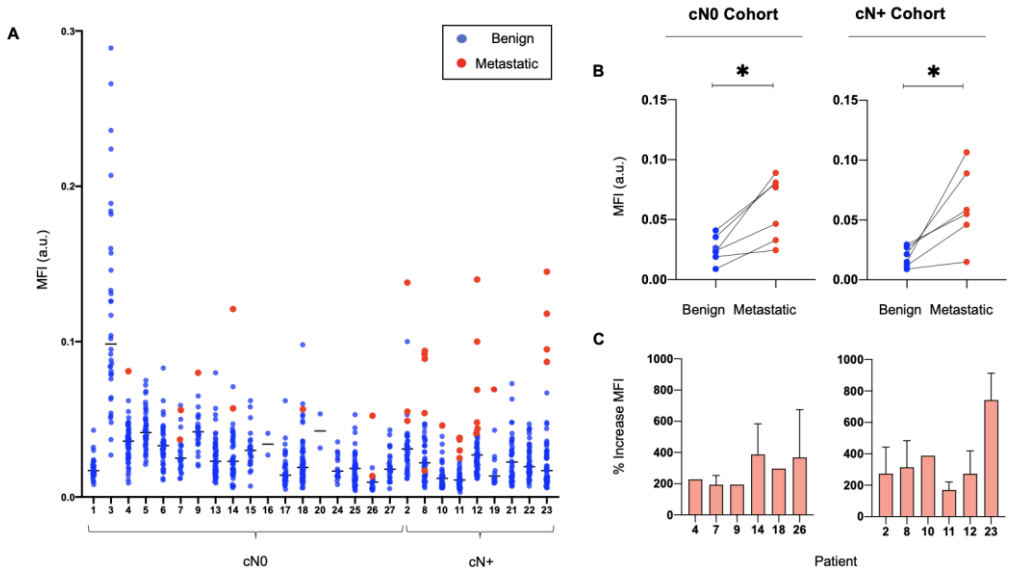

Figure 7.3 Metastatic LNs consistently exhibit a higher MFI than benign LNs in individual patients.

A. Graphical representation of the MFI of all resected metastatic and benign LNs per patient. B. Median MFI of benign LNs versus median MFI of metastatic LNs per patient in both cN0 and cN+ patient cohorts. C. Percentage increase in MFI of each resected metastatic LN above the median MFI of resected benign LNs per patient with pathologically positive neck disease.

Isolation of metastatic LNs based on preferential Panitumumab IRDye800CW uptake

All LNs from individual patient lymphadenectomy specimens were ordered by descending MFI providing an indication of preferential panitumumab-IRDye800CW delivery. To understand if this tracer could isolate metastatic LNs during a SLNB procedure, we examined the 5 LNs with the highest fluorescent intensity in each cohort (Figure 7.4A). Due to the anatomic complexity and variable lymphatic drainage in the head and neck, we chose to measure 5 LNs [179]. Using this method in the cN0 group, 100% of patients with positive LNs could be identified. In fact, 9 out of 10 (90%) metastatic LNs ranked 1st, 2nd, or 3rd in MFI relative all other LNs (Figure 3B). When evaluating cN+ patients, 16 out of 24 (66.7%) of the metastatic LNs ranked in the first 3 positions; 5 out of 24 (20.8%) ranked in the 4th and 5th positions; and 3 out of 24 (12.5%) ranked outside that range (Figure 7.4B).

ROC curves based on MFI ranking positions (Figure 7.4C) demonstrated that in the cN0 cohort, assessment of the highest 5 fluorescence LNs per patient allowed for 100% sensitivity, 85.8% specificity and 100% NPV for the detection of occult metastases. In the cN+ cohort, assessment of the highest 5 fluorescence LNs per patient had 87.5% sensitivity, 93.2% specificity and 99.1% NPV for the detection of metastatic nodes. Therefore, by setting a threshold of the highest 5 ranking LNs per patient for examination, in the cN0 cohort, of the 90 LNs examined, 80 were negative for tumour. In the cN+ cohort, of the 45 LNs examined, 24 were negative for tumour.

Nodal Staging using Panitumumab IRDye800CW

To understand if IV panitumumab-IRDye800CW could accurately stage the cN0 neck, we performed pathological staging and assessment of the overall metastatic status of the neck based on the 5 highest MFI LNs from each patient and correlated these results with the final staging of complete lymphadenectomy specimens. In the cN0 cohort we found that analysis of only three LNs with highest tracer uptake allowed for accurate staging of the overall metastatic status of the neck in all cases (Figure 7.4D). To evaluate the potential clinical value of super-selecting high MFI LNs in the cN+ cohort, we found that examination of the highest four fluorescent LNs was all that was required in order to obtain accurate neck staging in each patient across the cohort (Figure 7.4D).

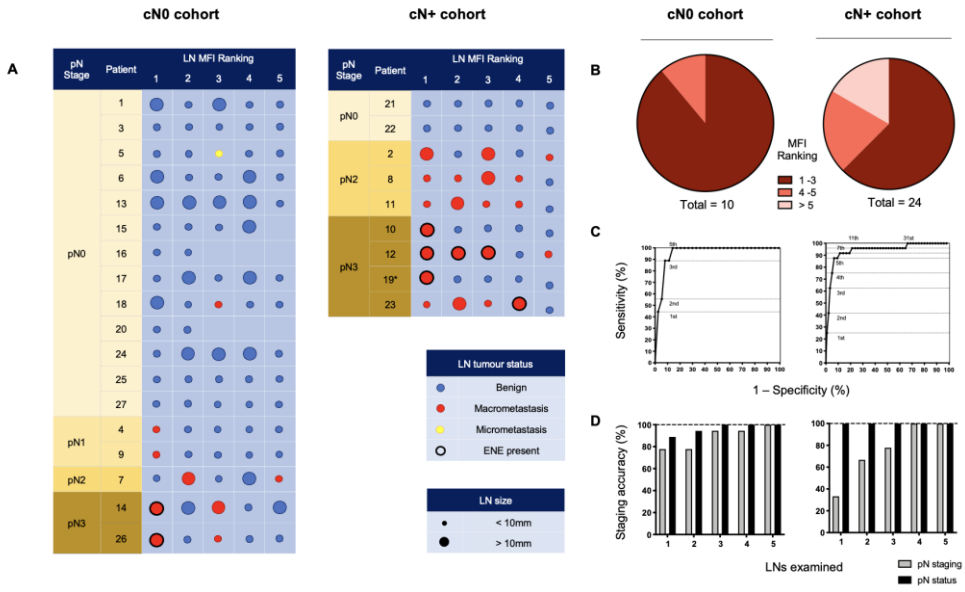

Figure 7.4 Ranking individually resected LNs by mean fluorescence intensity to isolate metastases and stage the neck.

A. The 5 LNs with the highest MFI from cN0 and cN+ patients, ranked from left to right by descending fluorescence signal demonstrating isolation of metastases. B. Pie charts

sorting metastatic LNs by relative fluorescent intensity ranking. C. ROC curves based on MFI ranking of LNs. Assessment of the top 5 fluorescence LNs per patient, in the cN0 cohort; resulted in 100% sensitivity, 85.8% specificity and 100% negative predictive value (NPV), and in the cN+ cohort; 87.5% sensitivity, 93.2% specificity and 99.1% NPV, for the detection of (occult) metastatic nodes. D. Accuracy of staging of the metastatic status and pathological status (according to the AJCC 8th edition) of the necks across cN0 and cN+ cohorts based on the number of highest relative fluorescent intensity LNs assessed.

As routine histopathology misses micrometastases, a SLNB pathology protocol was also performed on the highest three fluorescent LNs from cN0 patients (Figure 7.5) [159, 161]. Chance-sampling error was controlled for by examining size-matched LNs from the same patient in a blinded fashion. One micro-metastasis was revealed as a false negative (Figure 7.5), which upgraded the stage in one patient from pN0 to pN1. None of the control LNs were positive for metastases.

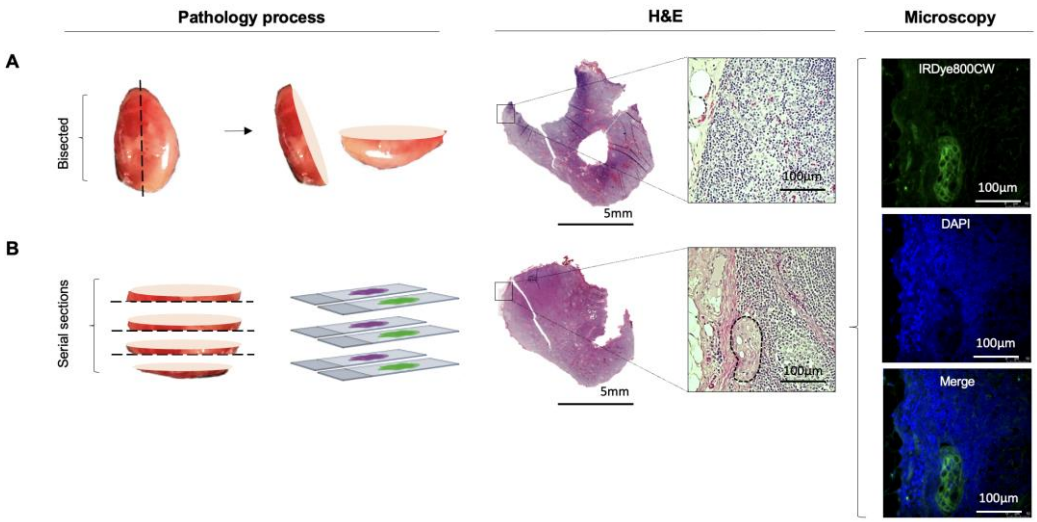

Figure 7.5 Further sectioning of LNs with high relative fluorescence can detect missed occult micrometastases.

A. Representative LN with high relative fluorescence, which upon routine histopathological processing showed no tumour deposit. B. Further sectioning of this LN using a standard SLNB pathological protocol revealed a missed microscopic tumour deposit. Microscopy fluorescence imaging demonstrates clear colocalization of fluorescent intensities at 800nm with uniform, strong cytoplasmic and membranous binding of IRDye800CW to the tumour cells, not observed in normal tissue as seen following DAPI staining of the nuclei of the surrounding tissue.

(DAPI: 4',6-diamidino-2-phenylinodole)

Comparison of IV Panitumumab IRDye800CW with peri-tumoural ^{99m}Tc-tilmanoscept

To evaluate whether IV panitumumab-IRDye800CW isolates SLNs identified with peri-tumoural injection of ^{99m}Tc-tilmanoscept, two patients received both IV panitumumab-IRDye800CW and peri-tumoural ^{99m}Tc-tilmanoscept. SLNs receiving direct ^{99m}Tc-

tilmanoscept drainage were identified with preoperative radionuclear imaging (Figure 5) [320].

In the first case (Case A), using a conventional SLNB technique, a cluster of two SLNs were identified in level II of the left neck; in the second case (Case B) one SLN was identified in level II of the right neck. Intraoperatively, all SLNs were successfully identified using a handheld gamma ray detection probe. In Case A (Figure 7.6A), the cluster of two SLNs were identified and registering gamma readings averaging 3475 and 3560, respectively. *In vivo* fluorescence imaging demonstrated signal in both of these SLNs (with MFIs of 0.043 and 0.040 respectively). In Case B (Figure 7.6B) the SLN recorded an average gamma reading of 1695 and was poorly visualized with the open-field near-infrared fluorescence camera and had an MFI of 0.019. In both patients an END was performed, and none of the SLNs contained metastatic disease on final pathology. However in Case B, two LNs on final pathology, that were not identified by ^{99m}Tc-tilmanoscept, were found to contain metastatic disease. These two metastatic LNs had the first and third highest MFI among all LNs from the specimen (MFIs of 0.052 and 0.019 respectively). This suggests that the injection may have been performed in a manner which did not accurately identify the SLN. In Case A, the two SLNs identified by conventional methods, were registered to have the highest fluorescence signals (Figure 7.6A).

We evaluated the microscopic distribution of panitumumab-IRDye800CW within the histological architecture of the LNs. Lymph nodes that were negative for metastases demonstrated florescent signal throughout the subcapsular and trabecular sinuses in the absence of EGFR expression. There was strong correlation of fluorescence with the

microvasculature based on CD31 staining. On the other hand, the fluorescence signal within metastatic LNs correlated strongly with EGFR expression. The microscopic distribution of fluorescence in benign LNs and metastatic LNs was not significantly changed depending on whether the LN was sentinel or non-sentinel.

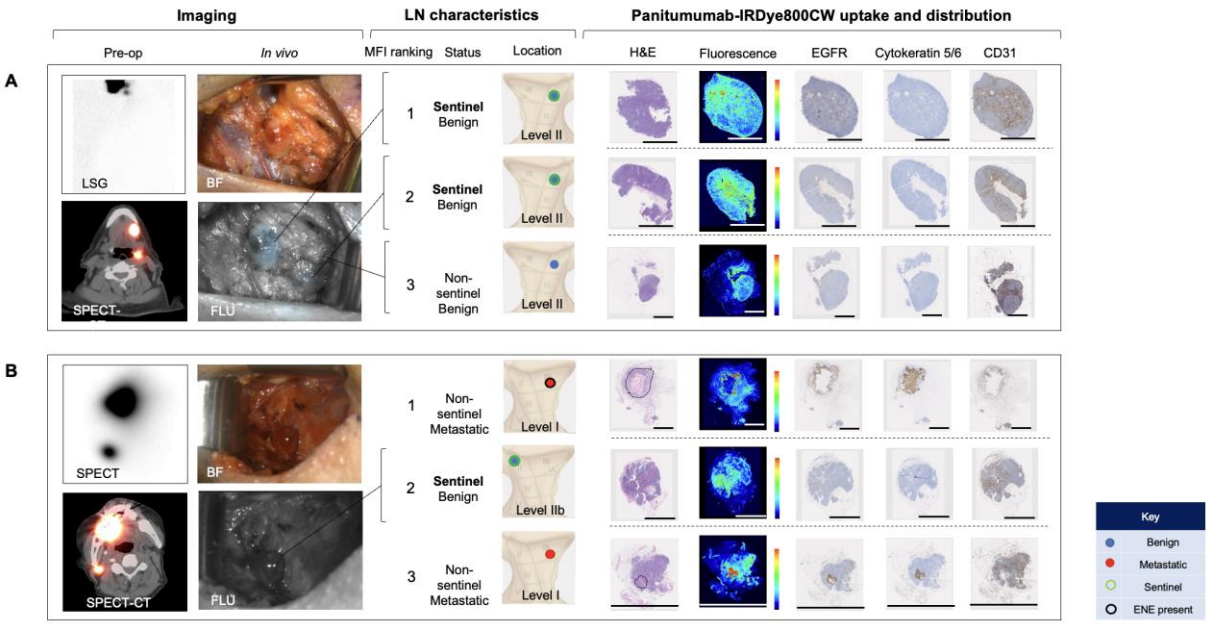

Figure 7.6 Systemically delivered panitumumab-IRDye800CW demonstrates high relative fluorescence in sentinel lymph nodes.

A. Case A demonstrates a patient with two level II SLNs following local radiotracer injection. These were the highest two fluorescent LNs following completion END. H&E staining showed no tumour deposits in these LNs and fluorescence imaging showed signal throughout the subcapsular and trabecular sinuses with minimal EGFR expression. B. Case B demonstrates a patient with one level II SLN. This was the second highest fluorescent LN following completion END. Fluorescence imaging and IHC showed a similar distribution pattern of panitumumab-IRDye800CW to the SLNs in case A. The first and third highest fluorescent LNs in this patient were metastatic (tumour deposit outlined on H&E). Fluorescence in these LNs correlated strongly with

EGFR expression. In the 12mm metastasis with ENE, fluorescence was highest around the periphery of the deposit. In the smaller metastasis, fluorescence was well distributed throughout the tumour deposit. Fluorescence also corelated strongly with CD31 staining in both metastatic LNs. Scale bars = 100 μm.

(LSG: Lymphoscintigraphy, FLU: Fluorescent image)

DISCUSSION

Since its description in 1977, the SLNB procedure has depended on peri-tumoural delivery of non-targeted agents [321]. To the best of our knowledge, this is the first study to identify a systemically delivered, SLN molecular agent in humans. By analysing fluorescence signal within individual LNs from resected lymphadenectomy specimens, we found that panitumumab-IRDye800CW identifies at-risk (metastatic and/or sentinel) LNs, allowing for accurate staging of cN0 patients.

We previously demonstrated in a dose escalation study, that fluorescence imaging of LNs at pathology of patients preoperatively infused with IV panitumumab-IRDye800CW enabled discrimination of metastatic and benign LNs based on a signal-to-background ratio (LN MFI divided by background tissue MFI) [243]. In the present study, we evaluated the feasibility of IV infusion of a molecularly-targeted fluorescent tracer to identify LNs most likely to harbour occult metastatic disease. We demonstrated that panitumumab-IRDye800CW preferentially reached SLNs, regardless of the tumour status of the LN. We demonstrated in two patients who underwent conventional SLNB, that IV panitumumab-IRDye800CW was preferentially delivered to the same LNs identified by ^{99m}Tc-tilmanoscept as being the first draining LNs from the primary tumour. Furthermore, identification of tumour-positive LNs based on preferential tracer uptake was not impeded by the presence of occult metastases within other LNs, which have potential to obstruct flow of locally delivered tracer, providing further support of this novel approach in the anatomically complex head and neck region.

The mechanism by which a systemically delivered agent identifies the SLNs is unclear, but it is possible that the antibody-dye bioconjugate first accumulates in the primary tumour and then drains non-specifically into the regional nodal basin in a stepwise pattern. It is likely that metastatic and sentinel LNs may be more likely to retain the panitumumab-IRDye800CW given the relatively large size (roughly 150kD) of the molecular tracer.

There are several key differences between this study and the study by Nishio et al. Firstly, the study by Nishio et al was a dose-escalation study where patients were divided into three different cohorts and received different weight-based doses of panitumuanmb-IRDye800CW. In the present study a fixed dose of 50 mg was used for all patients. Furthermore, to account for differences in tumour heterogeneity and regional nodal spread, only patients with oral squamous cell carcinoma were included in this study, while all HNSCC patients were included in Nishio's study. Finally, and most importantly, Nishio et al used a fixed thresholds for MFI and SBR to discriminate positive and negative LNs, whereas in the present study, LNs were ranked by decreasing order of MFI per patient and accuracy of positive tumour detection was calculated based on how many of the highest ranked LNs were needed. In both studies, MFI-based ranking of dissected LNs was used to identify how many LNs needed to be examined in order to accurately stage the neck. In our study 5 LNs from the cN0 group and 4 LNs from the CN+ group were required to achieve 100% accuracy with staging. In the study by Nishio et al, only 3 LNs were required across all patients to achieve 100% accuracy of staging.

Because all the patients underwent complete removal of all the LNs, we were able to identify all the sentinel and metastatic LNs through fluorescent analysis of all LNs. This study examined mostly cN0 patients, while inclusion of cN+ patients increased the number of metastatic LNs for analysis. All patients received the same dose of 50 mg of panitumumab-IRDye800CW, which is the established optimal dose for intra-operative imaging [300]. A notable limitation was that only two patients underwent conventional SLNB prior to END resulting in a small sample size for this direct comparison. In this study, patients were infused 1-5 days prior to surgery with panitumumab-IRDye800CW, which has been consistent with other trials conducted by our group studying this drug. Ideally, the timing of infusion prior to surgery would be kept constant, as our group have previously demonstrated that MFI significantly increased when the infusion-to-surgery window was reduced to within 2 days compared with 3 days or more [277], however this can be logistically challenging, and is subject to patient appointment availability and scheduling of surgery.

In this study, because of interpatient heterogeneity there was overlap in MFI between benign and malignant LNs over the population studied. Other groups have used techniques to improve cancer-specific discrimination, such as the radiometric imaging work by Ngyuen et al., where quantitative discrimination between target tissues and background based on the ratio of two fluorophores (rather than one) with intensities at different wavelengths, controls for variability in factors such as the amount of probe administered, patient-specific pharmacokinetics and imaging parameters.[330-332] Another example is the paired-agent molecular imaging method used by Ntziachristos and Pogue, where the kinetics of a control imaging agent is used to account for the nonbinding related

kinetics of a cancer-targeted imaging agent.[333, 334] Unfortunately significant additional regulatory requirements and costs have limited our ability for the moment to apply these techniques clinically.

This study in a clear demonstration that a molecular imaging agent can be administered systemically to identify metastatic and sentinel LNs. However, implementation will require conjugation of panitumumab to an appropriate gamma emitting radiotracer to enable dual-modality surgical navigation, which has been established as the standard of care for non-targeted locally injected fluorescent tracers [335, 336]. As is current practice, the antibody-radiolabel bioconjugate could identify at-risk LNs pre-operatively on SPECT-CT or PET-CT and then enable intraoperative localization with a gamma-probe. The conjugated fluorescent dye would allow for optical imaging with NIR-cameras to identify and isolate the node during dissection [337, 338]. Consistent with our previous work, this could also identify non-sentinel metastatic LNs in a positive neck [243].

By using fluorescence intensity to evaluate the delivery of panitumumab-IRDye800CW to individual LNs in lymphadenectomy specimens, we provide evidence that systemic delivery of this tumour-targeted tracer can identify sentinel and metastatic LNs. This study therefore demonstrates feasibility of SLN mapping using a systemically delivered tumour-targeted tracer, and provides impetus for further trials evaluating this strategy in lung, oesophageal, colorectal, urological and gynaecologic malignancies, using a different appropriately targeted antibody. Broad translation of this novel approach when combined with radioguidance holds promise to expand the potential role of SLNB in oncological surgery.

CHAPTER 8: PRECLINICAL EVALUATION OF A MANNOSE-LABELLED MAGNETIC TRACER FOR ENHANCED SENTINEL LYMPH NODE RETENTION IN THE HEAD AND NECK

STATEMENT OF AUTHORSHIP

Title of paper	Preclinical evaluation of a mannose-labelled magnetic tracer for enhanced sentinel lymph node retention in the head and neck
Publication status	☐ Published ☐ Accepted for Publication ☐ Submitted for Publication ✓ Unpublished and Unsubmitted work written in manuscript style
Publication details	Krishnan G, Cousins A, Pham N, Milanova V, Nelson M, Krishnan S, Shetty A, van den Berg N, Rosenthal EL, Krishnan S, Wormald PJ, Foreman A, Thierry B. Preclinical evaluation of a mannose-labelled magnetic tracer for enhanced sentinel lymph node retention in the head and neck. *Prepared for submission.*

Principal Author

Name of Principal Author (candidate)	Giri Krishnan		
Contribution to the Paper	Study conception and design. Data collection, analysis and interpretation. Manuscript writing and figure creation.		
Overall percentage (%)	60%		
Certification	This paper reports on original research I conducted during the period of my Higher Degree by Research candidature and is not subject to any obligations or contractual agreements with a third party that would constrain its inclusion in this thesis. I am the primary author of this paper		
		Date	20.09.2021

Co-Author Contributions

By signing the State of Authorship, each author certifies that:

i. The candidate's stated contribution to the publication is accurate (as detailed above);
ii. Permission is granted for the candidate in including the publication in thesis; and
iii. The sum of all co-author contributions is equal to 100% less the candidate's stated contribution.

Name of Co-Author	Aidan Cousins
Contribution to the Paper	Study conception and design. Data collection, analysis and interpretation. Manuscript preparation.

Signature		Date	28.09.2021

Name of Co-Author	Nguyen Pham		
Contribution to the Paper	Study conception and design. Data collection, analysis and interpretation. Manuscript preparation.		
Signature		Date	24.09.2021

Name of Co-Author	Valentina Milanova		
Contribution to the Paper	Data collection, analysis and interpretation.		
Signature		Date	24.09.2021

Name of Co-Author	Melanie Nelson		
Contribution to the Paper	Data collection, analysis and interpretation.		
Signature		Date	24.09.2021

Name of Co-Author	Shridhar Krishnan		
Contribution to the Paper	Data collection, analysis and interpretation.		
Signature		Date	11.10.2021

Name of Co-Author	Anil Shetty		
Contribution to the Paper	Data analysis and interpretation. Manuscript preparation.		
Signature		Date	05.10.2021

Name of Co-Author	Nynke van den Berg		
Contribution to the Paper	Data analysis and interpretation. Manuscript preparation.		
Signature		Date	28.09.2021

Name of Co-Author	Eben Rosenthal		
Contribution to the Paper	Data interpretation. Manuscript preparation.		
Signature		Date	24.09.2021

Name of Co-Author	Suren Krishnan
Contribution to the Paper	Data interpretation. Manuscript preparation.

Signature		Date	11.10.2021

Name of Co-Author	PJ Wormald		
Contribution to the Paper	Data interpretation. Manuscript preparation.		
Signature		Date	27.09.2021

Name of Co-Author	Andrew Foreman		
Contribution to the Paper	Data interpretation. Manuscript preparation.		
Signature		Date	23.09.2021

Name of Co-Author	Benjamin Thierry		
Contribution to the Paper	Study conception, design and responsibility for supervision. Data analysis and interpretation. Manuscript preparation.		
Signature		Date	24.09.2021

ABSTRACT

SLNB in cancers of the head and neck offers demonstrated clinical and diagnostic value, but adoption of this technique has been limited. The aim of this study was to demonstrate in a large animal model the ability to overcome these limitations via application of a novel mannose-labelled magnetic iron oxide tracer. A combination of preoperative imaging and intraoperative magnetometer detection was used to identify magnetic nodes. Iron quantification was used to map the distribution of tracer within the various lymphatic levels. Over the 4-week test period, uptake of magnetic tracer in the LNs increased in a linear-like fashion, with a substantial percentage of the accumulated iron (83%) being deposited in the SLN. This result indicates a high affinity of the mannose-labelled particles to the sentinel node, while providing a means for the magnetometer probe to indicate node status based on intraoperative signal.

Highlights

- Magnetic tracers facilitate accurate SLNB in the head and neck
- Mannose-labelled magnetic tracers result in enhanced retention in SLNs
- Magnetometer probes may identify SLNs based on iron content

BACKGROUND

OSCC has an annual worldwide incidence of over 350,0000 cases, making it the 8th most common cancer.[339] It is established that OSCC has a propensity to metastasise to the neck with a resultant 50% reduction in survival.[37, 38] Metastatic spread occurs in 25% of cases making optimal management of the cN0 neck an area of ongoing investigation. END is most widely practised but results in overtreatment of 75% of patients,[44] with morbidity related to shoulder dysfunction from spinal accessory nerve injury, [54, 55] as well as lymphoedema resulting in facial or neck swelling, chyle leak and post-operative haemorrhage.[56-58] SLNB has been established to accurately stage the neck with significantly less morbidity and improved cost efficacy but routine implementation has been limited.[193, 195] This is because cervical lymphatic drainage pathways are complex, and SLNs lie in close proximity to oral cavity tumours, both of which enhance the significance of well-known limitations of radiotracers (e.g. technetium radiocolloids); mainly, injection site shine-through masking SLN signals on preoperative lymphoscintigraphy and intraoperative gamma probe localisation.[340] The net result is the detrimental risk of false negatives in a highly curable setting.[198, 341]

Despite being the 'gold standard' in breast cancer SLNB, the pairing of blue dyes with radiotracers to improve accuracy introduces additional risks. Anaphylactic reactions to isosulfan blue dye occur in approximately 1% of patients[342, 343] and injection of methylene blue can result in tissue necrosis and DNA damage.[343, 344]

In the cervical basin SLNB paradigm, the use of SPIONs for SLN mapping offers a potentially significant advantage. Preoperative MRI provides excellent spatial resolution with high sensitivity to soft tissues, making it ideal for lymphatic mapping and surgical planning.[251] Additionally, SPIONs can be magnetised to generate a signal for detection

by handheld probes (analogous to the use of gamma probes) for intraoperative SLN localisation.[254] Unlike gamma rays, the magnetic signal is greatly reduced over distance, effectively removing the issue of shine-through,[254] These properties have already been leveraged for magnetic SLNB in breast cancer by the CE-mark and FDA-approved SPION agent 'Magtrace' (*Endomag, UK)*, with randomised controlled trials demonstrating diagnostic non-inferiority to the radiotracer and blue dye gold standard.[267, 345]

The addition of mannose to conventional radiopharmaceuticals for macrophage binding via the mannose-receptor CD206 has been demonstrated to increase tracer uptake and retention within first echelon LNs, thereby improving intraoperative signal detection and accuracy.[246, 248] To combine these properties with the demonstrated benefits of the magnetic particle approach, a novel mannose-labelled SPION tracer "FerroTrace" has been developed. In this study, a large animal model was used to evaluate the performance of FerroTrace with respect to SLN uptake and distribution into lower echelon nodes of the neck. These results were compared over the short- and long-term to evaluate if mannose-labelling could enhance SLN retention, reduce flow-through, and provide flexibility to the timing of injection, MRI, and surgery.

METHODS

Mannose-labelled SPION

The FerroTrace mannose-labelled SPION was provided by Ferronova (*Adelaide, Australia*). The core maghemite iron oxide (γ-Fe_2O_3) SPIONs are synthesised using an optimised nanoprecipitation of iron salts and controlled oxidation. To ensure in vivo colloidal stability, the SPIONs are sterically stabilised by block copolymers synthesised using reversible addtion-fragmentation chain-transfer (RAFT) polymerisation. The RAFT block copolymer coating was previously developed as a highly-stable coating for SPIONs, and yielded excellent biocompatibility and clearance following intraperitoneal injection.[272-274] In the present study, two types of block copolymer were attached to the SPION surface: a stabilising-polymer (70%) and a macrophage-targeting mannose-polymer (30%). Briefly, the stabilising block copolymer consisted of anchoring (methacryloyloxy)ethyl phosphonate groups (n = 5), a polyacrylamide stabilising polymer (n = 50 monomers), and a hydrophilic methoxy PEG group (n = 17). The stabilising block has been designed to prevent degradation and aggregation of nanoparticles in a biological environment. [272-275] The targeting block copolymer consisted of anchoring (methacryloyloxy)ethyl phosphonate groups (n = 5), a polyacrylamide linking polymer (n = 70 monomers), and a targeting group of mannose.

The tracer suspension was purified via centrifugation to remove excess polymer, redispersed in 0.9% saline and sterile filtered through a 0.22 μm membrane. Iron concentration was measured by atomic absorption spectroscopy (AAS) or inductively coupled plasma mass spectrometry (ICP-MS) and diluted with sterile 0.9% saline to a final iron concentration of either 50 mg/mL or 25 mg/mL. Aliquots of the tracer were

packaged into sterile vials under aseptic conditions, after which they could be stored at room temperature. No further processing or filtration was required prior to injection.

Tracer characterisation

Iron concentration was analysed by AAS (AAS, Varian AA800 spectrometer). The SPION core size and hydrodynamic diameter was measured using transmission electron microscopy (TEM; JEM-2100, *JEOL, Japan*) and dynamic light scattering (DLS; Zetasizer Nano ZS, *Malvern, USA*), respectively. The phase of SPION core was identified by X-ray diffraction (XRD; PANalytical XPert Powder). The polymer content was quantified by thermogravimetry analysis (TGA, TA Instrument). Magnetic characteristics of the tracer were measured using vibrating sample magnetometry (VSM; PPMS, *Quantum Design, Germany*), whereby both the mass susceptibility and saturation magnetisation could be determined.

Magnetometer probe

A prototype handheld magnetometer probe was developed for intraoperative detection of SPION-positive LNs, and provided by Ferronova (Figure 8.1). This experimental device consists of a small excitation coil to transmit an alternating magnetic field (0.4 mT, 375 Hz) and solid-state magnetic tunnel junction (MTJ) sensors for magnetic field detection.[254] The magnetometer probe is used during surgery in an analogous manner to gamma probes for radiocolloid detection; i.e. the user directs the probe at LNs in the neck, and signal strength is relayed to the user as an audible tone, light display on the probe, and numerical value on the base station. User interface, signal processing, and control of probe functions were managed by a custom LabVIEW executable. Unlike gamma probes, the magnetometer used in this study has a relatively short signal range (~10 mm), but

very high spatial resolution (4 mm). This effectively eliminates injection site signal interference at LNs, and introduces the unique ability to differentiate magnetic nodes within closely-packed chains.[254]

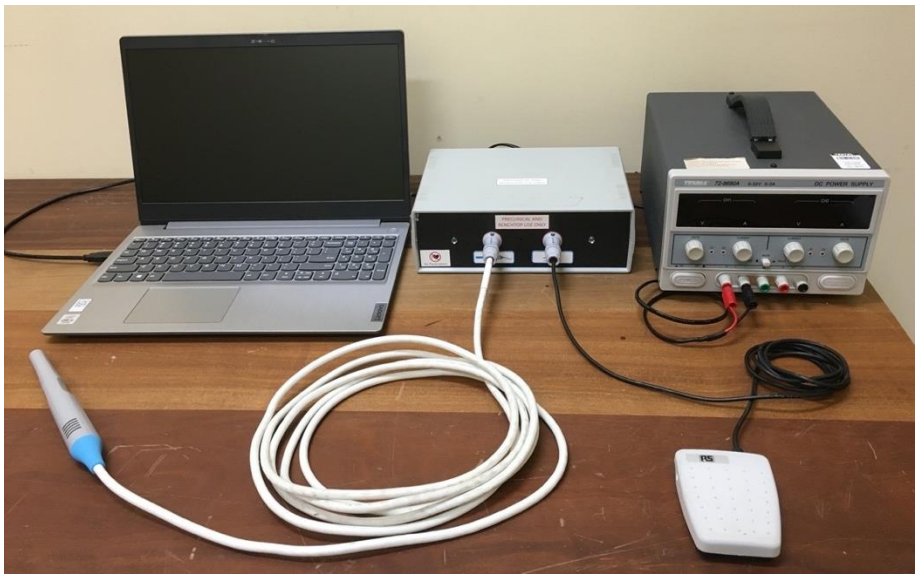

Figure 8.1 Prototype magnetometer probe used for intraoperative localisation of magnetic lymph nodes.

Animal experiments

All animal experiments were performed according to a protocol approved by the Animal Ethics Committee of the South Australian Health and Medical Research Institute (SAHMRI). All animal work was performed on site at the SAHMRI preclinical imaging and research laboratory (PIRL) in compliance with "The Australian Code of Practice for the Care and Use of Animals for Scientific Purposes, National Health and Medical Research Council (NHMRC)" and The Animal Welfare Act. Five domesticated female Large White pigs weighing approximately 40-50 kg were obtained and maintained

according to institutional standards. Animals were anaesthetised with 1 mg/kg Xylazil-100 and 10 mg/kg ketamine administered intramuscularly. Endotracheal anaesthesia was induced and maintained with 5% and 2% isoflurane, respectively. Venous catheters were placed for administration of drugs. Heart rate, oxygen saturation and body temperature were monitored while animals were anaesthetised. In all but one animal, tracer retention was studied over multiple days, in which case, animals were recovered from anaesthesia between procedures. At the completion of surgery, animals were humanely euthanized with a lethal overdose of barbiturate.

Tracer delivery and retention

All pigs were injected submucosally with FerroTrace anteriorly in the dorsal surface of the tongue in a quadrature pattern. Injections were performed using 19G insulin needles, bevel up, at a depth of approximately 5 mm and at a 20˚ angle to the tongue's surface. Animals were administered FerroTrace at volumes of either 0.25 mL or 1.0 mL, and concentrations of 25 mg[Fe]/mL or 50 mg[Fe]/mL. Injection sites were massaged for 2 minutes immediately following injection of tracer into the tongue in order to promote lymphatic uptake. FerroTrace was retained in the body for between 6 hours and 4 weeks, after which a full neck dissection was performed on the animals to remove draining LNs containing tracer. The total FerroTrace dosage and retention time for each animal is listed in Table 8.1.

Table 8.1 Summary of the various injected doses and retention times across 5 pigs.

Animal	Total volume	Iron concentration	Retention time
1	1.0 mL	25 mg/mL	6 hours
2	1.0 mL	25 mg/mL	16 days
3	1.0 mL	25 mg/mL	4 weeks
4	0.25 mL	25 mg/mL	4 weeks
5	0.25 mL	50 mg/mL	4 weeks

Pre-operative magnetic resonance imaging

Imaging was performed on a clinical 3.0T Magnetom Skyra MRI (*Siemens Healthineers, Germany*), with the anaesthetised animals in the supine position. Early in the study, pigs were scanned pre- and post-injection using a modified 2D T2 FLASH sequence (TE = 6 ms; TR = 1100 ms; FA = 20˚; 5 mm slice thickness) in axial and coronal planes. Tracer uptake within LNs was characterised by a negative change in contrast as a result of the tracers' magnetic susceptibility; as such the scan was revised part way through the study in favour of a shorter echo time to reduce the susceptibility 'bloom' artefact produced by the tracer (TE = 2.77 ms; TR = 540 ms; FA = 20˚; 3 mm slice thickness). Follow-up scans were performed shortly after injection of FerroTrace (15 to 30 minutes), and again 6 hours post-injection of the tracer. For animals where neck dissection was delayed 16 to 28 days, additional follow-up scans were performed one week after injection, and again on the day of neck dissection.

Sentinel lymph node harvest and magnetic signal detection

Lymphatic draining patterns were determined based on the known anatomical location of LNs.[346] and progressive uptake seen on post-injection MRI scans. Anaesthetised pigs were positioned supine on the operating table. A vertical skin incision was made ventral to the mandible from the mentum to clavicle. Subplatysmal flaps were raised with monopolar diathermy to expose the parotid gland. The gland was divided to reach the deep fascial plane where the LN clusters are located. A 'triple method' approach (Figure 8.2**)** was used for SLN identification, using pre-operative imaging, intra-operative optical visualisation of the tracer by its dark staining appearance, and confirmation of signal with the magnetometer probe. SLNB was performed by targeted dissection of individual SLNs as identified by pre-operative MRI. The magnetic signal of draining nodes was measured both *in vivo* and *ex vivo* using the probe by scanning it over MRI-hot nodes in a manner analogous to conventional gamma probes.

After retrieval of identified SLNs, further neck exploration was performed to inspect for additional LNs, which were also dissected and labelled non-sentinel. Bilateral neck dissection and exploration were performed on all pigs regardless of imaging results.

At euthanasia, the injection site at the tongue was removed. All tissue samples were stored in 10% buffered formalin solution until required for further analysis. Select node and injection site samples were embedded in paraffin and sectioned for pathological examination (*Gribbles Veterinary Pathology, Australia)*. Samples were examined to determine location of tracer accumulation and for signs of inflammation, necrosis, or other tissue damage in the presence of the tracers after 4-weeks retention.

All node samples (including two SPION-free control nodes) were analysed for total iron content by first digesting nodes in a mixture of 4-parts 65% ultrapure nitric acid to 1-part 36% hydrochloric acid, heated to 90˚C. Aliquots of digested tissue were then diluted as required and analysed via ICP-MS or AAS.

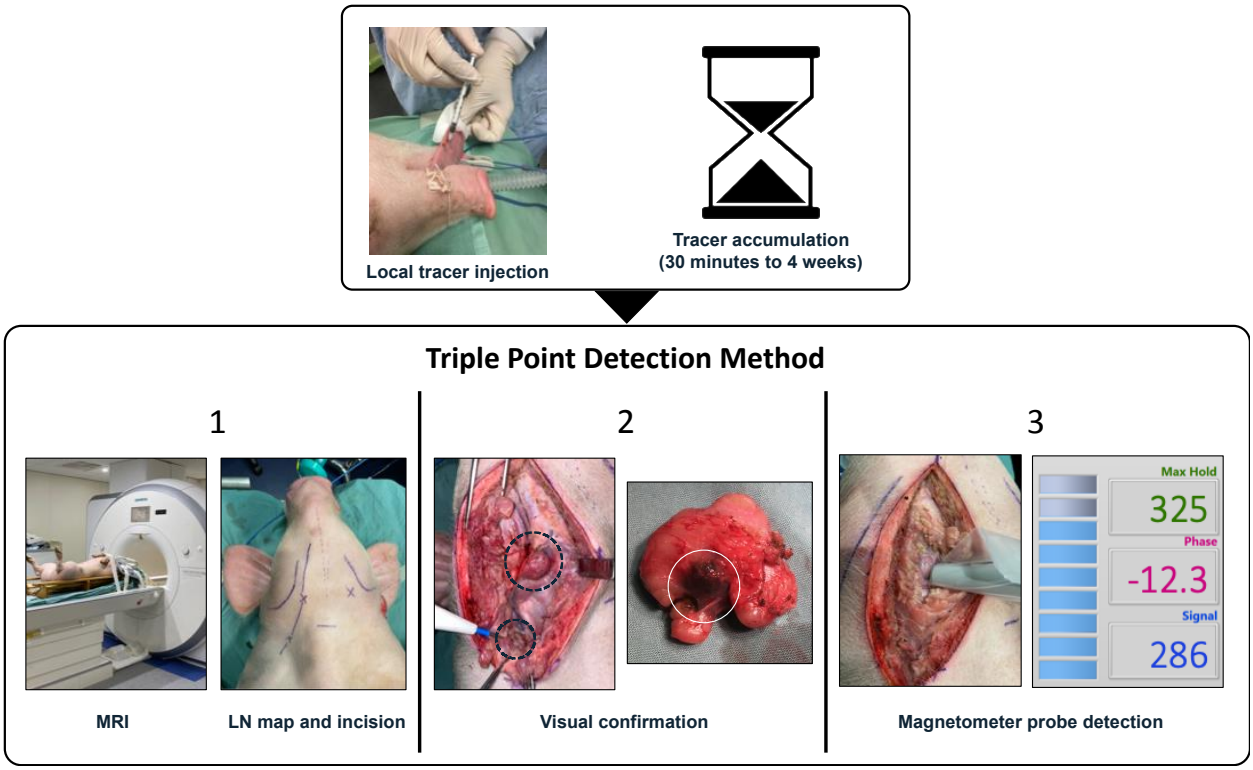

Figure 8.2 Workflow of the 'triple method' SLNB procedure of FerroTrace, using preoperative MRI, intraoperative visual node discolouration, and magnetometer probe signal.

RESULTS

Tracer characterisation

Through X-ray diffractometry, the FerroTrace cores were shown to be single crystal maghemite (γ-Fe_2O_3). TEM characterisation revealed the FerroTrace particles to have a mean core diameter of 16 ± 4 nm, with a mean hydrodynamic size (z-average) of 73.9 nm as measured by DLS. Shelf-life stability was tested after 12 months by way of remeasuring the z-average diameter without sonication or filtration, which was found to have increased marginally to 84.6 nm (+14%).

FerroTrace produces a magnetic saturation of 66 emu/g (Fe_2O_3) in an applied field of ±2.0 T, with an initial mass susceptibility of 0.087 emu/gOe in an applied field of ±40 mT. Visually, FerroTrace presents as a brown liquid suspension, even when diluted up to 50 times the injected concentration; hence, is expected to provide an exogenous brown discolouration to draining LNs.

Patterns of lymphatic drainage on preoperative MRI

Following injection into the tongue, MRI scans of the neck demonstrated flow of tracer from the injection site to three groups of LNs in an ordered pathway as follows: the submandibular LN, the accessory mandibular LN; and the superficial ventral cervical (SVC) chain of LNs, which include the cranial, middle and caudal LNs (Figure 8.3A).[346] Drainage was ipsilateral in 2 cases, contralateral in 1 case and bilateral in 2 cases. In all animals, the submandibular node was the first to receive drainage from the injection site, hence designated the 'sentinel' status. From here, the flow would progress to the accessory mandibular node (second echelon), then SVC chain (third echelon). In animals

where the accessory submandibular node was not present (n = 2), the middle SVC node took second echelon status. When drainage was bilateral, each side of the neck was treated separately; i.e. a SLN was identified for both left and right side. A total of 17 MRI-positive LNs were identified (average 3.4 per animal), of which 7 were first echelon, 7 were second echelon and 3 were third echelon.

Given the very high magnetic susceptibility of FerroTrace, even low levels of accumulation produce strong negative contrast on the MRI scans, and contrast was clearly visible from the first scans after injection (typically 15 to 30 minutes post-injection) (Figure 8.3B). Over the course of 6 hours, an increasing level of negative contrast in draining nodes over time was evident by visual observation alone. While the short echo time of the scan allowed for more precise localisation of the magnetic nodes, it also reduced soft-tissue contrast; however, this loss of contrast did not impede the researchers' ability to preoperatively determine the location of draining nodes, and often enhanced the contrast between soft tissue and the magnetic nodes. For animals where tracer accumulation was imaged over several days, no additional nodes were identified on MRI after the 6-hour post-injection scan.

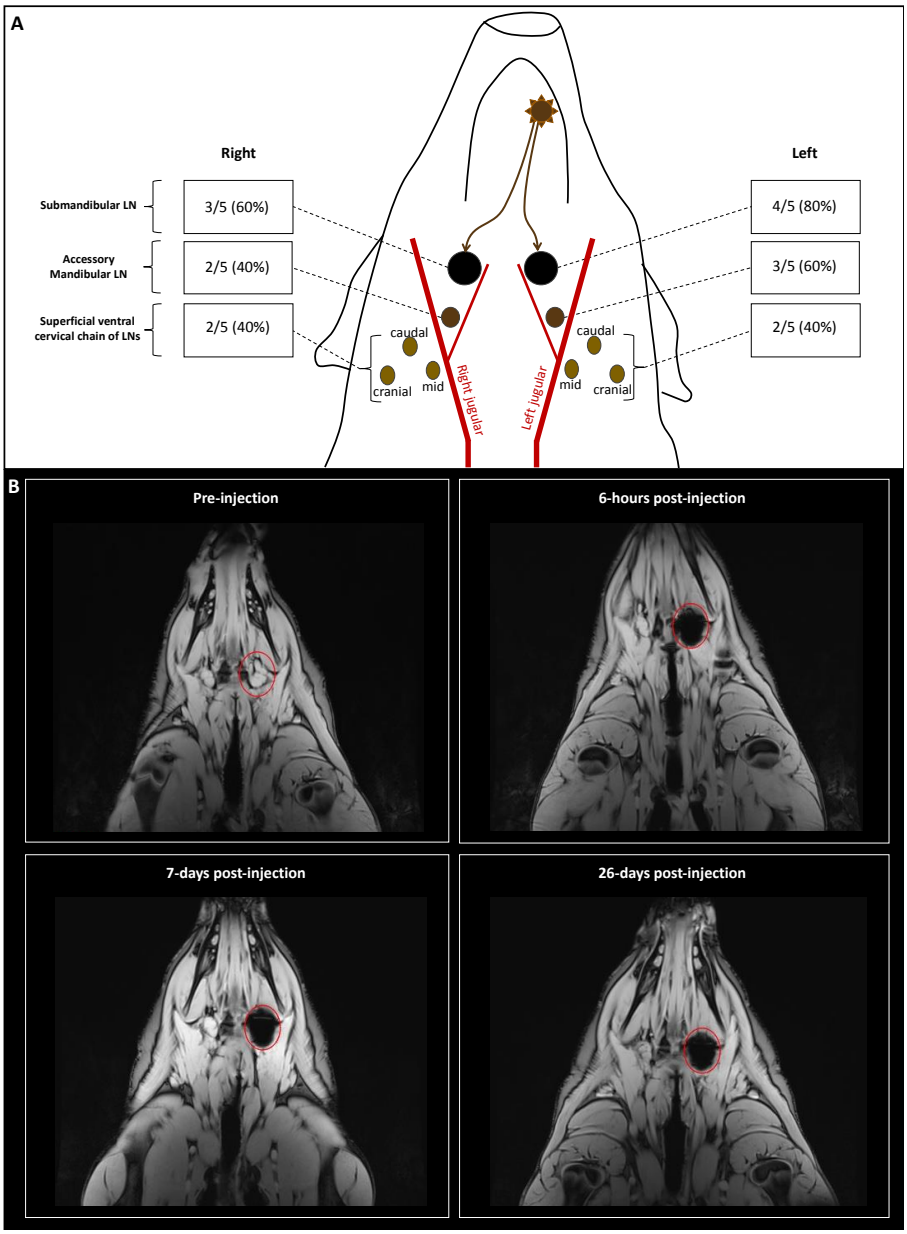

Figure 8.3 Sentinel lymph node mapping in the porcine model.

A. Lymphatic drainage map of the oral cavity of swine following lateral oral tongue injection, indicating the three main levels of lymph node. B. Example of the negative contrast produced by the magnetic tracers (animal 4) – in this instance, within the left submandibular node (circled). MRI contrast produced by FerroTrace remained high throughout the 4-week retention period, and did not significantly differ after 6-hours accumulation.

In vivo and ex vivo magnetic signal detection in draining LNs

In all but one instance, the draining LNs identified on MRI were detected *in vivo* with the magnetometer probe. In this instance, the false-negative LN was located cranially, deep in the parotid tissue and was initially not picked up when planning the neck dissection surgery using the MRI scans. This node was subsequently not located or removed during the neck dissection, and only discovered upon review of the MRI scans, after dissection had been completed. In addition to the MRI and magnetometer detection, positive nodes could be identified by a distinctive exogenous brown-black stain resulting from accumulation of SPIONs.

When comparing the total iron content of all draining nodes after 4 weeks, a directly proportional relationship was found between total injected iron dose and total node iron uptake, independent of the injected volume: 1.80 mg (29%), 3.71 mg (30%), and 7.46 mg (30%) total accumulation at doses of 6.25, 12.5 and 25 mg, respectively. Given this relationship, iron content in LNs could be normalised to the injected dose (%ID) to facilitate more accurate comparison between different timepoints and doses. By this method, FerroTrace is seen to continue to be taken up into the draining LNs over a 4-week period, in a generally linear fashion (Figure 8.4A).

On average, the SLN contained 14 ± 8 %ID of iron, compared to 2.3 ± 2.0 %ID for second echelon and 1.7 ± 0.6 %ID for third echelon nodes (Figure 8.4B). However, given the differences in node uptake based on accumulation time, comparing the iron content for each node relative to the total iron in all draining nodes within that basin may be more appropriate. In this instance, an average of 83 % (0.63 – 0.98; n = 7) of the total

accumulated iron resided in the SLN, compared to 15 % (0.024 – 0.37; n = 7) for the second echelon and 6 % (0.056, 0.070; n = 2) for third echelon nodes (Figure 8.4C).

When plotting maximum magnetometer probe signal of dissected LNs against their iron content (excluding one outlier), a linear correlation with r = 0.924 is observed (Figure 8.4D), indicating the magnetometer probe can be used to approximate iron quantity in the LN. Given the differential uptake between SLN and lower echelon nodes observed with FerroTrace, this could allow for discrimination of upper and lower echelon nodes based on magnetometer probe signal alone.

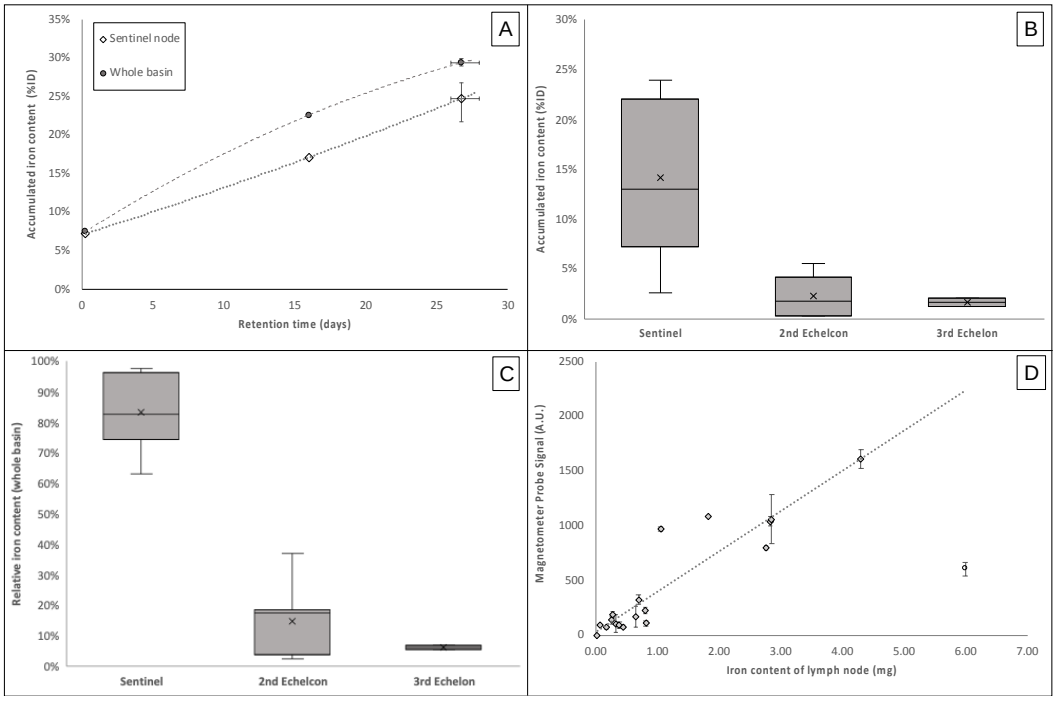

Figure 8.4 FerroTrace flow dynamics, retention and signal data.

A. Progression of FerroTrace content in lymph nodes over a 4-week period shows continued uptake into the SLN (line to guide the eye) and whole basin. B. Accumulated iron (percent injected dose, %ID) for each of the three echelons of node, for all time

points. C. Relative uptake of iron in the three echelons of node, normalised to the total iron content of draining basin. D. Linear correlation between magnetometer probe signal and iron content in lymph nodes (all samples, outlier indicated with unfilled circle). Deviations from this linear trend were typically from large nodes where the distribution of tracer is dispersed through a region larger than the sensing volume of the probe.

Pathological examination of dissected LNs and tongue injection sites demonstrated accumulation of mannose-labelled FerroTrace in the cytoplasm of macrophages, which in turn were predominantly located in the trabecular sinuses of LNs and the interstitial connective stroma between skeletal muscle bundles in the tongue (Figure 8.5). In all node and tongue samples, there was no sign of inflammatory cells (such as neutrophils, lymphocytes, or plasma cells) to indicate inflammation as a result of the tracer injection or accumulation. Furthermore, there was no sign of necrosis or cell degeneration, and the macrophages containing tracer particles were considered viable and healthy.

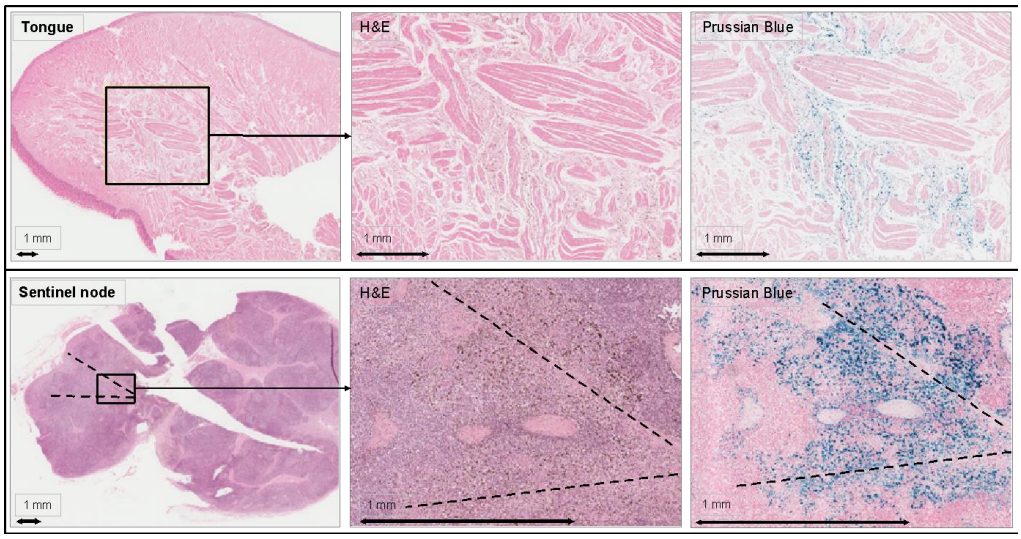

Figure 8.5 FerroTrace distribution in tissue at injection site and sentinel lymph node.

Examples of H&E and Prussian Blue staining of the tongue injection site (top row) and sentinel lymph node (bottom row) – taken from animal 3; 1.0 mL of 25 mg[Fe]/mL accumulated over 4 weeks. In the tongue, SPIONs collected predominantly in the interstitial connective stroma and between muscle bundles, whereas in lymph nodes accumulation was predominantly in the trabecular sinuses (dashed lines added to highlight trabeculae).

DISCUSSION

The magnetic technique for SLNB was first demonstrated to be clinically feasible in 2014 in a multicentre trial for breast cancer using the SentiMag magnetometer probe in combination with the Magtrace predecessor, Sienna+.[253] Since then, there have been several other large prospective non-inferiority trials for breast cancer evaluating this technology. A meta-analysis published in 2016 by Zada et al. found seven clinical trials comparing magnetic SLNB to the standard technique, with pooled data demonstrating that although the magnetic technique was non-inferior to the standard technique, it had an associated higher LN retrieval rate.[267]

To further develop the magnetic-approach, improve SLN retention, and reduce the number of draining nodes, FerroTrace was designed with a maghemite iron oxide core coated with a 2-part block copolymer consisting of a 70:30 mixture of stabilising and targeting polymers. The targeting block copolymer incorporates mannose to recognise and bind to the CD206 mannose-receptors on macrophages in the same fashion as technetium radiotracer Lymphoseek, which has been FDA approved and indicated for use in SLNB practice.[248]

While application of conventional lymphotropic tracers (radiotracers, radiotracers + dye) for SLNB in OSCC is capable of ~ 95% accuracy; high false negative rates, radiation shine-though from the injection site, tracer flow-though, and lack of soft-tissue anatomical detail in preoperative imaging[341] create opportunities for an improved approach. Such options are worth pursuing, given the less invasive approach of SLNB over END in cN0 patients not only reduces patient morbidity, but the number of nodes

requiring pathological resection is drastically reduced. In a multicentre trial using Lymphoseek in OSCC, Agrawal and colleagues[167] reported a reduction from an average of 37.9 resected LNs via END (sentinel and non-sentinel) to 3.9 if only SLNB was performed. Such a significant reduction in the number of LNs not only reduces the complexity and length of surgery, it also eases the burden on pathologists performing sample preparation and sectioning, and provides opportunity to use additional pathological techniques (such as serial sectioning and immunohistochemistry), which can increase upstaging rates.[340]

This preclinical study into the efficacy of mannose-labelled FerroTrace in the head and neck, while preliminary, shows promising results. Uptake of FerroTrace into the SLN could be clearly distinguished via MRI 15 to 30-minutes after injection and remained for the maximum 4-week test period. While we have not demonstrated complete clearance of FerroTrace from the injection site, a somewhat linear accumulation of tracer into the LNs over time suggests clearance is ongoing at the end of our 4-week test period, and may be expected to continue beyond that. Though the mannose-coating did not completely eliminate flowthrough to lower echelon nodes, FerroTrace had a significantly greater uptake in the SLN, and comparatively reduced uptake in lower echelon nodes. These characteristics, in combination with use of an intraoperative magnetometer probe allowed the SLN to be identified based on probe signal (relative to lower echelon nodes in the same draining basin) for all retention times.

The lymphotropic-profile of FerroTrace described in this study (fast migration, high SLN affinity, long retention) is potentially clinically significant. Swift migration of tracer to the SLN in concert with good retention over time will allow for both early imaging and

imaging over a long time-window; thereby increasing flexibility of the diagnostic aspect of the procedure in relation to timing of surgery. This is in opposition to the conventional use of radiotracers, where the windows of optimal use are dictated by a short radioactive half-live and the need to generate fresh radiotracers daily within the nuclear medicine department. In addition, pivoting to a magnetic approach holds great potential to overcome some of the inherent shortcomings associated with conventional radionuclear SLNB approaches. For example, unlike lymphoscintigraphy, MRI provides excellent spatial resolution with high sensitivity to soft tissues, which makes it ideal for lymphatic mapping and surgical planning.[251] In addition to spatial resolution inherent to the acquired images, MRI sequences can be designed to minimise the magnetic susceptibility artefacts produced by large quantities of tracer at the injection site, as opposed to scintigraphic images where injection site shine-through can occlude nearby SLNs[347]; thus limiting the resolving power of nodes close to the primary tumour. Furthermore, using magnetic tracers and MRI avoids exposure to ionising radiation which is highly attractive from a safety viewpoint. From a logistical viewpoint, magnetic tracers are not burdened by considerations associated with short half-life radioactive compounds that impact shelf-life, and timing of injection, imaging and surgery.[252] In addition, unlike radiocolloids, magnetic tracers produce a dark brown to black colour in the LNs to provide optical feedback without the use of an additional blue-dye injection.[253] With these advantages in mind, a magnetic approach presents an attractive next generation technique with significant potential to increase adoption of SLNB in the complex head and neck lymphatic environment.

While the results from this preclinical study are promising and provide proof-of-concept for use of this new tracer, several limitations of this study should be highlighted. As a

preliminary study, only a small number of animals were included, and future studies should focus on repeating a fixed dose or injection-to-dissection timepoint for increased confidence. Furthermore, in all the pigs studied, the submandibular node was typically larger in size compared to lower echelon nodes; hence, in order to uncouple any effects the node size might have on passive tracer accumulation, additional complex sites should also be explored in future studies (such as upper-gastrointestinal or colorectal). With respect to sensitivity and specificity of SLN detection, a small-animal tumour model would be preferential over healthy large animals, though in this instance use of a small animal comes at the cost of potentially affecting clinical translation of knowledge gained from human-relevant dosages and accumulation times.

Though the addition of a mannose-label to this magnetic tracer resulted in high levels of SLN retention for all timepoints, flow-through to second and third echelon nodes was still observed. Despite this, we showed that based on the total iron content of draining nodes, the SLN accounts for an average of 83 % of FerroTrace uptake. In addition, linear correlation between tracer uptake into LNs and magnetic signal indicates the potential for magnetometer probes to approximate iron quantity and may allow discrimination of SLNs from lower echelons. Development of a sequence of short MRI scans performed immediately after injection of the tracer may further help differentiate the SLN from lower echelon nodes, as the 'sentinel' status would be defined more accurately based on temporal data – i.e. which nodes are the first to receive drainage from the injection site. In addition, MRI protocols interrogating changes in magnetic susceptibility artefacts with changing echo time could potentially be used to approximate iron quantity in the nodes. In clinical application, a single MRI scan performed after injection is preferable to scans at multiple timepoints (with respect to both cost and logistics of planning multiple scans),

so exploring options which allow sentinel status to be identified either immediately after injection or some arbitrary time later will be of interest for future studies.

While node locations could be reasonable ascertained from preoperative MRI, the anatomy of the pig neck presented a learning curve for the surgical team and some lower echelon nodes proved difficult to isolate based on visual confirmation and probe signal alone. In future animal studies, anatomy of the swine neck could be better studied with the addition of a lymphotropic dye to more clearly highlight the lymphatic vessels and draining nodes. It is anticipated that this approach will reduce the time taken to locate draining nodes while providing a complete map of the draining lymphatic basin, given non-targeted dyes should flow through all levels of LN. As such, future studies will look to employ the fluorescent tracer ICG, which when paired with a specialised infrared camera is expected expedite localisation of the FerroTrace laden SLN, facilitate complete mapping of the lymphatic vessels and nodes, and (unlike blue dyes) will not obscure the brown staining provided by the magnetic tracer.

When LNs in animals were examined at 4 weeks there was still increasing uptake of FerroTrace in lower echelon LNs indicating that a small quantity of tracer was still ‘leaking through’ to lower-echelon nodes. This may be due to non-optimised labelling of mannose on the particles, and therefore it should be the focus of future studies to increase the binding affinity of the particles to macrophages.

When increasing the injected dose from 6.25 mg to 25 mg of iron, the amount of FerroTrace accumulating in draining nodes increased proportionally, independent of the injected volume. Though greater levels of uptake can aid intraoperative detection using magnetometer probes, consequences of higher injected doses include significant

susceptibility artefacts on MRI scans that may conceal or distort nearby anatomical landmarks, and larger injected volumes resulting in greater patient discomfort and tissue discolouration.[348] Based on the results of this study, a dose of between 0.25 to 0.5 mL, 50 mg[Fe]/mL FerroTrace is suggested as a compromise between reducing injected volume while maintaining sufficient iron dose for intraoperative detection.

This study demonstrates highly promising lymphatic flow properties of FerroTrace, a novel lymphotropic mannose-labelled magnetic tracer with significant potential for use in head and neck SLNB. Early phase clinical trials are underway to establish the safety and feasibility of this novel tracer in humans, the management of which has been guided, in part, by the findings of this study.

CHAPTER 9: MANNOSE LABELLED MAGNETIC TRACER FOR SENTINEL LYMPH NODE BIOPSY IN ORAL SQUAMOUS CELL CARCINOMA: INITIAL RESULTS FROM A PHASE 1 FERROTRACE CLINICAL TRIAL

STATEMENT OF AUTHORSHIP

Title of paper	Mannose-labelled magnetic tracer for sentinel lymph node biopsy in oral squamous cell carcinoma: Initial results from a phase 1 FerroTrace clinical trial
Publication status	☐ Published ☐ Accepted for Publication ☐ Submitted for Publication ✓ Unpublished and Unsubmitted work written in manuscript style
Publication details	Krishnan G, Cousins A, Krishnan S, Wormald PJ, Dhatrak D, Otto S, Walls A, Dwyer A, Thierry B, Badlani J, Krishnan S, Forema A. Mannose-labelled magnetic tracer for sentinel lymph node biopsy in oral squamous cell carcinoma: Initial results from a phase 1 FerroTrace clinical trial. *Prepared for submission.*

Principal Author

Name of Principal Author (candidate)	Giri Krishnan		
Contribution to the Paper	Study conception and design. Clinical trial coordinator. Recruitment of patients. Assisted in surgery. Data collection, analysis and interpretation. Manuscript preparation.		
Overall percentage (%)	75%		
Certification	This paper reports on original research I conducted during the period of my Higher Degree by Research candidature and is not subject to any obligations or contractual agreements with a third party that would constrain its inclusion in this thesis. I am the primary author of this paper		
		Date	20.09.2021

Co-Author Contributions

By signing the State of Authorship, each author certifies that:

i. The candidate's stated contribution to the publication is accurate (as detailed above);
ii. Permission is granted for the candidate in including the publication in thesis; and
iii. The sum of all co-author contributions is equal to 100% less the candidate's stated contribution.

Name of Co-Author	Aidan Cousins		
Contribution to the Paper	Study conception and design. Data collection, analysis and interpretation. Manuscript preparation.		
Signature		Date	28.09.2021

Name of Co-Author	Shridhar Krishnan		
Contribution to the Paper	Assistance in patient recruitment. Assistance in surgery. Clinical management of patients. Data collection, analysis and interpretation.		
Signature		Date	11.10.2021

Name of Co-Author	PJ Wormald		
Contribution to the Paper	Project supervision. Data interpretation. Manuscript preparation.		
Signature		Date	27.09.02021

Name of Co-Author	Deepak Dhatrak		
Contribution to the Paper	Pathological supervision. Pathology processing design. Data interpretation. Manuscript editing.		
Signature		Date	24.09.2021

Name of Co-Author	Sophie Otto		
Contribution to the Paper	Pathological supervision. Pathology processing design. Data interpretation. Manuscript preparation.		
Signature		Date	24.09.2021

Name of Co-Author	Angela Walls		
Contribution to the Paper	Radiological sequence development, analysis and interpretation. Manuscript preparation.		
Signature		Date	05.10.2021

Name of Co-Author	Andrew Dwyer		
Contribution to the Paper	Radiological data analysis and interpretation. Manuscript preparation.		
Signature		Date	24.09.2021

Name of Co-Author	Benjamin Thierry		
Contribution to the Paper	Project supervision. Study conception and design. Data interpretation. Manuscript preparation.		
Signature		Date	24.09.2021

Name of Co-Author	James Badlani		
Contribution to the Paper	Performed surgery and assisted in tissue sample collection. Data interpretation. Manuscript editing.		
Signature		Date	25.09.2021

Name of Co-Author	Suren Krishnan		
Contribution to the Paper	Project supervision. Study conception and design. Performed surgery and assisted in tissue sample collection. Data interpretation. Manuscript preparation.		
Signature		Date	11.10.2021

Name of Co-Author	Andrew Foreman		
Contribution to the Paper	Project supervision. Study conception and design. Performed surgery and assisted in tissue sample collection. Data interpretation. Manuscript preparation.		
Signature		Date	23.09.2021

ABSTRACT

Aims

SLNB promises less morbidity than END in patients with cN0 OSCC. Despite this, it is not widely practiced because of limitations of radiotracers that affect logistical feasibility and accuracy in the complex head and neck environment. To circumvent this, we evaluated the feasibility of a novel magnetic approach using a mannose-labelled magnetic nanoparticle.

Methodology

A phase 1 prospective clinical trial was conducted at the Royal Adelaide Hospital, recruiting patients with cN0 OSCC. An injection of a SPION (FerroTrace Ferronova Ltd Adelaide, Australia) was delivered around the tumour. Patients underwent MRI with pseudo-dynamic and static sequences prior to SLNB, which was performed using a hand-held magnetometer probe. SLNs were sent for serial-sectioning and patients underwent END in the same procedure to allow for comparison with gold-standard.

Results

Eight patients were enrolled with T2 lesions located in either the lateral tongue (4/8), RMT (3/8) or FOM (1/8). A total of 227 LNs were dissected of which, one returned positive for metastatic disease. 23 SLNs were identified on MRI and 22 (95.7%) of these were identified intraoperatively. Overall, the magnetic technique had a sensitivity of 100%, specificity 90.3% and NPV of 100% for identification of metastatic disease in the 227 LNs resected across the cohort. No adverse events were recorded.

Conclusion

This study demonstrates the procedural feasibility of a novel magnetic approach to SLNB in OSCC using a first-in-human magnetic tracer. These promising early results lay the foundation for an attractive next generation technique with significant potential to increase adoption of SLNB in the complex head and neck lymphatic environment.

INTRODUCTION

OSCC metastasises to the neck with high affinity.[37, 38] Neck disease is the most important prognostic factor as it halves survival, and 25% of patients with no clinical or radiological evidence of neck disease (cN0) will have occult metastases.[39] SLNB is an accepted approach for the management of the neck in these patients and has equivalent diagnostic and oncological outcomes.[182, 185, 186] In addition, it has decreased morbidity and improved cost-efficacy when compared to END.[193, 195] Despite this, it is not widely practiced.[196, 197]

While many reasons have been cited for the poor adoption of SLNB in OSCC, ultimately, the fundamental barrier is the potential and detrimental risk of yielding a false negative result in a highly curable setting.[203] Relative to other sites in the body, this risk is high in the oral cavity because of its uniquely complex cervical lymphatic drainage pathways where SLNs can be multiple and lie in close proximity to the primary tumour.[206, 207] This decreases the margin for error from inherent limitations of radiotracers like rapid "flow-through" to lower-echelon LNs, or "shine-through", where signal at the injection site masks the signal from the SLN.[198, 202]

The use of SPIONs for SLNB instead of conventional radionuclear technology, is anticipated to circumvent these limitations.[257, 258] Unlike gamma rays, magnetic signal is greatly reduced over distance, effectively removing the effect of shine-through.[254] MRI provides excellent spatial resolution with high sensitivity to soft tissues, making it ideal for lymphatic mapping and surgical planning.[251] Additionally, SPIONS can be

magnetised to generate a signal for detection by a hand-held probe, analogous to the use of a gamma probe for intraoperative SLN localisation.[254]

From a logistical viewpoint, a magnetic tracer has a long shelf-life, does not require any changes to infrastructure or licensing to handle and administer (unlike radioactive tracers), and the magnetic signal does not decay over time like radiation does, so injections can be performed in advance without the risk of losing signal over time.[349]

In order to leverage these benefits, a previously developed SPION with size and stability properties suitable for optimal migration in complex lymphatic environments has been labelled with mannose which recognises and binds to the CD206 mannose-receptor on macrophages, and consequently improves retention in draining LNs. [272-274] A comprehensive pre-clinical testing program in a large animal swine model demonstrated the excellent diagnostic performance of this tracer (*FerroTrace*, Ferronova) as well as excellent clearance from the injection site, a key feature as magnetic artefacts associated to residual magnetic tracer has limited the clinical use of *MagTrace*, a previously accepted magnetic tracer. The aim of this first-in-human phase 1 clinical trial was to evaluate its procedural feasibility and safety, as a first step, prior to moving to larger studies evaluating its accuracy

MATERIALS AND METHODS

Clinical trial

A prospective single-centre, non-randomized, phase I clinical trial was approved by the Central Adelaide Local Health Network Human Research Ethics Committee and conducted between July 2020 and July 2021. The study was performed in accordance with the Helsinki Declaration of 1975 and its amendments and FDA's ICH-GCP guidelines. Written informed consent was obtained from all patients.

For inclusion, patients required biopsy proven primary T1-T2 N0 OSCC scheduled for curative primary tumour resection and neck dissection. The N0 status of the neck was determined with either a CT neck and/or MRI neck, with or without FDG PET-CT as confirmed by both the surgical team and a board-certified radiologist. A performance status of ECOG 0 – 2 was required, and patients needed to be willing to provide informed consent. Exclusion criteria included a past history of head and neck cancer, previous head and neck radiotherapy, lip involvement, allergy or intolerance to iron oxide or dextran compounds, a metal implant at or close to the neck, iron overload disorder, pregnant or lactating and standard contraindications to MRI scanning.

Mannose-labelled 'FerroTrace'

To produce the mannose-labelled FerroTrace tracer (*Ferronova*, *Australia*), maghemite iron oxide (γ-Fe_2O_3) SPIONs were synthesised using coprecipitation of iron salts. A RAFT block copolymer was previously developed and shown to enable highly-stable

coating of SPIONs, demonstrating excellent systemic biocompatibility and clearance. Two types of block copolymer were coated to the SPION surface, a stabilising-RAFT (70%) and a macrophage-targeting mannose-RAFT (30%). The stabilising block copolymer consisted of an anchoring [(monoacryloyloxy)-ethyl]phosponic acid group (n = 5), a polyacrylamide stabilising polymer (n = 50 monomers), a hydrophilic PEG group (n = 17), and an end alkyl group. The targeting block copolymer consisted of an anchoring [(monoacryloyloxy)-ethyl]phosponic acid group (n = 5), a polyacrylamide linking polymer (n = 70 monomers), and a targeting group of mannose. The tracer suspension was purified via centrifugation to remove excess polymer and filtered with a 0.22 μm filter. Aliquots of the tracer were packaged into sterile vials under aseptic conditions, after which they could be stored at room temperature. No further processing or filtration was required prior to injection.

SPION administration and pre-operative MRI

SPION was administered with 4 submucosal injections around the tumour at 3, 6, 9 and 12 o'clock, at a distance of approximately 0.1- 0.5cm from the macroscopic margin. To confirm feasibility of the magnetic approach, three patients underwent magnetic SLNB with a commercial SPION tracer, MagTrace (*Endomaeg, UK*). This was purchased off-the-shelf and delivered in four aliquots of 0.25mL at a concentration of 28 mg[Fe]/mL as indicated by the instructions for use. All other patients received FerroTrace at a concentration of 50mg/mL in 4 aliquots of 0.1mLs. Injections were performed ~24 hours prior to surgery. Lidocaine hydrochloride spray was used for local anaesthesia 20 minutes prior to injection. Following injection, patients were asked to score the pain level using a 1-10 level pain scale.

Imaging was performed on a clinical 3.0T MRI system (*Siemen Healthineers, Erlangen, Germany*). Patients were scanned pre-injection using T1 diffusion weighted images and normal TE GRE sequences. A 'pseudo-dynamic' imaging protocol was used immediately post-injection in order to identify lymphatic vessels that drain from the tumour to the first echelon LN(s). This consisted of 4 - 5 low-TE sequenced scans at 100 second intervals in the axial plane only for the first 10 minutes commencing immediately following injection. At four separate time-points following injection (30 minutes, 1 hour, 4 hours and 24 hours) patients underwent a complete scanning sequence of T1 and T2 weighted images, diffusion weighted images and normal TE GRE sequences in axial and coronal planes.

The 'MRI-hot' SLN was identified as the first LN in the pseudo-dynamic scans to demonstrate a change in negative contrast as a result of the tracers' magnetic susceptibility. All SLNs were labelled and annotated individually. In cases of multiple LN uptake at a single time point (ie multiple first echelon LNs), LNs were labelled 'SN1', 'SN2', etc, in order of largest percent of LN area filled.

Magnetometer probe

For intraoperative magnetic signal detection, a handheld magnetometer probe (FerroMag, *Ferronova, Australia*) was used (Figure 9.1). The probe consists of a small excitation coil to transmit an alternating magnetic field and solid-state MTJ sensors for high-resolution detection.[247, 254] The probe was used intraoperatively *in vivo* to confirm the identity of draining nodes containing SPIONs, and again *ex vivo* to determine the average maximum signal strength, which is typically correlated to the level of iron uptake in the LN.[350]

Figure 9.1 Intraoperative use of magnetometer probe.

Intraoperative sentinel lymph node detection

The operative approach followed the steps of a typical neck dissection. Prior to performing SLNB, a routine transverse supraomohyoid neck dissection skin incision was made and subplatysmal-flaps were raised. In order to localise the SLN, a 'triple method' approach was employed. Firstly, a pre-operative MRI was used to locate and target the neck level for dissection of individual SLNs. Secondly, during tissue dissection, surgeons attempted to optically discriminate SLNs by their dark appearance, due to the brown/black staining effect of the SPION tracer. In vivo and ex vivo photographic images were taken of LNs and they were graded by darkness by the surgeon according to a scale used for other magnetic SLNB clinical trials (no stain, some discolouration, black).[267] Thirdly, the FerroMag probe was used to record magnetic signal within draining LNs, with measurements taken both *in vivo* and *ex vivo*. In addition, in two patients enrolled in the trial (patient 5 and 6), the fluorescent ICG dye was used. In these two cases, a total of 0.4mL of 2.5 mg/mL ICG was injected in 4 equal aliquots in a quadrant around the tumour

at the same sites of magnetic tracer injection. A fluorescent camera (SPY-PHI, *Stryker, USA*) was used to image ICG tracer spread and fluorescent signal uptake in the SLN in real-time with the neck opened. For the first all patients, surgical resection of the oral cancer was performed prior to treatment of the neck to minimise possibility of shine-through. For the two patients where fluorescence was used, neck flaps were raised first, in order to facilitate injection of ICG and real-time imaging of the flow to first echelon LNs.

Pathological analysis

Dissected SLNs were sent individually to pathology and labelled as per the pre-defined annotation on pre-operative MRI. At pathology they were fixed in formalin and cut transversely along the long axis at 2mm intervals. Slides from these sections underwent initial evaluation with standard H&E staining, and if these returned negative, further evaluation was undertaken with IHC staining for the pancytokeratin marker AE1/AE3. In addition, slides underwent Prussian blue staining to identify the presence of ferric particles. The rest of the END specimen underwent routine histopathological analysis following orientation with resected nodal levels sent to pathology separately.

Safety testing

Serum iron level measurements and complete blood exams were performed at 2 weeks and 3 months postoperatively to monitor safety. The wound at the primary site was examined at follow-up visits for evidence of staining from tracer injection and a routine diagnostic MRI was performed at 6 months post-surgery to assess for clearance of the tracer and identify any residual levels within LNs or at the injection site that might impair future diagnostic MRI scans of the head and neck.

RESULTS

Patient characteristics

Between July 2020 and July 2021, eight adult patients were enrolled in this trial. Five patients were female and two male, with ages ranging from 37 to 75 years old. All patients had clinically T2 lesions located in the lateral tongue (4/8), RMT (3/8) or FOM (1/8). Primary tumours were located on the right in 4/8 cases, on the left in 3/8 cases and midline in 1/8 cases. Seven out of eight patients underwent surgical resection of their primary tumour and unilateral neck dissections of levels 1- 4 (in three cases level 5 was also dissected). In the patient with a FOM tumour, a bilateral neck dissection was performed (levels 2-4 on the left and 1-4 on the right). A total of 227 LNs were dissected, with an average of 28.4 LNs per patient. Of these, only 1 LN in the patient cohort returned positive for metastatic disease (patient 3). Overall the primary tumour staging in all patients remained the same following final pathological analysis. Nodal staging was upgraded in one patient (patient 3) from N0 to N1. A summary of patient characteristic data is presented in Table 9.1.

Table 9.1 Summary of patient, tumour and nodal characteristics.

	Patient number							
	1	2	3	4	5	6	7	8
Tumour	Left Lateral tongue	Right RMT	Left Lateral tongue	Right RMT	Left Lateral tongue	Right Lateral tongue	Midline FOM	Left RMT
Stage	T2 N0	T2 N0	T2 N0	T2 N0	T2 N0	T2 N0	T2 N0	T2 N0
Tracer	FerroTrace	Magtrace	FerroTrace	FerroTrace	FerroTrace + ICG	FerroTrace + ICG	Magtrace	Magtrace
SPION dose (mg [Fe])	10	28	20	20	20	20	11	11
Pseudodynamic MRI nodes	-	2	4	2	3	1	1	1
30-minute MRI nodes	5	29	9	4	10	18	2	2
Final MRI nodes	27	69	51	30	18	41	34	30
Drainage	Unilateral	Unilateral	Unilateral	Unilateral	Unilateral	Unilateral	Bilateral	Unilateral
Nodes dissected	34	44	19	29	16	28	38	19
Metastatic nodes	0	0	1	0	0	0	0	0

Preoperative MRI

Twenty-three SLNs were identified on pre-operative MRI. Locations for identified SLNs included level Ib (7/23, 30.4%), IIa (11/23, 47.8%), III (2/23, 8.7%) and IV (3/23, 13%). Pseudodynamic imaging allowed identification of lymphatic vessels that drain to the tumour in all patients in which it was performed as demonstrated in Figure 9.2A-C. In patients injected with FerroTrace, time from tracer injection to uptake in the first draining LN averaged 5 mins (range 3- 6mins). There was a much larger range of timing of uptake in the three patients injected with MagTrace from 3 – 30 minutes.

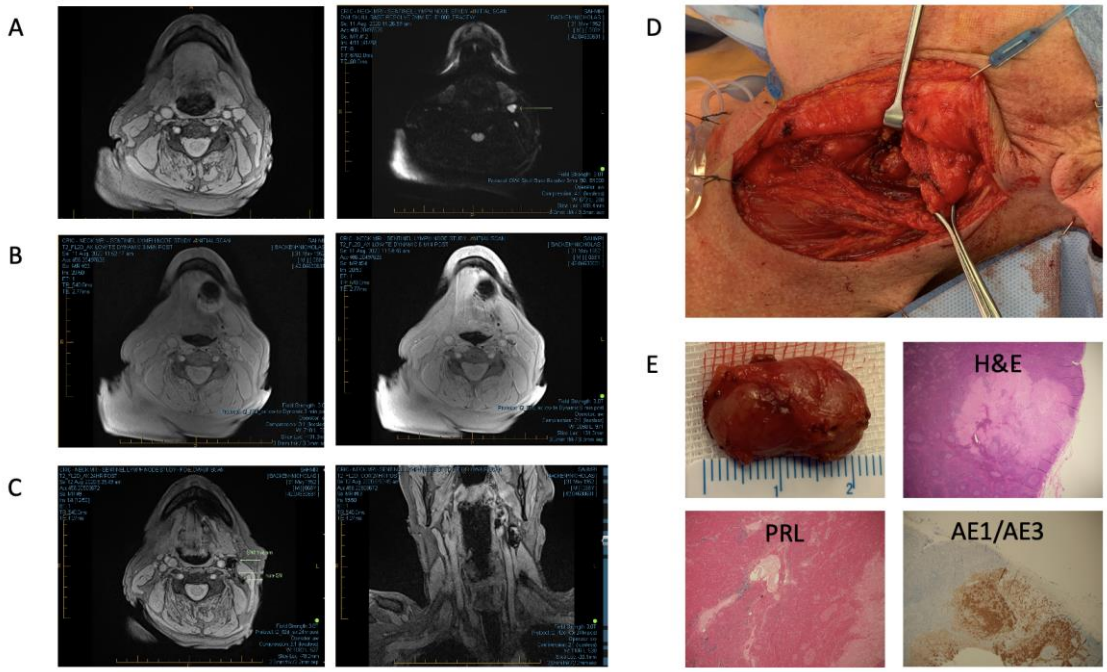

Figure 9.2 Figure 2. Successful identification of tumour positive lymph node with the magnetic approach using FerroTrace.

A. Pre-injection T2WI and DWI. B. Pseudo dynamic images taken at 3 and 6 minutes post-injection demonstrating tracer flow from injection site in left lateral tongue to first echelon LN at level IIA. C. Full-sequence T1WI scans in the axial and coronal plane clearly demonstrating MRI-hot SLNs in in relation to surrounding anatomic structures for three-dimensional localisation. D. Identification of dark-staining SLN following elevation of subplatysmal flaps. E. Macroscopic appearance of dissected SLN, and H&E slide demonstrating metastatic tumour deposition. Prussian blue (PRL) slide demonstrating ferric iron deposition, and IHC slide demonstrating AE1/AE3 positivity.

Sentinel lymph node data

SLN data is presented in Table 9.2. Overall 22/23 (95.6%) of SLNs identified on MRI were located and resected intraoperatively. In patient 4, a cluster of 3 LNs in level 1B was identified as being first echelon on MRI, but following resection of this cluster, only 2 LNs were identified within it at pathology. All resected SLNs registered magnetic signal with the magnetometer probe both in vivo and ex vivo and demonstrated iron deposition on Prussian blue staining at pathology. Average probe signal *in vivo* was 73 (range 45 – 209, n = 12), versus *ex vivo* 94 (range 73 – 235, n = 18). The short axis diameter of SLNs averaged 5.8mm (range 2 – 10mm), and on average the presence of SPIONs in the SLNs caused a light brown discolouration.

Table 9.2 Summary of sentinel lymph node data.

Patient	SLN	Level	Colour grade	Size (mm)	Average probe signal (in vivo)	Average probe signal (ex vivo)
1	1	1b	Mild	15 x 10 x 7	52	43
	2	2a	Mild	20 x 10 x 5	61	84
	3	3	Mild	15 x 8 x 5	62	63
	4	2a	Mild	8 x 7 x 5	62	71
	5	4	Mild	7 x 3 x 3	N/A	43
2	1	2a	Dark	30 x 15 x 7	209	191
	2	2a	Dark	12 x 6 x 5	91	85
3	1	2a	Mild	20 x 12 x 9	40	46
	2	2a	Minimal	5 x 3 x 2	N/A	180

	3	2a	Minimal	10 x 7 x 4	N/A	170
	4	4	Mild	12 x 8 x 6	N/A	97
4	1	1b (cluster)	Minimal	11 x 7 x 5	40	40
	2	1b (cluster)	Minimal	13 x 7 x 4	30	39
	3	1b (cluster)	Minimal	SMG tissue	Below threshold	Below threshold
	4	2a	Mild	20 x 13 x 10	59	80
5	1	2a	Mild	30 x 11 x 8	83	68
	2	2a	Mild	25 x 15 x 6	45	46
	3	4	Mild	25 x 10 x 5	N/A	78
6	1	2a	Dark	17 x 9 x 9	80	73
7	1	1b	Minimal	10 x 8 x 5	38	40
	1	3	Minimal	8 x 4 x 4	61	61
8	1	1b	Mild	18 x 5 x 8	N/A	131
	2	1b	Mild	10 x 7 x 6	N/A	80

Highlighted row indicated tumour positive SLN. (SMG: submandibular gland; N/A indicates measurement not performed).

The one metastatic LN in the patient cohort was MRI-hot on preoperative imaging (Figure 9.2A-C). During surgery it had a dark appearance (Figure 9.2D) and magnetic signal was detected with an *in vivo* and *ex vivo* probe signal of 40 and 46 respectively. This LN measured 20 x 12 x 9mm and had a tumour deposit detected at pathology with H&E staining of 4.5mm in maximal dimension (Figure 9.2E). Overall, the magnetic technique

had a sensitivity of 100%, specificity 90.3% and negative predictive value of 100% for identification of metastatic disease in the 227 LNs resected across the cohort.

In the two patients where ICG was used in addition to the magnetic tracer, intraoperative fluorescent imaging demonstrated tracer uptake in the LNs that correlated with MRI-hot SLNs and were confirmed with magnetic signal registration with the magnetometer probe. This is demonstrated in the representative case (patient 6) in Figure 9.3, where intraoperative fluorescence imaging aided discrimination of two dark appearing LNs in close proximity at the site of the MRI-hot SLN.

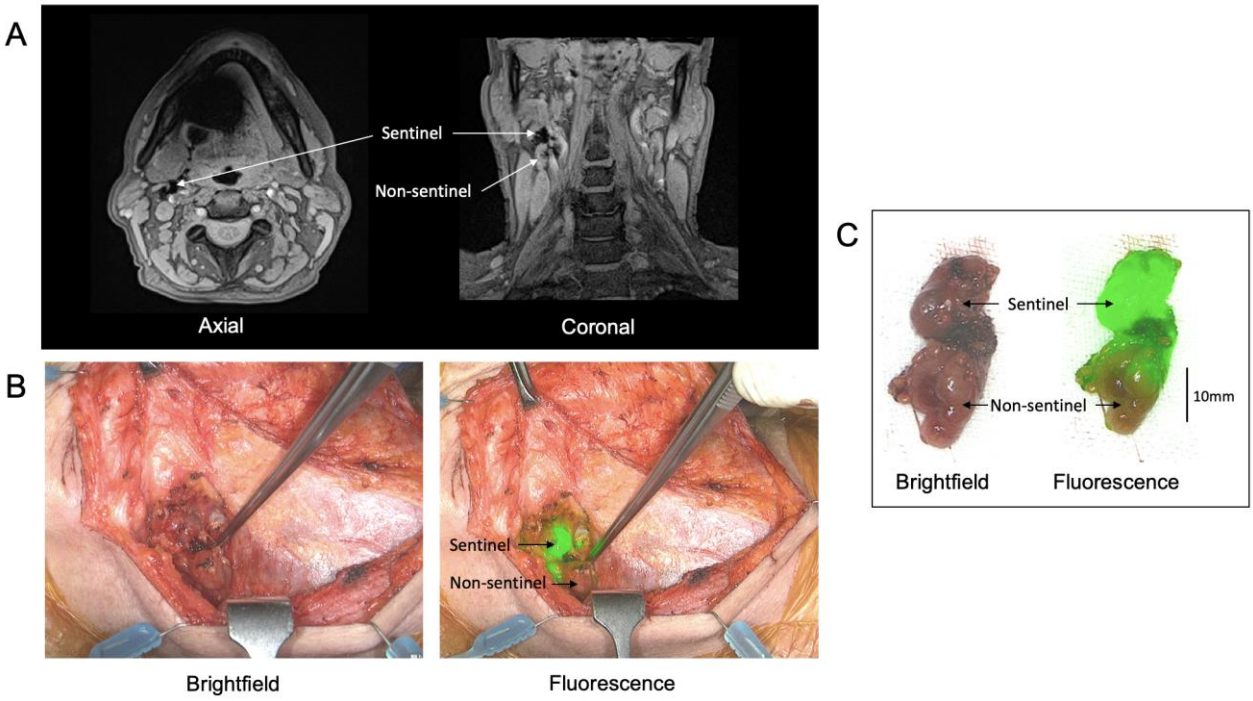

Figure 9.3 Figure 3. intraoperative real-time fluorescent imaging to aid SLN discrimination.

A. T1WI axial and coronal scans taken at 10 minutes from patient 6. On the coronal scan early filling of a LN inferior to the MRI-hot first echelon LN can be seen. B.

Intraoperatively following elevation of flaps both LNs can be seen and are both dark in appearance at 24-hour post-injection. Fluorescence imaging was able to discriminate first from second echelon in real-time. C. Following dissection of both LNs together, the superior LN demonstrates superior fluorescent signal.

Safety

All patients completed follow-up to 6-months post-operatively with no adverse events recorded. Average pain score of injection was 7.5/10. Serum iron levels remained normal at 2 weeks and 3 months post-operatively. In all patients, there was no residual tracer staining at the primary site at 2-week follow-up and no reports of persisting pain or skin damage relating to tracer administration. Residual tracer susceptibility artefact was not seen on diagnostic MRI scans performed at 6 months in any patients. (Figure 9.4).

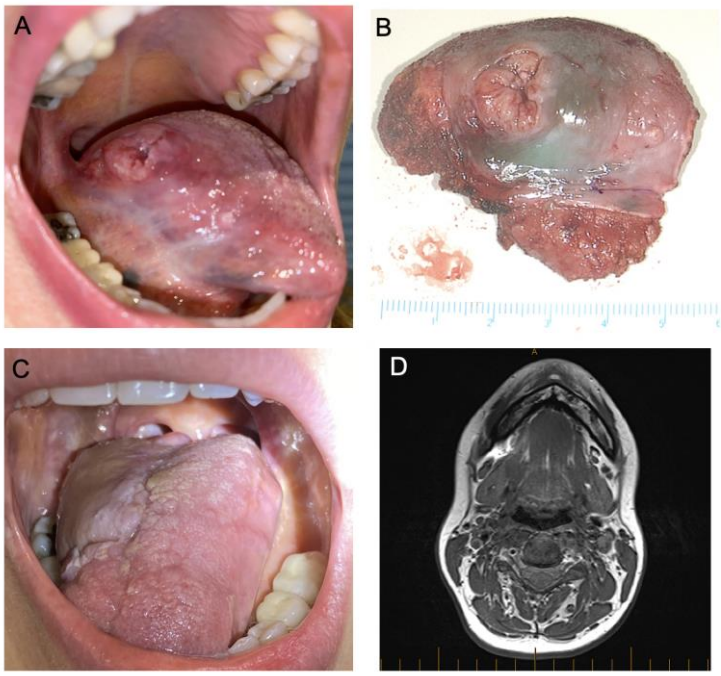

Figure 9.4 Figure 4. Demonstration of tracer clearance from injection site.

Representative images from patient 5. A. T2 right lateral tongue ulcer prior to FerroTrace injection. B. Resected tumour demonstrating dark staining appearance of tracer around the ulcer. C. Clinical photograph of patient's wound (with radial forearm flap filling defect) at 2 weeks. No tracer staining can be seen. D. Post-operative diagnostic T1WI MRI at 6-months showing no residual susceptibility artefact.

DISCUSSION

This first-in-human study demonstrates feasibility and safety of a novel magnetic SLNB approach for early-stage OSCC with a mannose-labelled superparamagnetic iron oxide nanoparticle tracer. In the 8 patients studied, 23 SLNs were identified on MRI. In all instances our pseudodynamic scanning sequence was able to demonstrate tracer flow through the lymphatics into the draining LN sinus. Overall 22/23 (95.7%) of MRI-hot SLNs were successfully located intraoperatively via visualisation of the optically dark tracer, and all of these were confirmed with magnetic signal via a hand-held magnetometer probe. Tracer was able to accurately identify the only tumour metastasis detected in the cohort, resulting in a sensitivity of 100%, specificity of 90.3% and NPV of 100% after assessment of all 227 resected LNs. No adverse events relating to the procedure were recorded and there was no evidence of residual tracer aggregation on follow-up MRI scans at 6-months.

Current best practice for conventional SLNB for OSCC involves a 'triple-method' of detection, with the injection of a radioisotope conjugated with a colloid followed by dynamic and static imaging with lymphoscintigraphy and SPECT-CT.[159-162] In addition, optical tracers, such as blue or fluorescent dyes delivered at time of surgery are recommended, with evidence suggesting that the additional modality improves sensitivity.[169] During surgery a gamma probe is used to guide SLN identification, where a SLN must have a count that is at least 10-times that of the background and more than 10% of the hottest node excised.[159]

To the best of our knowledge, the present study is one of the only clinical trials published evaluating a novel magnetic approach for SLN in OSCC and is the first to study the use of a lymphotropic magnetic particle. In the magnetic paradigm employed in this study, early scanning using the described pseudodynamic sequence allowed identification of tracer spread to first echelon LN after an average time of 5 minutes. Full-sequence scans at 10 minutes enabled localisation of SLNs in three dimensions with excellent anatomic resolution whereby SLNs could be mapped in relation to bony, soft tissues and vascular structures seen on MRI such as the skull base, mandible, SCM, submandibular gland, carotid artery and IJV. While in this study full-sequence scans were performed at 30-minutes and 4-hours post-injection in order to understand the flow-dynamics of this tracer, no further useful data for surgical planning was obtained at these timepoints. On the other hand, the 24 hours scans identified LNs that received a slower drainage from the tumour, which was helpful to distinguish between surgically relevant and irrelevant higher echelon nodes prior to SLNB. Given the speed of tracer spread, it is feasible that SLNB could be performed immediately following injection and imaging to avoid the need for another pre-operative scan. Conversely, future studies extending the time window between injection and SLN dissection will be useful for testing the efficacy of nodal retention in this lymphotropic tracer.

It is noteworthy that magnetic tracers, unlike radiocolloids, have a dark brown or black colour. In this study all identified SLNs demonstrated evidence of colour contrast as per the Magtrace grading system used by the surgeon and yielded satisfactory optical feedback. Therefore, in this SLNB paradigm, there is no need for an additional blue-dye injection, which carries a small risk of anaphylaxis. However, despite the mannose-target on Ferrotrace, it was observed during surgery 24-hours following injection, that LNs

surrounding the SLN were often also discoloured because of flow-throw (as demonstrated in Figure 9.3B). We therefore explored the benefit of combining the magnetic SLNB approach with intraoperative fluorescence guidance. To this end, in two patients ICG was additionally injected peri-tumourally at time of surgery.

Fluorescence imaging demonstrated ICG uptake that correlated with MRI and magnetometer probe findings for the SLNs. In the two patients where fluorescence imaging was additionally performed at time of surgery, the revised protocol afforded excellent discrimination of the true SLN(s) in what was really a 'quadruple approach'.

'Flow-through' of tracer is a pervasive issue with SLNB, and to minimise false negative results in the conventional radionuclear approach, all nodes in the area of the scintigraphic first echelon LN that are hot and coloured, only hot, or only coloured, are harvested.[160, 174] This can be a confusing and time-intensive protocol, that interrupts surgical work-flow. Based on the preliminary findings from this study, we are proposing a SLNB strategy using a quadruple approach for SLN detection hinged on the anatomic detail afforded by MRI to localise the level of the SLN, and then using optical imaging (dark stain) to detect and (real-time) fluorescence to discriminate first echelon LNs. This strategy has potential to expedite the procedure and improve overall specificity. This strategy is summarised in Figure 9.5 and should be further evaluated in future studies.

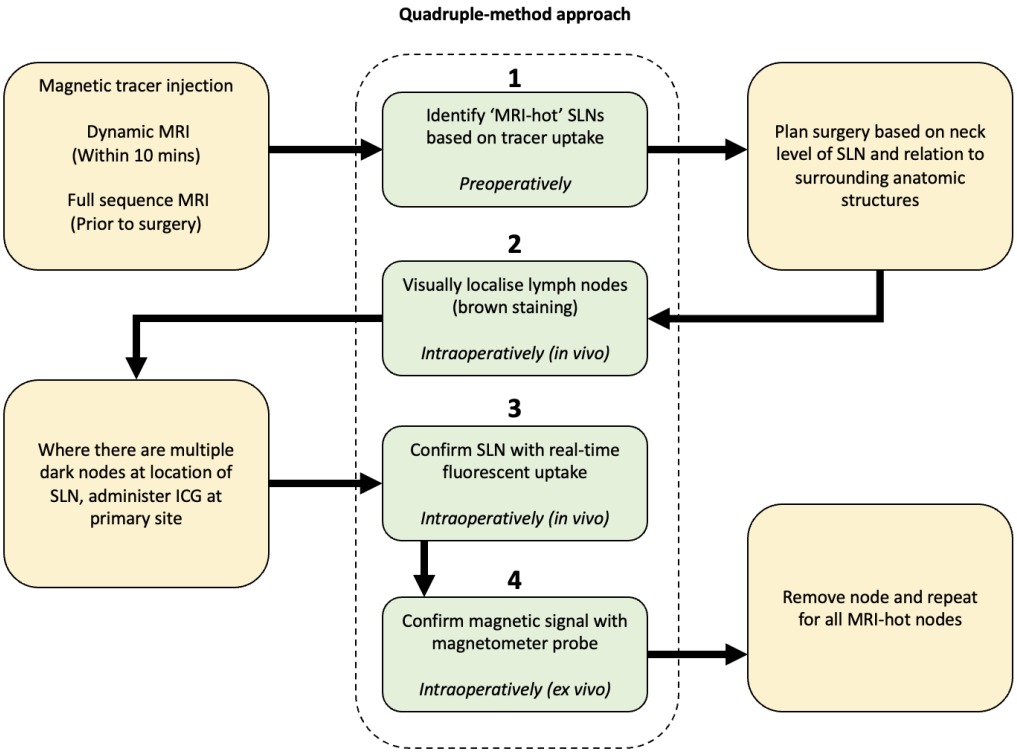

Figure 9.5 Proposed 'Quadruple method' for magnetic SLNB.

There is precedent for magnetic SLNB in breast cancer and melanoma. It was first demonstrated to be clinically feasible in 2014 in a multicentre trial for breast cancer using Sienna + (the predecessor of Magtrace) with the SentiMag magnetometer probe (both produced by *Endomagnetics, UK*). [253] Several large prospective non-inferiority trials followed and a metanalysis published in 2016 showed that the magnetic technique was non-inferior to the standard technique with a high identification rate but with a significantly higher LN retrieval rate.[267] However, poor clearance of the SPION tracer from the injection and resulting MRI artefacts were subsequently reported, limiting the clinical usability in breast cancer. Similarly, poor clearance in melanoma SLNB trials were reported, leading to high rates of skin staining, which caused issues with pain and skin necrosis. [268, 269] This was also identified in the MELAMAG trial for melanoma.[266]

Therefore, despite the fast rate of early diffusion, the significantly higher LN retrieval rate of Sienna+ or Magtrace compared with standard nanocolloid, and the clinically adverse outcome of skin staining, have been two critical shortcomings that have stunted ongoing practice [268, 270]

To address these problems, FerroTrace was designed with a maghemite iron oxide core coated with a 2-part block copolymer consisting of a 70:30 mixture of stabilising and targeting polymers. The nanoparticle has a hydrodynamic diameter of roughly 70nm and a high iron content (60%). The stability block consists of anchoring, stabilising and hydrophilic polymers and an end alkyl group to prevent degradation and aggregation in a biological environment. The targeting block copolymer incorporates mannose to recognise and bind to the CD206 mannose-receptors on macrophages in the same fashion as Lymphoseek.[248] While this study was not designed to verify the improved retention of mannose-labelled FerroTrace, our yet to be published preclinical studies in a large animal model support the benefit of the introduction of mannose onto the SPIONs. The preclinical studies also supported the improved clearance from the injection site of FerroTrace vs MagTrace, likely due to the excellent physicochemical properties of the tracer resulting from the application of a high performance coating. In the present study, at 2-week follow-up, no patient demonstrated tracer staining at the injection site on clinical exam. Furthermore, at 6-months, diagnostic MRI scans showed no residual susceptibility artefact at the primary injection site or in the neck. While FerroTrace particles have been designed for stability and decreased particle aggregation, it was not possible to determine the clinical benefit of this in this study as resection of tissue at the injection site with a clear margin will remove some tracer on the mucosal surface of the injection site.

As evaluation of safety and feasibility were the main objectives of this first-in-human study, there are some limitations to the assessment of the efficacy of this technology. While the steps of SLNB were tested, intraoperative identification of the SLN was probably made easier by widened access through a routine END incision which likely introduces bias as to the ease of feasibility of the approach. An END approach was necessary to preserve oncological safety as a priority in this phase 1 study and had the benefit of having all resected LNs for analysis. Despite this, the small sample size of eight patients makes meaningful conclusions on the efficacy of this approach impossible. Furthermore, tracer dynamics such as SLN retention by way of the mannose target were not formally evaluated, as this was not an objective of this study. Next steps are a phase II trial with a higher recruitment target to better evaluate accuracy and oncological safety, as well as testing a more streamlined MRI workflow, prior to phase III trials comparing FerroTrace against current standard of care to test non-inferiority.

CONCLUSION

This study demonstrates the procedural feasibility of a novel magnetic approach to SLNB in OSCC using a first-in-human magnetic tracer designed with enhanced stability properties. These promising early results lay the foundation for an attractive next generation technique with significant potential to increase adoption of SLNB in the complex head and neck lymphatic environment.

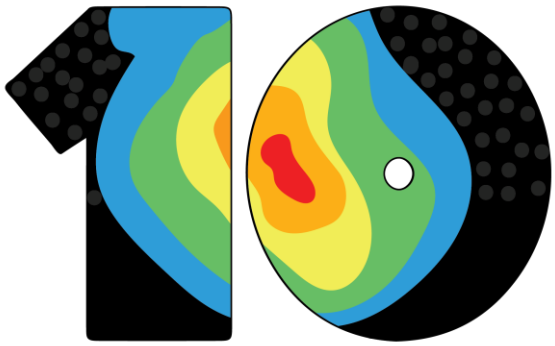

CHAPTER 10: FEASIBILITY OF ROBOT-ASSISTED SENTINEL LYMPH NODE BIOPSY IN THE HEAD AND NECK USING MULTI-MODALITY MAGNETIC AND FLUORESCENCE GUIDANCE

STATEMENT OF AUTHORSHIP

Title of paper	Feasibility of head and neck robot-assisted sentinel lymph node biopsy using multi-modality magnetic and fluorescence guidance
Publication status	☐ Published ☐ Accepted for Publication ☐ Submitted for Publication ✓ Unpublished and Unsubmitted work written in manuscript style
Publication details	Krishnan G, Cousins A, Milanova V, Krishnan S, van den Berg N, Rosenthal EL, Krishnan S, Wormald PJ, Thierry B, Foreman A, Krishnan S. Feasibility of head and neck robot-assisted sentinel lymph node biopsy using multi-modality magnetic and fluorescence guidance. *Prepared for submission.*

Principal Author

Name of Principal Author (candidate)	Giri Krishnan		
Contribution to the Paper	Study conception and design. Performed surgical procedures. Data collection, analysis and interpretation. Primary driver of manuscript writing.		
Overall percentage (%)	75%		
Certification	This paper reports on original research I conducted during the period of my Higher Degree by Research candidature and is not subject to any obligations or contractual agreements with a third party that would constrain its inclusion in this thesis. I am the primary author of this paper		
		Date	20.09.2021

Co-Author Contributions

By signing the State of Authorship, each author certifies that:

i. The candidate's stated contribution to the publication is accurate (as detailed above);
ii. Permission is granted for the candidate in including the publication in thesis; and
iii. The sum of all co-author contributions is equal to 100% less the candidate's stated contribution.

Name of Co-Author	Aidan Cousins
Contribution to the Paper	Study conception and design. Assisted with surgery. Data collection, analysis and interpretation. Manuscript editing.

Signature		Date	28.09.2021

Name of Co-Author	Ngyuen Pham		
Contribution to the Paper	Data analysis and interpretation. Manuscript editing.		
Signature		Date	24.09.2021

Name of Co-Author	Valentina Milanova		
Contribution to the Paper	Data analysis and interpretation. Manuscript editing.		
Signature		Date	24.09.2021

Name of Co-Author	Shridhar Krishnan		
Contribution to the Paper	Data analysis and interpretation. Manuscript editing.		
Signature		Date	11.10.2021

Name of Co-Author	Nynke van den Berg		
Contribution to the Paper	Data analysis and interpretation. Manuscript editing.		
Signature		Date	28.09.2021

Name of Co-Author	Eben Rosenthal		
Contribution to the Paper	Data analysis and interpretation. Manuscript editing.		
Signature		Date	24.09.2021

Name of Co-Author	Peter-John Wormald		
Contribution to the Paper	Data analysis and interpretation. Manuscript editing.		
Signature		Date	27.09.2021

Name of Co-Author	Benjamin Thierry		
Contribution to the Paper	Data analysis and interpretation. Manuscript editing.		
Signature		Date	24.09.2021

Name of Co-Author	Andrew Foreman
Contribution to the Paper	Project supervision. Data interpretation. Manuscript editing.

Signature		Date	23.09.2021

Name of Co-Author	Suren Krishnan		
Contribution to the Paper	Project supervision. Study design. Assistance in conducting experiments and performing surgery. Data interpretation. Manuscript preparation.		
Signature		Date	11.10.2021

ABSTRACT

Objectives

SLNB is a minimally invasive staging procedure that maps the spread of cancer from its primary site to regional LNs. It is poorly adopted in the head and neck where the lymphatic environment is uniquely complex. The objective of this study was to test the feasibility of a novel robot-assisted approach with magnetic and fluorescent guidance that could improve access to and accuracy of detection of cervical SLNs.

Materials and Methods

A SPION tracer and ICG were injected locally into the tongues of five pigs. Tracer spread to the first draining LN(s) was mapped with post-injection MRI. The da Vinci Xi surgical robot was used to access sentinel LNs through a retroarticular approach with intraoperative fluorescence image guidance using Firefly technology. A prototype hand-held magnetometer probe was used for confirmation of magnetic signal within dissected SLN.

Results

Robot-assisted SLNB was successfully performed in all pigs with adequate access to targeted LNs. Pre-operative MRI provided excellent anatomic resolution to map the location of SLNs in relation to surrounding landmarks. Fluorescence imaging provided valuable intraoperative guidance.

Conclusion

This study demonstrates pre-clinical feasibility of a novel robot-assisted approach to SLNB using dual-modality magnetic and fluorescence guidance in the head and neck. Clinical translation will enable improved access to SLNs across multiple neck levels with a single incision, holding promise for better adoption with improved oncological and aesthetic outcomes.

Key words

Head and neck cancer, Oral cancer, sentinel lymph node biopsy, Robotic surgery, Nanotechnology, Magnetic particles, Fluorescent molecular imaging, Translational science

INTRODUCTION

SLNB is a minimally invasive staging procedure that can avoid END in cN0 patients with oral and oropharyngeal cancer.[43] It has equivalent diagnostic yield to END with less morbidity due to the requirement for less tissue dissection.[186]

Despite promising benefits, conventional SLNB using radionuclear techniques for guidance has been poorly adopted in the head and neck where the complex anatomic and lymphatic environment presents several unique challenges. Firstly, primary head and neck tumours commonly drain to multiple first echelon LNs which are often scattered across numerous different neck levels presenting the surgeon with significant challenges in incision placement, or the need for multiple incisions; both of which can result in poor surgical access to the SLNs, and/or unsatisfactory aesthetic outcomes.[206] Secondly, guidance with conventional radionuclear tracers and nuclear imaging modalities has anatomic and spatial resolution limitations which can be unsatisfactory in the head and neck where level 1 LNs can lie in close proximity to the primary tumour and where elucidation of LN relationship to neurovascular structures is important.[351, 352] Finally, because there is a high concentration of LNs in the neck, precise intraoperative visualisation of the SLN is critical for accuracy.[353]

We hypothesised that these specific challenges could be addressed with a robot-assisted approach to SLNB in conjunction with the use of magnetic technology as an alternative to radionuclear technology. In this paradigm, robotic access to multiple nodal levels could be achieved via a modified face-lift incision resulting in a single incision hidden in the hairline. Adoption of magnetic resonance lymphangiography would provide localisation

of SLNs with excellent anatomical detail and provide better spatial resolution than nuclear imaging techniques. During surgery, the dark stain of the magnetic tracer would provide intraoperative SLN visualisation, removing the need for a separate methylene blue dye injection. Furthermore, the robot affords the opportunity for intraoperative NIR fluorescence image guidance with ICG.

Therefore, the objective of the present study was to evaluate the feasibility of performing robot-assisted SLNB in the head and neck using a multi-modality magnetic- and fluorescence-guided approach in a porcine model.

MATERIALS AND METHODS

Animals, anaesthesia and monitoring

All animal experiments were performed according to a protocol approved by the Animal Ethics Committee of the Institute of Medical and Veterinary Science, Adelaide, South Australia. All animal work was performed on site at the SAHMRI PIRL in compliance with "The Australian Code of Practice for the Care and Use of Animals for Scientific Purposes, NHMRC" and the ARRIVE guidelines. Five female pigs weighing approximately 40-50 kg were obtained and maintained according to institutional standards. Animals were anaesthetised with 1 mg/kg Xylazil-100 and 10 mg/kg ketamine administered intramuscularly. Endotracheal anaesthesia was induced and maintained with 5% and 2% isoflurane, respectively. Venous catheters were placed for administration of drugs. Heart rate, oxygen saturation and body temperature were monitored while animals were anaesthetised. At the completion of surgery animals were humanely killed with a lethal overdose of barbiturate.

Magnetic and fluorescent tracer

A proprietary SPION tracer, which has recently been approved for human use in Australia, was used in conjunction with ICG dye to perform SLN mapping. Briefly, the tracer consists of a crystalline iron oxide (maghemite) nanoparticle core and a polymer coating consisting of a 70:30 mixture of stabiliser (PEG) and macrophage-targeting (mannose) polymers. These particles have very high magnetic susceptibilities, which creates strong negative contrast in MRI, and can be detected with handheld magnetometer probes.[254, 354] Hence these particles can be used in an analogous manner to radiocolloids, without exposing patient or clinical team to any ionising radiation.[355]

For each pig, four equal SPION injections were delivered submucosally using an insulin syringe around a quadrant in the left ventrolateral surface of the oral tongue. In addition, each pig received four 0.1mL injections of 2.5mg/mL of ICG in the same location delivered immediately prior to neck incision (Figure 10.1A).

SPION tracer concentration and volume was delivered to the five pigs as follows: Pigs 1-3 received 0.4mL of 50mg/mL SPION, pig 4 received 0.35mL of 50mg/mL SPION premixed with 0.1mL of 8mg/mL of ICG (and therefore did not received a separate additional ICG injection), and pig 5 received 0.8mL of 25mg/mL of SPION.

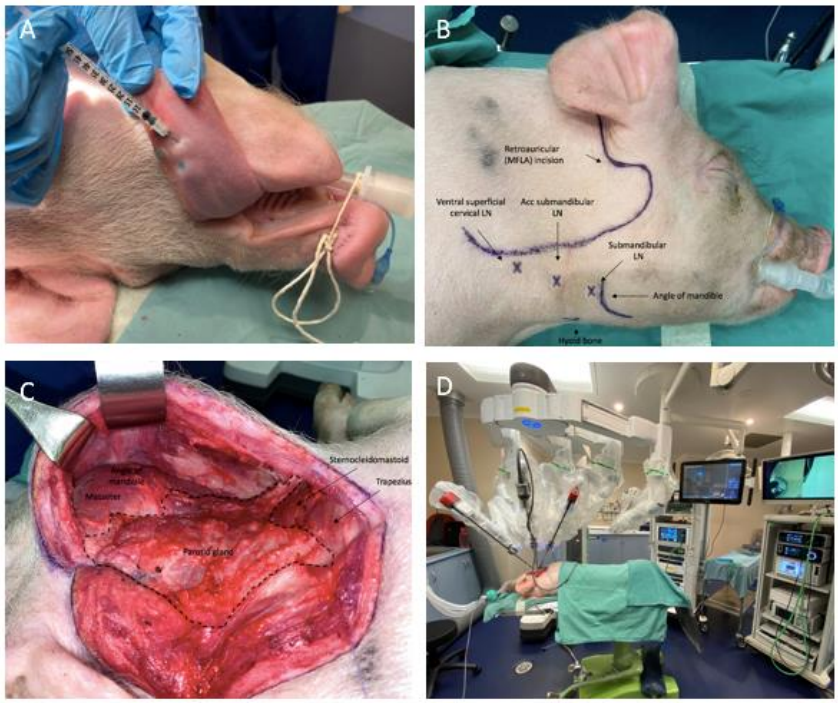

Figure 10.1 Representative workflow of tracer injection and cervical dissection.

(A) Injection of tracer in a quadrant in the left anterior ventrolateral tongue. (B) Neck incision marking for retroauricular approach designed to simulate a modified-face lift

incision. (C) Demonstration of dissection tunnel with key anatomic landmarks exposed following skin incision and raising of subplatysmal flaps. (D) The da Vinci Xi robot is docked, with endoscope and instruments placed into the dissection tunnel.

Pre-operative sentinel lymph node mapping with MRI

Imaging was performed on a clinical 3.0T MRI system (Siemen, Erlangen, German). Pigs were scanned pre-injection using T1WI, diffusion weighted images (DWI) and normal TE GRE sequences. A 'pseudo-dynamic imaging protocol' was used immediately post-injection, whereby pigs were scanned at 100 second intervals with low TE sequences in the axial plane only. At 1 hour post-injection, pigs underwent a final scan using T1 and T2 weighted images, diffusion weighted images (DWI) and normal TE GRE sequences. Axial and coronal planes were acquired in both the pre-injection and 1 hour post-injection scans. The SLN was identified as the first LN in the pseudo-dynamic scans to demonstrate a change in negative contrast as a result of the tracers' magnetic susceptibility.

Robot-assisted SLNB procedure

Pigs were positioned in a lateral decubitus position on the operating table to best replicate the standard extended and laterally rotated neck position used for human neck dissection. The skin incision began behind the pinna and was carried forward and then posteroinferiorly behind the ramus of the mandible (Figure 10.1B) to replicate a hair-line modified face-lift approach (MFLA) used for robot-assisted neck dissection (RAND) in humans.[356] Subplatysmal flaps were raised with monopolar diathermy to expose the three-cornered parotid gland to the masseter muscle anteriorly, the angle of mandible and

sternohyoid muscle inferiorly and the SCM and trapezius muscles posteriorly (Figure 10.1C).

The da Vinci Xi surgical system (Intuitive Surgical, Sunnyvale, CA) was docked on the contralateral side of the bed to the side of neck dissection (Figure 10.1D). Vision was provided by a 30˚ endoscopic camera equipped with 'Firefly' technology for ICG fluorescence imaging. A 5 mm Maryland forceps was introduced on the left side and harmonic curved shears on the right side. Dorsal flaps were retracted with a silk suture and ventral flaps were retracted by an assistant with 5 inch langenbeck retractors.

SLNB was performed by targeted dissection of individual SLNs in order of afferent tracer drainage from the injection site as identified by pre-operative MRI. The pig typically has three LN groups that drain from the oral tongue: The submandibular LN; the accessory mandibular LN; and the SVC chain of LNs, which include the cranial, middle and caudal LNs.[346] The location and surgical landmarks for identification of these LN clusters are schematically outlined in Figure 10.2.

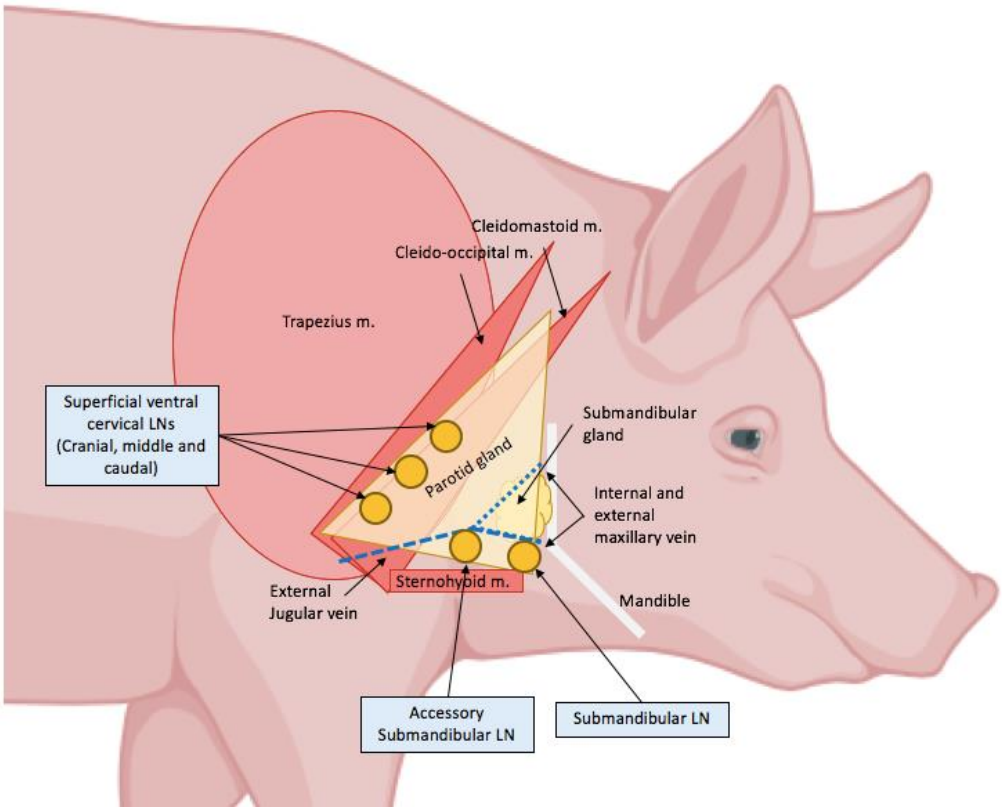

Figure 10.2 Schematic diagram of position of the submandibular, accessory mandibular and superficial ventral cervical chain of lymph nodes in relation to other key surgical landmarks for nodal dissection.

(m: muscle)

For dissection of the submandibular LN, the robotic endoscope was placed in the dissected tunnel and directed to the angle of mandible (Figure 10.3A). The anterior edge of the parotid gland was skeletonised and retracted posteriorly to reveal the submandibular gland. The submandibular LN lies anterior to the submandibular gland, lateral to the sternohyoid muscle and ventromedial to the angle of mandible. Caution was taken to identify and preserve or ligate the external maxillary vein on which the LN lies dorsal or ventromedial to.

The accessory mandibular LN was found by following the external maxillary vein distally to where it terminates into the external jugular vein. Here this LN lies ventral to the vein and is covered and partially embedded by the ventral edge of the parotid gland. Skeletonization and posterior retraction of the ventral aspect of the parotid gland allowed excellent visualisation of the lymph duct through the parotid tissue when the Firefly camera was activated, allowing the LN to be traced and excised (Figure 10.3B).

For best access to the superficial ventral cervical chain of LNs, the robotic endoscope was re-directed posteriorly in the tunnel to a groove between the trapezius and SCM muscles. These LNs form a row on the ventrolateral side of the SCM muscle. The posterior border of the parotid gland was skeletonised and retracted anteriorly. Again, the Firefly camera was activated allowing the LNs to be traced deep in the fascia between the muscle bellies (Figure 10.3C).

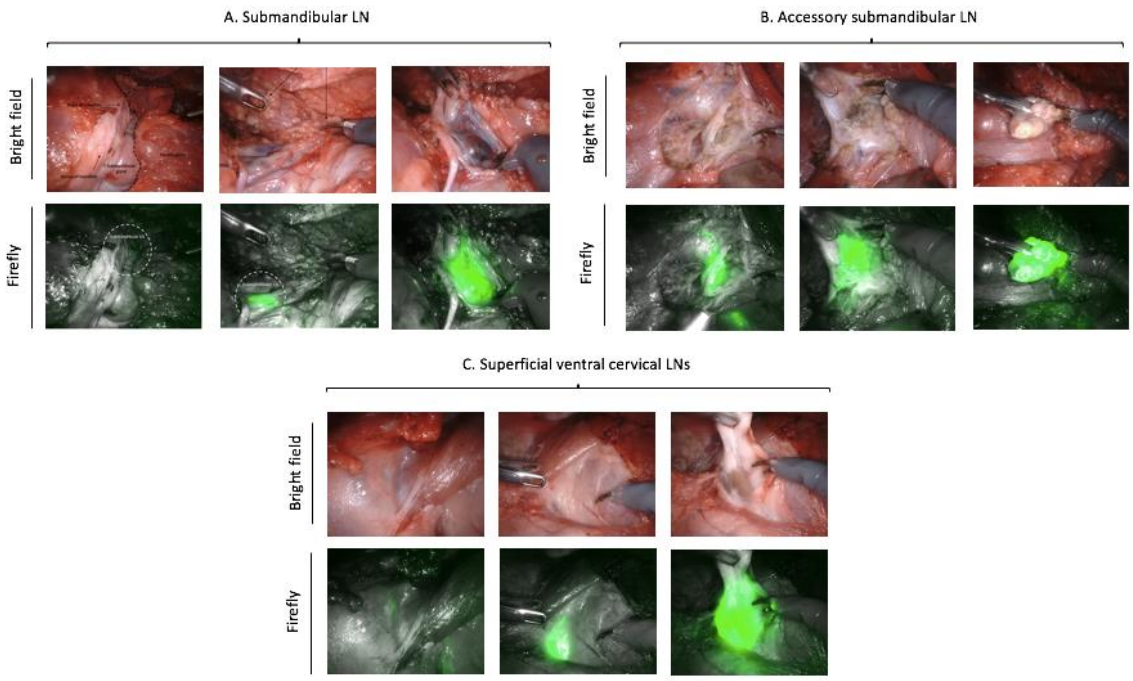

Figure 10.3 Endoscopic steps of Robot-assisted SLNB viewed in brightfield and with Firefly.

(A) The submandibular LN is accessed by skeletonising the anterior edge of the parotid gland at the angle of the mandible and retracting it posteriorly and dissecting deep to the submandibular gland. (B) Skeletonization and posterior retraction of the ventral aspect of the parotid gland demonstrates visualisation of the lymph duct through the parotid tissue with Firefly allowing the accessory mandibular LN to be traced and excised. (C) The superficial ventral cervical LNs form a row on the ventrolateral side of the sternocleidomastoid muscle which can be traced with dissection deep in the fascia between the muscle bellies.

The dark staining of the LN from the magnetic tracer was used for visual confirmation. Images were captured of LNs and they were graded by darkness by the surgeon according to a scale (no stain, some discolouration, black). All identified SLNs were dissected with

the robot and delivered from the dissection tunnel with forceps prior to ex vivo confirmation with a prototype hand-held magnetometer probe of LN magnetic signal (measured in arbitrary units).

Open exploration and Ex vivo LN analysis

After completion of the robot-assisted SLNB, an open neck exploration was performed to inspect the surgical site for additional LNs found with fluorescence using a Stryker 1688 fluorescent camera (Stryker, Michigan, USA). All individually excised LNs underwent 'closed-field' fluorescent imaging using the Stryker camera in a pitch-dark room. A custom MATLAB script was used to calculate MFI from ROIs drawn around captured LN images.

RESULTS

Pre-operative MRI findings

A total of 17 LNs were identified with pre-operative MRI following SPION injection. 'Pseudo-dynamic' imaging with short TE sequences 100 seconds apart successfully demonstrated tracer drainage from the primary to first, second and tertiary echelon LNs. Tracer uptake into LNs was clearly visualised in the pseudo-dynamic scans as early as 2 minutes post-injection. Over the following hour of imaging, the negative contrast steadily increased, indicating a prolonged uptake of the magnetic tracer over this time. Of the SLNs identified on MRI, six were first tier, ten were second tier and one was third tier. The submandibular LN was involved in four pigs, the accessory mandibular LN in one pig and the superficial ventral chain of cervical LNs in three pigs (Figure 10.4). SPION drained ipsilaterally in two pigs, contralaterally in two pigs and bilaterally in one pig (Figure 10.5).

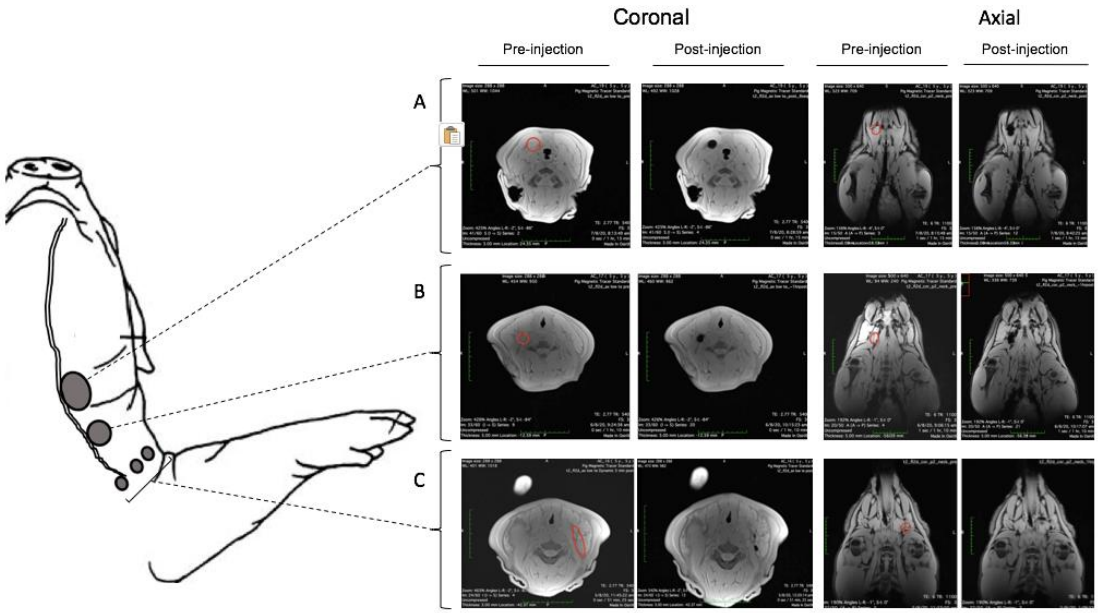

Figure 10.4 Representative T2 weighted MRI scans demonstrating a change in negative contrast at 1-hour post-injection of tracer as a result of its magnetic susceptibility.

Slices are taken from three different planes to demonstrate uptake in the (A) submandibular LN, (B) accessory mandibular LN, and (C) superficial ventral cervical chain of LNs.

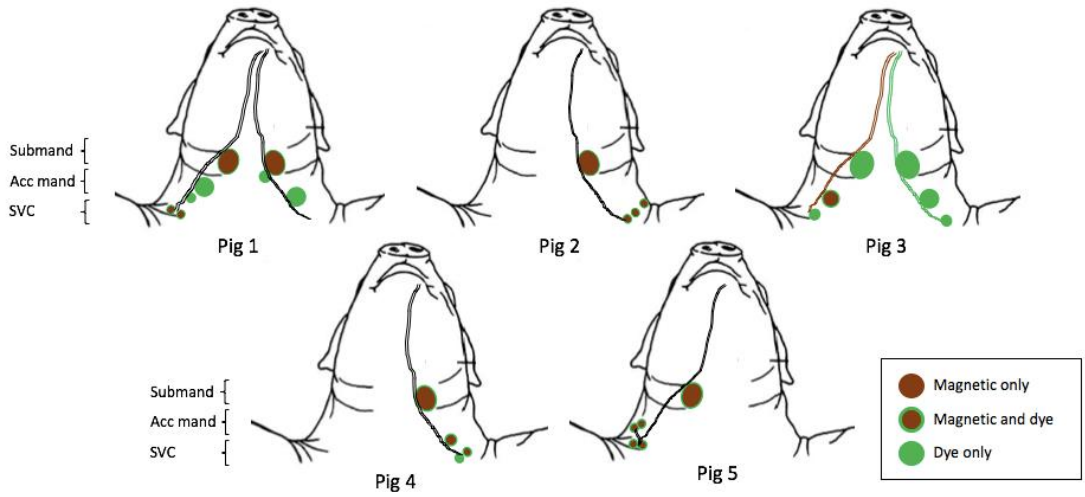

Figure 10.5 Summary of tracer drainage patterns.

(Submand = submandibular lymph node cluster, Acc mand = accessory mandibular lymph node cluster, SVC = superficial ventral cervical cluster of LNs).

Feasibility of robotic approach

Robot-assisted SLNB was successfully performed in all five pigs. The simulated MFLA incision and dissection tunnel described in this pig model provided adequate access to all targeted LN groups. All blood vessels encountered were able to be controlled with diathermy or surgical clips and blood loss was minimal. There were no operative complications and all animal survived to completion of procedure.

Intraoperative magnetic and fluorescent guidance findings

Pre-operative MR images provided excellent anatomic resolution allowing clear planning of approach to SLN location in relation to bony, vascular and soft tissue landmarks. Intraoperatively, MRI positive SLNs demonstrated a clear visual contrast because of the dark stain of SPION taken up within the node (Figure 10.6A and C). Fluorescence imaging provided excellent guidance to MRI positive LNs embedded deep within tissue.

Following robot-assisted SLNB, conversion to open exploration identified an additional 24 LNs which received ICG, demonstrating superior retention of SPION in first draining SLNs. SLN size and colouration characteristics as well as ex vivo magnetic and fluorescent signal results are summarised in Table 10.1.

Figure 10.6 Sentinel lymph node appearance.

(A) Endoscopic brightfield image, (B) Endoscopic fluorescent image and (C) Ex vivo brightfield.

Table 10.1 Correlation of MRI positive SLNs with magnetic and fluorescent findings.

Pig	MRI positive SLNs	Tier	LN size Length x Width (mm)	LN colouration	Magnetic signal (AU)	Fluorescent signal *(Yes/No) (MFI)	Number of additional fluorescent LNs
1	L submandibular R submandibular R caudal SVC R middle SVC	1 1 2 2	20 x 30 25 x 30 12 x 16 10 x 20	Dark Dark Mild Mild	0.39 0.51 0.00 0.21	Yes (12.28) Yes (19.08) Yes (3.49) Yes (4.42)	Left: 2 Right: 2 Total: 4
2	L submandibular L caudal SVC L middle SVC L cranial SVC	1 2 2 2	25 x 35 12 x 12 8 x 10 6 x 7	Dark Dark Dark Dark	2.28 0.34 0.38 0.40	Yes (20.81) Yes (8.69) Yes (2.50) Yes (2.24)	Left: 0 Right: 0 Total: 0
3	R acc mandibular	1	15 x 20	Mild	0.00	Yes (1.29)	Left: 3 Right: 2 Total: 5
4	L submandibular L caudal SVC L middle SVC	1 2 3	20 x 25 10 x 17 5 x 5	Dark Mild Mild	2.36 0.20 0.00	Yes (4.74) Yes (1.30) Yes (0.33)	Left: 0 Right: 1 Total: 1
5	R submandibular R middle SVC R middle SVC R cranial SVC R cranial SVC	1 2 2 2 2	25 x 30 10 x 20 8 x 10 15 x 20 5 x 6	Dark Dark Dark Dark Dark	2.72 1.31 1.76 0.46 0.08	Yes(27.15) Yes (4.85) Yes (1.53) Yes (9.47) Yes (1.21)	Left: 0 Right: 2 Total: 2

*Intraoperative visualisation, L: Left, R: Right, acc: accessory, SVC: superficial ventral cervical, AU: arbitrary units

DISCUSSION

To the best of our knowledge this study presents the first description of a robot-assisted SLNB procedure in the head and neck with multi-modality guidance.[357] Here we demonstrate in a porcine model, technical feasibility of this highly novel minimally-invasive approach. Pre-operative local injection of SPION provided a clear map for surgical dissection by demonstrating tracer flow to first, second and third echelon draining LNs with excellent anatomic resolution. A retro auricular approach provided adequate access with a single incision to all targeted nodal groups. Endoscopic localisation of SLNs was significantly enhanced by fluorescence imaging following ICG injection, with visualisation of lymphatic ducts through tissue providing guidance to the SLN. The dark stain of SPION provided clear visual identification of the SLN, which was further confirmed with ex vivo magnetic signal detection using a magnetometer probe.

There have been two previous reports of endoscopic SLNB approaches in the head and neck using traditional laparoscopic instruments in porcine models.[358, 359] In both studies, stab incisions were made in the neck followed by insertion of endoscopic trocars and carbon dioxide (C02) insufflation prior to nodal dissection. Pitman et al. pre-operatively injected pigs with technetium-labelled sulfa colloid as well as isosulfan blue dye and used a gamma probe transcutaneously prior to incision and then endoscopically during nodal resection.[359] Rosen et al. used only visual localisation of SLNs with an injected solution of carbon and methylene blue dye.[358] While these studies successfully demonstrated feasibility of minimally invasive endoscopic approaches, no pre-operative imaging of tracer flow to SLNs was performed. Furthermore, these endoscopic approaches relied

upon C02 insufflation, which has known risks of C02 air embolism and subcutaneous emphysema in the neck.[360, 361]

More recently, there have been two reports of robot-assisted sentinel LN mapping in humans using ICG only.[362, 363] Again, in both instances, no pre-operative SLN mapping was performed. Kim et al. reported a study of nine patients with cN0 OSCC who underwent SLN sampling following RAND. Patients were injected with ICG peri-tumourally roughly 12 hours prior to surgery to guide ex vivo sampling of fluorescence-positive LNs from the completely resected neck dissection specimen using the da Vinci Firefly system. Chow et al. reported results from ten cN0 OSCC patients who underwent real-time SLN mapping with injection of ICG around the tumour following retroarticular tans-hairline incision and positioning of the da Vinci Xi endoscope into the wound.[363] Here, the first LN(s) to receive ICG as detected by Firefly, was resected followed by END. While both approaches demonstrate an opportunity for improved detection of occult micrometastases at pathology, unlike conventional SLNB procedures, in both cases there was no opportunity to preoperatively map tracer flow, and therefore complete selective-neck dissections were required. In the study by Kim et al. there was a high volume of fluorescent positive LNs sent for histopathological assessment because of the extended time interval between tracer injection and LN biopsy. By injecting SPIONs in our study, individual first echelon SLNs could be identified pre-operatively and then targeted intra-operatively, with ex vivo confirmation of tracer uptake using a magnetometer probe. Clinical translation of this approach would limit both the extent of robotic dissection, and the volume of LNs sent for detailed histopathological analysis. Furthermore, this technique conforms with the wide belief that the gold-standard for

SLNB requires the use of both pre-operative and intra-operative SLN detection methods.[171, 207, 364]

By following all of the steps envisaged for use in clinical practice, this study has successfully demonstrated technical and practical feasibility of this highly novel SLNB approach. The porcine model has been used extensively for SLNB and magnetic lymphangiography studies and provides a well-established large animal model to investigate the steps of this procedure.[365] Cadaveric studies have already established the utility of a MFLA for RAND, and therefore pig positioning, incision placement and steps of dissection were planned to best stimulate human surgery according to this.[366] A live animal was chosen over a human cadaver in order to best test lymphatic flow dynamics of our tracer.[367] Several different combinations of SPION concentration and volume were used, however it was not the objective of this study to compare their flow properties as this is already under investigation by our group in a separate study. Accuracy of this SPION for tumour detection was also not examined in this study, and this is under evaluation in a preliminary Phase 1 clinical trial at our institution (Trial registration number: ACTRN12620000831987). While our magnetometer probe was useful for ex vivo confirmation of magnetic signal, future development of a smaller 'drop-in' probe would aid endoscopic magnetic signal confirmation, as has been demonstrated with gamma-guidance during robotic SLNB surgery in the abdomen and pelvis.[368]

The novel approach described in this study presents several significant potential clinical benefits. Firstly, the use of a retroauricular robot-assisted approach will improve aesthetic results and circumvent the difficulties with incision placement and nodal access that have been major short comings of conventional SLNB in the head and neck. Despite this, a

case for using the robot for this procedure needs to weighed against its substantial added expense. From a resource utilisation standpoint, an economically feasible case could be made for patients with cN0 oropharyngeal cancer being treated with transoral robotic surgery (TORS), where a combination of robotic primary resection followed by a minimally invasive robot-assisted SLNB approach could optimise robotic theatre utilisation.[369]

Secondly, up until now, the 'shine-through effect' from the radionuclear technique, which refers to the background scatter of signal when the first draining LN lies in close proximity to the primary tumour, has been an extensively-documented reason for poor adoption of SLNB in the head and neck. The MRI guided approach described in this study circumvents this issue because of its improved spatial resolution.[355] In addition to this, MRI is an easily accessible imaging modality that avoids the use of radionuclear material and, by using pseudo-dynamic sequences, enables temporal and anatomic localisation of the SLN with one imaging modality.

Finally, in our treatment paradigm, the surgeon is empowered to lead this procedure. The excellent anatomic detail afforded from pre-operative magnetic lymphangiography allows independence in surgical planning. The SPION injection results in a darkly stained SLN, removing the need for methylene blue dye injection, thereby minimising disruption to surgical workflow. The utility of the da Vinci Firefly system allows seamless transition between imaging capabilities for enhanced surgical guidance and by using multi-modality guidance the surgeon can have increased confidence in the sensitivity of SLN detection.

CONCLUSION

By demonstrating pre-clinical feasibility of a novel robot-assisted approach using multi-modality magnetic and fluorescence guidance, this study heralds an exciting new paradigm for SLNB. Clinical translation of this approach has great potential to circumvent the significant limitations currently hampering adoption of SLNB in head and neck cancer with hope for advancement in minimally-invasive surgical staging.

SUMMARY AND FUTURE PERSPECTIVES

The research contained within this thesis broadly examines how two contemporary fluorescent and magnetic tracer technologies can be utilised to innovate areas of shortcoming in the current surgical management paradigm of OSCC in order to deliver improved overall benefit to the patient and health system.

The thesis begins with an up-to-date summary of our understanding of OSCC and a critical analysis of the literature relating to the current treatment model for this disease. This was unpacked into two parts; 1. treatment of the primary tumour in the oral cavity, and 2. treatment of the neck, where there is a high rate of, often occult, tumour metastases. An area of limitation at each step of treatment was identified that was hypothesised to be amenable to improvement with our novel tracer technology; Firstly, margin analysis during primary tumour resection and, secondly, SLNB for staging of the neck.

Part one of this thesis focuses on the first issue and evaluates how fluorescence imaging can improve intraoperative margin analysis during resection of the primary tumour. Positive margins during surgical resection are associated with an increased risk of local recurrence and an associated decreased in overall survival. Current methods for intraoperative margin assessment involve surgeon palpation of the resected specimen, with areas of concern sampled for intraoperative pathological FSA. This system is prone to sampling error by the surgeon, which is consistent with data demonstrating unchanged positive margins rates across all surgically treated tumour resections over the last 30 years despite advances in surgery.[278]

To address this critical short-coming, a role for fluorescent molecular imaging was investigated. The fluorescent tracer examined was Panitumumab-IRDye800CW, which is a tumour-targeted antibody-dye conjugate that is infused IV into patients prior to surgery. In a scoping investigation of five tumour resection specimens that underwent *ex vivo* fluorescent imaging from patients pre-operatively infused with this tracer, points of highest fluorescence on the periptery of the specimens correlated with the points where the margin distance was the narrowest, leading to the hypothesis that fluorescent molecular imaging could be used to identify the point on a resection specimen where tumour came closest to the resection edge. This point was coined "the sentinel margin".

To further investigate the value of a novel sentinel margin identification strategy using fluorescence, a prospective clinical trial was established. Here, *ex vivo* fluorescent imaging of resected tumour specimens resulted in improved detection of the true closest margin at final pathology compared to the surgeon's margin assessment based on conventional methods of visual inspection and palpation of the specimen. Furthermore, margin distances at areas of highest fluorescence correlated highly with final closest margin distances at pathology. Broad clinical translation of this novel strategy holds promise to improve the accuracy and efficiency of intraoperative margin assessment with associated oncological and functional benefits to the patient as well as systems benefits from a more streamlined intraoperative pathological assessment process.

Part two of this thesis shifted focus to management of the neck and examined new strategies for SLNB in OSCC. SLNB provides a minimally invasive approach to stage the neck in patients, which is critical in OSCC where the presence of nodal disease is associated with a 50% decrease in survival and is the most important single prognostic

factor.[37] Despite this, SLNB has not been widely adopted in the head and neck, and following a critical review of the literature, the reasons for this were distilled into three core themes. These are: 1. Difficult access for local injection of tracers in the pharynx, 2. Inadequate spatial resolution of currently used radionuclear technology in the complex head and neck anatomic environment, and 3. The unique complexity of head and neck lymphatics that results in there often being multiple first draining LNs, which can be located at several different neck levels.

To address the first issue of limited access, a molecular fluorescent imaging technique was evaluated whereby patients were infused pre-operatively with IV Panitumumab-IRDye800CW instead of being injected with a radiotracer locally around the primary tumour in the pharynx. *Ex vivo* closed-field fluorescent imaging of close to 1000 individual LNs from END specimens from 23 patients revealed that the studied tumour-targeted tracer, when IV infused, preferentially reached SLNs, as well as metastatic LNs. Furthermore, examination of the highest five fluorescent LNs from each patient demonstrated excellent sensitivity and specificity for occult metastatic LN identification and 100% accuracy for staging the neck. The clinical significance of this is that a SLNB technique centred on IV delivery of a fluorescent tumour-targeted tracer could overcome the technical difficulties of local tracer injection, thereby eliminating this particular barrier to adoption.

To address the second issue relating to the inadequate spatial resolution afforded by radionuclear technology in the head and neck, an alternative magnetic approach was investigated. Here a novel proprietary magnetic tracer was studied, consisting of a crystalline iron oxide nanoparticle core and an outer PEG coating with macrophage-

targeting (mannose) polymers attached. Initial preclinical studies demonstrated high magnetic susceptibilities of these particles in pigs following local tracer delivery into their tongues, with associated strong negative contrast in first draining LNs on MRI and good signal detection in SLNs identified with a novel handheld magnetometer probe during dissection. Magnetic tracer was shown to have excellent retention in first echelon LNs as evidenced by increased magnetic probe signal when compared to lower echelon nodes, even when the time-window between injection and LN biopsy was extended over a 4-week period. In addition, total iron content in LNs was shown to correlate with probe signal supporting the use of this device for *in vivo* SLN detection. Following from this, a first-in-human phase 1 clinical trial was opened which demonstrated the procedural feasibility of this novel magnetic approach to SLNB. Eight patients were enrolled with a total of 227 LNs dissected of which, one returned positive for metastatic disease. 23 SLNs were identified on MRI and 22 (95.7%) of these were identified intraoperatively. Overall, the magnetic technique had a sensitivity of 100%, specificity 90.3% and NPV of 100% for identification of metastatic disease in the 227 LNs resected across the cohort and no adverse events were recorded. These promising early results lay the foundation for an attractive next generation technique with significant potential to increase adoption of SLNB in the complex head and neck lymphatic environment.

Finally, with an eye to the future, and in addressing the final issue relating to the propensity for multiple first echelon LNs in the neck, a novel robotic approach was described with dual-modality magnetic and fluorescence guidance. A mixture of magnetic tracer with ICG was injected locally and tracer flow to the SLNs was mapped with MRI. Instead of a standard neck incision to access SLNs, a retro-auricular approach through a single hidden incision was employed and SLNs were identified and dissected

robotically with the aid of real-time fluorescence image guidance. Preclinical feasibility of this technique was demonstrated, providing imminent potential for translation of this strategy to humans with promise for improved aesthetic and functional outcomes without compromising access to multiple SLNs scattered across different neck levels.

The two tracer technologies evaluated in this thesis have in common the fact that they both target specific tumour or tissue ligands for molecular imaging but have both been studied separately. While this thesis has demonstrated that both panitumumab-IRDye800CW and Ferro Trace could be used for SLNB, no work has yet been undertaken to compare the two tracers against each other. Each tracer as studied in this thesis has demonstrated a different means of overcoming some of the separate issues inherent to SLNB adoption for OSCC – for example using IV panitumumab-IRDye800CW avoids difficulties with injecting tracer at the local site and using Ferro Trace has potential to avoid issues relating to the shine-through phenomenon. In the future, it is my belief these tracer technologies should both be available as tools for SLNB and selected by surgeons for use depending on patient, tumour and institution specific factors. There is possibly also benefit to use both technologies together in a multi-modal manner harnessing the strengths of each for enhanced overall accuracy. Of course, this would need to be weighed against additional cost and resource requirements.

While there have been some break-through discoveries made as part of this thesis, these findings are very much in the early phase of the technology adoption cycle for both tracers and significant work is still required to see complete translation and adoption. For example, further study needs to be conducted to understand if and how fluorescence can

be used to identify tumour invasion into bone, as well as hoe sensitive it is to perineural invasion, complex 3D anatomical resections and discohesive growth patterns. Close and involved margins are often not a function of not realising that the surgeon is too close, but frequently result from attempting to preserve critical structures and navigating complex geometries. In this respect, the video recordings generated from intraoperative fluorescence imaging following panitumumab-IRDye800CW administration could be of significant value in understanding limitations of the resection and identifying anatomical locations at risk of recurrence. This could be used when collaborating with pathologists and with radiation oncologists at an MDT to plan adjuvant treatment.

The next step to for ex vivo strategies using fluorescence for margin analysis is a large prospective trial. This would likely need to be multi-centre to recruit sufficient patients to meet power calculations. This should test both mucosal and deep margins for all specimens and ideally patients of all OSCC types and TNM stages (being treated with curative intent) should be included. Following on from prospective case series, I suspect ultimately RCTs showing overall oncologic benefit will be required before this strategy becomes accepted.

Similarly, further research is required to see the development of IV targeted florescence for SLNB. It is my belief that for this to strategy to work in practice, panitumumab-IRDye800CW will need to be conjugated with either a radiotracer or a magnetic tracer to harness the important benefits that these tracers bring, like pre-operative localisation with nuclear imaging or MRI respectively, and the ability to localise/ plan the incision with a probe. The idea of multi-modal SLNB using hybrid fluorescent-radiotracers is not new,

but previous studies have not looked at tumour-targeted tracers. The strong evidence built in this thesis will provide a solid foundation for ongoing future investigation in this area.

Finally, with respect to future directions for magnetic SLNB, a larger prospective study should follow-on from the pilot study included in this thesis. While our pilot study showed that FerroTrace was able to accurately detect the only tumour metastasis in the cohort, a much larger patient cohort will be needed to appropriately evaluate accuracy. As part of this prospective study, patients should undergo a small incision as typically used for SLNB and should only have a completion neck dissection if the SLN returns positive at pathology. Diagnostic and functional outcomes as well as adverse events should be investigated, and patients should be followed up for at least 3 years (or up to 5 years for gold-standard) to analyse oncological outcomes. Following on from a prospective case series, again I suspect ultimately RCTs showing overall oncologic benefit will be required before this strategy becomes widely accepted.

As with any innovative technology or disruptive approach, the usual logistics need to be taken into consideration as part of analysing how successful it will be in crossing the chasm between the early adopters and the early majority in the adoption cycle.

For all strategies outlined in this thesis there is certainly a learning curve. There is definite benefit to be gained by studying the learning curve in each of the strategies. It is my belief that this may be a significant barrier to adoption, and it may be that in the future, some of these techniques become localised to high volume academic centres with specific expertise in these techniques. Further work should be conducted to explore techniques to

train surgeons in these new procedures, including the value of well-run courses, textbooks and online educational resources.

Cost will be another significant factor influencing uptake and adoption of these technologies. Both panitumumab-IRDye800CW and FerroTrace are currently research drugs so their commercial retail price is as yet unknown. When they do become commercially available other infrastructure will be required to enable their use. For example, for fluorescent ex vivo margin analysis, a closed-field imaging device and appropriate software will be required. Similarly, for fluorescent SLN mapping a hand-held fluorescent camera and display monitor will be required, and for magnetic SLNB a hand-held magnetometer probe and display monitor will be required. Purchase of this equipment will be a once-off cost, but will come with costs of maintenance, upkeep, program updates and single-use sterile drapes.

While cost-utility analyses comparing magnetic SLNB to traditional techniques have not been undertaken, it is anticipated that a magnetic technique would be more accessible, avoiding the requirement for specific infrastructure for safe storage and transport of radionuclear products. Having said this, MRI comes with its own unique set of challenges such as patients who have contraindications to MR imaging (such as implantable devices, metallic foreign bodies or implants and issues with claustrophobia), motion artefact and access.

While very specific strategies for margin analysis and SLNB have been evaluated using the two tracers studied in this thesis, there is certainly room for investigation of other approaches to modernise surgery using these technologies. For example, one of the

barriers to use of SLNB is in patients undergoing free flap reconstruction. In many units, most patients undergo free flap reconstruction for T2 tumours and many T1 tumours and re-entering the neck for these patients in the case of a positive SLN is problematic. In this instance, there certainly may be a role for using these technologies to ensure that all potential sentinel nodes are removed, rather than as a modality to minimise morbidity.

REFERENCES

1. Drake RL, Vogl, W., Mitchell, A. W. M., & Gray, H. Gray's anatomy for students. Philadelphia: Elsevier/Churchill Livingstone; 2005.

2. Wenig BM. Atlas of head and neck pathology. Philadelphia, Pa: Saunders/Elsevier; 2008.

3. Cancer TIAfRo. Pathology and Genetics of Head and Neck Tumours: World Health Organization; 2005.

4. In Flint PW, & Cummings, C. W. Cummings otolaryngology head & neck surgery2010.

5. Kumar V, Abbas, A. K., & Aster, J. C. Robbins and Cotran pathologic basis of disease. Ninth edition ed. Philadelphia, PA: Elsevier/Saunders; 2015.

6. Mao L, Lee JS, Fan YH, Ro JY, Batsakis JG, Lippman S, et al. Frequent microsatellite alterations at chromosomes 9p21 and 3p14 in oral premalignant lesions and their value in cancer risk assessment. Nature medicine. 1996 Jun;2(6):682-5.

7. Boyle JO, Hakim J, Koch W, van der Riet P, Hruban RH, Roa RA, et al. The incidence of p53 mutations increases with progression of head and neck cancer. Cancer research. 1993 Oct 1;53(19):4477-80.

8. Rosin MP, Cheng X, Poh C, Lam WL, Huang Y, Lovas J, et al. Use of allelic loss to predict malignant risk for low-grade oral epithelial dysplasia. Clin Cancer Res. 2000 Feb;6(2):357-62.

9. Michalides R, van Veelen N, Hart A, Loftus B, Wientjens E, Balm A. Overexpression of cyclin D1 correlates with recurrence in a group of forty-seven operable squamous cell carcinomas of the head and neck. Cancer research. 1995 Mar 1;55(5):975-8.

10. Hoffman HT, Karnell LH, Funk GF, Robinson RA, Menck HR. The National Cancer Data Base report on cancer of the head and neck. Arch Otolaryngol Head Neck Surg. 1998 Sep;124(9):951-62.

11. Jemal A, Tiwari RC, Murray T, Ghafoor A, Samuels A, Ward E, et al. Cancer statistics, 2004. CA Cancer J Clin. 2004 Jan-Feb;54(1):8-29.

12. Farah CS, Simanovic B, Dost F. Oral cancer in Australia 1982-2008: a growing need for opportunistic screening and prevention. Australian dental journal. 2014 Sep;59(3):349-59. DOI: 10.1111/adj.12198.

13. Singh JPSSGPB. Jatin Shah's head and neck surgery and oncology. Philadelphia: Elsevier/Mosby; 2012.

14. de Bondt RB, Nelemans PJ, Hofman PA, Casselman JW, Kremer B, van Engelshoven JM, et al. Detection of lymph node metastases in head and neck cancer: a meta-analysis comparing US, USgFNAC, CT and MR imaging. European journal of radiology. 2007 Nov;64(2):266-72. DOI: 10.1016/j.ejrad.2007.02.037.

15. Goerres GW, Schmid DT, Schuknecht B, Eyrich GK. Bone invasion in patients with oral cavity cancer: comparison of conventional CT with PET/CT and SPECT/CT. Radiology. 2005 Oct;237(1):281-7. DOI: 10.1148/radiol.2371041228.

16. Moreira MA, Lessa LS, Bortoli FR, Lopes A, Xavier EP, Ceretta RA, et al. Meta-analysis of magnetic resonance imaging accuracy for diagnosis of oral cancer. PloS one. 2017;12(5):e0177462. DOI: 10.1371/journal.pone.0177462.

17. Pasha MA, Marcus C, Fakhry C, Kang H, Kiess AP, Subramaniam RM. FDG PET/CT for Management and Assessing Outcomes of Squamous Cell Cancer of the Oral Cavity. AJR Am J Roentgenol. 2015 Aug;205(2):W150-61. DOI: 10.2214/ajr.14.13830.

18. Amin MB, Edge, S., Greene, F., Byrd, D.R., Brookland, R.K., Washington, M.K., Gershenwald, J.E., Compton, C.C., Hess, K.R., Sullivan, D.C., Jessup, J.M., Brierley, J.D., Gaspar, L.E., Schilsky, R.L., Balch, C.M., Winchester, D.P., Asare, E.A., Madera, M., Gress, D.M., Meyer, L.R. (Eds.). AJCC Cancer Staging Manual (8th edition): Springer International Publishing: American Joint Commission on Cancer; 2017.

19. Pfister DG, Spencer S, Brizel DM, Burtness B, Busse PM, Caudell JJ, et al. Head and Neck Cancers, Version 1.2015. J Natl Compr Canc Netw. 2015 Jul;13(7):847-55; quiz 56. DOI: 10.6004/jnccn.2015.0102.

20. Miller MC, Goldenberg D. AHNS Series: Do you know your guidelines? Principles of surgery for head and neck cancer: A review of the National Comprehensive Cancer Network guidelines. Head & neck. 2017 Apr;39(4):791-6. DOI: 10.1002/hed.24654.

21. Genden EM, Ferlito A, Silver CE, Takes RP, Suárez C, Owen RP, et al. Contemporary management of cancer of the oral cavity. European archives of oto-rhino-laryngology : official journal of the European Federation of Oto-Rhino-Laryngological Societies (EUFOS) : affiliated with the German Society for Oto-Rhino-Laryngology - Head and Neck Surgery. 2010 Jul;267(7):1001-17. DOI: 10.1007/s00405-010-1206-2.

22. Montero PH, Patel SG. Cancer of the oral cavity. Surg Oncol Clin N Am. 2015 Jul;24(3):491-508. DOI: 10.1016/j.soc.2015.03.006.

23. Brown JS, Lowe D, Kalavrezos N, D'Souza J, Magennis P, Woolgar J. Patterns of invasion and routes of tumor entry into the mandible by oral squamous cell carcinoma. Head & neck. 2002 Apr;24(4):370-83. DOI: 10.1002/hed.10062.

24. Chaukar DA, Dandekar M, Kane S, Arya S, Purandare N, Rangarajan V, et al. Invasion of the mandible in gingivobuccal complex cancers: Histopathological

analysis of routes of tumour entry and correlation with preoperative assessment. Oral Oncol. 2018 Nov;86:181-7. DOI: 10.1016/j.oraloncology.2018.09.022.

25. O'Brien CJ, Adams JR, McNeil EB, Taylor P, Laniewski P, Clifford A, et al. Influence of bone invasion and extent of mandibular resection on local control of cancers of the oral cavity and oropharynx. International journal of oral and maxillofacial surgery. 2003 Oct;32(5):492-7.

26. Gou L, Yang W, Qiao X, Ye L, Yan K, Li L, et al. Marginal or segmental mandibulectomy: treatment modality selection for oral cancer: a systematic review and meta-analysis. International journal of oral and maxillofacial surgery. 2018 Jan;47(1):1-10. DOI: 10.1016/j.ijom.2017.07.019.

27. Schrag C, Chang YM, Tsai CY, Wei FC. Complete rehabilitation of the mandible following segmental resection. J Surg Oncol. 2006 Nov 1;94(6):538-45. DOI: 10.1002/jso.20491.

28. Urken ML, Buchbinder D, Weinberg H, Vickery C, Sheiner A, Parker R, et al. Functional evaluation following microvascular oromandibular reconstruction of the oral cancer patient: A comparative study of reconstructed and nonreconstructed patients. The Laryngoscope. 2015 Jul;125(7):1512. DOI: 10.1002/lary.25279.

29. Ragbir M, Brown JS, Mehanna H. Reconstructive considerations in head and neck surgical oncology: United Kingdom National Multidisciplinary Guidelines. The Journal of laryngology and otology. 2016 May;130(S2):S191-s7. DOI: 10.1017/s0022215116000621.

30. Batstone MD. Reconstruction of major defects of the jaws. Australian dental journal. 2018 Mar;63 Suppl 1:S108-s13. DOI: 10.1111/adj.12596.

31. Chien SH, Hsu H, Lin CM, Chiu CH, Huang CC. Reconstruction of extensive head and neck defects with multiple simultaneous free flaps. Plast Reconstr Surg. 2009 Jul;124(1):318. DOI: 10.1097/PRS.0b013e3181a837e0.

32. Taberna M, Gil Moncayo F, Jané-Salas E, Antonio M, Arribas L, Vilajosana E, et al. The Multidisciplinary Team (MDT) Approach and Quality of Care. Front Oncol. 2020;10:85. DOI: 10.3389/fonc.2020.00085.

33. Gooi Z, Fakhry C, Goldenberg D, Richmon J, Kiess AP. AHNS Series: Do you know your guidelines?Principles of radiation therapy for head and neck cancer: A review of the National Comprehensive Cancer Network guidelines. Head & neck. 2016 Jul;38(7):987-92. DOI: 10.1002/hed.24448.

34. Shin JY, Yoon JK, Shin AK, Diaz AZ. Locoregionally advanced oral cavity cancer: A propensity-score matched analysis on overall survival with emphasis on the impact of adjuvant radiotherapy. Head & neck. 2018 Sep;40(9):1934-46. DOI: 10.1002/hed.25185.

35. Nair D, Mair M, Singhvi H, Mishra A, Nair S, Agrawal J, et al. Perineural invasion: Independent prognostic factor in oral cancer that warrants adjuvant treatment. Head & neck. 2018 Aug;40(8):1780-7. DOI: 10.1002/hed.25170.

36. Fridman E, Na'ara S, Agarwal J, Amit M, Bachar G, Villaret AB, et al. The role of adjuvant treatment in early-stage oral cavity squamous cell carcinoma: An international collaborative study. Cancer. 2018 Jul 15;124(14):2948-55. DOI: 10.1002/cncr.31531.

37. Shah JP, Candela FC, Poddar AK. The patterns of cervical lymph node metastases from squamous carcinoma of the oral cavity. Cancer. 1990 Jul 1;66(1):109-13. DOI: 10.1002/1097-0142(19900701)66:1<109::aid-cncr2820660120>3.0.co;2-a.

38. Byers RM, Wolf PF, Ballantyne AJ. Rationale for elective modified neck dissection. Head Neck Surg. 1988 Jan-Feb;10(3):160-7. DOI: 10.1002/hed.2890100304.

39. Shah JP. Cervical lymph node metastases--diagnostic, therapeutic, and prognostic implications. Oncology (Williston Park). 1990 Oct;4(10):61-9; discussion 72, 6.

40. Ferlito A, Robbins KT, Shaha AR, Pellitteri PK, Kowalski LP, Gavilan J, et al. Current considerations in neck dissection. Acta oto-laryngologica. 2002 Apr;122(3):323-9. DOI: 10.1080/00016480275364825 9.

41. Crile G. Landmark article Dec 1, 1906: Excision of cancer of the head and neck. With special reference to the plan of dissection based on one hundred and thirty-two operations. By George Crile. Jama. 1987 Dec 11;258(22):3286-93. DOI: 10.1001/jama.258.22.3286.

42. Martin H, Del Valle B, Ehrlich H, Cahan WG. Neck dissection. Cancer. 1951 May;4(3):441-99. DOI: 10.1002/1097-0142(195105)4:3<441::aid-cncr2820040303>3.0.co;2-o.

43. Colevas AD, Sue SY, David GP, Sharon S, David A, Douglas A, et al. NCCN Guidelines Insights: Head and Neck Cancers, Version 1.2018. Journal of the National Comprehensive Cancer Network J Natl Compr Canc Netw. 2018;16(5):479-90. DOI: 10.6004/jnccn.2018.0026.

44. Koyfman SA, Ismaila N, Crook D, D'Cruz A, Rodriguez CP, Sher DJ, et al. Management of the Neck in Squamous Cell Carcinoma of the Oral Cavity and Oropharynx: ASCO Clinical Practice Guideline. Journal of clinical oncology : official journal of the American Society of Clinical Oncology. 2019 Jul 10;37(20):1753-74. DOI: 10.1200/jco.18.01921.

45. de Bree R, Takes RP, Shah JP, Hamoir M, Kowalski LP, Robbins KT, et al. Elective neck dissection in oral squamous cell carcinoma: Past, present and future. Oral Oncol. 2019 Mar;90:87-93. DOI: 10.1016/j.oraloncology.2019.01.016.

46. Shah JP. Patterns of cervical lymph node metastasis from squamous carcinomas of the upper aerodigestive tract. American journal of surgery. 1990 Oct;160(4):405-9.

47. Ferlito A, Rinaldo A, Robbins KT, Silver CE. Neck dissection: past, present and future? The Journal of laryngology and otology. 2006 Feb;120(2):87-92. DOI: 10.1017/s0022215105004512.

48. Silver CE, Rinaldo A, Ferlito A. Crile's neck dissection. The Laryngoscope. 2007 Nov;117(11):1974-7. DOI: 10.1097/MLG.0b013e31813544b7.

49. Ferlito A, Rinaldo A, Silver CE, Shah JP, Suarez C, Medina JE, et al. Neck dissection: then and now. Auris, nasus, larynx. 2006 Dec;33(4):365-74. DOI: 10.1016/j.anl.2006.06.001.

50. Fisch UP, Sigel ME. CERVICAL LYMPHATIC SYSTEM AS VISUALIZED BY LYMPHOGRAPHY. The Annals of otology, rhinology, and laryngology. 1964 Dec;73:870-82.

51. Popescu B, Bertesteanu SV, Grigore R, Scaunasu R, Popescu CR. Functional implications of radical neck dissection and the impact on the quality of life for patients with head and neck neoplasia. Journal of medicine and life. 2012 Dec 15;5(4):410-3.

52. Gane EM, Michaleff ZA, Cottrell MA, McPhail SM, Hatton AL, Panizza BJ, et al. Prevalence, incidence, and risk factors for shoulder and neck dysfunction after neck dissection: A systematic review. European journal of surgical oncology : the journal of the European Society of Surgical Oncology and the British Association of Surgical Oncology. 2017 Jul;43(7):1199-218. DOI: 10.1016/j.ejso.2016.10.026.

53. Saunders JR, Jr., Hirata RM, Jaques DA. Considering the spinal accessory nerve in head and neck surgery. American journal of surgery. 1985 Oct;150(4):491-4.

54. Short SO, Kaplan JN, Laramore GE, Cummings CW. Shoulder pain and function after neck dissection with or without preservation of the spinal accessory nerve. American journal of surgery. 1984 Oct;148(4):478-82.

55. Leipzig B, Suen JY, English JL, Barnes J, Hooper M. Functional evaluation of the spinal accessory nerve after neck dissection. American journal of surgery. 1983 Oct;146(4):526-30.

56. Delaney SW, Shi H, Shokrani A, Sinha UK. Management of Chyle Leak after Head and Neck Surgery: Review of Current Treatment Strategies. International journal of otolaryngology. 2017;2017:8362874. DOI: 10.1155/2017/8362874.

57. Sugarbaker ED, Wiley HM. Intracranial-pressure studies incident to resection of the internal jugular veins. Cancer. 1951 Mar;4(2):242-50.

58. Chen YJ, Wang CP, Wang CC, Jiang RS, Lin JC, Liu SA. Carotid blowout in patients with head and neck cancer: associated factors and treatment outcomes. Head & neck. 2015 Feb;37(2):265-72. DOI: 10.1002/hed.23590.

59. Ferlito A, Rinaldo A, Devaney KO, Nakashiro K, Hamakawa H. Detection of lymph node micrometastases in patients with squamous carcinoma of the head and neck. European archives of oto-rhino-laryngology : official journal of the European Federation of Oto-Rhino-Laryngological Societies (EUFOS) : affiliated with the German Society for Oto-Rhino-Laryngology - Head and Neck Surgery. 2008 Oct;265(10):1147-53. DOI: 10.1007/s00405-008-0715-8.

60. Fasunla AJ, Greene BH, Timmesfeld N, Wiegand S, Werner JA, Sesterhenn AM. A meta-analysis of the randomized controlled trials on elective neck dissection versus therapeutic neck dissection in oral cavity cancers with clinically node-negative neck. Oral Oncol. 2011 May;47(5):320-4. DOI: 10.1016/j.oraloncology.2011.03.009.

61. Liao LJ, Lo WC, Hsu WL, Wang CT, Lai MS. Detection of cervical lymph node metastasis in head and neck cancer patients with clinically N0 neck-a meta-analysis comparing different imaging modalities. BMC Cancer. 2012 Jun 12;12:236. DOI: 10.1186/1471-2407-12-236.

62. Merritt RM, Williams MF, James TH, Porubsky ES. Detection of cervical metastasis. A meta-analysis comparing computed tomography with physical examination. Arch Otolaryngol Head Neck Surg. 1997 Feb;123(2):149-52. DOI: 10.1001/archotol.1997.01900020027004.

63. van den Brekel MW, Castelijns JA, Stel HV, Luth WJ, Valk J, van der Waal I, et al. Occult metastatic neck disease: detection with US and US-guided fine-needle aspiration cytology. Radiology. 1991 Aug;180(2):457-61. DOI: 10.1148/radiology.180.2.2068312.

64. Wu LM, Xu JR, Liu MJ, Zhang XF, Hua J, Zheng J, et al. Value of magnetic resonance imaging for nodal staging in patients with head and neck squamous cell carcinoma: a meta-analysis. Acad Radiol. 2012 Mar;19(3):331-40. DOI: 10.1016/j.acra.2011.10.027.

65. Sun R, Tang X, Yang Y, Zhang C. (18)FDG-PET/CT for the detection of regional nodal metastasis in patients with head and neck cancer: a meta-analysis. Oral Oncol. 2015 Apr;51(4):314-20. DOI: 10.1016/j.oraloncology.2015.01.004.

66. Weiss MH, Harrison LB, Isaacs RS. Use of decision analysis in planning a management strategy for the stage N0 neck. Arch Otolaryngol Head Neck Surg. 1994 Jul;120(7):699-702. DOI: 10.1001/archotol.1994.01880310005001.

67. Leusink FK, van Es RJ, de Bree R, Baatenburg de Jong RJ, van Hooff SR, Holstege FC, et al. Novel diagnostic modalities for assessment of the clinically node-negative neck in oral squamous-cell carcinoma. Lancet Oncol. 2012 Dec;13(12):e554-61. DOI: 10.1016/s1470-2045(12)70395-9.

68. Nieuwenhuis EJ, Castelijns JA, Pijpers R, van den Brekel MW, Brakenhoff RH, van der Waal I, et al. Wait-and-see policy for the N0 neck in early-stage oral and oropharyngeal squamous cell carcinoma using ultrasonography-guided cytology: is there a role for identification of the sentinel node? Head & neck. 2002 Mar;24(3):282-9. DOI: 10.1002/hed.10018.

69. Rodrigo JP, Shah JP, Silver CE, Medina JE, Takes RP, Robbins KT, et al. Management of the clinically negative neck in early-stage head and neck cancers after transoral resection. Head & neck. 2011 Aug;33(8):1210-9. DOI: 10.1002/hed.21505.

70. Pantvaidya G, Rao K, D'Cruz A. Management of the neck in oral cancers. Oral Oncol. 2020 Jan;100:104476. DOI: 10.1016/j.oraloncology.2019.104476.

71. Yuen AP, Ho CM, Chow TL, Tang LC, Cheung WY, Ng RW, et al. Prospective randomized study of selective neck dissection versus observation for N0 neck of early tongue carcinoma. Head & neck. 2009 Jun;31(6):765-72. DOI: 10.1002/hed.21033.

72. Kligerman J, Lima RA, Soares JR, Prado L, Dias FL, Freitas EQ, et al. Supraomohyoid neck dissection in the treatment of T1/T2 squamous cell carcinoma of oral cavity. The American Journal of Surgery. 1994 1994/11/01/;168(5):391-4. DOI: https://doi.org/10.1016/S0002-9610(05)80082-0.

73. Fakih AR, Rao RS, Borges AM, Patel AR. Elective versus therapeutic neck dissection in early carcinoma of the oral tongue. The American Journal of Surgery. 1989 1989/10/01/;158(4):309-13. DOI: https://doi.org/10.1016/0002-9610(89)90122-0.

74. Vandenbrouck C, Sancho-Garnier H, Chassagne D, Saravane D, Cachin Y, Micheau C. Elective versus therapeutic radical neck dissection in epidermoid carcinoma of the oral cavity: results of a randomized clinical trial. Cancer. 1980 Jul 15;46(2):386-90. DOI: 10.1002/1097-0142(19800715)46:2<386::aid-cncr2820460229>3.0.co;2-9.

75. D'Cruz AK, Vaish R, Kapre N, Dandekar M, Gupta S, Hawaldar R, et al. Elective versus Therapeutic Neck Dissection in Node-Negative Oral Cancer. New England Journal of Medicine. 2015;373(6):521-9. DOI: 10.1056/NEJMoa1506007.

76. Garden AS, Reddy JP. Postoperative Radiation Therapy for Metastatic Cervical Adenopathy. Semin Radiat Oncol. 2019 Apr;29(2):144-9. DOI: 10.1016/j.semradonc.2018.11.007.

77. Orosco RK, Tapia VJ, Califano JA, Clary B, Cohen EEW, Kane C, et al. Positive Surgical Margins in the 10 Most Common Solid Cancers. Scientific Reports. 2018 2018/04/09;8(1):5686. DOI: 10.1038/s41598-018-23403-5.

78. Looser KG, Shah JP, Strong EW. The significance of "positive" margins in surgically resected epidermoid carcinomas. Head Neck Surg. 1978 Nov-Dec;1(2):107-11. DOI: 10.1002/hed.2890010203.

79. Batsakis JG. Surgical excision margins: a pathologist's perspective. Adv Anat Pathol. 1999 May;6(3):140-8. DOI: 10.1097/00125480-199905000-00002.

80. Loree TR, Strong EW. Significance of positive margins in oral cavity squamous carcinoma. American journal of surgery. 1990 Oct;160(4):410-4. DOI: 10.1016/s0002-9610(05)80555-0.

81. Sutton DN, Brown JS, Rogers SN, Vaughan ED, Woolgar JA. The prognostic implications of the surgical margin in oral squamous cell carcinoma. International journal of oral and maxillofacial surgery. 2003 Feb;32(1):30-4. DOI: 10.1054/ijom.2002.0313.

82. Luryi AL, Chen MM, Mehra S, Roman SA, Sosa JA, Judson BL. Positive surgical margins in early stage oral cavity cancer: an analysis of 20,602 cases. Otolaryngol Head Neck Surg. 2014 Dec;151(6):984-90. DOI: 10.1177/0194599814551718.

83. Hinni ML, Ferlito A, Brandwein-Gensler MS, Takes RP, Silver CE, Westra WH, et al. Surgical margins in head and neck cancer: a contemporary review. Head & neck. 2013 Sep;35(9):1362-70. DOI: 10.1002/hed.23110.

84. Anderson CR, Sisson K, Moncrieff M. A meta-analysis of margin size and local recurrence in oral squamous cell carcinoma. Oral Oncol. 2015 May;51(5):464-9. DOI: 10.1016/j.oraloncology.2015.01.015.

85. Colevas AD, Yom SS, Pfister DG, Spencer S, Adelstein D, Adkins D, et al. NCCN Guidelines Insights: Head and Neck Cancers, Version 1.2018. J Natl Compr Canc Netw. 2018 May;16(5):479-90. DOI: 10.6004/jnccn.2018.0026.

86. Meier JD, Oliver DA, Varvares MA. Surgical margin determination in head and neck oncology: current clinical practice. The results of an International American Head and Neck Society Member Survey. Head & neck. 2005 Nov;27(11):952-8. DOI: 10.1002/hed.20269.

87. Ettl T, El-Gindi A, Hautmann M, Gosau M, Weber F, Rohrmeier C, et al. Positive frozen section margins predict local recurrence in R0-resected squamous cell carcinoma of the head and neck. Oral Oncol. 2016 Apr;55:17-23. DOI: 10.1016/j.oraloncology.2016.02.012.

88. Buchakjian MR, Tasche KK, Robinson RA, Pagedar NA, Sperry SM. Association of Main Specimen and Tumor Bed Margin Status With Local Recurrence and Survival in Oral Cancer Surgery. JAMA otolaryngology-- head & neck surgery. 2016 Dec 1;142(12):1191-8. DOI: 10.1001/jamaoto.2016.2329.

89. Williams MD. Determining Adequate Margins in Head and Neck Cancers: Practice and Continued Challenges. Curr Oncol Rep. 2016 Sep;18(9):54. DOI: 10.1007/s11912-016-0540-y.

90. Bulbul MG, Zenga J, Tarabichi O, Parikh AS, Sethi RK, Robbins KT, et al. Margin Practices in Oral Cavity Cancer Resections: Survey of American Head and Neck Society Members. The Laryngoscope. 2020 Aug 22. DOI: 10.1002/lary.28976.

91. Pimenta Amaral TM, Da Silva Freire AR, Carvalho AL, Pinto CA, Kowalski LP. Predictive factors of occult metastasis and prognosis of clinical stages I and II squamous cell carcinoma of the tongue and floor of the mouth. Oral Oncol. 2004 Sep;40(8):780-6. DOI: 10.1016/j.oraloncology.2003.10.009.

92. Weijers M, Snow GB, Bezemer DP, van dr Wal JE, van der Waal I. The status of the deep surgical margins in tongue and floor of mouth squamous cell carcinoma and risk of local recurrence; an analysis of 68 patients. International journal of oral and maxillofacial surgery. 2004 Mar;33(2):146-9. DOI: 10.1054/ijom.2002.0469.

93. Kademani D, Bell RB, Bagheri S, Holmgren E, Dierks E, Potter B, et al. Prognostic factors in intraoral squamous cell carcinoma: the influence of histologic grade. J Oral Maxillofac Surg. 2005 Nov;63(11):1599-605. DOI: 10.1016/j.joms.2005.07.011.

94. Brandwein-Gensler M, Teixeira MS, Lewis CM, Lee B, Rolnitzky L, Hille JJ, et al. Oral squamous cell carcinoma: histologic risk assessment, but not margin status, is strongly predictive of local disease-free and overall survival. Am J Surg Pathol. 2005 Feb;29(2):167-78. DOI: 10.1097/01.pas.0000149687.90710.21.

95. Wong LS, McMahon J, Devine J, McLellan D, Thompson E, Farrow A, et al. Influence of close resection margins on local recurrence and disease-specific survival in oral and oropharyngeal carcinoma. British Journal of Oral and Maxillofacial Surgery. 2012 2012/03/01/;50(2):102-8. DOI: https://doi.org/10.1016/j.bjoms.2011.05.008.

96. Alicandri-Ciufelli M, Bonali M, Piccinini A, Marra L, Ghidini A, Cunsolo EM, et al. Surgical margins in head and neck squamous cell carcinoma: what is 'close'? European archives of oto-rhino-laryngology : official journal of the European Federation of Oto-Rhino-Laryngological Societies (EUFOS) : affiliated with the German Society for Oto-Rhino-Laryngology - Head and Neck Surgery. 2013 Sep;270(10):2603-9. DOI: 10.1007/s00405-012-2317-8.

97. Glenny AM, Furness S, Worthington HV, Conway DI, Oliver R, Clarkson JE, et al. Interventions for the treatment of oral cavity and oropharyngeal cancer: radiotherapy. Cochrane Database Syst Rev. 2010 Dec 8(12):Cd006387. DOI: 10.1002/14651858.CD006387.pub2.

98. Sieczka E, Datta R, Singh A, Loree T, Rigual N, Orner J, et al. Cancer of the buccal mucosa: are margins and T-stage accurate predictors of local control? Am J Otolaryngol. 2001 Nov-Dec;22(6):395-9. DOI: 10.1053/ajot.2001.28067.

99. Huang C-H, Chu S-T, Ger L-P, Hou Y-Y, Sun C-P. Clinicopathologic Evaluation of Prognostic Factors for Squamous Cell Carcinoma of the Buccal Mucosa. Journal of the Chinese Medical Association. 2007 2007/04/01/;70(4):164-70. DOI: https://doi.org/10.1016/S1726-4901(09)70351-X.

100. Shaw RJ, McGlashan G, Woolgar JA, Lowe D, Brown JS, Vaughan ED, et al. Prognostic importance of site in squamous cell carcinoma of the buccal mucosa. British Journal of Oral and Maxillofacial Surgery. 2009 2009/07/01/;47(5):356-9. DOI: https://doi.org/10.1016/j.bjoms.2008.09.017.

101. Sutton DN, Brown JS, Rogers SN, Vaughan ED, Woolgar JA. The prognostic implications of the surgical margin in oral squamous cell carcinoma. International journal of oral and maxillofacial surgery. 2003 2003/02/01/;32(1):30-4. DOI: https://doi.org/10.1054/ijom.2002.0313.

102. Nason RW, Binahmed A, Pathak KA, Abdoh AA, Sándor GKB. What is the adequate margin of surgical resection in oral cancer? Oral Surgery, Oral Medicine, Oral Pathology, Oral Radiology, and Endodontology. 2009 2009/05/01/;107(5):625-9. DOI: https://doi.org/10.1016/j.tripleo.2008.11.013.

103. Binahmed A, Nason RW, Abdoh AA. The clinical significance of the positive surgical margin in oral cancer. Oral oncology. 2007 2007/09/01/;43(8):780-4. DOI: https://doi.org/10.1016/j.oraloncology.2006.10.001.

104. Helliwell T, Woolgar J. Dataset for histopathology reporting of mucosal malignancies of the oral cavity. Stand Datasets report Cancers London: the Royal College of Pathologists. 2013.

105. Weijers M, Snow GB, Bezemer DP, van der Wal JE, van der Waal I. The status of the deep surgical margins in tongue and floor of mouth squamous cell carcinoma and risk of local recurrence; an analysis of 68 patients. International journal of oral and maxillofacial surgery. 2004 2004/03/01/;33(2):146-9. DOI: https://doi.org/10.1054/ijom.2002.0469.

106. Mishra RC, Parida G, Mishra TK, Mohanty S. Tumour thickness and relationship to locoregional failurein cancer of the buccal mucosa. European Journal of Surgical Oncology (EJSO). 1999 1999/04/01/;25(2):186-9. DOI: https://doi.org/10.1053/ejso.1998.0624.

107. Vered M, Dayan D, Dobriyan A, Yahalom R, Shalmon B, Barshack I, et al. Oral tongue squamous cell carcinoma: recurrent disease is associated with histopathologic risk score and young age. Journal of Cancer Research and Clinical Oncology. 2010 2010/07/01;136(7):1039-48. DOI: 10.1007/s00432-009-0749-3.

108. Ferlito A, Shaha AR, Silver CE, Rinaldo A, Mondin V. Incidence and sites of distant metastases from head and neck cancer. ORL J Otorhinolaryngol Relat Spec. 2001 Jul-Aug;63(4):202-7. DOI: 10.1159/000055740.

109. Müller S, Boy SC, Day TA, Magliocca KR, Richardson MS, Sloan P, et al. Data Set for the Reporting of Oral Cavity Carcinomas: Explanations and Recommendations of the Guidelines From the International Collaboration of Cancer Reporting. Archives of Pathology & Laboratory Medicine. 2018;143(4):439-46. DOI: 10.5858/arpa.2018-0411-SA.

110. Johnson RE, Sigman JD, Funk GF, Robinson RA, Hoffman HT. Quantification of surgical margin shrinkage in the oral cavity. Head & neck. 1997 Jul;19(4):281-6. DOI: 10.1002/(sici)1097-0347(199707)19:4<281::aid-hed6>3.0.co;2-x.

111. Mistry RC, Qureshi SS, Kumaran C. Post-resection mucosal margin shrinkage in oral cancer: quantification and significance. J Surg Oncol. 2005 Aug 1;91(2):131-3. DOI: 10.1002/jso.20285.

112. Umstattd LA, Mills JC, Critchlow WA, Renner GJ, Zitsch RP, 3rd. Shrinkage in oral squamous cell carcinoma: An analysis of tumor and margin measurements in vivo, post-resection, and post-formalin fixation. Am J Otolaryngol. 2017 Nov-Dec;38(6):660-2. DOI: 10.1016/j.amjoto.2017.08.011.

113. Pangare TB, Waknis PP, Bawane SS, Patil MN, Wadhera S, Patowary PB. Effect of Formalin Fixation on Surgical Margins in Patients With Oral Squamous Cell Carcinoma. J Oral Maxillofac Surg. 2017 Jun;75(6):1293-8. DOI: 10.1016/j.joms.2016.11.024.

114. Wick MR, Mills SE. Evaluation of surgical margins in anatomic pathology: technical, conceptual, and clinical considerations. Semin Diagn Pathol. 2002 Nov;19(4):207-18.

115. McIntosh ER, Harada S, Drwiega J, Brandwein-Gensler MS, Gordetsky J. Frozen section: guiding the hands of surgeons? Ann Diagn Pathol. 2015 Oct;19(5):326-9. DOI: 10.1016/j.anndiagpath.2015.07.004.

116. Arcega RS, Woo JS, Xu H. Performing and Cutting Frozen Sections. Methods Mol Biol. 2019;1897:279-88. DOI: 10.1007/978-1-4939-8935-5_24.

117. Winship T, Rosvoll RV. Frozen sections; an evaluation of 1,810 cases. Surgery. 1959 Mar;45(3):462-6.

118. Kain JJ, Birkeland AC, Udayakumar N, Morlandt AB, Stevens TM, Carroll WR, et al. Surgical margins in oral cavity squamous cell carcinoma: Current practices and future directions. The Laryngoscope. 2020 Jan;130(1):128-38. DOI: 10.1002/lary.27943.

119. Guillemaud JP, Patel RS, Goldstein DP, Higgins KM, Enepekides DJ. Prognostic impact of intraoperative microscopic cut-through on frozen section in oral cavity squamous cell carcinoma. J Otolaryngol Head Neck Surg. 2010 Aug;39(4):370-7.

120. Patel RS, Goldstein DP, Guillemaud J, Bruch GA, Brown D, Gilbert RW, et al. Impact of positive frozen section microscopic tumor cut-through revised to negative on oral carcinoma control and survival rates. Head & neck. 2010 Nov;32(11):1444-51. DOI: 10.1002/hed.21334.

121. Szewczyk M, Golusinski W, Pazdrowski J, Masternak M, Sharma N, Golusinski P. Positive fresh frozen section margins as an adverse independent prognostic factor for local recurrence in oral cancer patients. The Laryngoscope. 2018 May;128(5):1093-8. DOI: 10.1002/lary.26890.

122. Mair M, Nair D, Nair S, Dutta S, Garg A, Malik A, et al. Intraoperative gross examination vs frozen section for achievement of adequate margin in oral cancer surgery. Oral Surg Oral Med Oral Pathol Oral Radiol. 2017 May;123(5):544-9. DOI: 10.1016/j.oooo.2016.11.018.

123. Pathak KA, Nason RW, Penner C, Viallet NR, Sutherland D, Kerr PD. Impact of use of frozen section assessment of operative margins on survival in oral cancer. Oral Surg Oral Med Oral Pathol Oral Radiol Endod. 2009 Feb;107(2):235-9. DOI: 10.1016/j.tripleo.2008.09.028.

124. Bulbul MG, Tarabichi O, Sethi RK, Parikh AS, Varvares MA. Does Clearance of Positive Margins Improve Local Control in Oral Cavity Cancer? A Meta-analysis. Otolaryngol Head Neck Surg. 2019 Aug;161(2):235-44. DOI: 10.1177/0194599819839006.

125. Chang AM, Kim SW, Duvvuri U, Johnson JT, Myers EN, Ferris RL, et al. Early squamous cell carcinoma of the oral tongue: comparing margins obtained from

the glossectomy specimen to margins from the tumor bed. Oral Oncol. 2013 Nov;49(11):1077-82. DOI: 10.1016/j.oraloncology.2013.07.013.

126. Yahalom R, Dobriyan A, Vered M, Talmi YP, Teicher S, Bedrin L. A prospective study of surgical margin status in oral squamous cell carcinoma: a preliminary report. J Surg Oncol. 2008 Dec 15;98(8):572-8. DOI: 10.1002/jso.21034.

127. Maxwell JH, Thompson LD, Brandwein-Gensler MS, Weiss BG, Canis M, Purgina B, et al. Early Oral Tongue Squamous Cell Carcinoma: Sampling of Margins From Tumor Bed and Worse Local Control. JAMA otolaryngology--head & neck surgery. 2015 Dec;141(12):1104-10. DOI: 10.1001/jamaoto.2015.1351.

128. Amit M, Na'ara S, Leider-Trejo L, Akrish S, Cohen JT, Billan S, et al. Improving the rate of negative margins after surgery for oral cavity squamous cell carcinoma: A prospective randomized controlled study. Head & neck. 2016 Apr;38 Suppl 1:E1803-9. DOI: 10.1002/hed.24320.

129. Black C, Marotti J, Zarovnaya E, Paydarfar J. Critical evaluation of frozen section margins in head and neck cancer resections. Cancer. 2006 Dec 15;107(12):2792-800. DOI: 10.1002/cncr.22347.

130. Scholl P, Byers RM, Batsakis JG, Wolf P, Santini H. Microscopic cut-through of cancer in the surgical treatment of squamous carcinoma of the tongue. Prognostic and therapeutic implications. American journal of surgery. 1986 Oct;152(4):354-60. DOI: 10.1016/0002-9610(86)90304-1.

131. Kerawala CJ, Ong TK. Relocating the site of frozen sections--is there room for improvement? Head & neck. 2001 Mar;23(3):230-2. DOI: 10.1002/1097-0347(200103)23:3<230::aid-hed1023>3.0.co;2-v.

132. van Lanschot CGF, Mast H, Hardillo JA, Monserez D, Ten Hove I, Barroso EM, et al. Relocation of inadequate resection margins in the wound bed during oral cavity oncological surgery: A feasibility study. Head & neck. 2019 Jul;41(7):2159-66. DOI: 10.1002/hed.25690.

133. DiNardo LJ, Lin J, Karageorge LS, Powers CN. Accuracy, utility, and cost of frozen section margins in head and neck cancer surgery. The Laryngoscope. 2000 Oct;110(10 Pt 1):1773-6. DOI: 10.1097/00005537-200010000-00039.

134. Nieweg OE, Tanis PJ, Kroon BB. The definition of a sentinel node. Annals of surgical oncology. 2001 Jul;8(6):538-41.

135. Dogan NU, Dogan S, Favero G, Köhler C, Dursun P. The Basics of Sentinel Lymph Node Biopsy: Anatomical and Pathophysiological Considerations and Clinical Aspects. J Oncol. 2019;2019:3415630. DOI: 10.1155/2019/3415630.

136. Gould EA, Winship T, Philbin PH, Kerr HH. Observations on a "sentinel node" in cancer of the parotid. Cancer. 1960 Jan-Feb;13:77-8. DOI: 10.1002/1097-0142(196001/02)13:1<77::aid-cncr2820130114>3.0.co;2-d.

137. Cabanas RM. An approach for the treatment of penile carcinoma. Cancer. 1977 Feb;39(2):456-66. DOI: 10.1002/1097-0142(197702)39:2<456::aid-cncr2820390214>3.0.co;2-i.

138. Morton DL, Wen DR, Wong JH, Economou JS, Cagle LA, Storm FK, et al. Technical details of intraoperative lymphatic mapping for early stage melanoma. Arch Surg. 1992 Apr;127(4):392-9. DOI: 10.1001/archsurg.1992.01420040034005.

139. Reintgen M, Kerivan L, Reintgen E, Swaninathan S, Reintgen D. Breast Lymphatic Mapping and Sentinel Lymph Node Biopsy: State of the Art: 2015. Clin Breast Cancer. 2016 Jun;16(3):155-65. DOI: 10.1016/j.clbc.2016.02.014.

140. Donker M, van Tienhoven G, Straver ME, Meijnen P, van de Velde CJ, Mansel RE, et al. Radiotherapy or surgery of the axilla after a positive sentinel node in breast cancer (EORTC 10981-22023 AMAROS): a randomised, multicentre, open-label, phase 3 non-inferiority trial. Lancet Oncol. 2014 Nov;15(12):1303-10. DOI: 10.1016/s1470-2045(14)70460-7.

141. Veronesi U, Viale G, Paganelli G, Zurrida S, Luini A, Galimberti V, et al. Sentinel lymph node biopsy in breast cancer: ten-year results of a randomized controlled study. Annals of surgery. 2010 Apr;251(4):595-600. DOI: 10.1097/SLA.0b013e3181c0e92a.

142. Qiu SQ, Zhang GJ, Jansen L, de Vries J, Schröder CP, de Vries EGE, et al. Evolution in sentinel lymph node biopsy in breast cancer. Critical reviews in oncology/hematology. 2018 Mar;123:83-94. DOI: 10.1016/j.critrevonc.2017.09.010.

143. Taghizadeh Kermani A, Bagheri R, Tehranian S, Shojaee P, Sadeghi R, D NK. Accuracy of sentinel node biopsy in the staging of non-small cell lung carcinomas: systematic review and meta-analysis of the literature. Lung Cancer. 2013 Apr;80(1):5-14. DOI: 10.1016/j.lungcan.2013.01.001.

144. Schulze T, Bembenek A, Schlag PM. Sentinel lymph node biopsy progress in surgical treatment of cancer. Langenbecks Arch Surg. 2004 Nov;389(6):532-50. DOI: 10.1007/s00423-004-0484-9.

145. Mulsow J, Winter DC, O'Keane JC, O'Connell PR. Sentinel lymph node mapping in colorectal cancer. Br J Surg. 2003 Jun;90(6):659-67. DOI: 10.1002/bjs.4217.

146. van der Poel HG, Meershoek P, Grivas N, KleinJan G, van Leeuwen FW, Horenblas S. Sentinel node biopsy and lymphatic mapping in penile and prostate cancer. Urologe A. 2017 Jan;56(1):13-7. DOI: 10.1007/s00120-016-0270-7.

147. Holloway RW, Abu-Rustum NR, Backes FJ, Boggess JF, Gotlieb WH, Jeffrey Lowery W, et al. Sentinel lymph node mapping and staging in endometrial cancer: A Society of Gynecologic Oncology literature review with consensus recommendations. Gynecol Oncol. 2017 Aug;146(2):405-15. DOI: 10.1016/j.ygyno.2017.05.027.

148. Alex JC, Krag DN. The gamma-probe-guided resection of radiolabeled primary lymph nodes. Surg Oncol Clin N Am. 1996 Jan;5(1):33-41.

149. de Bree R, Nieweg OE. The history of sentinel node biopsy in head and neck cancer: From visualization of lymphatic vessels to sentinel nodes. Oral oncology. 2015 2015/09/01/;51(9):819-23. DOI: https://doi.org/10.1016/j.oraloncology.2015.06.006.

150. Pitman KT, Johnson JT, Edington H, Barnes EL, Day R, Wagner RL, et al. Lymphatic mapping with isosulfan blue dye in squamous cell carcinoma of the head and neck. Arch Otolaryngol Head Neck Surg. 1998 Jul;124(7):790-3. DOI: 10.1001/archotol.124.7.790.

151. Koch WM, Choti MA, Civelek AC, Eisele DW, Saunders JR. Gamma Probe–Directed Biopsy of the Sentinel Node in Oral Squamous Cell Carcinoma. Archives of Otolaryngology–Head & Neck Surgery. 1998;124(4):455-9. DOI: 10.1001/archotol.124.4.455.

152. Shoaib T, Soutar DS, Prosser JE, Dunaway DJ, Gray HW, McCurrach GM, et al. A suggested method for sentinel node biopsy in squamous cell carcinoma of the head and neck. Head & neck. 1999 Dec;21(8):728-33. DOI: 10.1002/(sici)1097-0347(199912)21:8<728::aid-hed8>3.0.co;2-p.

153. Ross GL, Shoaib T, Soutar DS, MacDonald DG, Camilleri IG, Bessent RG, et al. The First International Conference on Sentinel Node Biopsy in Mucosal Head and Neck Cancer and adoption of a multicenter trial protocol. Annals of surgical oncology. 2002 May;9(4):406-10. DOI: 10.1007/bf02573877.

154. Stoeckli SJ, Pfaltz M, Ross GL, Steinert HC, MacDonald DG, Wittekind C, et al. The second international conference on sentinel node biopsy in mucosal head and neck cancer. Annals of surgical oncology. 2005 Nov;12(11):919-24. DOI: 10.1245/aso.2005.11.024.

155. Alkureishi LW, Ross GL, Shoaib T, Soutar DS, Robertson AG, Thompson R, et al. Sentinel node biopsy in head and neck squamous cell cancer: 5-year follow-up of a European multicenter trial. Annals of surgical oncology. 2010 Sep;17(9):2459-64. DOI: 10.1245/s10434-010-1111-3.

156. Kovács AF, Stefenelli U, Seitz O, Middendorp M, Diener J, Sader R, et al. Positive sentinel lymph nodes are a negative prognostic factor for survival in T1-2 oral/oropharyngeal cancer-a long-term study on 103 patients. Annals of surgical oncology. 2009 Feb;16(2):233-9. DOI: 10.1245/s10434-008-0150-5.

157. Broglie MA, Haile SR, Stoeckli SJ. Long-term experience in sentinel node biopsy for early oral and oropharyngeal squamous cell carcinoma. Annals of surgical oncology. 2011 Oct;18(10):2732-8. DOI: 10.1245/s10434-011-1780-6.

158. Pfister DG, Ang KK, Brizel DM, Burtness BA, Busse PM, Caudell JJ, et al. Head and neck cancers, version 2.2013. Featured updates to the NCCN guidelines. J Natl Compr Canc Netw. 2013 Aug;11(8):917-23. DOI: 10.6004/jnccn.2013.0113.

159. Giammarile F, Schilling C, Gnanasegaran G, Bal C, Oyen WJG, Rubello D, et al. The EANM practical guidelines for sentinel lymph node localisation in oral cavity squamous cell carcinoma. Eur J Nucl Med Mol Imaging. 2019 Mar;46(3):623-37. DOI: 10.1007/s00259-018-4235-5.

160. Alkureishi LW, Burak Z, Alvarez JA, Ballinger J, Bilde A, Britten AJ, et al. Joint practice guidelines for radionuclide lymphoscintigraphy for sentinel node localization in oral/oropharyngeal squamous cell carcinoma. Eur J Nucl Med Mol Imaging. 2009 Nov;36(11):1915-36. DOI: 10.1007/s00259-009-1248-0.

161. Schilling C, Stoeckli SJ, Vigili MG, de Bree R, Lai SY, Alvarez J, et al. Surgical consensus guidelines on sentinel node biopsy (SNB) in patients with oral cancer. Head & neck. 2019 Aug;41(8):2655-64. DOI: 10.1002/hed.25739.

162. Garrel R, Poissonnet G, Temam S, Dolivet G, Fakhry N, de Raucourt D. Review of sentinel node procedure in cN0 head and neck squamous cell carcinomas. Guidelines from the French evaluation cooperative subgroup of GETTEC. Eur Ann Otorhinolaryngol Head Neck Dis. 2017 Apr;134(2):89-93. DOI: 10.1016/j.anorl.2016.10.004.

163. Hornstra MT, Alkureishi LW, Ross GL, Shoaib T, Soutar DS. Predictive factors for failure to identify sentinel nodes in head and neck squamous cell carcinoma. Head & neck. 2008 Jul;30(7):858-62. DOI: 10.1002/hed.20787.

164. Flach GB, Broglie MA, van Schie A, Bloemena E, Leemans CR, de Bree R, et al. Sentinel node biopsy for oral and oropharyngeal squamous cell carcinoma in the previously treated neck. Oral Oncol. 2012 Jan;48(1):85-9. DOI: 10.1016/j.oraloncology.2011.08.015.

165. Wilhelm AJ, Mijnhout GS, Franssen EJ. Radiopharmaceuticals in sentinel lymph-node detection - an overview. Eur J Nucl Med. 1999 Apr;26(4 Suppl):S36-42. DOI: 10.1007/pl00014793.

166. Strand SE, Persson BR. Quantitative lymphoscintigraphy I: Basic concepts for optimal uptake of radiocolloids in the parasternal lymph nodes of rabbits. J Nucl Med. 1979 Oct;20(10):1038-46.

167. Agrawal A, Civantos FJ, Brumund KT, Chepeha DB, Hall NC, Carroll WR, et al. [(99m)Tc]Tilmanocept Accurately Detects Sentinel Lymph Nodes and Predicts Node Pathology Status in Patients with Oral Squamous Cell Carcinoma of the Head and Neck: Results of a Phase III Multi-institutional Trial. Annals of surgical oncology. 2015 Oct;22(11):3708-15. DOI: 10.1245/s10434-015-4382-x.

168. Alazraki N, Glass EC, Castronovo F, Olmos RA, Podoloff D. Procedure guideline for lymphoscintigraphy and the use of intraoperative gamma probe for sentinel lymph node localization in melanoma of intermediate thickness 1.0. J Nucl Med. 2002 Oct;43(10):1414-8.

169. van den Berg NS, Brouwer OR, Klop WM, Karakullukcu B, Zuur CL, Tan IB, et al. Concomitant radio- and fluorescence-guided sentinel lymph node biopsy in squamous cell carcinoma of the oral cavity using ICG-(99m)Tc-nanocolloid. Eur

J Nucl Med Mol Imaging. 2012 Jul;39(7):1128-36. DOI: 10.1007/s00259-012-2129-5.

170. Barthelmes L, Goyal A, Newcombe RG, McNeill F, Mansel RE. Adverse reactions to patent blue V dye - The NEW START and ALMANAC experience. European journal of surgical oncology : the journal of the European Society of Surgical Oncology and the British Association of Surgical Oncology. 2010 Apr;36(4):399-403. DOI: 10.1016/j.ejso.2009.10.007.

171. Stoffels I, Dissemond J, Pöppel T, Schadendorf D, Klode J. Intraoperative Fluorescence Imaging for Sentinel Lymph Node Detection: Prospective Clinical Trial to Compare the Usefulness of Indocyanine Green vs Technetium Tc 99m for Identification of Sentinel Lymph Nodes. JAMA Surg. 2015 Jul;150(7):617-23. DOI: 10.1001/jamasurg.2014.3502.

172. Christensen A, Juhl K, Charabi B, Mortensen J, Kiss K, Kjaer A, et al. Feasibility of Real-Time Near-Infrared Fluorescence Tracer Imaging in Sentinel Node Biopsy for Oral Cavity Cancer Patients. Annals of surgical oncology. 2016 Feb;23(2):565-72. DOI: 10.1245/s10434-015-4883-7.

173. Valdés Olmos RA, Jansen L, Muller SH, Hoefnagel CA, Nieweg O. [Contribution of nuclear medicine to lymphatic mapping and sentinel node identification in oncology]. Rev Esp Med Nucl. 1999;18(2):111-21.

174. Chakera AH, Hesse B, Burak Z, Ballinger JR, Britten A, Caracò C, et al. EANM-EORTC general recommendations for sentinel node diagnostics in melanoma. Eur J Nucl Med Mol Imaging. 2009 Oct;36(10):1713-42. DOI: 10.1007/s00259-009-1228-4.

175. Stoeckli SJ, Huebner T, Huber GF, Broglie MA. Technique for reliable sentinel node biopsy in squamous cell carcinomas of the floor of mouth. Head & neck. 2016 Sep;38(9):1367-72. DOI: 10.1002/hed.24440.

176. Atula T, Shoaib T, Ross GL, Gray HW, Soutar DS. How many sentinel nodes should be harvested in oral squamous cell carcinoma? European archives of oto-rhino-laryngology : official journal of the European Federation of Oto-Rhino-Laryngological Societies (EUFOS) : affiliated with the German Society for Oto-Rhino-Laryngology - Head and Neck Surgery. 2008 Jul;265 Suppl 1(Suppl 1):S19-23. DOI: 10.1007/s00405-007-0548-x.

177. Woolgar JA. Micrometastasis in oral/oropharyngeal squamous cell carcinoma: incidence, histopathological features and clinical implications. Br J Oral Maxillofac Surg. 1999 Jun;37(3):181-6. DOI: 10.1054/bjom.1999.0037.

178. Stoeckli SJ, Pfaltz M, Steinert H, Schmid S. Histopathological features of occult metastasis detected by sentinel lymph node biopsy in oral and oropharyngeal squamous cell carcinoma. The Laryngoscope. 2002 Jan;112(1):111-5. DOI: 10.1097/00005537-200201000-00019.

179. Sloan P. Head and neck sentinel lymph node biopsy: current state of the art. Head Neck Pathol. 2009 Sep;3(3):231-7. DOI: 10.1007/s12105-009-0132-3.

180. Hermanek P, Hutter RV, Sobin LH, Wittekind C. International Union Against Cancer. Classification of isolated tumor cells and micrometastasis. Cancer. 1999 Dec 15;86(12):2668-73.

181. Burcia V, Costes V, Faillie JL, Gardiner Q, de Verbizier D, Cartier C, et al. Neck restaging with sentinel node biopsy in T1-T2N0 oral and oropharyngeal cancer: Why and how? Otolaryngol Head Neck Surg. 2010 Apr;142(4):592-7.e1. DOI: 10.1016/j.otohns.2009.12.016.

182. Schilling C, Stoeckli SJ, Haerle SK, Broglie MA, Huber GF, Sorensen JA, et al. Sentinel European Node Trial (SENT): 3-year results of sentinel node biopsy in oral cancer. European journal of cancer (Oxford, England : 1990). 2015 Dec;51(18):2777-84. DOI: 10.1016/j.ejca.2015.08.023.

183. Schiefke F, Akdemir M, Weber A, Akdemir D, Singer S, Frerich B. Function, postoperative morbidity, and quality of life after cervical sentinel node biopsy and after selective neck dissection. Head & neck. 2009 Apr;31(4):503-12. DOI: 10.1002/hed.21001.

184. Huang SH, Hahn E, Chiosea SI, Xu ZY, Li JS, Shen L, et al. The role of adjuvant (chemo-)radiotherapy in oral cancers in the contemporary era. Oral Oncol. 2020 Mar;102:104563. DOI: 10.1016/j.oraloncology.2019.104563.

185. Govers TM, Hannink G, Merkx MA, Takes RP, Rovers MM. Sentinel node biopsy for squamous cell carcinoma of the oral cavity and oropharynx: a diagnostic meta-analysis. Oral Oncol. 2013 Aug;49(8):726-32. DOI: 10.1016/j.oraloncology.2013.04.006.

186. Liu M, Wang SJ, Yang X, Peng H. Diagnostic Efficacy of Sentinel Lymph Node Biopsy in Early Oral Squamous Cell Carcinoma: A Meta-Analysis of 66 Studies. PloS one. 2017;12(1):e0170322. DOI: 10.1371/journal.pone.0170322.

187. Murer K, Huber GF, Haile SR, Stoeckli SJ. Comparison of morbidity between sentinel node biopsy and elective neck dissection for treatment of the n0 neck in patients with oral squamous cell carcinoma. Head & neck. 2011 Sep;33(9):1260-4. DOI: 10.1002/hed.21622.

188. Taylor RJ, Chepeha JC, Teknos TN, Bradford CR, Sharma PK, Terrell JE, et al. Development and validation of the neck dissection impairment index: a quality of life measure. Arch Otolaryngol Head Neck Surg. 2002 Jan;128(1):44-9. DOI: 10.1001/archotol.128.1.44.

189. Constant CR, Murley AH. A clinical method of functional assessment of the shoulder. Clin Orthop Relat Res. 1987 Jan(214):160-4.

190. O'Connor R, Pezier T, Schilling C, McGurk M. The relative cost of sentinel lymph node biopsy in early oral cancer. Journal of cranio-maxillo-facial surgery : official publication of the European Association for Cranio-Maxillo-Facial Surgery. 2013 Dec;41(8):721-7. DOI: 10.1016/j.jcms.2013.01.012.

191. Kosuda S, Kusano S, Kohno N, Ohno Y, Tanabe T, Kitahara S, et al. Feasibility and cost-effectiveness of sentinel lymph node radiolocalization in stage N0 head

and neck cancer. Arch Otolaryngol Head Neck Surg. 2003 Oct;129(10):1105-9. DOI: 10.1001/archotol.129.10.1105.

192. Govers TM, Takes RP, Baris Karakullukcu M, Hannink G, Merkx MA, Grutters JP, et al. Management of the N0 neck in early stage oral squamous cell cancer: a modeling study of the cost-effectiveness. Oral Oncol. 2013 Aug;49(8):771-7. DOI: 10.1016/j.oraloncology.2013.05.001.

193. Lai SY, Ferris RL. Evolving Evidence in Support of Sentinel Lymph Node Biopsy for Early-Stage Oral Cavity Cancer. Journal of clinical oncology : official journal of the American Society of Clinical Oncology. 2020 Dec 1;38(34):3983-6. DOI: 10.1200/jco.20.02716.

194. Hasegawa Y, Tsukahara K, Yoshimoto S, Miura K, Yokoyama J, Hirano S, et al. Neck dissections based on sentinel lymph node navigation versus elective neck dissections in early oral cancers: A randomized, multicenter, non-inferiority trial. Journal of Clinical Oncology. 2019 2019/05/20;37(15_suppl):6007-. DOI: 10.1200/JCO.2019.37.15_suppl.6007.

195. Garrel R, Poissonnet G, Moyà Plana A, Fakhry N, Dolivet G, Lallemant B, et al. Equivalence Randomized Trial to Compare Treatment on the Basis of Sentinel Node Biopsy Versus Neck Node Dissection in Operable T1-T2N0 Oral and Oropharyngeal Cancer. Journal of clinical oncology : official journal of the American Society of Clinical Oncology. 2020 Dec 1;38(34):4010-8. DOI: 10.1200/jco.20.01661.

196. Abdul-Razak M, Chung H, Wong E, Palme C, Veness M, Farlow D, et al. Sentinel lymph node biopsy for early oral cancers: Westmead Hospital experience. ANZ J Surg. 2017 Jan;87(1-2):65-9. DOI: 10.1111/ans.13853.

197. Cramer JD, Sridharan S, Ferris RL, Duvvuri U, Samant S. Sentinel Lymph Node Biopsy Versus Elective Neck Dissection for Stage I to II Oral Cavity Cancer. The Laryngoscope. 2019 Jan;129(1):162-9. DOI: 10.1002/lary.27323.

198. Bluemel C, Rubello D, Colletti PM, de Bree R, Herrmann K. Sentinel lymph node biopsy in oral and oropharyngeal squamous cell carcinoma: current status and unresolved challenges. Eur J Nucl Med Mol Imaging. 2015 Aug;42(9):1469-80. DOI: 10.1007/s00259-015-3049-y.

199. Pedersen NJ, Jensen DH, Hedbäck N, Frendø M, Kiss K, Lelkaitis G, et al. Staging of early lymph node metastases with the sentinel lymph node technique and predictive factors in T1/T2 oral cavity cancer: A retrospective single-center study. Head & neck. 2016 Apr;38 Suppl 1:E1033-40. DOI: 10.1002/hed.24153.

200. Den Toom IJ, Heuveling DA, Flach GB, van Weert S, Karagozoglu KH, van Schie A, et al. Sentinel node biopsy for early-stage oral cavity cancer: the VU University Medical Center experience. Head & neck. 2015 Apr;37(4):573-8. DOI: 10.1002/hed.23632.

201. Civantos FJ, Zitsch RP, Schuller DE, Agrawal A, Smith RB, Nason R, et al. Sentinel Lymph Node Biopsy Accurately Stages the Regional Lymph Nodes for T1-T2 Oral Squamous Cell Carcinomas: Results of a Prospective Multi-

Institutional Trial. Journal of Clinical Oncology. 2010;28(8):1395-400. DOI: 10.1200/jco.2008.20.8777.

202. den Toom IJ, Mahieu R, van Rooij R, van Es RJJ, Hobbelink MGG, Krijger GC, et al. Sentinel lymph node detection in oral cancer: a within-patient comparison between [(99m)Tc]Tc-tilmanocept and [(99m)Tc]Tc-nanocolloid. Eur J Nucl Med Mol Imaging. 2020 Aug 25. DOI: 10.1007/s00259-020-04984-8.

203. Civantos FJ, Moffat FL, Goodwin WJ. Lymphatic mapping and sentinel lymphadenectomy for 106 head and neck lesions: contrasts between oral cavity and cutaneous malignancy. The Laryngoscope. 2006 Mar;112(3 Pt 2 Suppl 109):1-15. DOI: 10.1097/01.mlg.0000200750.74249.79.

204. Farmer RW, McCall L, Civantos FJ, Myers JN, Yarbrough WG, Murphy B, et al. Lymphatic drainage patterns in oral squamous cell carcinoma: findings of the ACOSOG Z0360 (Alliance) study. Otolaryngol Head Neck Surg. 2015 Apr;152(4):673-7. DOI: 10.1177/0194599815572585.

205. Dias FL, Lima RA, Kligerman J, Farias TP, Soares JR, Manfro G, et al. Relevance of skip metastases for squamous cell carcinoma of the oral tongue and the floor of the mouth. Otolaryngol Head Neck Surg. 2006 Mar;134(3):460-5. DOI: 10.1016/j.otohns.2005.09.025.

206. Werner JA, Dunne AA, Ramaswamy A, Folz BJ, Brandt D, Kulkens C, et al. Number and location of radiolabeled, intraoperatively identified sentinel nodes in 48 head and neck cancer patients with clinically staged N0 and N1 neck. European archives of oto-rhino-laryngology : official journal of the European Federation of Oto-Rhino-Laryngological Societies (EUFOS) : affiliated with the German Society for Oto-Rhino-Laryngology - Head and Neck Surgery. 2002 Feb;259(2):91-6. DOI: 10.1007/s00405-001-0421-2.

207. Alex JC. The application of sentinel node radiolocalization to solid tumors of the head and neck: a 10-year experience. The Laryngoscope. 2004 Jan;114(1):2-19. DOI: 10.1097/00005537-200401000-00002.

208. Ferris RL, Xi L, Seethala RR, Chan J, Desai S, Hoch B, et al. Intraoperative qRT-PCR for detection of lymph node metastasis in head and neck cancer. Clin Cancer Res. 2011 Apr 1;17(7):1858-66. DOI: 10.1158/1078-0432.Ccr-10-3110.

209. Tumati V, Hoang L, Sumer BD, Truelson JM, Myers LL, Khan S, et al. Association between treatment delays and oncologic outcome in patients treated with surgery and radiotherapy for head and neck cancer. Head & neck. 2019 Feb;41(2):315-21. DOI: 10.1002/hed.25457.

210. Goel AN, Frangos MI, Raghavan G, Lazaro SL, Tang B, Chhetri DK, et al. The impact of treatment package time on survival in surgically managed head and neck cancer in the United States. Oral Oncol. 2019 Jan;88:39-48. DOI: 10.1016/j.oraloncology.2018.11.021.

211. de Boer E, Harlaar NJ, Taruttis A, Nagengast WB, Rosenthal EL, Ntziachristos V, et al. Optical innovations in surgery. Br J Surg. 2015 Jan;102(2):e56-72. DOI: 10.1002/bjs.9713.

212. Lee Y-J, Krishnan G, Nishio N, van den Berg NS, Lu G, Martin BA, et al. Intraoperative Fluorescence-Guided Surgery in Head and Neck Squamous Cell Carcinoma. The Laryngoscope.n/a(n/a). DOI: https://doi.org/10.1002/lary.28822.

213. Zhu B, Godavarty A. Near-Infrared Fluorescence-Enhanced Optical Tomography. Biomed Res Int. 2016;2016:5040814. DOI: 10.1155/2016/5040814.

214. Vinegoni C, Razansky D, Figueiredo JL, Nahrendorf M, Ntziachristos V, Weissleder R. Normalized Born ratio for fluorescence optical projection tomography. Opt Lett. 2009 Feb 1;34(3):319-21. DOI: 10.1364/ol.34.000319.

215. van Keulen S, Nishio N, Fakurnejad S, van den Berg NS, Lu G, Birkeland A, et al. Intraoperative Tumor Assessment Using Real-Time Molecular Imaging in Head and Neck Cancer Patients. J Am Coll Surg. 2019 Dec;229(6):560-7.e1. DOI: 10.1016/j.jamcollsurg.2019.09.007.

216. Moore LS, Rosenthal EL, Chung TK, de Boer E, Patel N, Prince AC, et al. Characterizing the Utility and Limitations of Repurposing an Open-Field Optical Imaging Device for Fluorescence-Guided Surgery in Head and Neck Cancer Patients. J Nucl Med. 2017 Feb;58(2):246-51. DOI: 10.2967/jnumed.115.171413.

217. Teraphongphom N, Kong CS, Warram JM, Rosenthal EL. Specimen mapping in head and neck cancer using fluorescence imaging. Laryngoscope Investig Otolaryngol. 2017 Dec;2(6):447-52. DOI: 10.1002/lio2.84.

218. Moore GE. Fluorescein as an Agent in the Differentiation of Normal and Malignant Tissues. Science. 1947 Aug 8;106(2745):130-1. DOI: 10.1126/science.106.2745.130-a.

219. Zeng HC, Hu JL, Bai JW, Zhang GJ. Detection of Sentinel Lymph Nodes with Near-Infrared Imaging in Malignancies. Mol Imaging Biol. 2019 Apr;21(2):219-27. DOI: 10.1007/s11307-018-1237-4.

220. Rosenthal EL, Warram JM, Bland KI, Zinn KR. The status of contemporary image-guided modalities in oncologic surgery. Annals of surgery. 2015 Jan;261(1):46-55. DOI: 10.1097/sla.0000000000000622.

221. Miller SE, Tummers WS, Teraphongphom N, van den Berg NS, Hasan A, Ertsey RD, et al. First-in-human intraoperative near-infrared fluorescence imaging of glioblastoma using cetuximab-IRDye800. Journal of neuro-oncology. 2018 Aug;139(1):135-43. DOI: 10.1007/s11060-018-2854-0.

222. Rosenthal EL, Warram JM, de Boer E, Chung TK, Korb ML, Brandwein-Gensler M, et al. Safety and Tumor Specificity of Cetuximab-IRDye800 for Surgical Navigation in Head and Neck Cancer. Clin Cancer Res. 2015 Aug 15;21(16):3658-66. DOI: 10.1158/1078-0432.Ccr-14-3284.

223. Tummers WS, Miller SE, Teraphongphom NT, van den Berg NS, Hasan A, Longacre TA, et al. Detection of visually occult metastatic lymph nodes using molecularly targeted fluorescent imaging during surgical resection of pancreatic cancer. HPB (Oxford). 2019 Jul;21(7):883-90. DOI: 10.1016/j.hpb.2018.11.008.

224. Stummer W, Reulen HJ, Novotny A, Stepp H, Tonn JC. Fluorescence-guided resections of malignant gliomas--an overview. Acta Neurochir Suppl. 2003;88:9-12. DOI: 10.1007/978-3-7091-6090-9_3.

225. Terwisscha van Scheltinga AG, van Dam GM, Nagengast WB, Ntziachristos V, Hollema H, Herek JL, et al. Intraoperative near-infrared fluorescence tumor imaging with vascular endothelial growth factor and human epidermal growth factor receptor 2 targeting antibodies. J Nucl Med. 2011 Nov;52(11):1778-85. DOI: 10.2967/jnumed.111.092833.

226. Giusti RM, Shastri KA, Cohen MH, Keegan P, Pazdur R. FDA drug approval summary: panitumumab (Vectibix). Oncologist. 2007 May;12(5):577-83. DOI: 10.1634/theoncologist.12-5-577.

227. Adams KE, Ke S, Kwon S, Liang F, Fan Z, Lu Y, et al. Comparison of visible and near-infrared wavelength-excitable fluorescent dyes for molecular imaging of cancer. J Biomed Opt. 2007 Mar-Apr;12(2):024017. DOI: 10.1117/1.2717137.

228. Bhattacharyya S, Patel N, Wei L, Riffle LA, Kalen JD, Hill GC, et al. Synthesis and biological evaluation of panitumumab-IRDye800 conjugate as a fluorescence imaging probe for EGFR-expressing cancers. MedChemComm. 2014 Sep;5(9):1337-46. DOI: 10.1039/c4md00116h.

229. Kalyankrishna S, Grandis JR. Epidermal growth factor receptor biology in head and neck cancer. Journal of clinical oncology : official journal of the American Society of Clinical Oncology. 2006 Jun 10;24(17):2666-72. DOI: 10.1200/jco.2005.04.8306.

230. Marshall MV, Draney D, Sevick-Muraca EM, Olive DM. Single-dose intravenous toxicity study of IRDye 800CW in Sprague-Dawley rats. Mol Imaging Biol. 2010 Dec;12(6):583-94. DOI: 10.1007/s11307-010-0317-x.

231. Ter Weele EJ, Terwisscha van Scheltinga AG, Linssen MD, Nagengast WB, Lindner I, Jorritsma-Smit A, et al. Development, preclinical safety, formulation, and stability of clinical grade bevacizumab-800CW, a new near infrared fluorescent imaging agent for first in human use. Eur J Pharm Biopharm. 2016 Jul;104:226-34. DOI: 10.1016/j.ejpb.2016.05.008.

232. Zinn KR, Korb M, Samuel S, Warram JM, Dion D, Killingsworth C, et al. IND-directed safety and biodistribution study of intravenously injected cetuximab-IRDye800 in cynomolgus macaques. Mol Imaging Biol. 2015 Feb;17(1):49-57. DOI: 10.1007/s11307-014-0773-9.

233. Day KE, Sweeny L, Kulbersh B, Zinn KR, Rosenthal EL. Preclinical comparison of near-infrared-labeled cetuximab and panitumumab for optical imaging of head and neck squamous cell carcinoma. Mol Imaging Biol. 2013 Dec;15(6):722-9. DOI: 10.1007/s11307-013-0652-9.

234. Gao RW, Teraphongphom N, de Boer E, van den Berg NS, Divi V, Kaplan MJ, et al. Safety of panitumumab-IRDye800CW and cetuximab-IRDye800CW for fluorescence-guided surgical navigation in head and neck cancers. Theranostics. 2018;8(9):2488-95. DOI: 10.7150/thno.24487.

235. Pei J, Juniper G, van den Berg NS, Nisho N, Broadt T, Welch AR, et al. Safety and Stability of Antibody-Dye Conjugate in Optical Molecular Imaging. Mol Imaging Biol. 2021 Feb;23(1):109-16. DOI: 10.1007/s11307-020-01536-2.

236. Nishio N, van den Berg NS, van Keulen S, Martin BA, Fakurnejad S, Zhou Q, et al. Optimal Dosing Strategy for Fluorescence-Guided Surgery with Panitumumab-IRDye800CW in Head and Neck Cancer. Mol Imaging Biol. 2020 Feb;22(1):156-64. DOI: 10.1007/s11307-019-01358-x.

237. Gao RW, Teraphongphom NT, van den Berg NS, Martin BA, Oberhelman NJ, Divi V, et al. Determination of Tumor Margins with Surgical Specimen Mapping Using Near-Infrared Fluorescence. Cancer research. 2018 Sep 1;78(17):5144-54. DOI: 10.1158/0008-5472.can-18-0878.

238. van Keulen S, Nishio N, Fakurnejad S, van den Berg NS, Lu G, Birkeland A, et al. Intraoperative Tumor Assessment Using Real-Time Molecular Imaging in Head and Neck Cancer Patients. Journal of the American College of Surgeons. 2019 Dec;229(6):560-7 e1. DOI: 10.1016/j.jamcollsurg.2019.09.007.

239. van Keulen S, Nishio N, Fakurnejad S, Birkeland A, Martin BA, Lu G, et al. The Clinical Application of Fluorescence-Guided Surgery in Head and Neck Cancer. J Nucl Med. 2019 Jun;60(6):758-63. DOI: 10.2967/jnumed.118.222810.

240. van Keulen S, Nishio N, Birkeland A, Fakurnejad S, Martin B, Forouzanfar T, et al. The Sentinel Margin: Intraoperative Ex Vivo Specimen Mapping Using Relative Fluorescence Intensity. Clinical cancer research : an official journal of the American Association for Cancer Research. 2019 Aug 1;25(15):4656-62. DOI: 10.1158/1078-0432.Ccr-19-0319.

241. van Keulen S, van den Berg NS, Nishio N, Birkeland A, Zhou Q, Lu G, et al. Rapid, non-invasive fluorescence margin assessment: Optical specimen mapping in oral squamous cell carcinoma. Oral Oncol. 2019 Jan;88:58-65. DOI: 10.1016/j.oraloncology.2018.11.012.

242. Rosenthal EL, Moore LS, Tipirneni K, de Boer E, Stevens TM, Hartman YE, et al. Sensitivity and Specificity of Cetuximab-IRDye800CW to Identify Regional Metastatic Disease in Head and Neck Cancer. Clin Cancer Res. 2017 Aug 15;23(16):4744-52. DOI: 10.1158/1078-0432.ccr-16-2968.

243. Nishio N, van den Berg NS, van Keulen S, Martin BA, Fakurnejad S, Teraphongphom N, et al. Optical molecular imaging can differentiate metastatic from benign lymph nodes in head and neck cancer. Nat Commun. 2019 Nov 6;10(1):5044. DOI: 10.1038/s41467-019-13076-7.

244. Walkey CD, Olsen JB, Guo H, Emili A, Chan WC. Nanoparticle size and surface chemistry determine serum protein adsorption and macrophage uptake. J Am Chem Soc. 2012 Feb 1;134(4):2139-47. DOI: 10.1021/ja2084338.

245. P MS, Naha A, Shetty D, Nayak UY. Lymphatic Drug Transport and Associated Drug Delivery Technologies: A Comprehensive Review. Curr Pharm Des. 2020 Dec 3. DOI: 10.2174/1381612826999201203214247.

246. Wallace AM, Hoh CK, Ellner SJ, Darrah DD, Schulteis G, Vera DR. Lymphoseek: a molecular imaging agent for melanoma sentinel lymph node mapping. Annals of surgical oncology. 2007 Feb;14(2):913-21. DOI: 10.1245/s10434-006-9099-4.

247. Cousins AMF. Novel handheld magnetometer probe for improved intraoperative detection of sentinel lymph nodes in cancer patients / Aidan Mark Francis Cousins: Thesis (PhD)--University of South Australia, 2016.; 2016.

248. Azad AK, Rajaram MV, Metz WL, Cope FO, Blue MS, Vera DR, et al. γ-Tilmanocept, a New Radiopharmaceutical Tracer for Cancer Sentinel Lymph Nodes, Binds to the Mannose Receptor (CD206). J Immunol. 2015 Sep 1;195(5):2019-29. DOI: 10.4049/jimmunol.1402005.

249. Tausch C, Baege A, Rageth C. Mapping lymph nodes in cancer management - role of (99m)Tc-tilmanocept injection. Onco Targets Ther. 2014;7:1151-8. DOI: 10.2147/ott.S50394.

250. Leong SP, Kim J, Ross M, Faries M, Scoggins CR, Metz WL, et al. A phase 2 study of (99m)Tc-tilmanocept in the detection of sentinel lymph nodes in melanoma and breast cancer. Annals of surgical oncology. 2011 Apr;18(4):961-9. DOI: 10.1245/s10434-010-1524-z.

251. Notohamiprodjo M, Weiss M, Baumeister RG, Sommer WH, Helck A, Crispin A, et al. MR lymphangiography at 3.0 T: correlation with lymphoscintigraphy. Radiology. 2012 Jul;264(1):78-87. DOI: 10.1148/radiol.12110229.

252. Pouw JJ, Grootendorst MR, Bezooijen R, Klazen CA, De Bruin WI, Klaase JM, et al. Pre-operative sentinel lymph node localization in breast cancer with superparamagnetic iron oxide MRI: the SentiMAG Multicentre Trial imaging subprotocol. Br J Radiol. 2015;88(1056):20150634. DOI: 10.1259/bjr.20150634.

253. Douek M, Klaase J, Monypenny I, Kothari A, Zechmeister K, Brown D, et al. Sentinel node biopsy using a magnetic tracer versus standard technique: the SentiMAG Multicentre Trial. Annals of surgical oncology. 2014 Apr;21(4):1237-45. DOI: 10.1245/s10434-013-3379-6.

254. Cousins A, Balalis GL, Thompson SK, Forero Morales D, Mohtar A, Wedding AB, et al. Novel handheld magnetometer probe based on magnetic tunnelling junction sensors for intraoperative sentinel lymph node identification. Sci Rep. 2015 Jun 3;5:10842. DOI: 10.1038/srep10842.

255. Sun C, Lee JS, Zhang M. Magnetic nanoparticles in MR imaging and drug delivery. Adv Drug Deliv Rev. 2008 Aug 17;60(11):1252-65. DOI: 10.1016/j.addr.2008.03.018.

256. Kobayashi H, Kawamoto S, Bernardo M, Brechbiel MW, Knopp MV, Choyke PL. Delivery of gadolinium-labeled nanoparticles to the sentinel lymph node: comparison of the sentinel node visualization and estimations of intra-nodal gadolinium concentration by the magnetic resonance imaging. J Control Release. 2006 Apr 10;111(3):343-51. DOI: 10.1016/j.jconrel.2005.12.019.

257. Jun YW, Huh YM, Choi JS, Lee JH, Song HT, Kim S, et al. Nanoscale size effect of magnetic nanocrystals and their utilization for cancer diagnosis via magnetic resonance imaging. J Am Chem Soc. 2005 Apr 27;127(16):5732-3. DOI: 10.1021/ja0422155.

258. Amiri H, Mahmoudi M, Lascialfari A. Superparamagnetic colloidal nanocrystal clusters coated with polyethylene glycol fumarate: a possible novel theranostic agent. Nanoscale. 2011 Mar;3(3):1022-30. DOI: 10.1039/c0nr00603c.

259. Corot C, Robert P, Idée JM, Port M. Recent advances in iron oxide nanocrystal technology for medical imaging. Adv Drug Deliv Rev. 2006 Dec 1;58(14):1471-504. DOI: 10.1016/j.addr.2006.09.013.

260. Minamiya Y, Ito M, Katayose Y, Saito H, Imai K, Sato Y, et al. Intraoperative sentinel lymph node mapping using a new sterilizable magnetometer in patients with nonsmall cell lung cancer. Ann Thorac Surg. 2006 Jan;81(1):327-30. DOI: 10.1016/j.athoracsur.2005.06.005.

261. Nakagawa T, Minamiya Y, Katayose Y, Saito H, Taguchi K, Imano H, et al. A novel method for sentinel lymph node mapping using magnetite in patients with non-small cell lung cancer. J Thorac Cardiovasc Surg. 2003 Aug;126(2):563-7. DOI: 10.1016/s0022-5223(03)00216-2.

262. McDermott S, Thayer SP, Fernandez-Del Castillo C, Mino-Kenudson M, Weissleder R, Harisinghani MG. Accurate prediction of nodal status in preoperative patients with pancreatic ductal adenocarcinoma using next-gen nanoparticle. Transl Oncol. 2013 Dec 1;6(6):670-5. DOI: 10.1593/tlo.13400.

263. Winter A, Woenkhaus J, Wawroschek F. A novel method for intraoperative sentinel lymph node detection in prostate cancer patients using superparamagnetic iron oxide nanoparticles and a handheld magnetometer: the initial clinical experience. Annals of surgical oncology. 2014 Dec;21(13):4390-6. DOI: 10.1245/s10434-014-4024-8.

264. Ookubo T, Inoue Y, Kim D, Ohsaki H, Mashiko Y, Kusakabe M, et al. Characteristics of magnetic probes for identifying sentinel lymph nodes. Annu Int Conf IEEE Eng Med Biol Soc. 2013;2013:5485-8. DOI: 10.1109/embc.2013.6610791.

265. Teshome M, Wei C, Hunt KK, Thompson A, Rodriguez K, Mittendorf EA. Use of a Magnetic Tracer for Sentinel Lymph Node Detection in Early-Stage Breast Cancer Patients: A Meta-analysis. Annals of surgical oncology. 2016 May;23(5):1508-14. DOI: 10.1245/s10434-016-5135-1.

266. Anninga B, White SH, Moncrieff M, Dziewulski P, J LCG, Klaase J, et al. Magnetic Technique for Sentinel Lymph Node Biopsy in Melanoma: The MELAMAG Trial. Annals of surgical oncology. 2016 Jun;23(6):2070-8. DOI: 10.1245/s10434-016-5113-7.

267. Zada A, Peek MC, Ahmed M, Anninga B, Baker R, Kusakabe M, et al. Meta-analysis of sentinel lymph node biopsy in breast cancer using the magnetic technique. Br J Surg. 2016 Oct;103(11):1409-19. DOI: 10.1002/bjs.10283.

268. Rubio IT, Diaz-Botero S, Esgueva A, Rodriguez R, Cortadellas T, Cordoba O, et al. The superparamagnetic iron oxide is equivalent to the Tc99 radiotracer method for identifying the sentinel lymph node in breast cancer. European journal of surgical oncology : the journal of the European Society of Surgical Oncology and the British Association of Surgical Oncology. 2015 Jan;41(1):46-51. DOI: 10.1016/j.ejso.2014.11.006.

269. Ghilli M, Carretta E, Di Filippo F, Battaglia C, Fustaino L, Galanou I, et al. The superparamagnetic iron oxide tracer: a valid alternative in sentinel node biopsy for breast cancer treatment. Eur J Cancer Care (Engl). 2017 Jul;26(4). DOI: 10.1111/ecc.12385.

270. Huizing E, Anninga B, Young P, Monypenny I, Hall-Craggs M, Douek M. 4. Analysis of void artefacts in post-operative breast MRI due to residual SPIO after magnetic SLNB in SentiMAG Trial participants. Ejso. 2015;41.

271. Barranger E, Ihrai T. Comment on: Sentinel Node Biopsy Using Magnetic Tracer Versus Standard Technique: The SentiMAG Multicentre Trial. Annals of surgical oncology. 2017 Dec;24(Suppl 3):593. DOI: 10.1245/s10434-017-6191-x.

272. Bryce NS, Pham BTT, Fong NWS, Jain N, Pan EH, Whan RM, et al. The composition and end-group functionality of sterically stabilized nanoparticles enhances the effectiveness of co-administered cytotoxins. Biomater Sci. 2013 Dec 29;1(12):1260-72. DOI: 10.1039/c3bm60120j.

273. Jain N, Wang Y, Jones SK, Hawkett BS, Warr GG. Optimized steric stabilization of aqueous ferrofluids and magnetic nanoparticles. Langmuir. 2010 Mar 16;26(6):4465-72. DOI: 10.1021/la903513v.

274. Pham BT, Jain N, Kuchel PW, Chapman BE, Bickley SA, Jones SK, et al. The interaction of sterically stabilized magnetic nanoparticles with fresh human red blood cells. Int J Nanomedicine. 2015;10:6645-55. DOI: 10.2147/ijn.S93225.

275. Pham BTT, Colvin EK, Pham NTH, Kim BJ, Fuller ES, Moon EA, et al. Biodistribution and Clearance of Stable Superparamagnetic Maghemite Iron Oxide Nanoparticles in Mice Following Intraperitoneal Administration. Int J Mol Sci. 2018 Jan 10;19(1). DOI: 10.3390/ijms19010205.

276. Zanoni DK, Montero PH, Migliacci JC, Shah JP, Wong RJ, Ganly I, et al. Survival outcomes after treatment of cancer of the oral cavity (1985-2015). Oral Oncol. 2019 Mar;90:115-21. DOI: 10.1016/j.oraloncology.2019.02.001.

277. DeVita VT, Lawrence, T. S., & Rosenberg, S. A. (2015). DeVita, Hellman, and Rosenberg's cancer: Principles & practice of oncology: Tenth edition. Wolters Kluwer Health Adis (ESP).

278. Orosco RK, Tapia VJ, Califano JA, Clary B, Cohen EEW, Kane C, et al. Positive Surgical Margins in the 10 Most Common Solid Cancers. Sci Rep. 2018 Apr 9;8(1):5686. DOI: 10.1038/s41598-018-23403-5.

279. McMahon J, O'Brien CJ, Pathak I, Hamill R, McNeil E, Hammersley N, et al. Influence of condition of surgical margins on local recurrence and disease-

specific survival in oral and oropharyngeal cancer. Br J Oral Maxillofac Surg. 2003 Aug;41(4):224-31.

280. Zanoni DK, Migliacci JC, Xu B, Katabi N, Montero PH, Ganly I, et al. A Proposal to Redefine Close Surgical Margins in Squamous Cell Carcinoma of the Oral Tongue. JAMA otolaryngology-- head & neck surgery. 2017 Jun 1;143(6):555-60. DOI: 10.1001/jamaoto.2016.4238.

281. Tipirneni KE, Warram JM, Moore LS, Prince AC, de Boer E, Jani AH, et al. Oncologic Procedures Amenable to Fluorescence-guided Surgery. Annals of surgery. 2017 Jul;266(1):36-47. DOI: 10.1097/sla.0000000000002127.

282. Garofolo S, Piazza C, Del Bon F, Mangili S, Guastini L, Mora F, et al. Intraoperative narrow band imaging better delineates superficial resection margins during transoral laser microsurgery for early glottic cancer. The Annals of otology, rhinology, and laryngology. 2015 Apr;124(4):294-8. DOI: 10.1177/0003489414556082.

283. Muto M, Minashi K, Yano T, Saito Y, Oda I, Nonaka S, et al. Early detection of superficial squamous cell carcinoma in the head and neck region and esophagus by narrow band imaging: a multicenter randomized controlled trial. Journal of clinical oncology : official journal of the American Society of Clinical Oncology. 2010 Mar 20;28(9):1566-72. DOI: 10.1200/jco.2009.25.4680.

284. Gono K, Yamazaki K, Doguchi N, Nonami T, Obi T, Yamaguchi M, et al. Endoscopic Observation of Tissue by Narrowband Illumination. Optical Review. [journal article]. 2003 July 01;10(4):211-5. DOI: 10.1007/s10043-003-0211-8.

285. Wu C, Gleysteen J, Teraphongphom NT, Li Y, Rosenthal E. In-vivo optical imaging in head and neck oncology: basic principles, clinical applications and future directions. Int J Oral Sci. 2018 Mar 18;10(2):10. DOI: 10.1038/s41368-018-0011-4.

286. Low PS, Singhal S, Srinivasarao M. Fluorescence-guided surgery of cancer: applications, tools and perspectives. Current opinion in chemical biology. 2018 Aug;45:64-72. DOI: 10.1016/j.cbpa.2018.03.002.

287. Wang C, Wang Z, Zhao T, Li Y, Huang G, Sumer BD, et al. Optical molecular imaging for tumor detection and image-guided surgery. Biomaterials. 2018 Mar;157:62-75. DOI: 10.1016/j.biomaterials.2017.12.002.

288. Rosenthal EL, Warram JM, de Boer E, Basilion JP, Biel MA, Bogyo M, et al. Successful Translation of Fluorescence Navigation During Oncologic Surgery: A Consensus Report. J Nucl Med. 2016 Jan;57(1):144-50. DOI: 10.2967/jnumed.115.158915.

289. van Keulen S, Nishio N, Birkeland A, Fakurnejad S, Martin B, Forouzanfar T, et al. The Sentinel Margin: Intraoperative Ex Vivo Specimen Mapping Using Relative Fluorescence Intensity. Clin Cancer Res. 2019 May 29. DOI: 10.1158/1078-0432.ccr-19-0319.

290. Halicek M, Lu G, Little JV, Wang X, Patel M, Griffith CC, et al. Deep convolutional neural networks for classifying head and neck cancer using hyperspectral imaging. J Biomed Opt. 2017 Jun 1;22(6):60503. DOI: 10.1117/1.jbo.22.6.060503.

291. Grandis JR, Tweardy DJ. Elevated levels of transforming growth factor alpha and epidermal growth factor receptor messenger RNA are early markers of carcinogenesis in head and neck cancer. Cancer research. 1993 Aug 1;53(15):3579-84.

292. Yang XD, Jia XC, Corvalan JR, Wang P, Davis CG. Development of ABX-EGF, a fully human anti-EGF receptor monoclonal antibody, for cancer therapy. Critical reviews in oncology/hematology. 2001 Apr;38(1):17-23.

293. Heath CH, Deep NL, Sweeny L, Zinn KR, Rosenthal EL. Use of panitumumab-IRDye800 to image microscopic head and neck cancer in an orthotopic surgical model. Annals of surgical oncology. 2012 Nov;19(12):3879-87. DOI: 10.1245/s10434-012-2435-y.

294. Smits RW, Koljenović S, Hardillo JA, Ten Hove I, Meeuwis CA, Sewnaik A, et al. Resection margins in oral cancer surgery: Room for improvement. Head & neck. 2016 Apr;38 Suppl 1:E2197-203. DOI: 10.1002/hed.24075.

295. Chiosea SI. Intraoperative Margin Assessment in Early Oral Squamous Cell Carcinoma. Surg Pathol Clin. 2017 Mar;10(1):1-14. DOI: 10.1016/j.path.2016.10.002.

296. Fakurnejad S, Krishnan G, van Keulen S, Nishio N, Birkeland AC, Baik FM, et al. Intraoperative Molecular Imaging for ex vivo Assessment of Peripheral Margins in Oral Squamous Cell Carcinoma. Front Oncol. 2019;9:1476. DOI: 10.3389/fonc.2019.01476.

297. Kubik MW, Sridharan S, Varvares MA, Zandberg DP, Skinner HD, Seethala RR, et al. Intraoperative Margin Assessment in Head and Neck Cancer: A Case of Misuse and Abuse? Head Neck Pathol. 2020 Jun;14(2):291-302. DOI: 10.1007/s12105-019-01121-2.

298. Lubek JE, Magliocca KR. Evaluation of the Bone Margin in Oral Squamous Cell Carcinoma. Oral Maxillofac Surg Clin North Am. 2017 Aug;29(3):281-92. DOI: 10.1016/j.coms.2017.03.005.

299. Weinstock YE, Alava I, 3rd, Dierks EJ. Pitfalls in determining head and neck surgical margins. Oral Maxillofac Surg Clin North Am. 2014 May;26(2):151-62. DOI: 10.1016/j.coms.2014.01.003.

300. Nishio N, van den Berg NS, van Keulen S, Martin BA, Fakurnejad S, Zhou Q, et al. Optimal Dosing Strategy for Fluorescence-Guided Surgery with Panitumumab-IRDye800CW in Head and Neck Cancer. Mol Imaging Biol. 2019:10.1007/s11307-019-01358-x. DOI: 10.1007/s11307-019-01358-x. Cited in: PubMed.

301. Mizushima T, Ohnishi S, Shimizu Y, Hatanaka Y, Hatanaka KC, Hosono H, et al. Fluorescent imaging of superficial head and neck squamous cell carcinoma using a γ-glutamyltranspeptidase-activated targeting agent: a pilot study. BMC Cancer. 2016 Jul 7;16:411. DOI: 10.1186/s12885-016-2421-z.

302. Pan J, Deng H, Hu S, Xia C, Chen Y, Wang J, et al. Real-time surveillance of surgical margins via ICG-based near-infrared fluorescence imaging in patients with OSCC. World J Surg Oncol. 2020 May 15;18(1):96. DOI: 10.1186/s12957-020-01874-z.

303. Christensen A, Juhl K, Persson M, Charabi BW, Mortensen J, Kiss K, et al. uPAR-targeted optical near-infrared (NIR) fluorescence imaging and PET for image-guided surgery in head and neck cancer: proof-of-concept in orthotopic xenograft model. Oncotarget. 2017 Feb 28;8(9):15407-19. DOI: 10.18632/oncotarget.14282.

304. McCaul JA, Cymerman JA, Hislop S, McConkey C, McMahon J, Mehanna H, et al. LIHNCS - Lugol's iodine in head and neck cancer surgery: a multicentre, randomised controlled trial assessing the effectiveness of Lugol's iodine to assist excision of moderate dysplasia, severe dysplasia and carcinoma in situ at mucosal resection margins of oral and oropharyngeal squamous cell carcinoma: study protocol for a randomised controlled trial. Trials. 2013 Sep 24;14:310. DOI: 10.1186/1745-6215-14-310.

305. Petruzzi M, Lucchese A, Baldoni E, Grassi FR, Serpico R. Use of Lugol's iodine in oral cancer diagnosis: an overview. Oral oncology. 2010 Nov;46(11):811-3. DOI: 10.1016/j.oraloncology.2010.07.013.

306. Algadi HH, Abou-Bakr AA, Jamali OM, Fathy LM. Toluidine blue versus frozen section for assessment of mucosal tumor margins in oral squamous cell carcinoma. BMC Cancer. 2020 Nov 25;20(1):1147. DOI: 10.1186/s12885-020-07644-0.

307. Bray F, Ferlay J, Soerjomataram I, Siegel RL, Torre LA, Jemal A. Global cancer statistics 2018: GLOBOCAN estimates of incidence and mortality worldwide for 36 cancers in 185 countries. CA Cancer J Clin. 2018;68(6):394-424. DOI: 10.3322/caac.21492. Cited in: PubMed.

308. Pantel K, Brakenhoff RH. Dissecting the metastatic cascade. Nat Rev Cancer. 2004 Jun;4(6):448-56. DOI: 10.1038/nrc1370.

309. Grandi C, Alloisio M, Moglia D, Podrecca S, Sala L, Salvatori P, et al. Prognostic significance of lymphatic spread in head and neck carcinomas: therapeutic implications. Head Neck Surg. 1985 Nov-Dec;8(2):67-73. DOI: 10.1002/hed.2890080202.

310. Greenberg JS, El Naggar AK, Mo V, Roberts D, Myers JN. Disparity in pathologic and clinical lymph node staging in oral tongue carcinoma. Implication for therapeutic decision making. Cancer. 2003 Aug 1;98(3):508-15. DOI: 10.1002/cncr.11526.

311. Ferlito A, Rinaldo A, Devaney KO, Nakashiro K-i, Hamakawa H. Detection of lymph node micrometastases in patients with squamous carcinoma of the head and neck. European Archives of Oto-Rhino-Laryngology. [journal article]. 2008 October 01;265(10):1147-53. DOI: 10.1007/s00405-008-0715-8.

312. Schuller DE, McGuirt WF, McCabe BF, Young D. The prognostic significance of metastatic cervical lymph nodes. The Laryngoscope. 1980;90(4):557-70. DOI: 10.1288/00005537-198004000-00001. Cited in: PubMed.

313. Koyfman SA, Ismaila N, Holsinger FC. Management of the Neck in Squamous Cell Carcinoma of the Oral Cavity and Oropharynx: ASCO Clinical Practice Guideline Summary. Journal of Oncology Practice. 2019 2019/05/01;15(5):273-8. DOI: 10.1200/JOP.18.00727.

314. Argiris A, Karamouzis MV, Raben D, Ferris RL. Head and neck cancer. Lancet. 2008 May 17;371(9625):1695-709. DOI: 10.1016/s0140-6736(08)60728-x.

315. Gourin CG, Conger BT, Porubsky ES, Sheils WC, Bilodeau PA, Coleman TA. The effect of occult nodal metastases on survival and regional control in patients with head and neck squamous cell carcinoma. The Laryngoscope. 2008 Jul;118(7):1191-4. DOI: 10.1097/MLG.0b013e31816e2eb7.

316. Pitman KT, Johnson JT, Myers EN. Effectiveness of selective neck dissection for management of the clinically negative neck. Arch Otolaryngol Head Neck Surg. 1997 Sep;123(9):917-22. DOI: 10.1001/archotol.1997.01900090023004.

317. D'Cruz AK, Vaish R, Kapre N, Dandekar M, Gupta S, Hawaldar R, et al. Elective versus Therapeutic Neck Dissection in Node-Negative Oral Cancer. The New England journal of medicine. 2015 Aug 6;373(6):521-9. DOI: 10.1056/NEJMoa1506007.

318. Ferlito A, Rinaldo A, Silver CE, Gourin CG, Shah JP, Clayman GL, et al. Elective and therapeutic selective neck dissection. Oral Oncol. 2006 Jan;42(1):14-25. DOI: 10.1016/j.oraloncology.2005.03.009.

319. Dünne AA, Budach VG, Wagner W, Werner JA. Management of N0 neck in head and neck cancer: current controversies. Onkologie. 2004;27(4):363-7. DOI: 10.1159/000079089. Cited in: PubMed.

320. Nieweg OE, Tanis PJ, Kroon BBR. The Definition of a Sentinel Node. Annals of surgical oncology. 2001 2001/07/01;8(6):538-41. DOI: 10.1007/s10434-001-0538-y.

321. Cabanas RM. An approach for the treatment of penile carcinoma. Cancer. 1977;39(2):456-66. DOI: 10.1002/1097-0142(197702)39:2<456::aid-cncr2820390214>3.0.co;2-i. Cited in: PubMed.

322. Morton DL, Wen DR, Wong JH, Economou JS, Cagle LA, Storm FK, et al. Technical details of intraoperative lymphatic mapping for early stage melanoma. Arch Surg. 1992;127(4):392-9. DOI: 10.1001/archsurg.1992.01420040034005. Cited in: PubMed.

323. Thompson CF, St John MA, Lawson G, Grogan T, Elashoff D, Mendelsohn AH. Diagnostic value of sentinel lymph node biopsy in head and neck cancer: a meta-analysis. European archives of oto-rhino-laryngology : official journal of the European Federation of Oto-Rhino-Laryngological Societies (EUFOS) : affiliated with the German Society for Oto-Rhino-Laryngology - Head and Neck Surgery. 2013;270(7):2115-22. DOI: 10.1007/s00405-012-2320-0. Cited in: PubMed.

324. Liu M, Wang SJ, Yang X, Peng H. Diagnostic Efficacy of Sentinel Lymph Node Biopsy in Early Oral Squamous Cell Carcinoma: A Meta-Analysis of 66 Studies. PloS one. 2017;12(1):e0170322-e. DOI: 10.1371/journal.pone.0170322. Cited in: PubMed.

325. van den Brekel MW, van der Waal I, Meijer CJ, Freeman JL, Castelijns JA, Snow GB. The incidence of micrometastases in neck dissection specimens obtained from elective neck dissections. The Laryngoscope. 1996;106(8):987-91. DOI: 10.1097/00005537-199608000-00014. Cited in: PubMed.

326. Woolgar JA. Pathology of the N0 neck. British Journal of Oral and Maxillofacial Surgery. 1999;37(3):205-9. DOI: 10.1054/bjom.1999.0035.

327. Bogani G, Ditto A, Martinelli F, Signorelli M, Perotto S, Lorusso D, et al. A critical assessment on the role of sentinel node mapping in endometrial cancer. J Gynecol Oncol. 2015;26(4):252-4. DOI: 10.3802/jgo.2015.26.4.252. Cited in: PubMed.

328. Du J, Li Y, Wang Q, Batchu N, Zou J, Sun C, et al. Sentinel lymph node mapping in gynecological oncology. Oncol Lett. 2017;14(6):7669-75. DOI: 10.3892/ol.2017.7219. Cited in: PubMed.

329. Pei J, Juniper G, van den Berg NS, Nisho N, Broadt T, Welch AR, et al. Safety and Stability of Antibody-Dye Conjugate in Optical Molecular Imaging. Mol Imaging Biol. 2020 Sep 3. DOI: 10.1007/s11307-020-01536-2.

330. Tsien RY, Harootunian AT. Practical design criteria for a dynamic ratio imaging system. Cell Calcium. 1990 Feb-Mar;11(2-3):93-109. DOI: 10.1016/0143-4160(90)90063-z.

331. Nguyen QT, Tsien RY. Fluorescence-guided surgery with live molecular navigation--a new cutting edge. Nat Rev Cancer. 2013 Sep;13(9):653-62. DOI: 10.1038/nrc3566.

332. Miampamba M, Liu J, Harootunian A, Gale AJ, Baird S, Chen SL, et al. Sensitive in vivo Visualization of Breast Cancer Using Ratiometric Protease-activatable Fluorescent Imaging Agent, AVB-620. Theranostics. 2017;7(13):3369-86. DOI: 10.7150/thno.20678.

333. Tichauer KM, Wang Y, Pogue BW, Liu JT. Quantitative in vivo cell-surface receptor imaging in oncology: kinetic modeling and paired-agent principles from nuclear medicine and optical imaging. Phys Med Biol. 2015 Jul 21;60(14):R239-69. DOI: 10.1088/0031-9155/60/14/r239.

334. Weissleder R, Ntziachristos V. Shedding light onto live molecular targets. Nature medicine. 2003 Jan;9(1):123-8. DOI: 10.1038/nm0103-123.

335. van Leeuwen FW, Valdes-Olmos R, Buckle T, Vidal-Sicart S. Hybrid surgical guidance based on the integration of radionuclear and optical technologies. Br J Radiol. 2016 Jun;89(1062):20150797. DOI: 10.1259/bjr.20150797.

336. Hernot S, van Manen L, Debie P, Mieog JSD, Vahrmeijer AL. Latest developments in molecular tracers for fluorescence image-guided cancer surgery. Lancet Oncol. 2019 Jul;20(7):e354-e67. DOI: 10.1016/s1470-2045(19)30317-1.

337. van den Berg NS, Simon H, Kleinjan GH, Engelen T, Bunschoten A, Welling MM, et al. First-in-human evaluation of a hybrid modality that allows combined radio- and (near-infrared) fluorescence tracing during surgery. Eur J Nucl Med Mol Imaging. 2015 Oct;42(11):1639-47. DOI: 10.1007/s00259-015-3109-3.

338. KleinJan GH, van Werkhoven E, van den Berg NS, Karakullukcu MB, Zijlmans H, van der Hage JA, et al. The best of both worlds: a hybrid approach for optimal pre- and intraoperative identification of sentinel lymph nodes. Eur J Nucl Med Mol Imaging. 2018 Oct;45(11):1915-25. DOI: 10.1007/s00259-018-4028-x.

339. Miranda-Filho A, Bray F. Global patterns and trends in cancers of the lip, tongue and mouth. Oral Oncol. 2020 Mar;102:104551. DOI: 10.1016/j.oraloncology.2019.104551.

340. Ross GL, Soutar DS, Gordon MacDonald D, Shoaib T, Camilleri I, Roberton AG, et al. Sentinel node biopsy in head and neck cancer: preliminary results of a multicenter trial. Annals of surgical oncology. 2004 Jul;11(7):690-6. DOI: 10.1245/aso.2004.09.001.

341. Seim NB, Wright CL, Agrawal A. Contemporary use of sentinel lymph node biopsy in the head and neck. World J Otorhinolaryngol Head Neck Surg. 2016 Jun;2(2):117-25. DOI: 10.1016/j.wjorl.2016.05.008.

342. Albo D, Wayne JD, Hunt KK, Rahlfs TF, Singletary SE, Ames FC, et al. Anaphylactic reactions to isosulfan blue dye during sentinel lymph node biopsy for breast cancer. American journal of surgery. 2001 Oct;182(4):393-8. DOI: 10.1016/s0002-9610(01)00734-6.

343. Thevarajah S, Huston TL, Simmons RM. A comparison of the adverse reactions associated with isosulfan blue versus methylene blue dye in sentinel lymph node biopsy for breast cancer. American journal of surgery. 2005 Feb;189(2):236-9. DOI: 10.1016/j.amjsurg.2004.06.042.

344. Masannat YA, Hanby A, Horgan K, Hardie LJ. DNA damaging effects of the dyes used in sentinel node biopsy: possible implications for clinical practice. J Surg Res. 2009 Jun 15;154(2):234-8. DOI: 10.1016/j.jss.2008.07.039.

345. Alvarado MD, Mittendorf EA, Teshome M, Thompson AM, Bold RJ, Gittleman MA, et al. SentimagIC: A Non-inferiority Trial Comparing Superparamagnetic Iron Oxide Versus Technetium-99m and Blue Dye in the Detection of Axillary

Sentinel Nodes in Patients with Early-Stage Breast Cancer. Annals of surgical oncology. 2019 Oct;26(11):3510-6. DOI: 10.1245/s10434-019-07577-4.

346. Saar LI, Getty R. THE INTERRELATIONSHIP OF THE LYMPH VESSEL CONNECTIONS OF THE LYMPH NODES OF THE HEAD, NECK, AND SHOULDER REGIONS OF SWINE. Am J Vet Res. 1964 May;25:618-36.

347. Aarsvold JN, Alazraki NP. Update on detection of sentinel lymph nodes in patients with breast cancer. Semin Nucl Med. 2005 Apr;35(2):116-28. DOI: 10.1053/j.semnuclmed.2004.11.003.

348. Hersi AF, Pistiolis L, Dussan Luberth C, Vikhe-Patil E, Nilsson F, Mohammed I, et al. Optimizing Dose and Timing in Magnetic Tracer Techniques for Sentinel Lymph Node Detection in Early Breast Cancers: The Prospective Multicenter SentiDose Trial. Cancers (Basel). 2021 Feb 9;13(4). DOI: 10.3390/cancers13040693.

349. Karakatsanis A, Daskalakis K, Stålberg P, Olofsson H, Andersson Y, Eriksson S, et al. Superparamagnetic iron oxide nanoparticles as the sole method for sentinel node biopsy detection in patients with breast cancer. Br J Surg. 2017 Nov;104(12):1675-85. DOI: 10.1002/bjs.10606.

350. Ahmed M, Anninga B, Pouw JJ, Vreemann S, Peek M, Van Hemelrijck M, et al. Optimising magnetic sentinel lymph node biopsy in an in vivo porcine model. Nanomedicine. 2015 May;11(4):993-1002. DOI: 10.1016/j.nano.2015.01.010.

351. Koch WM, Choti MA, Civelek AC, Eisele DW, Saunders JR. Gamma probe-directed biopsy of the sentinel node in oral squamous cell carcinoma. Arch Otolaryngol Head Neck Surg. 1998 Apr;124(4):455-9. DOI: 10.1001/archotol.124.4.455.

352. Payoux P, Dekeister C, Lopez R, Lauwers F, Esquerré JP, Paoli JR. Effectiveness of lymphoscintigraphic sentinel node detection for cervical staging of patients with squamous cell carcinoma of the head and neck. J Oral Maxillofac Surg. 2005 Aug;63(8):1091-5. DOI: 10.1016/j.joms.2005.04.026.

353. de Bree R, Takes RP, Castelijns JA, Medina JE, Stoeckli SJ, Mancuso AA, et al. Advances in diagnostic modalities to detect occult lymph node metastases in head and neck squamous cell carcinoma. Head & neck. 2015 Dec;37(12):1829-39. DOI: 10.1002/hed.23814.

354. Gloag L, Mehdipour M, Ulanova M, Mariandry K, Nichol MA, Hernández-Castillo DJ, et al. Zero valent iron core-iron oxide shell nanoparticles as small magnetic particle imaging tracers. Chem Commun (Camb). 2020 Mar 25;56(24):3504-7. DOI: 10.1039/c9cc08972a.

355. Cousins A, Thompson SK, Wedding AB, Thierry B. Clinical relevance of novel imaging technologies for sentinel lymph node identification and staging. Biotechnol Adv. 2014 Mar-Apr;32(2):269-79. DOI: 10.1016/j.biotechadv.2013.10.011.

356. Park YM, Holsinger FC, Kim WS, Park SC, Lee EJ, Choi EC, et al. Robot-assisted selective neck dissection of levels II to V via a modified facelift or retroauricular approach. Otolaryngol Head Neck Surg. 2013 May;148(5):778-85. DOI: 10.1177/0194599813478934.

357. Accorona R, D'Onghia A, Pignataro L, Capaccio P. Head and neck robotic surgery combined with sentinel lymph node biopsy. Fascinating, but feasible? Oral Oncol. 2020 Jul 31;111:104939. DOI: 10.1016/j.oraloncology.2020.104939.

358. Malloy KM, Cognetti DM, Wildemore BM, Cunnane MF, Keane WM, Pribitkin EA, et al. Feasibility of endoscopic sentinel node biopsy in the porcine neck. Otolaryngol Head Neck Surg. 2007 May;136(5):806-10. DOI: 10.1016/j.otohns.2006.11.025.

359. Pitman KT, Sisk JD. Endoscopic sentinel lymph node biopsy in a porcine model. The Laryngoscope. 2006 May;116(5):804-8. DOI: 10.1097/01.mlg.0000209098.99831.1a.

360. Kang SW, Jeong JJ, Yun JS, Sung TY, Lee SC, Lee YS, et al. Gasless endoscopic thyroidectomy using trans-axillary approach; surgical outcome of 581 patients. Endocr J. 2009;56(3):361-9. DOI: 10.1507/endocrj.k08e-306.

361. Gottlieb A, Sprung J, Zheng X-M, Gagner M. Massive Subcutaneous Emphysema and Severe Hypercarbia in a Patient During Endoscopic Transcervical Parathyroidectomy Using Carbon Dioxide Insufflation. Anesthesia & Analgesia. 1997;84(5).

362. Kim JH, Byeon HK, Kim DH, Kim SH, Choi EC, Koh YW. ICG-Guided Sentinel Lymph Node Sampling during Robotic Retroauricular Neck Dissection in cN0 Oral Cancer. Otolaryngol Head Neck Surg. 2020 Mar;162(3):410-3. DOI: 10.1177/0194599819900264.

363. Chow VL, Ng JC, Chan JY, Gao W, Wong TS. Robot-assisted real-time sentinel lymph node mapping in oral cavity cancer: preliminary experience. J Robot Surg. 2020 Jun 27. DOI: 10.1007/s11701-020-01112-4.

364. Acar C, Kleinjan GH, van den Berg NS, Wit EM, van Leeuwen FW, van der Poel HG. Advances in sentinel node dissection in prostate cancer from a technical perspective. Int J Urol. 2015 Oct;22(10):898-909. DOI: 10.1111/iju.12863.

365. Torchia MG, Misselwitz B. Combined MR lymphangiography and MR imaging-guided needle localization of sentinel lymph nodes using Gadomer-17. AJR Am J Roentgenol. 2002 Dec;179(6):1561-5. DOI: 10.2214/ajr.179.6.1791561.

366. Koh YW, Chung WY, Hong HJ, Lee SY, Kim WS, Lee HS, et al. Robot-assisted selective neck dissection via modified face-lift approach for early oral tongue cancer: a video demonstration. Annals of surgical oncology. 2012 Apr;19(4):1334-5. DOI: 10.1245/s10434-011-2155-8.

367. Ito R, Suami H. Lymphatic Territories (Lymphosomes) in Swine: An Animal Model for Future Lymphatic Research. Plast Reconstr Surg. 2015 Aug;136(2):297-304. DOI: 10.1097/prs.0000000000001460.

368. van Oosterom MN, Simon H, Mengus L, Welling MM, van der Poel HG, van den Berg NS, et al. Revolutionizing (robot-assisted) laparoscopic gamma tracing using a drop-in gamma probe technology. Am J Nucl Med Mol Imaging. 2016;6(1):1-17.

369. Byrd JK, Paquin R. Cost Considerations for Robotic Surgery. Otolaryngol Clin North Am. 2020 Dec;53(6):1131-8. DOI: 10.1016/j.otc.2020.07.019.